AN INVESTIGATION INTO THE IMPACT FRACTURE BEHAVIOUR OF POLY (PROPYLENE – ETHYLENE) COPOLYMERS USING AN INSTRUMENTED LOW TEMPERATURE DROP WEIGHT IMPACT TESTER

Ravindra Patil

A dissertation submitted to the Faculty of Engineering and the Built Environment at the University of Cape Town in fulfillment of the requirements for the degree of
Master of Science in Engineering.

Department of Mechanical Engineering
Centre for Materials Engineering
University of Cape Town

October
2001

ACKNOWLEDGEMENTS

I would like to express my sincere gratitude to my parents, Dr D G Patil and Mrs Vimlabai Patil and my younger brother, Ajay Patil, for motivating, guiding and always encouraging me throughout my path in life.

I would also like to thank and show my appreciation to the following people for their kind assistance in my masters research project.

- Dr Kashif Marcus, who is my supervisor, for his guidance, patience and sincere dedication.
- Dr Brian Sole, my co-supervisor, for his helpful input into this research project.
- Mr Glen Newins and his assistant, Peter Jacobs, for their help in the construction of my cryogenic temperature set-up, and helpful words of advice.
- Mr Dave Dean, for setting up the Gefran Temperature Controller Unit and other electrical connections required for my test apparatus.
- Mr James Petersen for his assistance with photography.
- My friends and fellow students at the Centre for Materials Engineering for their words of advice and support.
- Sasol Polymers for their supplying the testing copolymer specimens.
- Mrs Mira Topic for always cheerfully helping me to understand the operational procedure of the SEM.
- Sasol Polymers and the National Research Foundation for their financial support during my postgraduate study.

A special thanks to my fiancé, Florina-Maria Moodley and my close friends in Cape Town.

KEYWORD GLOSSARY

- Brittle-to-ductile transition
- Brittle-to-ductile transition temperature
- Cavitation
- Copolymer
- Copolymerization
- Crazing
- Crack initiation energy
- Crack propagation energy
- Cryogenic
- Crystallinity
- Drop weight impact
- Ductility
- Ethylene content
- Ethylene propylene rubber
- Fracture toughness
- Homopolymer
- Impactor
- Impact copolymers
- Impact strength
- Isotactic
- Matrix ligament thickness
- Melt flow index
- Microfibrils
- Micro-mechanical damage
- Micro-morphological
- Microvoid
- Modifier particles
- Polypropylene
- Poly (propylene-ethylene) copolymer
- Rubber content
- Rubber toughening
- Shear bands
- Stress whitening
- Shear yielding

ABSTRACT

This dissertation examines the drop weight impact behaviour and fracture of poly (propylene – ethylene) copolymers at cryogenic temperatures. A cryogenic temperature facility was incorporated into the existing instrumented drop weight impact tester to allow for variation of the impact test temperatures. Sasol Polymer grades with varying ethylene content (0 to 13.4 weight %) were comprehensively tested to determine their brittle-to-ductile transition temperatures. The effect of melt flow index, melt temperature, rubber particle size and distribution were also examined to determine their effect on impact energy.

A cooling disk system was built and used to lower the impact test temperatures down to -50°C within a tolerance of 2°C of the desired test temperature. It was found that increasing additions of ethylene into the polypropylene matrix suppressed the brittle-to-ductile temperatures of the copolymers. Interestingly, the impact energy of the copolymers shows an increase in impact energy with decreasing temperature until the brittle-to-ductile transition is reached. It was found that the magnitude of crazing decreases with temperature especially at temperatures below the transition. A large amount of the stress whitening phenomena is observed in the copolymer above its brittle-to-ductile transition temperature. Brittle failure in the form of radial and circumferential cracks dominates the impact behaviour below the copolymer's brittle-to-ductile transition temperature.

The effect of decreasing ethylene content at constant temperature is analogous to decreasing the test temperature at constant ethylene. The copolymers show a dramatic increase in impact energy dissipation at ethylene contents above 11%. The impact tests also show that low melt flow indices lead to significant improvements in impact performance. At constant ethylene content it is important for the rubber particles to have a narrow particle distribution and be uniformly distributed within the matrix.

TABLE OF CONTENTS

CHAPTER 1

GENERAL INTRODUCTION

1.1 INTRODUCTION

Isotactic polypropylene (PP) is a versatile semi-crystalline polymer exhibiting good mechanical properties coupled with an advantageous price-performance ratio. It is widely used due to its ease of processing in various manufacturing methods. Thus, polypropylene is used in applications ranging from commodities in packaging to fabrics in textiles to under hood engineering applications in the automobile industry. The percentage of polypropylene consumption in Western Europe and their respective applications are shown in figure 1.1 for the year 1999[1]. The South African polypropylene market is similar to that of Europe with regard to the high growth rates in the local packaging industry.

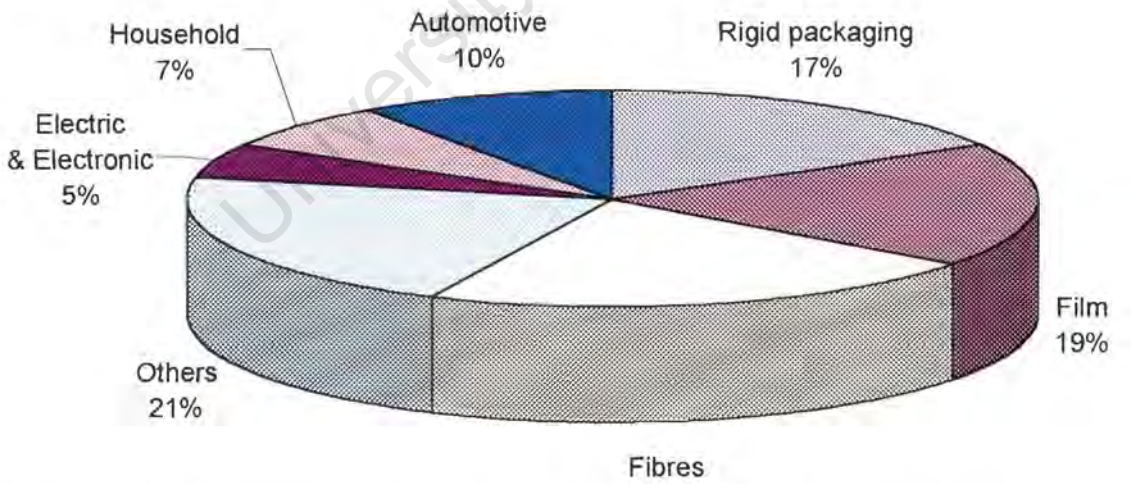

Figure 1.1: *Western Europe polypropylene consumption details in the year 1999 [after ref. 1].*

So it is therefore not surprising that polypropylene continues to show such phenomenal growth in the near future as the worldwide polypropylene demand information in figure 1.2 illustrates. Polypropylene is produced either

as a homopolymer or a copolymer. The copolymers can be subdivided into two main categories, namely random and impact copolymers. The projected growth rates for the three polypropylene grades until the year 2004 is shown in table 1.1. The total worldwide polypropylene production is estimated to increase by 49% by the year 2004 to a gross of about 41 million tons[1].

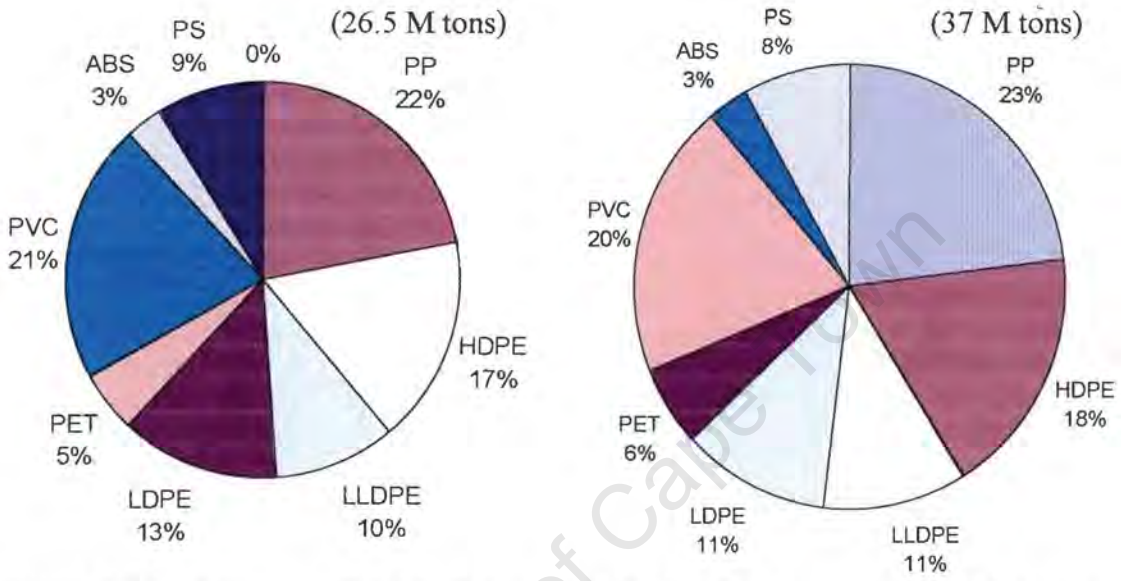

Figure 1.2: *Worldwide increase in the demand of polypropylene compared with other major polymer types [after ref. 1].*

	Year 1999 (million tons)	***Year 2004 (million tons)***
Homopolymers	18400	27500
Growth rate	49%	
Random copolymers	3040	4500
Growth rate	51%	
Impact copolymers	6100	8970
Growth rate	47%	

Table 1.1: *The world production of the three major categories of the polypropylene market and their respective projected growth rates to the year 2004 [after ref. 1].*

The polypropylene homopolymer is known to exhibit relatively low impact strength at temperatures below room temperature. Thus the use of polypropylene for engineering structural applications in the industrial sector is severely limited. The homopolymer typically finds uses in applications such as domestic food containers, package strapping tape and needle punched carpets. These items do not require high impact strength; the low impact strength of polypropylene can, to an extent, be attributed to its high glass transition temperature (T_g) of approximately 0°C.

An improvement in the impact toughness of polypropylene can be achieved through the addition of a secondary rubbery phase or impact modifier into its microstructure. This is known as rubber toughening and is achieved either by in situ copolymerization or by blending two or more compatible polymer species together. The copolymerization process involves the insertion of a different moiety into the backbone of the chain and therefore disrupts the chain structure regularity. As a consequence of the change in the polymer structure and in the morphology and microstructure, its properties are also altered. The crystallinity is lowered and so are properties that are influenced directly by crystallinity, such as the yield strength and modulus. Lowering the crystallinity of the copolymer also shifts the so-called brittle-to-ductile transition (BDT) temperature to lower values. It is clear then that improving the impact toughness of polypropylene has important significance in extending its range of applications. The impact toughness is a key parameter in influencing the performance of engineering applications produced from polypropylene.

Copolymer impact modifiers such ethylene propylene rubber (EPR) and ethylene propylene diene monomer (EPDM) is commonly used as the secondary phase in polypropylene systems. This type of copolymer is strictly speaking a bi-phasic copolymer but is commonly referred to as a block copolymer or impact copolymer in common parlance. The inclusion of these ductile rubber particles within the polypropylene homopolymer matrix lowers the ductile-to-brittle transition temperature of the impact copolymer due to the

effect of additional deformation mechanisms. However, an improvement in impact strength is accompanied by a noticeable reduction in the modulus, tensile strength and scratch resistance. These impact copolymers are used in applications such as luggage, car bumpers and outdoor stadium seats. Figure 1.1 shows that rigid packaging is also one of the main uses of impact copolymers. In many of these applications low temperature impact resistance is of critical importance for the polymer manufacturer. The material properties depend mainly on their micro-morphological structure, making the relationship between structure and properties such as the fracture behaviour in polymers an important branch within materials science. The fracture toughness of a material is strongly related to the ability of that material to dissipate energy before failure, thus impact testing such in as the instrumented drop weight impact testing can be carried out to examine the structure-property relationships.

As the applications for toughened polymeric materials become more common and severe, tests that simulate end-use conditions more stringently and accurately are required. The impact resistance of a polymer often determines its usefulness in applications, as a ductile polymer may even behave as a brittle one under impact conditions due to the inability of the chains to undergo compensating molecular relaxation. Drop weight impact tests provide a more accurate correlation of the loading mode applied to practical situations. Generally, these tests are carried out to the point of completion, which is the total penetration mode and the impact energy at ultimate failure is employed to evaluate the toughness of the copolymers. Under the influence of an external load, a multitude of micro-mechanical deformations such as crazing, cavitation and shear yielding develop in competition with one another in polypropylene copolymers. The composition, structure, size and distribution of the modifier particles govern the deformation mechanisms. The temperature and strain rates play a crucial role in allowing a specific mechanism to dominate the deformation. These factors affect the response of the impacted polymer to an external load, giving different fracture characteristics.

1.2 MOTIVATION FOR THE THESIS PROJECT

The increasing market demands for structural applications of polypropylene have triggered extensive research into improving the fracture toughness and impact resistance of polypropylene. A widely employed strategy to improve the toughness of a single-phase thermoplastic is to incorporate an elastomeric phase into the matrix such as in the case of poly (propylene-ethylene) copolymer where EPR particles are dispersed within the polypropylene homopolymer. From an industrial application point of view, the dependence of impact strength on temperature is crucial. The properties of the poly (propylene-ethylene) copolymers can be tailored and engineered via ethylene content and molecular weight to suit a wide range of products. This requires a good understanding of the material's behaviour in terms of molecular parameters as well as external factors such as temperature and strain rate.

1.3 RESEARCH OBJECTIVES

The objectives of this research is to:

1 Modify the in-house built impact tester to permit impact testing at cryogenic temperatures. The impact testing is to be carried out in the temperature range of 40°C to -50°C. The test temperature must lie within a tolerance level of 2°C of the selected temperature.

2 Study the impact and fracture behaviour of different grades of poly (propylene-ethylene) copolymers produced by Sasol Polymers. Of prime importance, is the effect of increasing the EPR modifier content on the impact behaviour.

3 Make a correlation between the rubber content, the testing temperature and the impact deformation modes.

1.4 SCOPE AND PLAN OF DEVELOPMENT

This research thesis is comprised of five parts:

- Design and construction of the cryogenic temperature facility which should be incorporated into the in-house built instrumented drop weight impact tester.
- Performing drop weight impact tests on different grades of polypropylene copolymers with varying ethylene content as well as on a reference polypropylene homopolymer.
- Testing the impact specimens within a temperature range of 40°C to -50°C.
- Analyse the dispersion and size of the EPR particles using scanning electron microscopy and the Joyce Loebl Image Analysis Software package.
- Analyse the results obtained from the experimental work.

This research project begins with a *review of the literature* surveyed regarding the research topic followed by the *design* of a cryogenic temperature facility. It then outlines the *experimental techniques* used in the impact testing of the copolymers. The *results* of the experiments are then presented and *discussed*. Lastly, *conclusions* are drawn and *recommendations* for future work are made.

CHAPTER 2

LITERATURE REVIEW

2.1 POLYMERIC STRUCTURES

2.1.1 Polypropylene Homopolymer

When all the repeating units along a chain are of the same type, the resulting polymer is known as a homopolymer[1]. In isotactic polypropylene the pendant methyl group (-CH_3) has the same configuration along the polymer backbone[2]. The degree of crystallinity is governed by the tacticity of the chain and hence isotactic polypropylene is highly crystalline. In syndiotactic polypropylene the methyl groups are situated in an alternating fashion around the chain whilst in atactic polypropylene the methyl groups are randomly distributed about the backbone[3]. Figure 2.1 shows a schematic of the three stereoisomers of polypropylene.

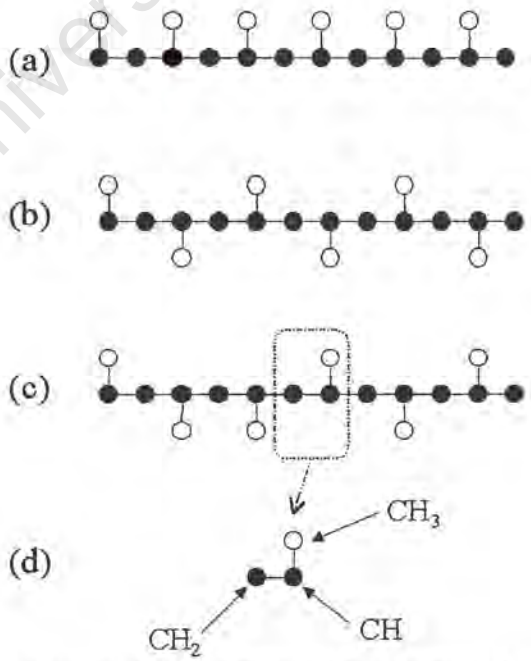

Figure 2.1: *Schematic illustration of (a) isotactic, (b) syndiotactic, (c) atactic polypropylene and (d) repeating unit [after ref. 3].*

2.1.2 Polypropylene Copolymers

A copolymer is a polymer that consists of two or more dissimilar mer units in various combinations along its molecular backbone chain. Depending on the polymerization process and the relative fractions of these mer units, different sequencing arrangements on the polymer chain are possible. When two different units are randomly dispersed along the chain a random copolymer is produced. An alternating copolymer has the two mer units in alternating positions along the chain. A block copolymer has identical mer units clustered in blocks along the chain. In the terminology used in the local polymer industry, the impact block copolymers refer to a polymer composite consisting of a homopolymer polypropylene matrix and an elastomeric EPR phase dispersed in it. This is strictly speaking a bi-phasic copolymer. A graft copolymer consists of a homopolymer side branch of one polymer type being grafted onto the homopolymer main chain of another type[2,3]. A schematic of these structures is shown in figure 2.2 below.

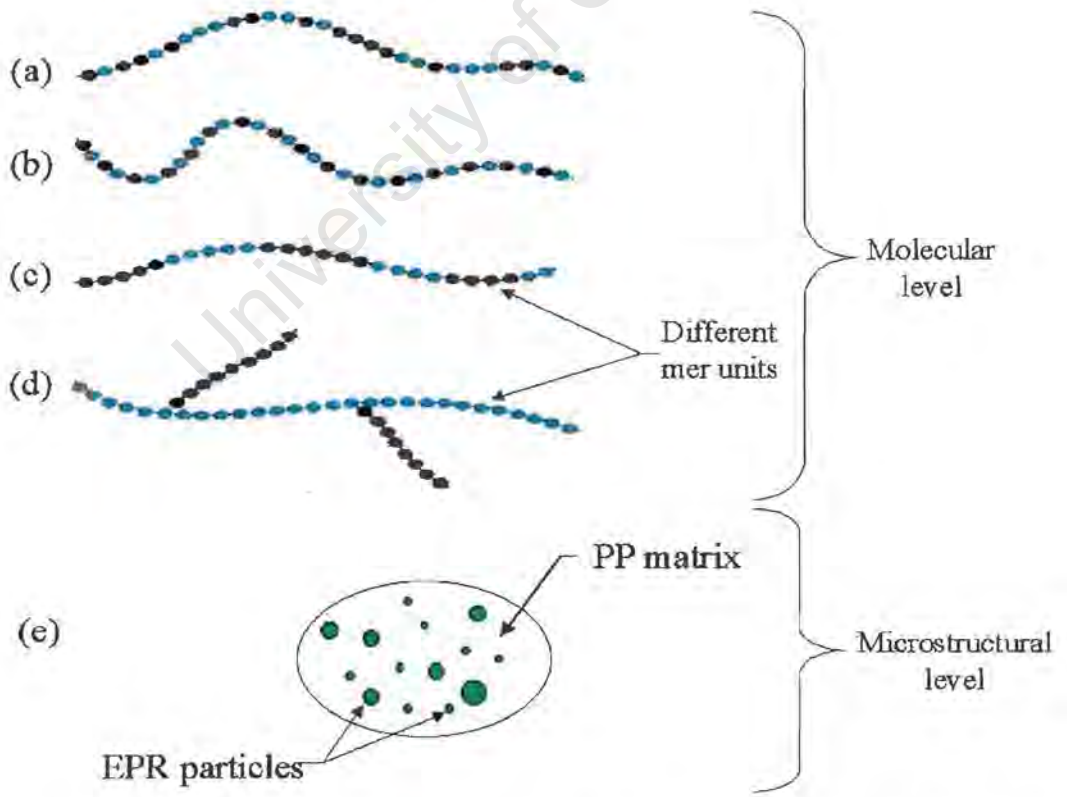

Figure 2.2: *Simplified schematic of the various types of copolymers described (a) random (b) alternating (c) block (d) graft (e) bi-phasic structure [after ref. 3].*

The blending or copolymerization of the polypropylene homopolymer with a more ductile or rubbery material that is compatible with the homopolymer is a widely employed strategy that alleviates the inherent brittleness of polypropylene. This procedure introduces one or more types of polymer into the matrix and the resultant microstructure is either bi-phasic or multi-phasic. In polypropylene impact modification, the levels of ethylene-propylene rubber (EPR) do not usually exceed 40% by volume as additions of a greater quantity leads to undesirable softening[4,5]. The relative chemical composition, configuration and molecular weight of the polypropylene and elastomeric phases involved determine the morphology of rubber-modified polypropylene. In the impact block copolymers the secondary phase consists of both ethylene-propylene molecules and linear polyethylene within the rubber particle. A transmission electron micrograph of rubber particles dispersed in polypropylene is shown in figure 2.3.

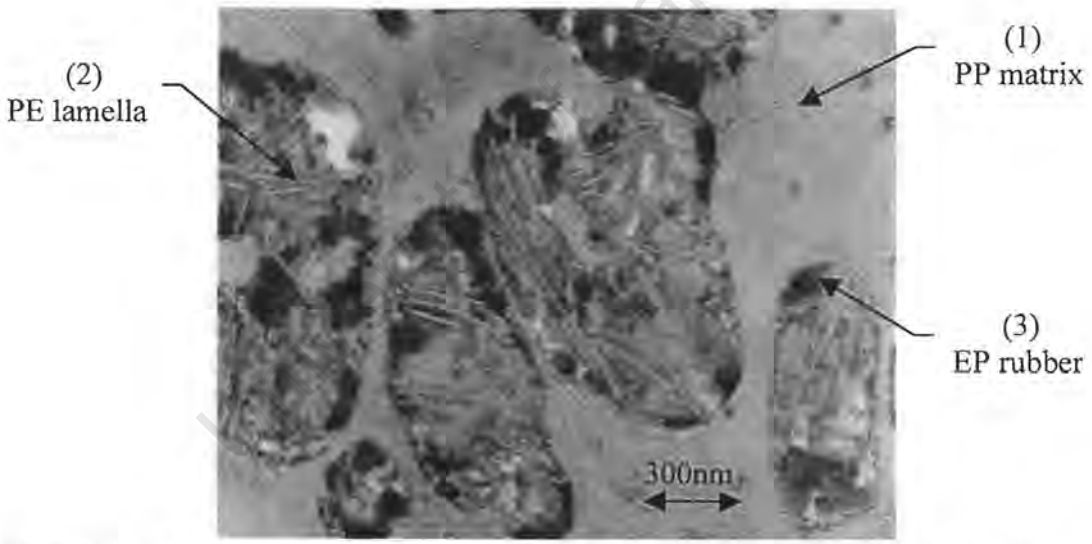

Figure 2.3: *TEM image of rubber-modified PP with crystalline PE dispersed in the rubber phase [after ref. 3].*

Three microstructural features are visible in the phase structure of the impact block copolymer shown in figure 2.3 above. The matrix of the semi-crystalline polypropylene contains fine lamellae (1). Some of polypropylene lamellae penetrate into the dispersed elastomeric particles and are typically normal to the rubber-matrix interface. This process assists adhesion between the two phases. Some of the dispersed particles have coalesced as seen in the figure

above. Within the rubber inclusions, coarser polyethylene lamellae can be seen (2). The polyethylene lamellae are surrounded by a region of EPR (3) which also forms the shell of the particle. Good adhesion between the matrix and the modifier particles is important for adequate impact strength. The combined concentration of the rubber content and the amorphous content in the matrix represent the total amorphous content in the copolymer[4,6,7].

2.2 PRINCIPLES OF RUBBER TOUGHENING

The extent of the toughening induced by copolymerization is dependent on the shape, size, EPR content, spatial distribution and morphology of the rubber particles as well as on the morphology of the polypropylene matrix. The rubber phase improves the fracture resistance of the copolymer by dissipating the energy present in the matrix phase before failure and by varying the crystalline structure of the polypropylene. However, the effect of the induced difference in the crystalline structure on the mechanical properties of the toughened polymer is insignificant.

The process of rubber toughening increases the fracture resistance of the matrix polymer but is also accompanied by an undesired limited reduction in the stiffness, yield stress and creep resistance of the polymer. The degree and nature of adhesion between the different phases are also important parameters in controlling the micro-mechanical and mechanical behaviour of the impact copolymers because the rubber particles must be effective as craze stoppers and shear force transmitters. The interfacial morphological structure between the modifier particles and the matrix is controlled by the functionality between the matrix and the rubber phase[5,7,8,9]. The average size of the dispersed EPR particles is largely dependent on the relative viscosity between polypropylene and EPR. Similar melt viscosities allow for better compatibility between the two phases, which results in a fine and uniform distribution of the EPR particles. Strong interfacial adhesion is also achieved from good compatibility[2].

2.3 TOUGHENING MECHANISMS

Various toughening mechanisms for the elastomer-modified polymers have been suggested[2-21]. The mechanisms mentioned below are preceded by the word "multiple" due to the initiation of the deformation mechanisms at numerous sites, resulting in the deformation micro-mechanisms occurring throughout a comparatively large volume of rubber-modified material. The modifier particles initiate the toughening mechanisms and limit the growth and breakdown of crazes and/or voids to prevent early crack initiation which leads to material failure. The micro-mechanisms mentioned below provide evidence of the occurrence of the damage process within the copolymer upon loading and are irreversible modes of deformation. The multiple crazing and voiding modes are known as dilatational deformation micro-mechanisms[2,8].

2.3.1 Multiple Crazing Theory

Bucknall and Smith proposed a multiple crazing theory primarily based on the role of the matrix polymer in the deformation and energy absorption process[2]. Upon the application of a critical load, stress whitening is observed on the specimens. This observation is attributed to the formation of many crazes in the vicinity of the elastomer-matrix interface and run between the elastomeric particles. Craze formation manifests itself as opaque striations in planes normal to the direction of the stress. Crazes are defined as regions of localised yielding that consists of microvoids in a plane perpendicular to the maximum principle stress that are stabilised by fibrillar bridges of plastically deformed and oriented polymeric material. This can be observed in the schematic shown in figure 2.4 on the following page.

Provided the load is sufficient to cause the microvoids to grow and coalesce, crack formation begins as indicated in the diagram. Crazes are *therefore* known as the precursors to fracture. The fracture toughness of the polypropylene is increased during the craze growth stage which occurs prior to cracking since the micro-mechanism of crazing absorbs the fracture

energy. Specifically, it is the orientated microfibrils that contribute significantly to further deformation resistance.

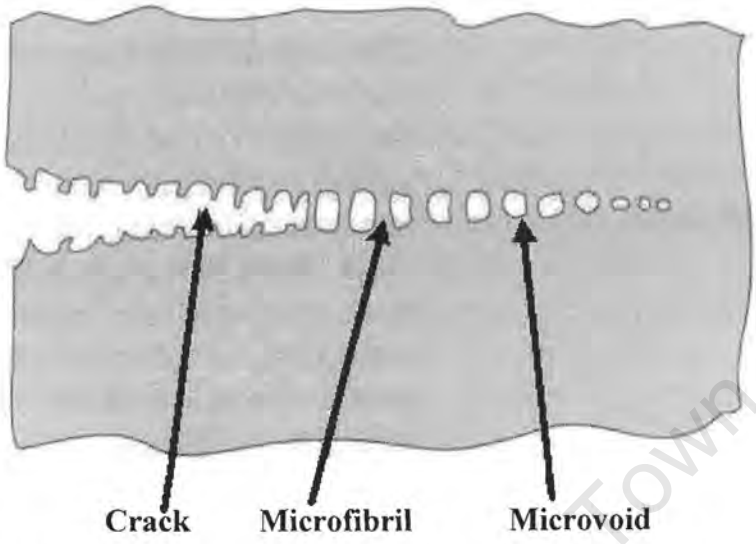

Figure 2.4: *A schematic representation of a craze within a polymer [after ref. 3].*

Polymers that usually fail by means of crazing have a low crack initiation (un-notched) energy and low crack propagation (notched) energy thus promoting the formation of crazes. In addition, tests done at low temperatures or high rate of loading promote the formation of crazes. Figure 2.5 below shows a photomicrograph of a craze with polymer fibrils spanning the craze length.

Figure 2.5: *An image of a craze in a polyphenylene oxide [after ref. 3].*

It was put forward that the function of the elastomeric particles was to act as stress concentrators and control craze growth by initiating a sufficient number of energy-absorbing crazes of a sub-critical size. Once they are initiated, the role of the particles is to attempt the termination of the crazes before they reach the critical catastrophic failure size and crack formation begins. The presence of rubber particles as well as the average particle size is crucial in the multiple crazing theory[2,8,10,11].

For the termination process to occur effectively, adequate adhesion of the dispersed phase to the matrix is required, because the rubber particles must be effective in the craze arresting process[2,8,12,13]. Thus a system possessing a strong interfacial adhesion between the two phases would support the multiple crazing deformation mechanism. The dimensions of the dispersed rubber phase particles also play an important role in the initiation and termination of the crazes. The optimum particle size is dependent on the crystallinity of the matrix and the rubber content. For polypropylene copolymers, an optimum particle size of 0.4 μm has been suggested. In figure 2.6 it is seen that the optimum particle size increases with rubber content and with increasing matrix crystallinity at a constant rubber content. The rubber particle size (d) is calculated using the equation shown below[8].

$$\mathrm{Log}_{10}(d_{optimum}) = 1.19 - \{4.51 * (1 - \text{rubber content}) * (1 - \text{matrix crystallinity})\}$$

where the rubber content is given by (χ%/100)
the matrix crystallinity is given by (χ%/100)
and $d_{optimum}$ is measured in (μm)

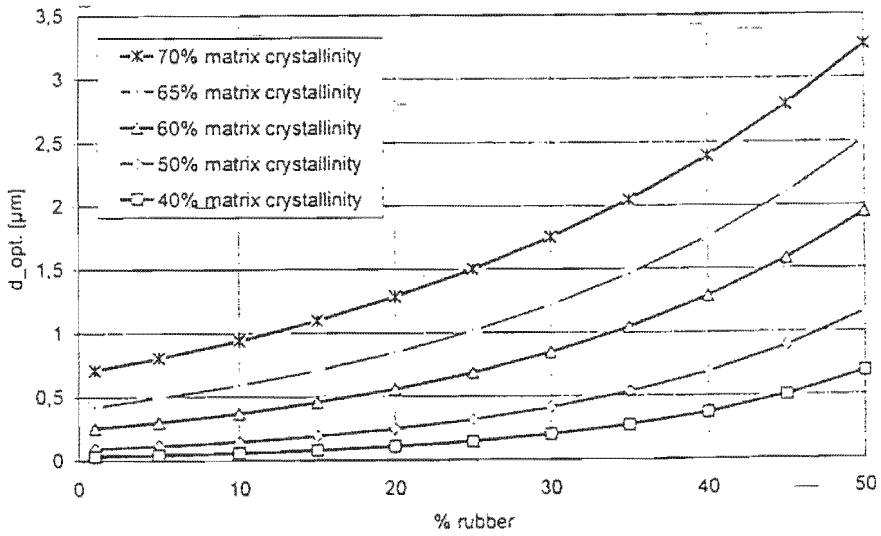

Figure 2.6: *Graph showing the effect of rubber content and crystallinity on* $d_{optimum}$ *[after ref. 8].*

2.3.2 Multiple Shear Yielding

An additional energy absorbing mechanism is the occurrence of shear yielding in the matrix. Unlike crazing or voiding, shear yielding is not a dilatational mechanism and may be assumed to occur at constant volume. For the shear yielding process to occur, the polymer must have a high crack initiation energy but low crack propagation energy. The decrease in crack propagation resistance energy is attributed to the inability of the material to relax and absorb a significant amount of fracture energy. High test temperatures or low strain rates favour the shear yielding mechanism of deformation as opposed to the multiple crazing mechanism in bulk polypropylene. However, the ability of sheet material to show chain flexibility and mobility even at low temperatures permit deformation via stretching and yielding rather than through crazing[8,14].

Localised yielding induces the formation of shear bands, which are deformation zones of high local strain at 45° to the applied stress direction. Their occurrence may also be attributed to a region of high stress concentration due to the presence of the elastomeric particles. A minimal

amount of stress whitening is associated with this deformation process, though permanent deformation occurs[2,8]. It has been suggested that the multiple crazing theory may occur simultaneously with shear yielding in elastomeric modified polymers. The interactions between the two mechanisms play a combined role in the reduction of crack size in the matrix thereby toughening the copolymer. The shear bands formed during deformation could act as barriers that limit the growth of the crazes since the shear bands are orientated at an angle to the direction of growth of the crazes. In addition, a reduction in the hydrostatic stresses required for craze growth occurs when the shear bands originate at the craze tip. These interactions arrest craze growth thereby reducing the craze size in the matrix and in so doing avert the probability of catastrophic failure[2].

The average interparticle distance as well as rubber particle size are important factors governing the toughening efficiency of the shear yielding mechanism. For matrices that deform by crazing the rubber particle size is important, whilst for matrices that deform by shear yielding the average interparticle distance is important. The propagation of the crack is dependent on the fracture ligament (plastic zone) of the crack. When the size of the fracture ligament is greater than the dimensions of the modifier particles, the particles cannot influence crack propagation and thus cannot contribute to increasing the toughness of the material. However, if the particle is large enough to hinder crack propagation, the material toughness is improved[2,8,15,16].

The following equation known as Wu's equation can be used to calculate the interparticle distance present between the dispersed rubber phase[8].

$$\text{Interparticle Distance} = d * k\left\{\left(\frac{\Pi}{6(V_r)}\right)^{\frac{1}{3}} - 1\right\} \qquad (\mu m)$$

where d is the particle size diameter (μm)

k is a geometric constant dependent on the crystal lattice type (no units)

and V_r is the particle volume fraction (no units)

The particle volume fraction (V_r) can be calculated by the following equation.

$$V_r = \left\{ \frac{W_r * \rho_m}{W_r * \rho_m + (1 - W_r)\rho_r} \right\} \quad \text{(no units)}$$

where W_r is the weight fraction of modifier particles (no units)

ρ_r is the modifier particle density (g/cm^3)

and ρ_m is the matrix density (g/cm^3)

2.3.3 Multiple Void Formation (Cavitation)

The concept of microvoid toughening in copolymers has also been proposed by a number of researchers[2,13,17]. Kim *et al* suggested that the deformation mechanism of voiding in tensile tests comprises of three stages, namely[6]:

1) Stress concentrations due to modifier particles

   During the initial stages of deformation, the inclusions (EPR modifier particles) act as stress concentrators and the stress field is distributed by the dispersed particles. Triaxial stresses develop in the rubber particles due to the effect of the stress concentration, providing adequate adhesion between the two phases exists. This leads to the dilation of the matrix. With increasing strain, the particles elongate with the matrix. Localised plastic deformation occurs within the ethylene propylene rubbery shell and weak shear bands are formed. The deformation processes are initiated in the rubber particles and not in the matrix or at the phase interfaces.

2) Void and shear band formation

   Due to the effect of stress concentrations, a higher hydrostatic stress, which constitutes between 60 – 70% of the applied load, builds up inside the particles. This leads to void formation through cavitation inside the plastically deformed EPR particles to relieve the imposed volume strain. These voids continue to grow in size with increasing

strain. The hydrostatic tension at any point inside the elastomeric inclusion can be given by:

$$S = \left(\frac{2}{3}\right)(\sigma_A)\left\{\frac{(1+\nu_0)(1-\nu)}{1+\left(\mu/\mu_0\right)(1-2\nu_0)}\right\}$$

where σ_A is the applied stress (MPa)

ν_0 is the Poisson ratio of the elastic inclusion (no units)

μ_0 is the shear modulus of the elastic inclusion (MPa)

ν is the Poisson ratio of the matrix (no units)

μ is the shear modulus of the matrix (MPa)

and S is the hydrostatic tension (MPa)

3) Shear yielding

Void formation due to cavitation and debonding locally relieves the triaxial stress state imposed on the dispersed particles, thereby lowering the yield strength. Cavitation of the rubber particles changes the stress distribution of the surrounding area causing a local decrease in the hydrostatic component of the stress and a corresponding sharp increase in the shear stress component. This change in the stress state facilitates the yielding of the matrix. Following the initiation of void formation, shear yielding is greatly enhanced in the parent polymer[6,15,18,19].

The cavitation of the rubber particles relieves the triaxial tension in the vicinity of the crack tip allowing the matrix to shear yield, thus absorbing energy and arresting crack propagation. Large modifier particles can contain several cavitation sites with the interface cavitation sites being more favourable than at the centre of the rubber sphere. The different sites of cavitation can be seen in figure 2.7 on the following page.

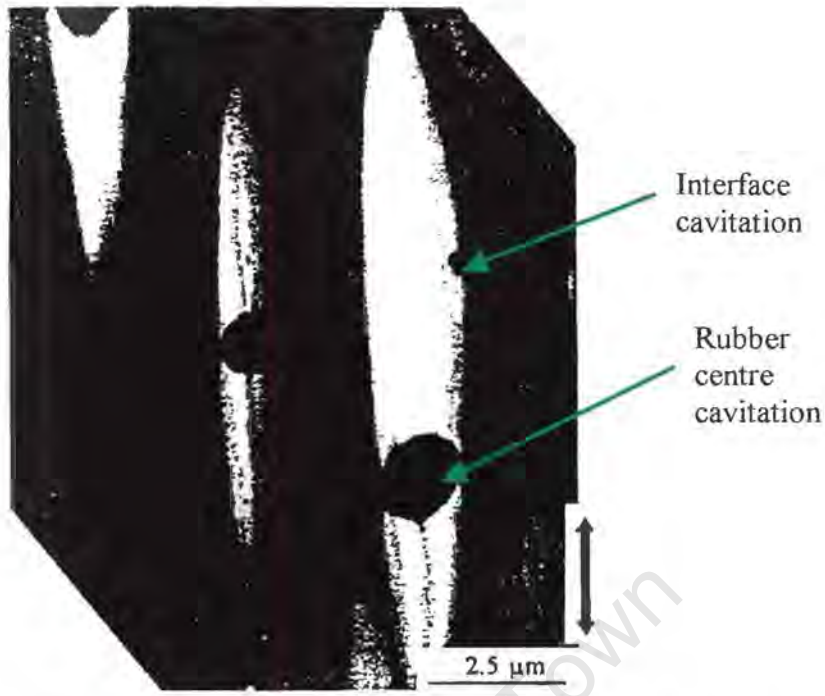

Figure 2.7: *Occurrence of cavitation within the modifier particles at different sites [after ref. 6].*

2.3.4 Damage Competition Theory

Essentially, the multiple crazing and shear yielding mechanisms are not mutually exclusive micro-mechanisms and therefore may occur within a copolymer as two coupled toughening mechanisms either sequentially or simultaneously. However, there exists a competition between them resulting in one of the mechanisms becoming the more dominant mode of deformation. This is commonly referred to as the damage competition theory.

Crazing in the matrix is initiated by chain scission. This is deduced by the presence of microvoids at the leading edge of the crazing zone. Once initiated, they are stabilised by entanglements and fibrillar polymer bridges or halted by modifier particles. In polymers with high entanglement densities, the applied load distribution occurs over various different entanglements and chains making high entanglement density an unsuitable environment for the craze initiation process. Therefore the stress required for craze initiation and growth increases with increasing matrix entanglement density. Since high entanglement densities hinder craze growth once initiated, it is a necessary

criterion for the modifier rubber particles to possess a molecular structure that has a high entanglement density to allow for craze termination[2,8,13,17].

A requirement for the occurrence of the shear yielding deformation mode is that the chains have sufficient mobility to allow for chain activity or movement. Thus, as the chain rigidity is lowered, so too is the initiation stress for shear yielding lowered, allowing yielding to occur. In summary, entanglement density is the primary factor controlling the intrinsic crazing behaviour whereas chain stiffness is the primary factor controlling the intrinsic yielding behaviour. Therefore crazing dominates the failure mechanism when the crazing stress is lower than the yield stress[8,13].

2.4 PRODUCTION OF POLYPROPYLENE IMPACT COPOLYMERS

The production process for polypropylene generally make use of the liquid monomer as the polymerization medium in order to maximise the rate of the polymerization reaction by providing a high monomer concentration. Processes using liquid monomer are often used to manufacture homopolymer polypropylene and random copolymers with less than 5% ethylene content. However, liquid phase processes are not well suited for the production of the rubber phase of impact-modified copolymers due to the high solubility of the rubber in the liquid monomer. Consequently a hybrid process is often made use of during the production of impact copolymers. The hybrid process consists of homopolymerization in the liquid phase followed by copolymerization in the gas phase. One reactor is used for the production of the polypropylene homopolymer and a second smaller reactor is used in series for the production of the ethylene-propylene rubber component of impact modified copolymers. This is a continuous and uninterrupted process[2].

The process shown in figure 2.8 is known as the BASF Gas – Phase process. In this process, the catalyst components and the monomer (liquid propylene) are fed into a loop reactor for homopolymerization through the bottom seal and into the top of each reactor. The product manufactured in the first reactor is the isotactic homopolymer polypropylene that forms the matrix of the ethylene-propylene copolymer. The molecular weight, molecular weight distribution of the polypropylene is primarily influenced by the choice as well as amount of catalyst employed and controlled by varying the reactor temperature and pressure. Hydrogen is added to the reactor for the termination of the polymer chain thus also controlling the molecular weight. The use of spherical form catalysts with a narrow particle size distribution, coupled with the high liquid velocities minimises reactor fouling. High isotacticity grades require a suitable catalyst, co catalyst and stereo-modifier. The process shown in figure 2.8 makes use of a PTK 4 high activity catalyst, which is suitable for a wide choice of products ranging from the high stiffness homopolymer to the high impact copolymers. Operating temperature conditions are typically in the range of 50°C to 90°C and pressures ranging from 35 bar to 50 bar are utilised. The polymerisation conditions are dependent and based on the grade of polymer being manufactured. The polymerisation reaction is exothermic and the reactor is cooled externally by cooling the gas above the power bed in the reactor[2,21].

Upon exiting the loop reactors, the polypropylene/propylene slurry is depressurised and flashed at a pressure that allows for the recycle of the vaporised monomer by condensation using a water-cooled condenser. The pressure must also be sufficient for the gas phase copolymerization. In addition to propylene and hydrogen, the feedstock consists of ethylene, which is fed into the secondary reactor. A fluidized bed gas phase reactor is used to produce ethylene-propylene rubber particles in the homopolymer produced from the first reactor thereby manufacturing impact copolymers. The ethylene and propylene react to form ethylene-propylene rubber (EPR), which is established as the dispersed phase incorporated in the polypropylene homopolymer matrix. Chain to chain linkage is achieved between the

dispersed phase and the matrix. The polymer exiting the polymerization section passes through a low pressure separator where the residual monomer is separated for recycling[2,8,20,21,22].

Twin screw extruders are used during the extrusion process to allow for a uniform distribution of the appropriate additives and stabilisers added to the polymer powder. Pelletisation of the polymer occurs with the aid of underwater die-face cutters. After the drying and classification procedure, the pellets are passed through a degassing unit to deodorise the pellets. The final manufactured polymer product is then stored in blending storage silos prior to being packaged and sold[8]. The various stages described during the manufacturing process of the copolymer product can be seen in a schematic diagram of the process in figure 2.8.

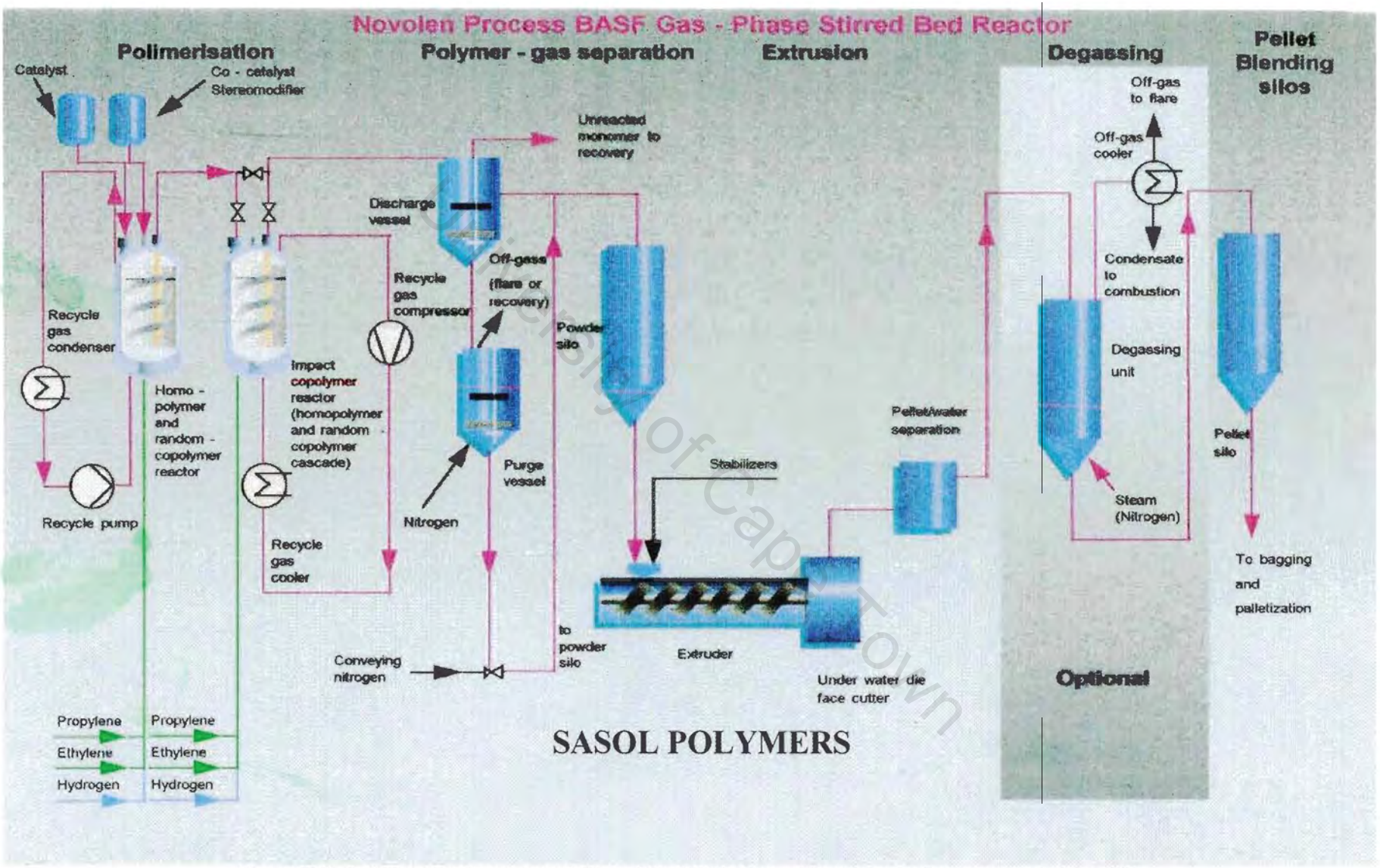

Figure 2.8: *A diagrammatic representation of the BASF Gas – Phase production process [after ref.8].*

2.5 MECHANICAL PROPERTIES

The rubber content of the poly (propylene-ethylene) impact copolymers primarily governs the mechanical properties of the final product. Several other parameters are involved too, but to a lesser extent[2]:

- Molecular weight, molecular weight distribution and isotacticity level of the PP homopolymer matrix and the EP rubber phase
- Ethylene/propylene ratio of the rubber phase
- Concentration of the crystalline PE sequences in the rubber phase
- Size and uniformity of dispersion of the rubber phase domains
- Melt viscosity ratio of the matrix and the rubber phase components

2.5.1 Instrumented Drop Weight Impact Testing

The impact performance of a material is assessed by means of a drop weight impact tester that can be instrumented to provide computerised information of the impact event. This type of test involves a striker which is a guided hemisperically tipped weight (tup) that is dropped under the influence of the gravitational force onto a specimen positioned over a circular opening. The striker is instrumented with a force transducer that permits a record of the force-time response continuously throughout the impact event. From this information, data such as the load/energy-deflection can be derived. The drop weight test imposes a biaxial stress state onto the specimen as opposed to the more severe triaxial stress state loading during an Izod test. Both qualitative and quantitative information can be derived from the load/energy versus deflection curves obtained during the impact test. Figure 2.9 is a schematic representation of the instrumentation of the drop weight test system[23].

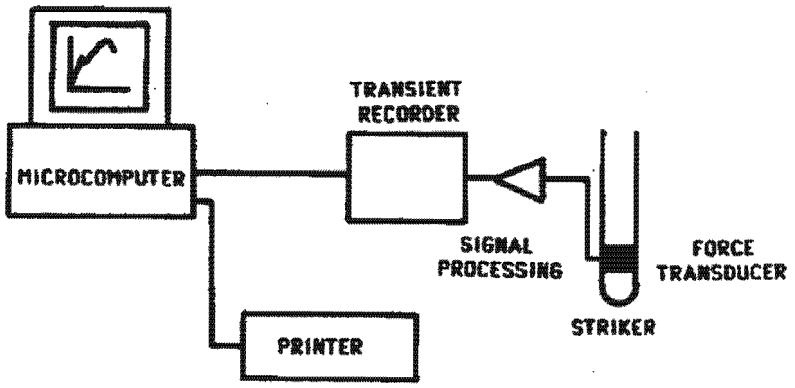

Figure 2.9: *Layout of the drop weight test instrumentation method [after ref. 23].*

The impact test results describe the complete impact event, including the initiation of failure, crack propagation and collapse of the specimen when sufficient damage is incurred by the specimen. The impact resistance of the tested material is evaluated in terms of the energy absorbed by the specimen during the impact process. However, the impact strength of a material is not a fundamental material property and is thus dependent upon specimen geometry, loading, test conditions and the particular test method employed.

The impact event involves high contact forces between the specimen plate and the tup occurring over a short duration of time, which varies typically between 2 to 30 milliseconds. The contact area on the specimen plate is dependent on the tup diameter. The fracture event consists of both the elastic and permanent plastic deformation.

Figure 2.10 below is a typical load versus displacement trace from an instrumented test. The figure also displays characteristic information that can be obtained such as yield load after which the specimen begins to plastically deform, the maximum load sustainable by the specimen, the failure point of the specimen as well as the corresponding deflections experienced by the specimen during the impact event. The maximum force is associated with a stage in the impact event at which the specimen has undergone sufficient damage to facilitate further penetration of the striker under reduced resistance. Thus, the large reductions in force thereafter are generally associated with considerable crack development.

The area under the load displacement curve represents the energy absorbed by the specimen. The energy absorbed by the specimen till the point of maximum loading (pre-maximum load energy) is known as the crack initiation energy and initiates the formation of cracks in the specimen. The post-maximum load energy is responsible for the propagation of the initiated crack and is thus known as crack propagation energy. This is the portion of plastic contribution to the total fracture energy and is strongly dependent on the rubber content of the copolymer. The plastic component usually constitutes approximately 70% of the final fracture energy and is primarily responsible for the continuous increase in fracture energy as the EPR content increases to a level limited by the deleterious effect on stiffness[23,24].

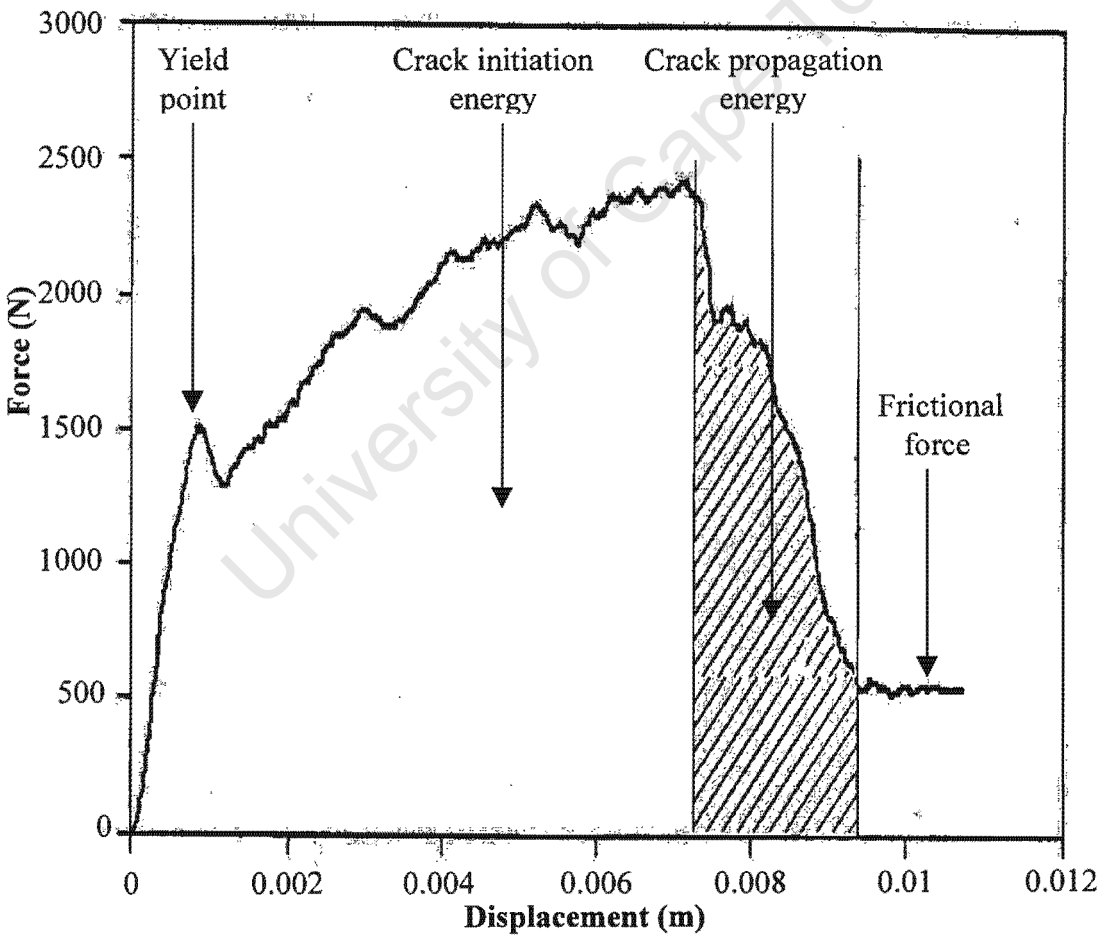

Figure 2.10: *Schematic showing a typical load versus displacement trace obtained from an instrumented impact test [after ref. 8].*

2.5.2 Impact Strength

Impact copolymers have characteristic properties as a result of their hetero-phasic nature but their impact strength is not a fundamental material property and is dependent on the test method employed, specimen geometry, test temperature and conditions used. The main end-use property of the copolymers is their low temperature impact strength. The introduction of the very low modulus elastomer in the polypropylene homopolymer matrix increases the impact strength of the material. This increase is a consequence of an improvement in the efficiency of the energy dissipation behaviour of the material, which is correlated to the structure and morphology of the copolymer. However, copolymerizing polypropylene with a rubbery elastomer also detrimentally affects other properties such as a lowering in the stiffness, hardness, and the tensile strength of the copolymer. Figure 2.11 illustrates the decrease in modulus that is observed in the ethylene-propylene copolymer as the rubber content present within a copolymer microstructure increases.

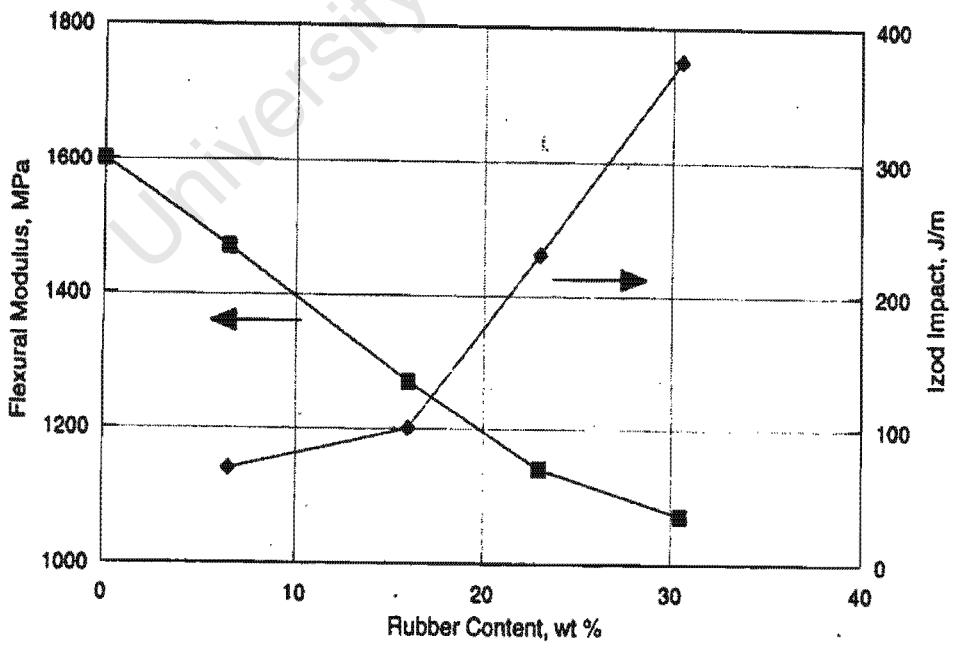

Figure 2.11: *Diagram showing the effect of the ethylene content in polypropylene on the end-use properties [after ref. 2].*

Other end-use properties such as the ultimate load bearing capacity and the scratch/mar resistance also suffer to allow for an enhancement in the impact resistance of impact copolymers. The factor governing the ideal compromise between the impact strength and stiffness is the degree of dispersion of the EPR component. The impact strength is related to the amount, particle size, composition and distribution of the rubbery phase within the matrix. The nature of the modifier determines the deformation behaviour of the copolymer and its ability to absorb the impact energy, whilst the particle size and spatial concentration define the possibility of initiating crazes and intercepting the fracture propagation path[2,25,26,27].

2.5.3 Tensile Strength

Investigations by Fernando and Williams using tensile tests to illustrate the toughness behaviour of polypropylene copolymers at sub-zero temperatures showed the results displayed in figure 2.12[4]. The results are obtained from tensile tests done at –60°C. The homopolymer fractured in a brittle manner at the test termination point as compared to the pronounced yielding accompanied by dense stress whitening at the ultimate tensile strength in the copolymer specimens. The ultimate tensile stress decreased with increasing ethylene content for the impact copolymers. What is also noticeable, is the decrease in the modulus of the copolymers compared to the homopolymer thus indicating that the stiffness of the polymer is negatively affected by the addition of the secondary phase ductile material due to a reduction in the crystallinity present in the copolymer and a limited degree of contribution through plasticization. The area under the curves shown in figure 2.12 is an indication of the toughness of the material being tested. Thus the copolymers show an increased toughness in comparison to the polypropylene homopolymer. The yield strain, however, remained constant at 3.2% and is independent of the ethylene content[4,18,28].

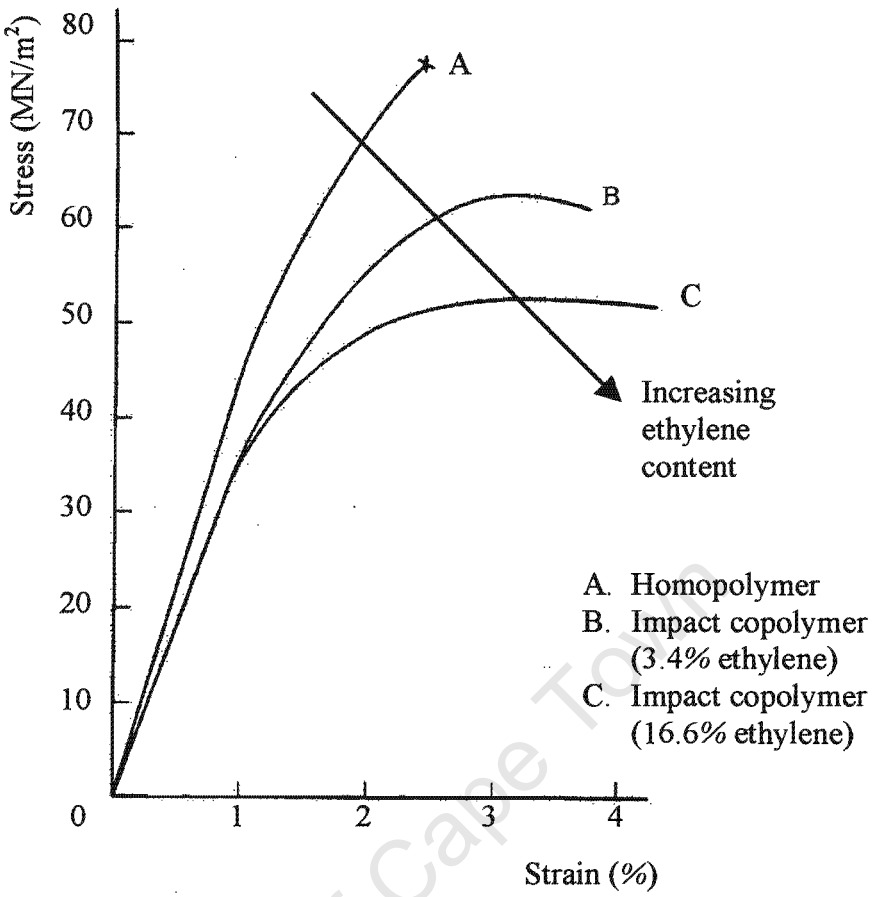

Figure 2.12: *Stress-strain curves indicating the property difference between the rubber modified polypropylene and the homopolymer [after ref. 4].*

2.5.4 Young's Modulus

The Young's modulus of the copolymer is dependent solely on the volume fraction of the rubber present in the polymer material. The relationship between the volume fraction of the secondary phase material and the resulting Young's modulus can, for example, be described by the Kernel equation for polypropylene as shown below[8].

$$E = E_M * \left\{ \frac{1 - 0.967(\chi)(1 + 0.879(\chi))}{1 + 0.829(\chi)} \right\}$$

where E is the Young's modulus of copolymer (MPa)

E_M is the Young's modulus of the matrix polymer (MPa)

and χ is the volume fraction of the modifier material (No units)

The Kernel equation does not have a variable to represent the rubber particle size and is therefore independent of that factor. Figure 2.13 is a graph showing the Young's modulus plotted against the volume fraction of the rubber in the copolymer. A linear relationship is observed between the two variables in which a constant decrease of the Young's modulus occurs as the volume fraction of the rubber increases. Thus the rubber content present in a copolymer should be limited by a compromise between the impact strength and modulus to allow for adequate polymer stiffness[8].

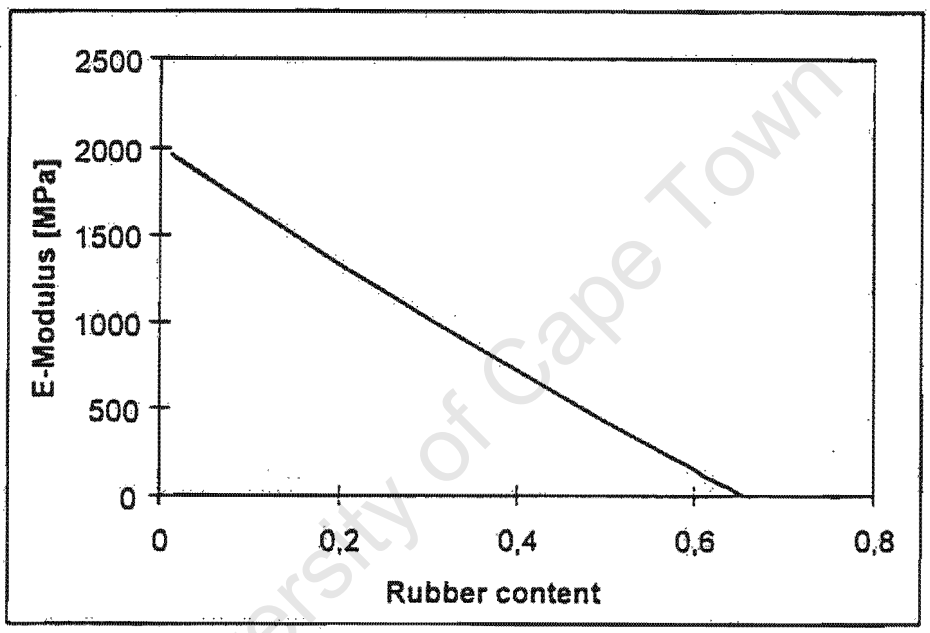

Figure 2.13: *Graph of Young's modulus as a function of the rubber content for PP/EPR system [after ref. 8].*

2.5.5 The Ductile Ratio

A parameter known as the Ductile Ratio (D.R.) is used to characterise the plastic yielding and elastic deformation of polymers. The ductile ratio is defined as the contribution or relative percentage of energy that is absorbed in deforming the polymer specimen plastically with regard to impact energy, which is the total energy absorbed by the specimen. The ductile ratio is used as an indication or measure of the ductility of the polymeric specimen. It is not an intrinsic material parameter and can therefore be used only to rank the

ductility of polymeric materials at the specific test conditions such as impact velocity, test temperature and the test specimen geometry[29]. It is calculated by the equation:

$$\text{Ductile Ratio} = \left\{\frac{(U_t - U_m)}{U_t}\right\} \qquad \text{(no units)}$$

where U_t is the total impact energy (J)

U_m is the initiation elastic deformation energy (J)

and $(U_t - U_m)$ is the energy of plastic deformation after yield (J)

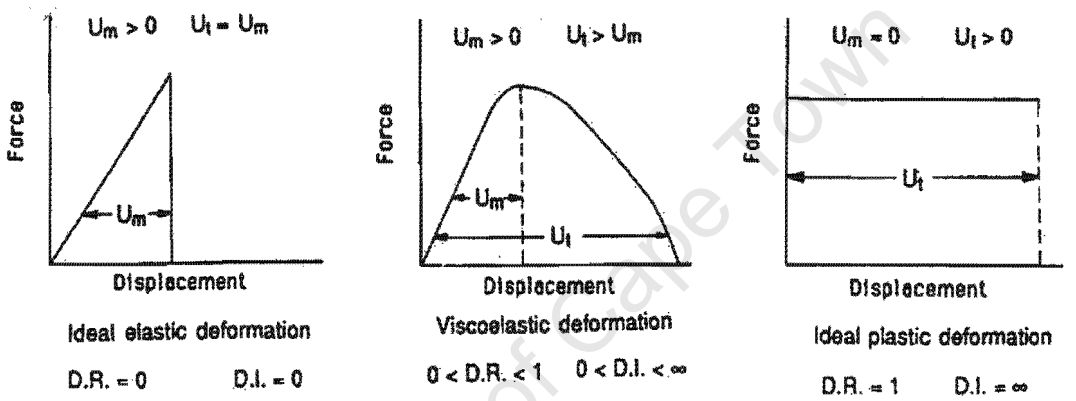

Figure 2.14: *Illustration of the ductile ratios for various types of materials [after ref. 29].*

Figure 2.14 shows that an ideally brittle material that does not exhibit any plasticity and has a D.R. value of zero because U_t is equal to U_m. Similarly, ideal ductile materials exhibit minimal or no elasticity thus making U_m almost equal to zero and the D.R. value tends to one. Viscoelastic materials show values of D.R. ranging from zero to one. Thus the energy supplied during crack propagation in the impact event is a measure of the ductility of a material[29,30].

2.6 THE GLASS TRANSITION TEMPERATURE

The glass transition temperature (T_g) is defined by a change in the expansion coefficient of the polymer material upon cooling from the liquid melt. It is an important parameter relative to the in-service applications of the polymer and

is indicated by a discontinuity in the rate of change of the specific volume with respect to temperature. Crystalline polymers display a discontinuous specific volume change at the melting temperature (T_m) whereas amorphous polymers are show a continuous behaviour past the T_m and a decrease in slope only at the T_g. Intermediate polymers show a discontinuity at both the melting and the glass transition temperature. This effect of specific volume discontinuity arises due to the onset of enhanced chain mobility as the temperature rises above the glass transition temperature. Thus the polymers experience a transition from the rubbery to a rigid state at the glass transition temperature[3,31]. Block copolymers consist of sequences of two different polymers and form a phase separated polymer system. Thus two different glass transition temperatures are observed and can be ascribed to the EPR and polypropylene components, respectively. The compatibility of the different component systems of an impact copolymer determines the difference in the T_g of the components.

Ethylene-propylene rubber copolymers exhibit transition temperatures identical to the pure components indicating total incompatibility and immiscibility between the polypropylene and the EPR phases. This is also evident in the microstructure of the impact copolymers as two distinct phases are observed. Figure 2.15 illustrates this concept by the results obtained from the dynamic mechanical analysis (DMA) of EPR toughened polypropylene. Separately detected tan δ peaks of polypropylene and EPR glass transition temperatures indicate that phase separation does take place during copolymerization.

Phase separation is essential for increasing the toughness of the rubber-modified systems as a rubber that dissolves in the matrix acts only as a plasticizer reducing the glass transition temperature as well as the stiffness of the matrix with only a moderate increase in its toughness[7,8]. However, the solubility parameters of the two components must be similar to achieve good adhesion properties between the two phases[2,7,31]. The mechanical response

of the elastomeric materials is greatly dependent on the difference between the glass transition temperature and the testing temperature[32].

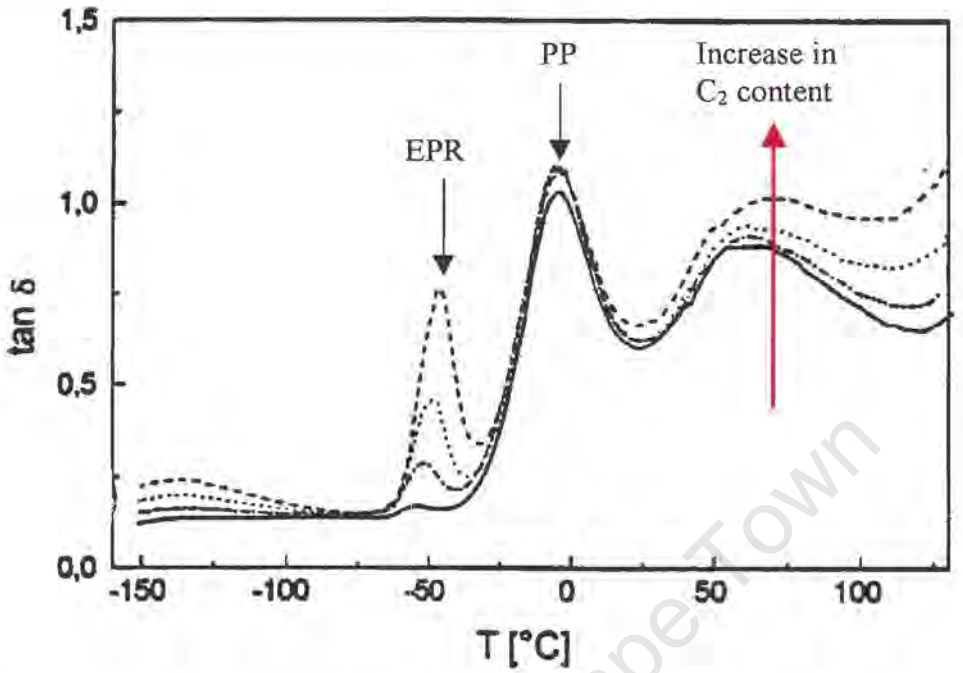

Figure 2.15: *Graph of the loss factor tan δ as a function of temperature for various copolymers. The arrows depict the glass transition temperatures of the EPR and PP phase [after ref. 7].*

The T_g of the EPR phase is crucial to impact enhancement. The viscoelastic response of the rubber-like nature of the EPR phase is responsible for increased impact strength. Thus there is a lower temperature limit below which the rubber-toughened system becomes ineffective. This is due to the rubber behaving essentially in a glassy, rigid and brittle manner due to insufficient molecular motion thereby restricting the toughening contribution to processes such as crack pinning due to the dispersed particles present in the matrix. These processes absorb much less energy in comparison to the shear yielding and multiple crazing mechanisms. This is due to the EPR phase undergoing a transition causing it to behave in a brittle manner[2].

2.7 THE BRITTLE-TO-DUCTILE TRANSITION (BDT)

The principle criterion, in the brittle-to-ductile transition of polymers, is a change from a brittle failure to a ductile one when the yield stress drops below the fracture stress. It is direct result of the existing competition between the different failure micro-mechanisms within the material as well as the yield and fracture stress. The polymer failure mode changes from brittle to ductile as the ambient temperature increases primarily due to the fracture stress being higher than the yield stress. Thus the BDT is defined as the onset of ductility and the energy supplied during crack propagation is a measure of ductility. The crack propagation energy is dependent on the crack propagation displacement and on the load experienced during crack propagation[33,34].

The polypropylene homopolymer and rubber modified polypropylene show a clear and sharp BDT temperature. Polypropylene copolymers show much lower transition temperature in comparison to the conventional polypropylene homopolymers. Figure 2.16 shows a representative graph of a polymer undergoing the brittle-ductile transition. The three regimes shown in the figure correspond to the brittle (1), brittle-to-ductile (2) and ductile behaviour (3) of the polymer while X denotes a parameter that influences the impact toughness of the polymer such as the temperature, rubber content, interparticle distance or even the particle size. X_c would therefore be the critical value at which the transition in toughness occurs[35].

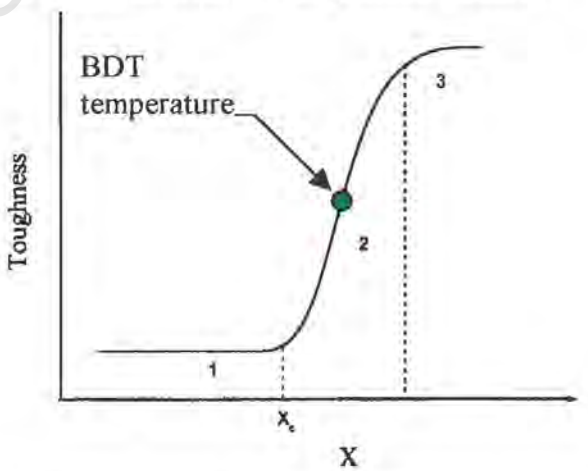

Figure 2.16: *Diagrammatic representation of the transition in a polymer with respect to its toughness [after ref. 35].*

The BDT temperature can be defined to be the temperature reading at the point of inflection in the impact strength temperature curve in regime 2 as shown in figure 2.16. The BDT occurs within a temperature band around the brittle-to-ductile transition temperature. The addition of a low modulus elastomer to polypropylene shifts the BDT to lower temperatures, whilst an increase in the crystallinity of polypropylene causes a shift in the BDT to higher temperatures. Crystallinity effectively increases the yield stress whilst simultaneously decreasing fracture strain thereby promoting brittle fracture.

Since the ductility and brittle strength of polymers are both temperature dependent, the fracture resistance is also temperature sensitive. A higher temperature provides a more suitable condition for molecular relaxation, thereby promoting the impact resistance of the polymer. The BDT temperature for a poly (propylene-ethylene) copolymer shows a dependence on the composition of the material and external variables such as temperature and strain rate[16,18,35,36]. The test procedures used are in accordance with the ASTM standards for determining the BDT temperature of plastics[(a)].

2.8 THE EFFECT OF ELASTOMER CONTENT ON THE BDT TEMPERATURE

Drop weight impact tests performed on impact modified polypropylene containing an increasing % of ethylene-propylene-diene elastomer (EPDM) indicate that the modified polypropylene shows an inadequate impact performance at cryogenic temperatures until a critical amount of impact modifier is reached within the modified polypropylene system. The effect of increasing the EPDM content within the copolymer composition is comparable to increasing the test temperature at which the impact event characteristics are captured. In figure 2.17, an increase in the modifier content shifts the transition to lower temperatures thereby extending the scope of use to encapsulate cryogenic temperature applications[30,35,37]. The plasticizing effect induced in the polypropylene copolymer upon the addition of up to 10%

(a) ASTM D746 – Brittleness temperature of plastics and elastomers by impact
ASTM D1790 – Brittleness temperature of plastic sheeting by impact

ethylene suppresses the occurrence of brittle-to-ductile transition temperature to lower temperatures by decreasing the copolymer yield strength[38].

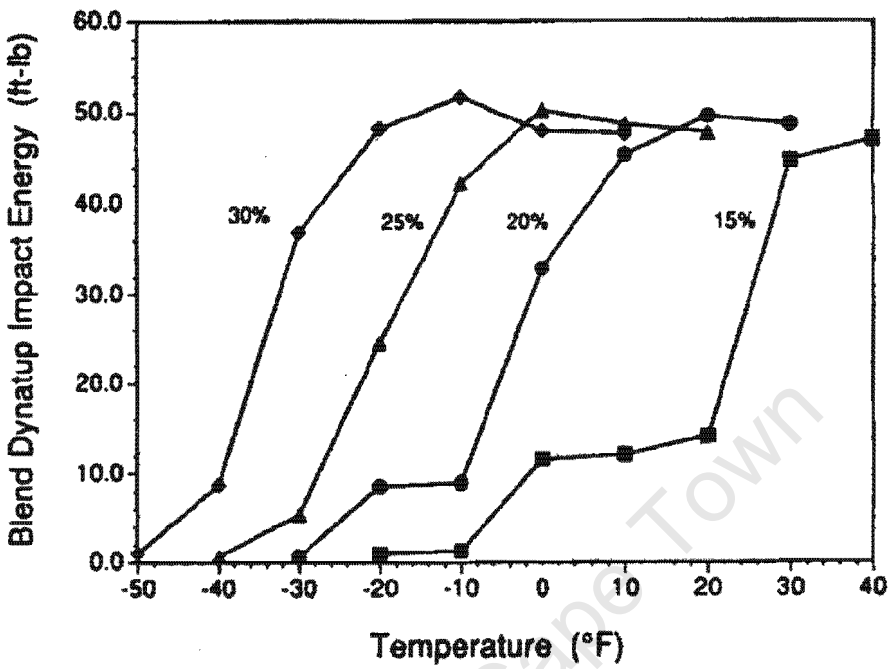

Figure 2.17: *Brittle-ductile transition temperatures of impact modified PP with increasing % elastomer content [after ref. 30].*

2.9 THE EFFECT OF RUBBER CONTENT ON SPHERULITE MORPHOLOGY

Spherulites consist of skeletal crystalline lamellae radiating outwards from a common centre. These lamellae fan out and branch out in a spherical entity. Generally, the addition of a rubber elastomer in a polypropylene matrix results in a change in the polypropylene spherulite morphology. The spherulites lose their form and tend to shrink in size and as the rubber content in the copolymer is increased resulting in smaller spherulites possessing irregular shapes. The dimension changes or defects in the spherulite morphology could be a consequence of the swift nucleation rate of the polypropylene spherulites in the presence of the rubber phase. However, the growth rate of the spherulites is not deeply affected by the secondary phase. This induced change in the spherulites increases the fracture resistance of polypropylene

which forms a inverse relationship between impact resistance and spherulite size and number[13,27,37].

2.10 CONSEQUENCE OF ELASTOMERIC CHARACTERISTICS ON PROPERTIES

Impact enhancement is dependent on several factors concerning the ethylene-propylene rubber modifier.

- *Amount of EPR added to the impact copolymer system*

Generally impact or hetero-phasic copolymers contain up to 40% ethylene-propylene intimately dispersed within the polypropylene matrix. The EPR particle itself consists of 50% to 60% ethylene. Therefore approximately 20% ethylene is present in the total final product. It is important to note that an increase in the EPR content affects only the degree of occurrence or the density of the rubber particles in the matrix and not the shape or size[2,8].

- *EPR particle size and distribution*

Optimum particle sizes vary according to the type and chemical structure of the matrix polymer and the secondary rubber phase incorporated during copolymerization. The particle size determines the number and interspacing of the particles for a particular concentration present in a system. The impact behaviour is influenced by the EPR size principally through the effect of initiation and termination of crazing and shear yielding. The molecular weight of the EPR phase controls the size of the rubber particles in the matrix. A critical particle size of 0.4 μm for PP/EPR systems is found to yield optimum toughness. Obtaining the correct melt phase viscosity ratio prevents agglomeration of the rubber particles. Figure 2.18 shows the effect that the rubber phase viscosity has on impact for a constant matrix viscosity[2].

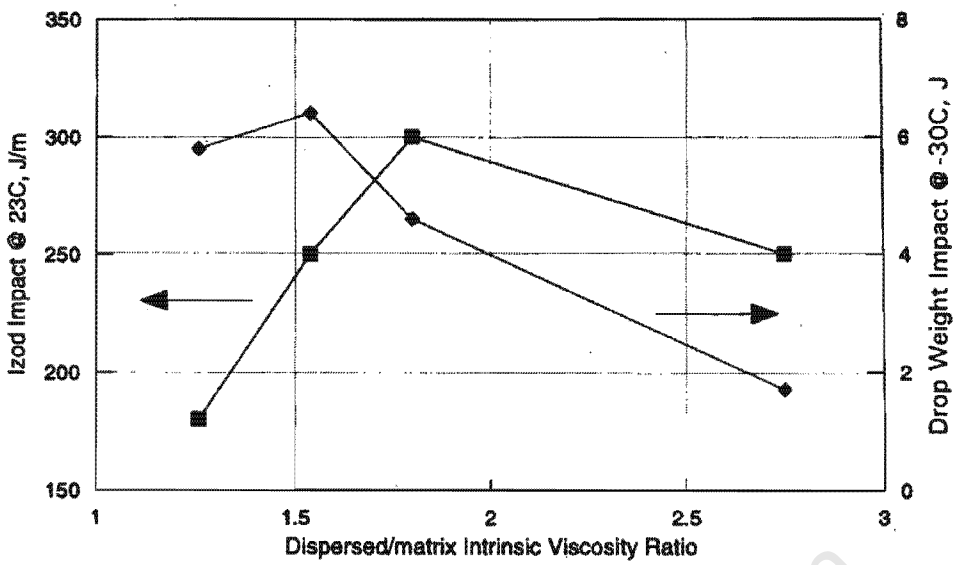

Figure 2.18: *Effect of EPR viscosity on the impact behaviour of hetero-phasic copolymer [after ref. 2].*

The degree of dispersion of EPR is also affected by the melt phase viscosity ratio i.e. the viscosity of the dispersed phase/viscosity of the matrix. Increasing the melt phase viscosity ratio by decreasing the matrix viscosity induces a coarser distribution of the EPR phase. This is a direct result of the inability of the matrix to transfer shear stress to the elastomer phase and break it apart into smaller particles. However the EPR mode of dispersion is independent of the EPR microstructure[2,7].

- *T_g of EPR and chemical affinity for the polypropylene matrix*

Interfacial adhesion can be promoted by selecting components with similar solubility parameters. Grafting agents can be used to assist in the adhesion between the two phases. The ethylene (C_2) and propylene (C_3) content of the EPR also affects the blend. At high C_3 contents, the T_g of the EPR phase increases and the impact strength is limited. The polypropylene crystallinity in the EPR reduces shrinkage stresses in the polypropylene matrix. In addition, the interphase between the matrix and modifier particles is indistinct. As the C_2 comonomer content increases, the polypropylene crystallinity decreases and the T_g begins to drop. However, a decrease in the tensile strength is observed. Further increases of the C_2 levels, typically above 50%, introduce polyethylene crystallinity within the rubber phase causing the rubber particle

to shrink more during cooling thereby reducing a build-up of stress in the matrix. Thus impact resistance reaches a maximum. However interfacial adhesion suffers as even more C_2 is introduced into the modifier particles. This has a negative effect on the impact behaviour since the rubber particles become stiffer. An optimum concentration of between 45 to 60 mole % of C_2 is found in the EPR. Thus the dispersed elastomer phase is able to maintain phase separation due to adequate immiscibility with the matrix and yet provide strong adhesion between the two phases[2,8].

2.11 INFLUENCE OF MATRIX LIGAMENT THICKNESS AND PARTICLE SIZE

The matrix ligament thickness (ID) is defined as the nearest distance of the matrix between two neighbouring rubber particles and can been calculated by the equation in section 2.3.2. The average ID increases with increasing particle size and particles size distribution at constant volume fraction. As the particle volume fraction is increased, the relationship between the average ID and particle size distribution becomes more sensitive. Figure 2.19 shows the concept of matrix ligament thickness and the stress interaction between adjacent rubber particles.

For every system, there exists a critical ligament thickness (ID_C) at which point the system will undergo a brittle-to-ductile transition. The ID_C is independent of particle volume fraction, particle size and is a characteristic of only the matrix for a given mode, temperature and rate of deformation. The ID_C increases substantially as the testing temperature increases to the T_g of the material and thereafter continues to increase with increasing test temperature. The ID_C value should therefore be reduced to ensure toughening in the copolymer system in a low temperature environment. Strain rates and ID_C values have an inverse relationship between them indicating that the ID_C value increases with an accompanied decrease in the applied deformation

rate. The ID_C value is also strongly dependent on the testing method employed to induce deformation[13].

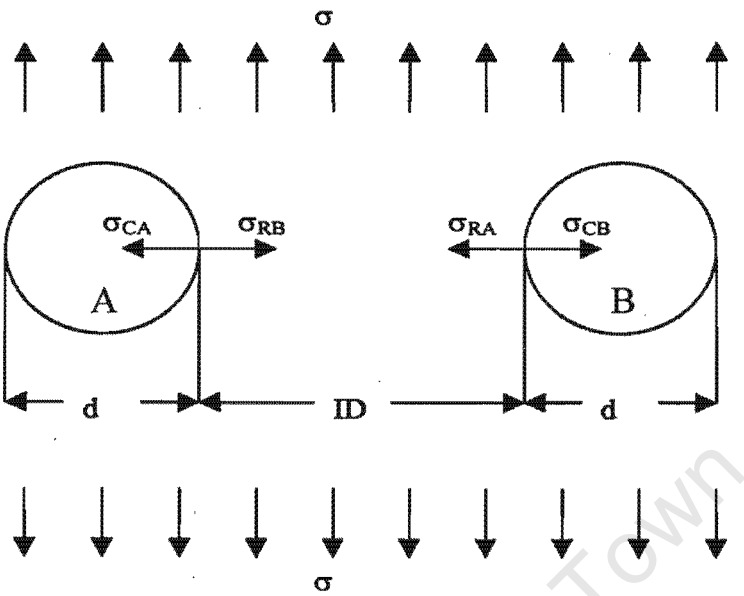

Figure 2.19: *Diagram of the stress interaction that occurs between the rubber particles. σ_C and σ_R are the compressive stresses imposed by the external load onto the particles and the matrix respectively [after ref. 13].*

If the concentration of the modifier particles is sufficiently large due to an increasing volume fraction, the adjacent particles A and B are positioned closer together thus reducing the ID. The compressive stresses σ_{CA} and σ_{CB} exerted on the particles under the action of the external load begin to overlap. Thus the compressive stresses imposed on the matrix surrounding the individual particles is reduced to $\sigma_{CA} - \sigma_{RB}$ and $\sigma_{CB} - \sigma_{RA}$ respectively, causing the copolymer to behave in a tough manner when the average ligament thickness, ID, of the system is lower than its critical matrix ligament thickness, ID_C. However, if the ID is much greater than the ID_C, there will be a low concentration of rubber particles in the system. The imposed external stress will then be borne mainly by the matrix, which renders the rubber toughening effectively insignificant. Thus the copolymer would be brittle[8,13,39].

Therefore, a greater number of matrix ligaments thinner than the critical ligament thickness in a system is a key factor for toughening by interparticle yielding. A value of 1.5 μm was found to represent the ID_C in polypropylene

systems. The critical rubber content within a system induces a transition from the brittle to the tough and ductile type behaviour as shown in figure 2.20 below.

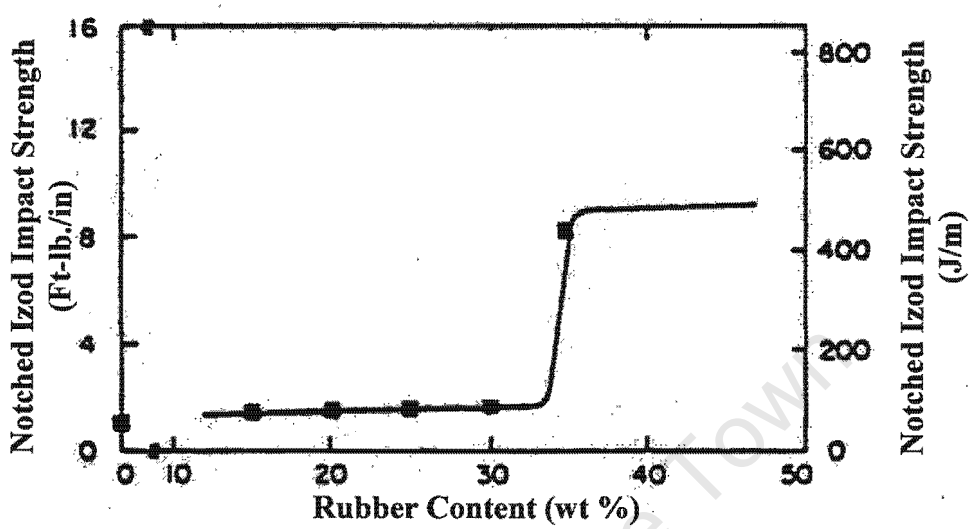

Figure 2.20: *Diagram showing the occurrence of BDT at a critical rubber content [after ref. 8].*

At particular conditions of temperature, modifier particle size and testing method employed, the matrix ligament thickness becomes thinner as the rubber content in a modified polypropylene system increases. The average matrix ligament continues to thin with higher weight percentages of rubber until it falls below the IDc value of that system leading to a transition in the impact strength of the material thus introducing the concept of critical rubber content[8].

2.12 THE MELT PROCESSING TEMPERATURE

An excessively high processing temperature leads to a significant degree of degradation in the homopolymer with a deterioration in its mechanical properties through an increase in brittleness. Moulding conditions such as barrel hold time, melt and mould temperature affect the properties of the copolymer by inducing changes in the rubber particle size. An increase in the melt temperature results in coalescence and growth of the rubber phase

leading to a larger average elastomer particle diameter. Increases in the melt temperature also reduces the nucleation of spherulites. However, the changes in the crystallinity, molecular weight and macro-morphology of the copolymer due to modifications in the moulding parameters are not very significant. Although the skin-core macrostructure formed during injection moulding is not altered, the thickness of the skin layer decreases as the melt temperature is increased[2,16,27].

2.13 THE MELT FLOW INDEX (MFI)

The melt flow index a measure of the flow rate in g/10min of polymer flowing through a die at a given temperature and dead weight on a piston. For polypropylene, test temperature conditions of 230°C and a load of 2.16 kg are used. The melt flow index is inversely related to the molecular weight (M_w) of polymer. More specifically, it is known that there exists an inverse log-linear relationship between molecular weight and MFI[40]. Thus to understand the influence of MFI on the properties of the copolymers, one can look at the influence of molecular weight and relate it back to the MFI of the copolymer.

Molecular weight is also important in terms of the material's response to an impact event. Low weight-average molecular weight samples have a brittle behaviour whereas a higher M_w of the same sample would be comparatively ductile. This is a result of an increase in the fracture stress of the material thus allowing it to yield before failure and absorb more impact energy leading to ductile failure. Also, craze nucleation is enhanced in the material within amorphous interlayers primarily due to a lower degree of crystallinity as the M_w increases. The critical fibril length before the breakdown of the crazes is also extended as the M_w increases.

The peak force experienced by a copolymer also increases as its M_w increases since there exists a greater amount of entanglements between the crystalline blocks in the craze fibrils allowing a higher external load to be

imposed onto the fibrils. Thus, increasing the M_w of a sample would effectively lower the brittle-to-ductile temperature. However, the effect of the rubber phase molecular weight on impact strength is small[33]. Figure 2.21 shows the influence of the melt flow index of the matrix on the brittle-to-ductile transition temperature of a copolymer containing 15% by volume EPDM. The notched Izod impact test was used to determine the transition temperatures.

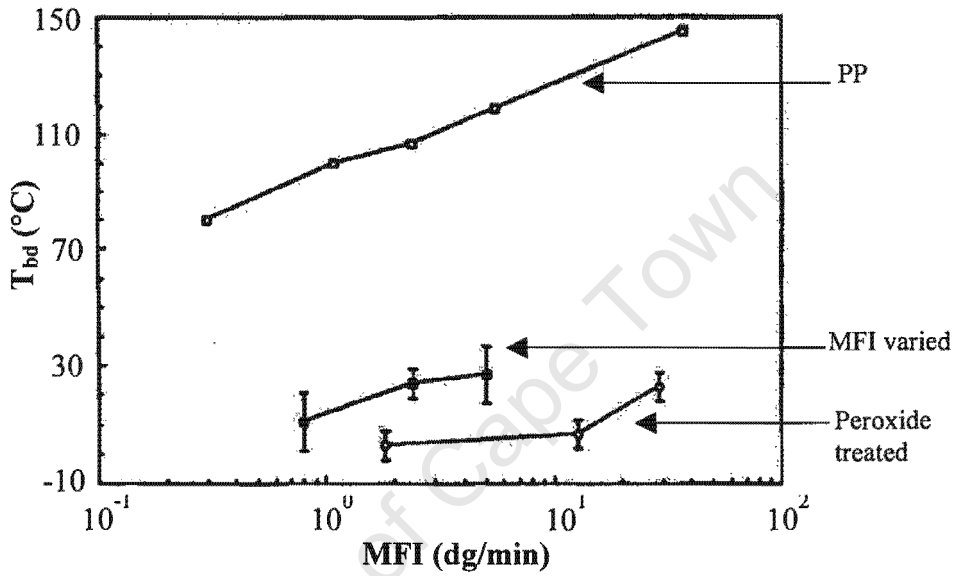

Figure 2.21: *Graph of various polypropylenes showing the effect of MFI on the brittle-to-ductile transition temperature [after ref. 33].*

These results show an associated increase in the BDT temperature with an increase in the melt flow index of the specimens. This effect is attributed to a decrease in the fracture stress experienced by the specimen as their melt flow index rises which would cause the specimens to fail prematurely below their yield stress as is characteristic of brittle failure. The M_w of the matrix also shifts critical rubber content required for ductile behaviour to lower values[33,37,41].

2.14 THE EFFECT OF CRYSTALLINITY ON THE BDT TEMPERATURE

Polypropylene with a high matrix crystallinity shows a low degree of ductility, which is a consequence of a high yield stress and decreased fracture strain. The influence of matrix crystallinity on the yield strength of the copolymer can be seen in figure 2.22 at varying rubber contents. There exists a direct relationship between polymer crystallinity and yield stress as shown in figure 2.22. However, the figure also shows that the yield stress decreases as the rubber content within the copolymer is increased at constant matrix crystallinity.

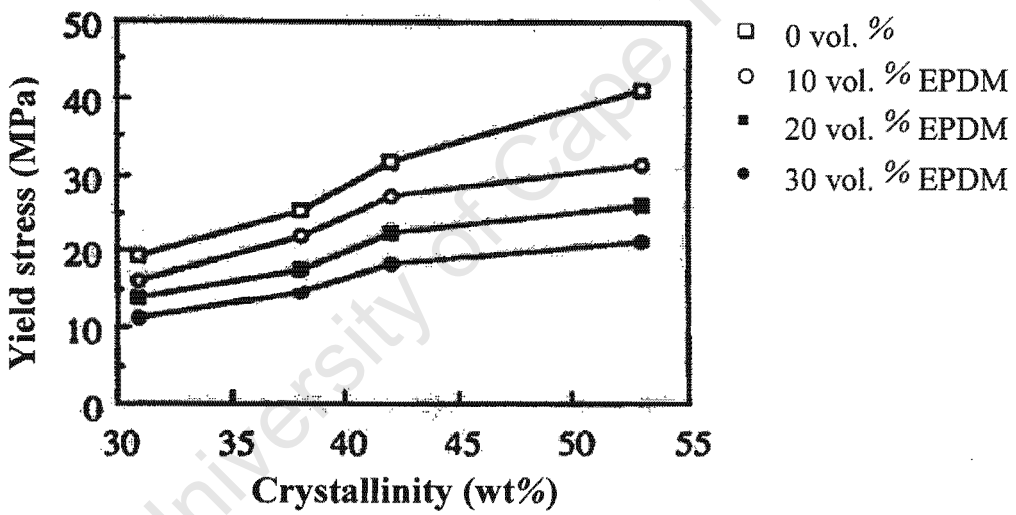

Figure 2.22: *Graph of the yield stress of the PP-EPDM copolymers as a function of the polypropylene matrix crystallinity [after ref. 34].*

The brittle-to-ductile transition temperature can be lowered appreciably by lowering the crystallinity of the copolymer since the yield stress of that copolymer would drop below the fracture stress inducing a ductile response from the copolymer during an impact event. This can be seen in the results shown in figure 2.23. The EPDM specimens maintained a constant particle size of about 0.4 μm whilst increasing the rubber content to the percentage level as indicated by the legends.

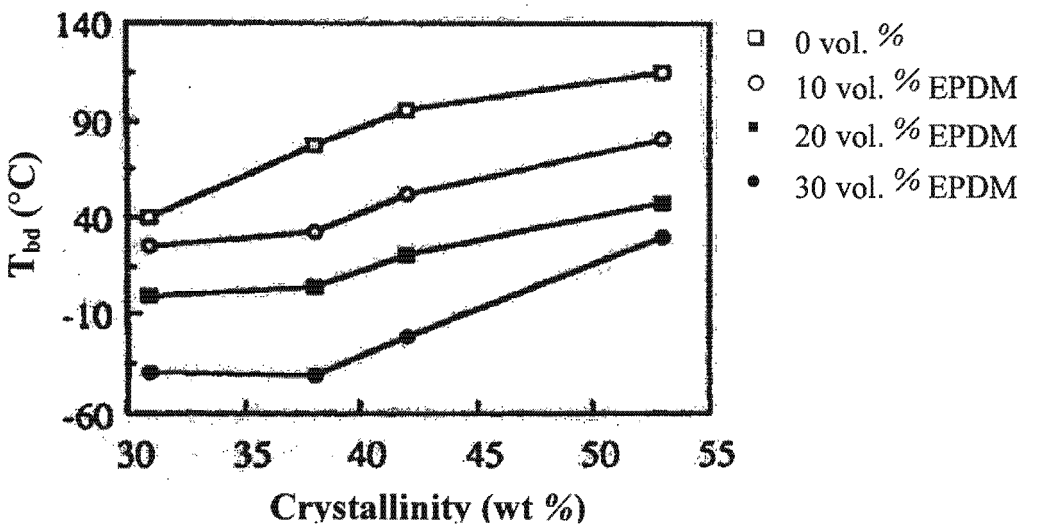

Figure 2.23: *Brittle-ductile transition temperature vs. matrix crystallinity [after ref. 34].*

The strength varies inversely with crystallinity, since crystallinity introduces brittleness in the material via a localised action of applied stress due to the stress concentration effect of the crystallites. The crystallites also reduce the action of the energy dissipative micro-mechanisms of the polymer matrix. The crystallinity of the polypropylene matrix phase is noticeably suppressed by the presence of the secondary EPR phase suggesting an interference between the crystallization process of the ethylenic EPR sequences and the polypropylene. It is hypothesised that the crystalline domains of the ethylenic sequences are entrapped within interlamellar amorphous regions of the polypropylene phase hindering the polypropylene crystal growth whilst increasing its thickness, thus lowering the crystallinity of the copolymer[8,27,42].

CHAPTER 3

CRYOGENIC APPARATUS DESIGN

3.1 DESIGN STATEMENT DEFINITION

Design a cooling rig capable of cooling the copolymer specimens clamped within the in-house built drop weight impact tester to any specific cryogenic temperature ranging from 40°C to -50°C. Due to the nature of the cooling requirements, the cooling rig should be incorporated onto the existing in-house built impact tester.

3.2 CONCEPT FORMATION OF THE COOLING RIG

Three different methods of cooling the drop weight impact specimens were investigated. These are reviewed in terms of their method of operation in the sub-sections that follow. Based on the advantages and disadvantages of the various cooling designs, the most viable design will be selected. Factors such as the ease of manufacture and operation are also considered.

3.2.1 Design A: Vapour Cooling System

The schematic shown in figure 3.1 is a possible design solution of the cooling rig required. The operational mode of the vapour cooler system is as follows. The compressed nitrogen gas tank acts as a storage unit containing nitrogen at room temperature. Upon operation of this system, the nitrogen gas is released from the storage unit via the regulator placed onto the tank. The nitrogen gas flows through a pipe that is tightly secured to a hollow copper tube.

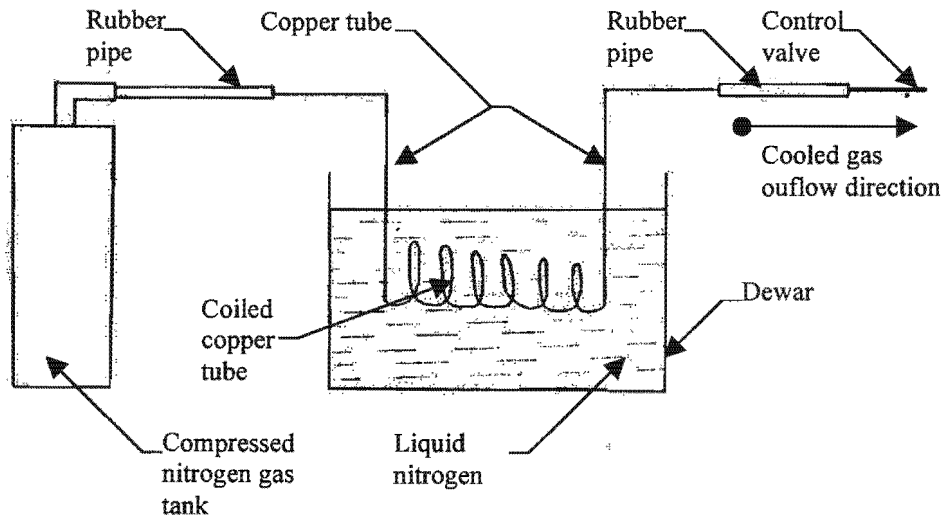

Figure 3.1: *Schematic diagram of the vapour cooling system*

The copper tube is immersed into a tank containing liquid nitrogen. Thus, the nitrogen gas is cooled as it passes through the copper tube positioned inside the liquid nitrogen tank. Heat dissipation or transfer from the nitrogen gas to the liquid nitrogen is the crucial step in this system. To improve the efficiency of heat transfer, the copper tube should be mechanically coiled to allow for a longer contact time period between the nitrogen gas in the copper tube and the liquid nitrogen in the tank.

The cooled nitrogen gas then flows out of the tank and back into a flexible rubber pipe. The pipe is required to have a very low glass transition temperature, typically lower than -150°C, to maintain flexibility at cryogenic temperatures. It is vital that appropriate steps be taken to ensure a good degree of insulation in this section of the system thus minimising the temperature rise of the cooled nitrogen gas. The pipe is directed towards the clamped specimen allowing the cooled nitrogen gas to make direct contact with the specimen. The gas is directed onto the specimen until it reaches the desired testing temperature. The specimen temperature is to be measured by means of a thermocouple located onto the specimen. The test commences upon achieving the desired specimen temperature by triggering the release of the impactor by a computer activated solenoid. The set-up of this system allows continuous cooling of the specimen even whilst the impact event occurs. The outflow of the cooled gas onto the specimen is controlled by

means of a control valve attached to the open end of the pipe. However, the nature of the design requires that the nitrogen gas be periodically replaced and particular attention be given to the insulation of the pipes. Another factor that may interfere with the impact results is the condensate formed on the specimen surface which may react with certain types of polymers.

3.2.2 Design B: Coiled Cooling System

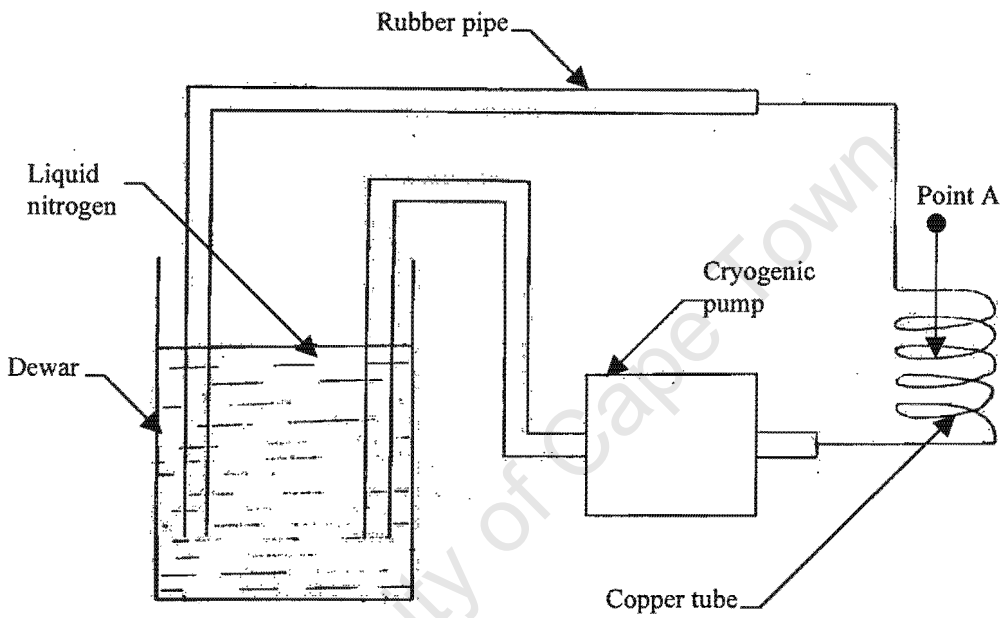

Figure 3.2: *Diagrammatic representation of the coiled cooling system*

The coiled cooling system utilises the flow of liquid nitrogen. The liquid nitrogen is stored in a dewar and is pumped into a flexible pipe by means of a cryogenic pump. The pump should be capable of operation at cryogenic temperatures and be able to pump cryogenic fluid. The pumped liquid nitrogen passes through a hollow copper tube that is attached to the outflow section of the cryogenic pump. The copper tube is coiled in order to enhance the effectiveness of this design. The polymer specimen is positioned within the circumference of the copper coils (point A), allowing the system to cool the specimen irrespective of the impacting procedure. The impact specimens are usually between 2 to 5 mm in thickness whilst the clamping plates generally measure a length of 50 mm. The coiled copper section should therefore measure a vertical length of approximately 70-100 mm. The diameter of the

coils is dependent on the geometry of the clamping platens as the coils are to be positioned around the specimen clamping plates of the impact tester. The design of the coiled cooling system prevents direct contact between the polymer specimen and the copper coils. Air is a poor conductor of heat, rendering the cooling design less efficient and thus requiring an added construction of an environmental chamber.

The temperature of the specimen can be regulated by means of an electrical heat source located within close proximity to the specimen. Increasing the temperature of the heat source would increase the temperature of the specimen, thereby providing a method of controlling the specimen temperature. The liquid nitrogen is pumped back into the dewar after passing through the copper coils allowing for a continuous flow cycle.

3.2.3 Design C: Cooling Disk System

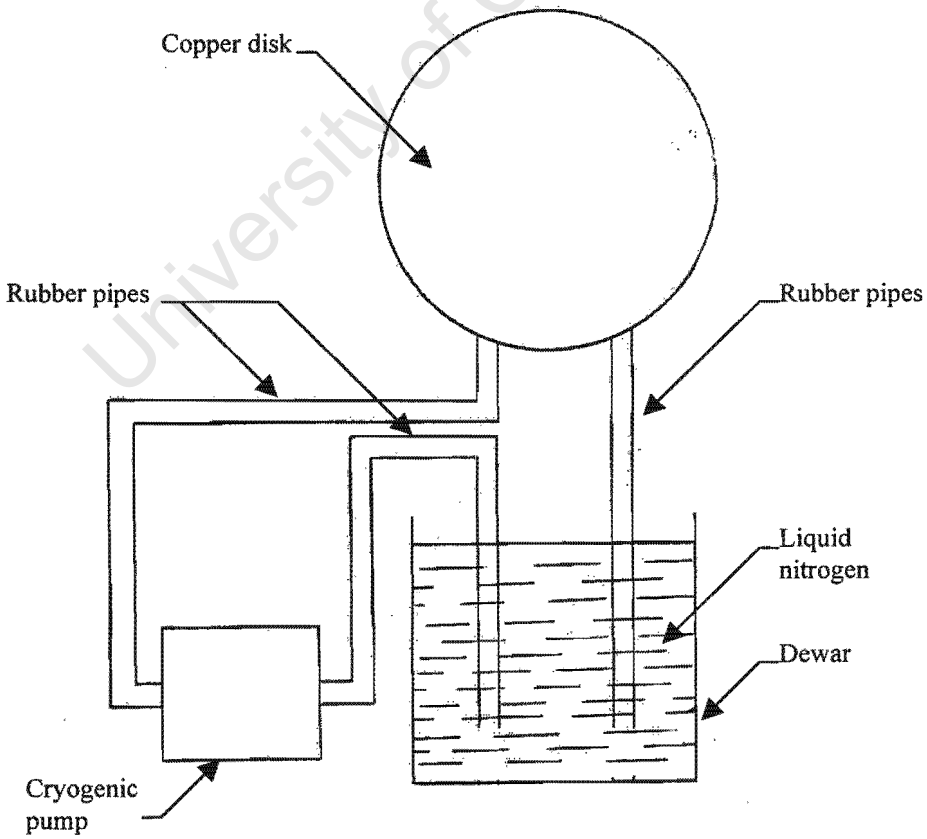

Figure 3.3: *Schematic illustration of the cooling disk system*

In the cooling disk system, a dewar is used to store a quantity of the cooling fluid that is used to cool the polymer specimen. The dewar is an appropriate choice of storage as it would minimise the loss of the cooling fluid due to evaporation.

This design also makes use of a cryogenic pump to pump the cooling fluid out of the dewar and through flexible rubber pipes. The pipes are connected to a copper disk containing a network of pathways allowing the cooling fluid to enter and circulate through the disk. The flow rate of the cooling medium can thus be varied to obtain the required cryogenic temperatures. Electronic devices such as the heating element and thermocouple are incorporated into the design to assist in regulating the polymer specimen temperature. The copper disk is located on top of the polymer specimen surface to be impacted, thus maintaining direct contact with the specimen in its clamped position. The location of the copper disk in the clamping base of the instrumented drop weight impact tester is shown in figure 3.4.

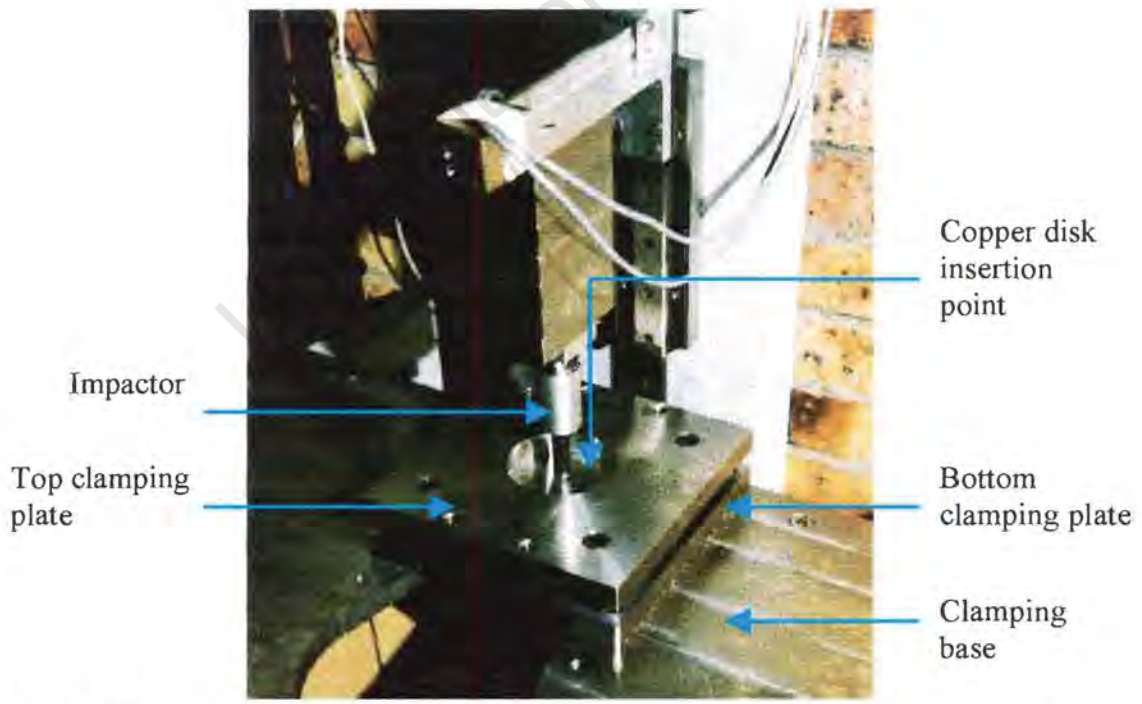

Figure 3.4: *Photograph showing the location of the copper disk and other components found at the base of the in-house instrumented drop weight impact tester*

However, the copper disk should be removed before the impact test is allowed to proceed when the specimen attains the required test temperature. The specimen and surrounding medium are cooled by means of heat transfer from the specimen to the cold copper disk. The cooling fluid circulates through the disk and is pumped back into the dewar. Although the design solution indicates a closed circuit in terms of the flow of the cooling medium, the medium would have to be replaced due to the evaporation of the medium in the storage unit. The tubing should be adequately insulated to minimise the heat loss to the atmosphere before the cooling fluid reaches the disk.

3.2.4 Design Solution

Design A (vapour cooling system) shows an attractive advantage in terms of the manufacture and machining of the required components and the design's simplicity. This reduces the overall cost of the apparatus as well as the production period of the system. However, the system requires frequent replacement of the nitrogen gas which is both expensive and time consuming. A further disadvantage is the formation of condensate on the polymer surface which may influence the impact behaviour of the polymer leading to erroneous results. The coiled cooling system shows a major disadvantage in terms of physical contact between the polymer and the copper coils. This would result in a longer period of cooling time as the coils would have to cool the clamping plates in order to be able to cool the specimen. A larger surface area would therefore be susceptible to heat transfer from the environment and an insulating environmental chamber would have to be constructed to avoid it. This translates to further cost and delay times.

The cooling disk system shows minimal machining costs as the copper disk is the only component that would need to be manufactured. A major advantage of this design is the physical contact that occurs between the copper disk and the clamped polymer specimen. The physical contact between the two increases the efficiency of the design by reducing the contact time required to attain the desired specimen temperature. In addition to this, upon removal of

the copper disk, the polymer specimen is ready to be impacted as it is positioned and clamped in place before the cooling operation begins. The disadvantage of this system is clearly the removal of the copper disk from the polymer surface which breaks the physical contact between them. However, this can be accommodated for by lowering the specimen temperature below the required impact test temperature. Replacement of the coolant is also necessary in this design but the frequency of replacement comparing to the vapour cooling system is decreased.

On the basis of the advantages and disadvantages of the possible design systems mentioned, the cooling disk system illustrated in figure 3.3 is chosen as the design solution to be used to incorporate the cryogenic test facility onto the in-house built instrumented drop weight impact tester.

3.3 THE CRYOGENIC FLUID MEDIUM

Various fluids were considered as the medium to cool the specimen down to cryogenic temperatures. The table below shows the fluids considered and their respective operating temperatures.

Cooling Medium	***Temperature (°C)***
Solid carbon dioxide with ethanol	-72
Solid carbon dioxide with acetone	-77
Solid carbon with ethyl ether	-100
Liquid air	-192
Liquid nitrogen	-196

Table 3.1: *Tabulation of the operating temperatures of the various fluid mediums considered*

According to table 3.1, any of these mediums would provide a suitable option to be used in the cooling disk design in terms of lowering the specimen temperature down to -50°C. However, due to the possibility of damage to the

cryogenic pump from the solid carbon dioxide chunks (dry ice), the first three possibilities were discarded. Liquid nitrogen is readily available, and was thus chosen as the cooling medium to be used in the cooling disk system.

3.4 THE CRYOGENIC PUMP

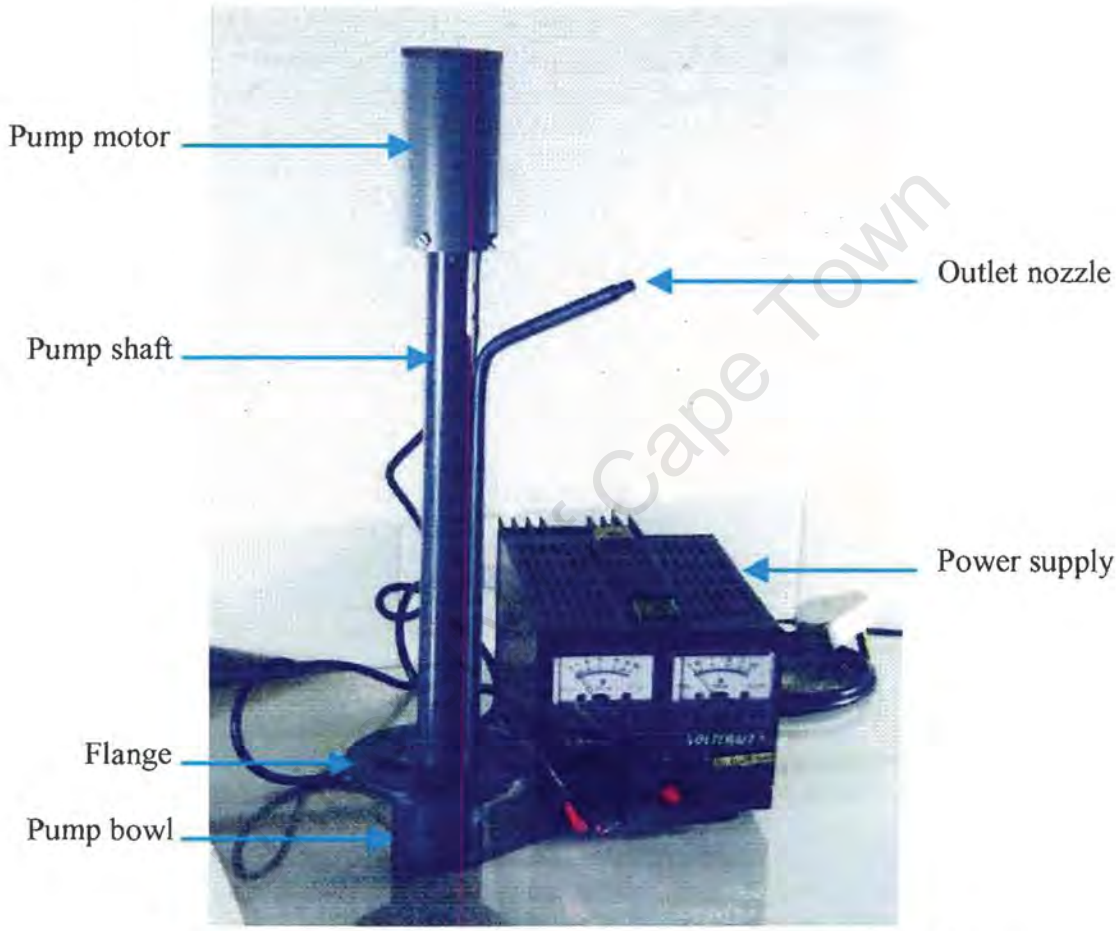

Figure 3.5: *Photograph of the Unipump and the power supply used*

The main criteria of the pump is that it should:

- operate at a minimum cryogenic temperature of –100°C if not lower
- be resistant to chemical attack from the coolant used
- be compact, lightweight, easy to handle and install
- be easy to operate

Various types of peristaltic and gear pumps were considered during the pump selection process. The lowest operating temperature of a small peristaltic

pump in South Africa was -45°C. The Unipump shown in figure 3.5 is a cryogenic pump designed specifically to pump liquid nitrogen and thus is able to operate at a temperature of -196°C whilst still satisfying the criteria mentioned. The Unipump is supplied by Materials Science Ltd based in the United Kingdom. It is built by using components of stainless steel, solid polyvinylchloride (PVC) and polytetrafluoroethylene (PTFE). It makes use of a propeller device which is run by a 12 volt direct current power source. The power source used has a variable voltage output thus allowing control of the coolant flow rate through the design circuit. The Unipump motor requires approximately 0.5 amps and has a fuse rated at 1 amp.

The top housing of the Unipump contains the motor and drive unit whilst the elongated section consists of the pump shaft. The pump bowl is located at the bottom of the Unipump. The flange can be positioned anywhere along the pump shaft housing tolerating a variety of sizes of flasks. The outlet nozzle of the Unipump has a flow diameter of 4 mm which is attached to a polysiloxane (silicone) tube with a useful working temperature range of –115 to 315°C. The polysiloxane material possess a self-insulation property eliminating the use of external insulation methods. The pump has a length of 35 cm with a diameter of 10 cm and weighs only 0.635 kilograms making it a convenient tool to use.

3.5 THE TEMPERATURE REGULATION APPARATUS

Apart from the control of the specimen temperature by varying the flow rate of the coolant into the disk, various other electronic devices are incorporated into the design to regulate the specimen test temperature. A teflon (type "T") thermocouple is used in conjunction with a heating cartridge element to provide heat to the disk when the actual disk temperature falls below the desired temperature. These thermal instruments are incorporated into the design as mentioned in the section describing the manufacture of the disk.

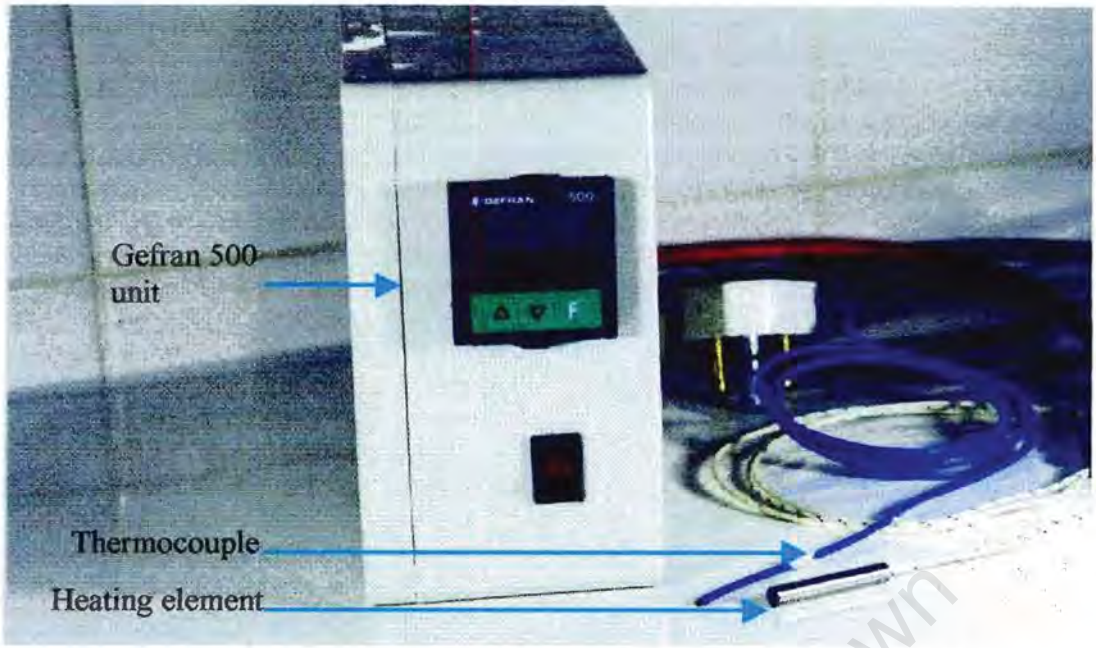

Figure 3.6: *Photograph of the temperature controlling devices used*

Figure 3.6 is a photograph of the Gefran 500 unit, the thermal instruments used in the cooling disk system and their appropriate electrical connections. The Gefran 500 is a temperature controller unit that was supplied by Unitemp in South Africa. It is used to control the voltage input to the heating element cartridge. Feedback of the disk temperature to the Gefran unit is provided by the type "T" thermocouple which has an operating temperature range of 200°C to -100°C. To separately determine the in-situ temperature of the specimen, a Testo 826 - T4 infrared thermal instrument is used. A picture of this device is shown in figure 3.7 and operates by shining an infrared beam onto the polymer specimen surface to be measured. This unit also has the ability to perform contact temperature measurements and has a measuring temperature range between –50 and 400°C with an accuracy of ±2°C.

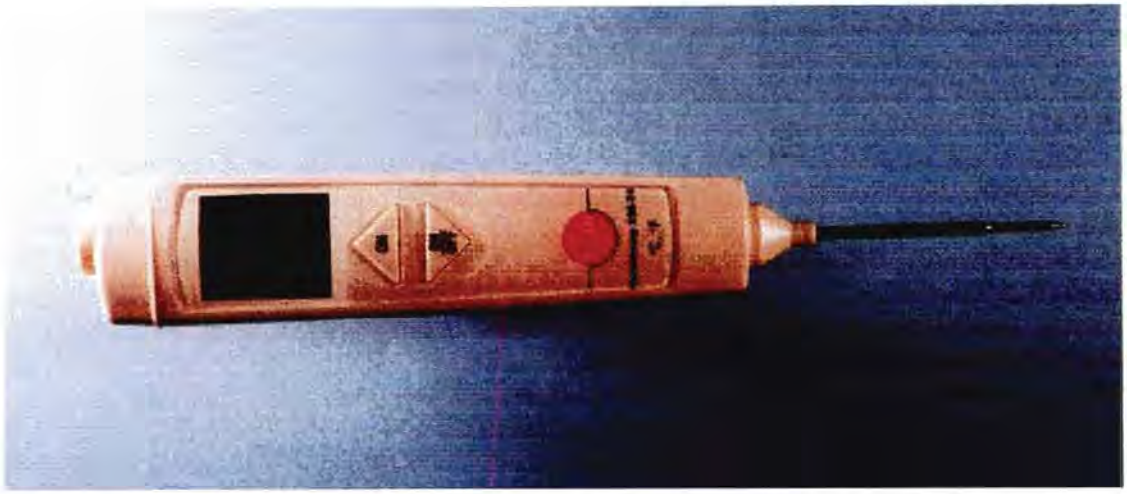

Figure 3.7: *The hand held Quicktemp Testo 826 – T4 temperature measuring device*

3.6 THE COPPER DISK

The following subsections describe the copper disk in detail as it is an integral part of the cooling disk design.

3.6.1 The Disk Material

To facilitate the cooling process, it is necessary to select an appropriate material for the disk in terms of its thermal properties as well as the nominal price which also contributes towards the cost of manufacture. Table 3.2 below describes the thermal properties of the materials from which a material selection for the disk was made.

Material Choice	***Coefficient of Thermal Expansion [10^{-6} (°C)$^{-1}$]***	***Thermal Conductivity [W/m-K]***
Aluminium	23.6	247
Copper	17.0	398
Magnesium	25.0-27.0	418
Stainless Steel	9.9-17.5	14.4-17.2

Table 3.2: *Tabulation of the thermal properties of various metallic materials*

From the information displayed in table 3.2, stainless steel shows the lowest coefficient of thermal expansion but has a relatively low thermal conductivity which is an important property required for the disk material. Magnesium and aluminium show a good balance of thermal properties. However, copper possesses a lower thermal expansion coefficient and a high thermal conductivity. The added bonus of copper is its corrosion resistant property which is especially useful considering the occurrence of condensation on the disk during the cooling procedure. These factors coupled with the economic benefits of copper make it an ideal choice for the material from which the disk is to be manufactured.

3.6.2 The Disk Manufacture Drawings

Owing to the limited amount of space available in the clamping mechanism, it is necessary to design the disk to be small and compact whilst still maintaining functionality. The figures 3.8, 3.9 and 3.10 describe the respective drawing manufacturing views of the disk in detail.

The disk has a diameter of 45 mm and a total thickness of 20 mm. The two holes shown in figure 3.8 on the top surface of the disk with a diameter of 6 mm are the inflow and outflow channels through which the coolant enters and leaves the disk. The inflow channel is connected to the silicone tube from the outlet nozzle of the Unipump thus providing a channel for the flow of the coolant. The coolant circulates through the disk upon entering it and exits the disk through the outflow channel via another silicone tube and is deposited back into the dewar flask. A special cover lid manufactured from polystyrene was used to facilitate the upright positioning of the Unipump and to cover the dewar flask minimising the evaporation of the coolant during storage, although evaporation of the coolant whilst in the dewar and the disk, is inevitable due to its inherent cryogenic temperature of -196°C.

The centre hole (7 mm) which is also located on the top surface of the disk is drilled to allow for an insertion point of the heating element into the disk. Due

to the compact size of the disk, part of the heating element remains exposed to the atmosphere. This portion of the heating element is inserted into a hollow ceramic tube to aid the heat dissipation process and prevent damage to the heating element. The 2.5 mm diameter hole is drilled for the insertion of the thermocouple into the disk at a strategic location in the disk thereby providing a means of obtaining a legitimate disk temperature measurement.

Figure 3.9 is also a schematic view of the disk from the top but sectioned halfway through the thickness of the disk. This allows for a closer examination of the detail inside the thickness of the disk. The hatched area represents the copper material whilst the rest of the drawings shows the network of holes drilled into the disk. The inflow and the outflow channels link up with the two parallel pathways drilled in the disk. Another pathway is drilled perpendicular to the parallel ones thereby creating a network of passages through which the coolant is able to circulate in the disk and in so doing, cool the disk and the specimens upon which the disk is located. The three holes on the surface of the disk circumference are formed as a result of the manufacturing procedure. These are sealed off with screws to prevent leakage of the cooling fluid during the circulation process. Precaution was taken during the designing process to ensure that the thermocouple and heating element locating holes did not intersect or lie in the immediate vicinity of the coolant pathways considering the overall dimensions of the disk.

An important feature indicated in figure 3.10 is that the heating element is located a distance away from the bottom surface of the disk and thus the copolymer specimen surface. This is done to avoid excessive heating of the specimen during the periods in which the heating element stabilises the disk temperature to the designated temperature. The final manufactured component is exhibited in figure 3.11.

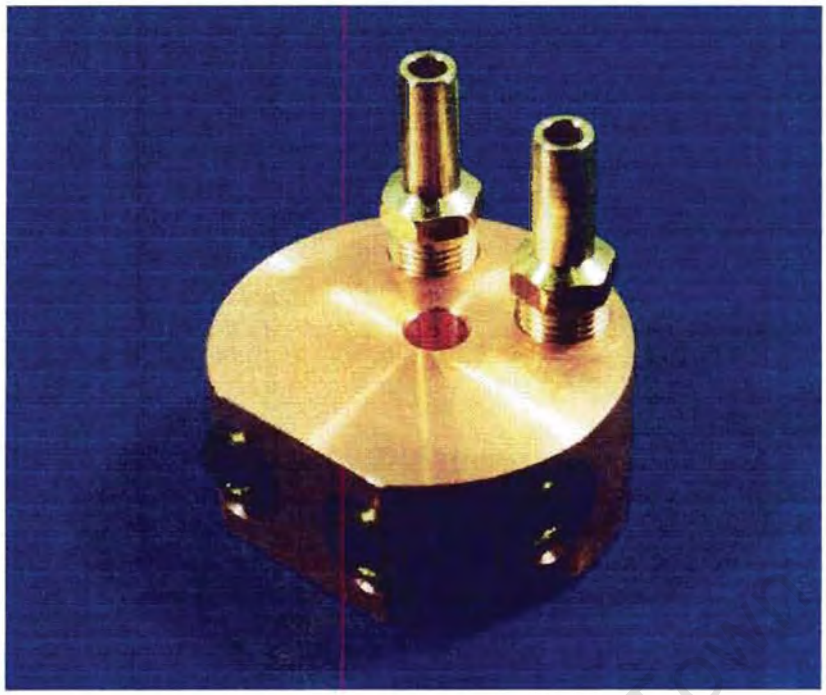

Figure 3.11: *Photograph of the manufactured part known as the disk*

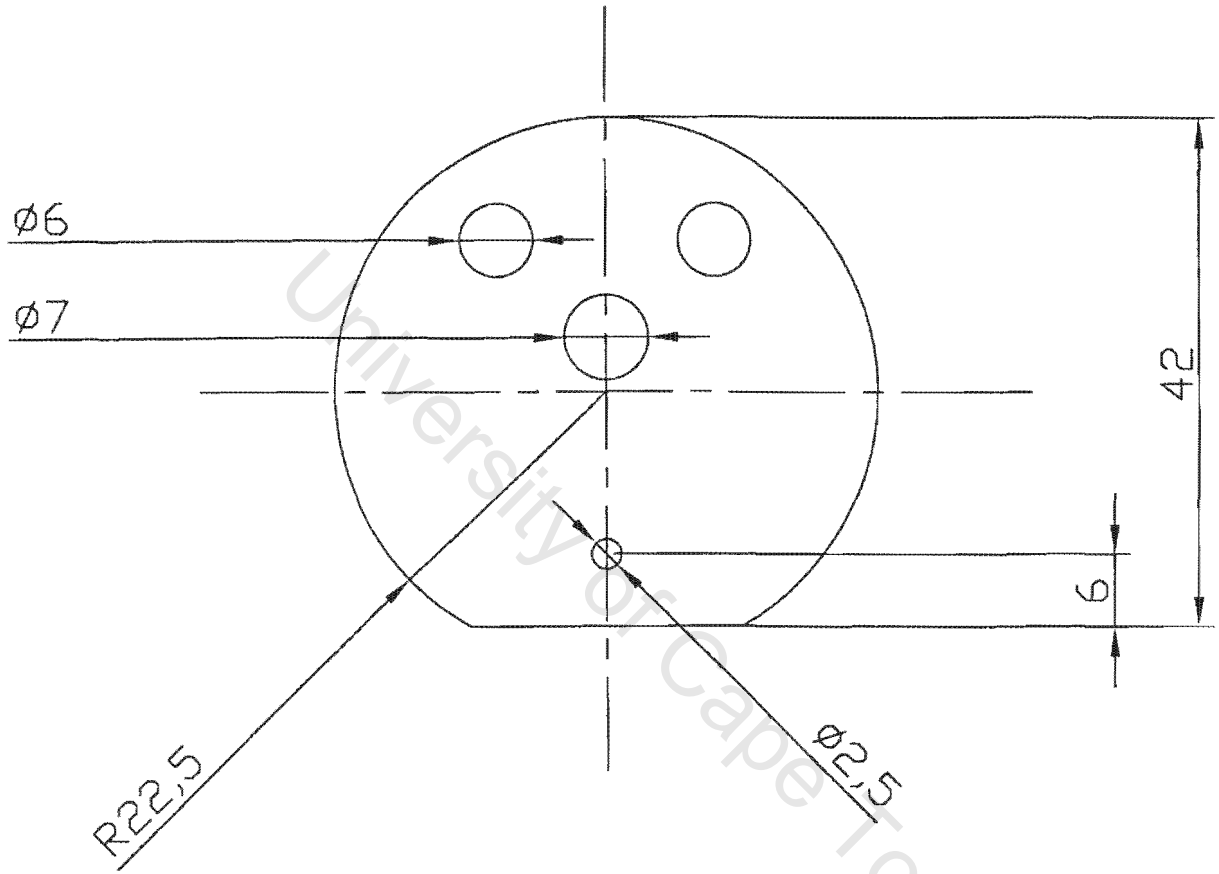

NOTES:

1. All dimensions in millimetres
2. All sharp edges and burrs to be chamfered.
3. All tolerances unless otherwise stated: ±0.1 mm.
4. Manufacturing material to be used: Copper.

Figure 3.8: *A top view of the copper disk with the respective manufacturing dimensions*

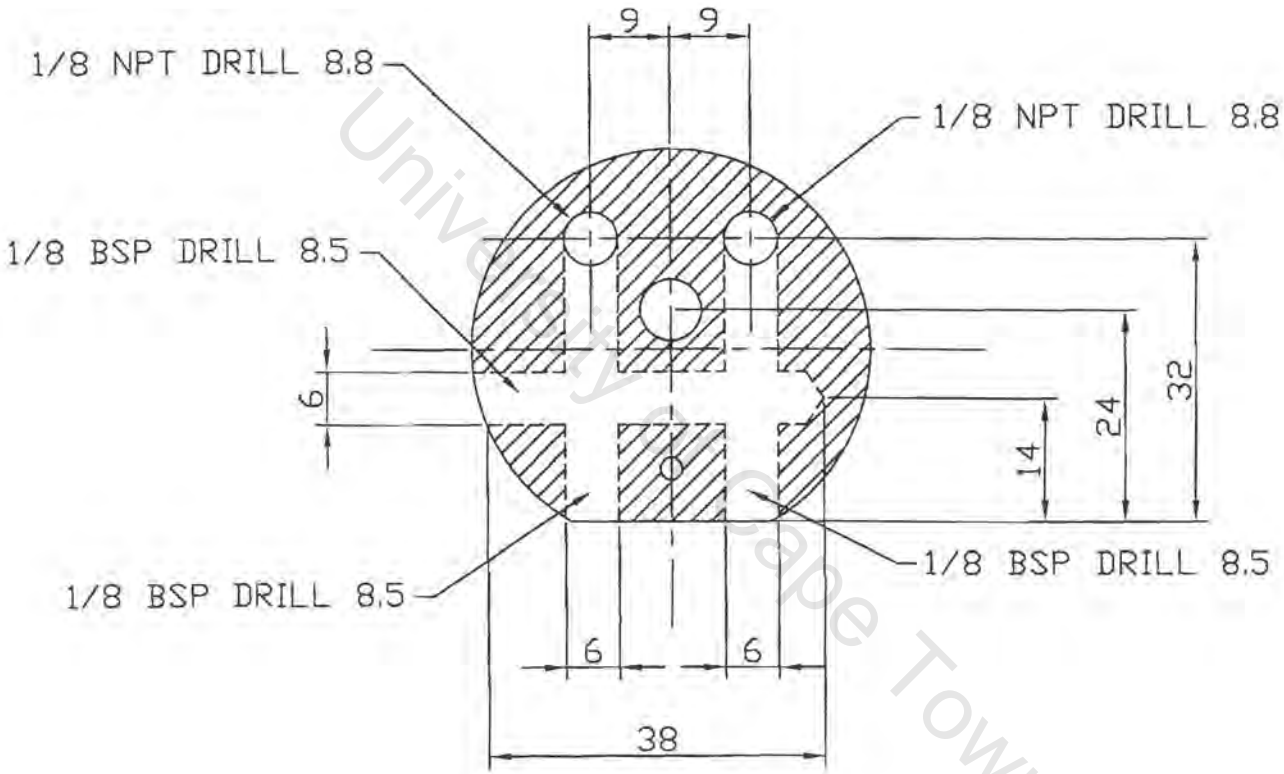

Figure 3.9: *A sectioned top view of the copper disk exposing the coolant pathways inside*

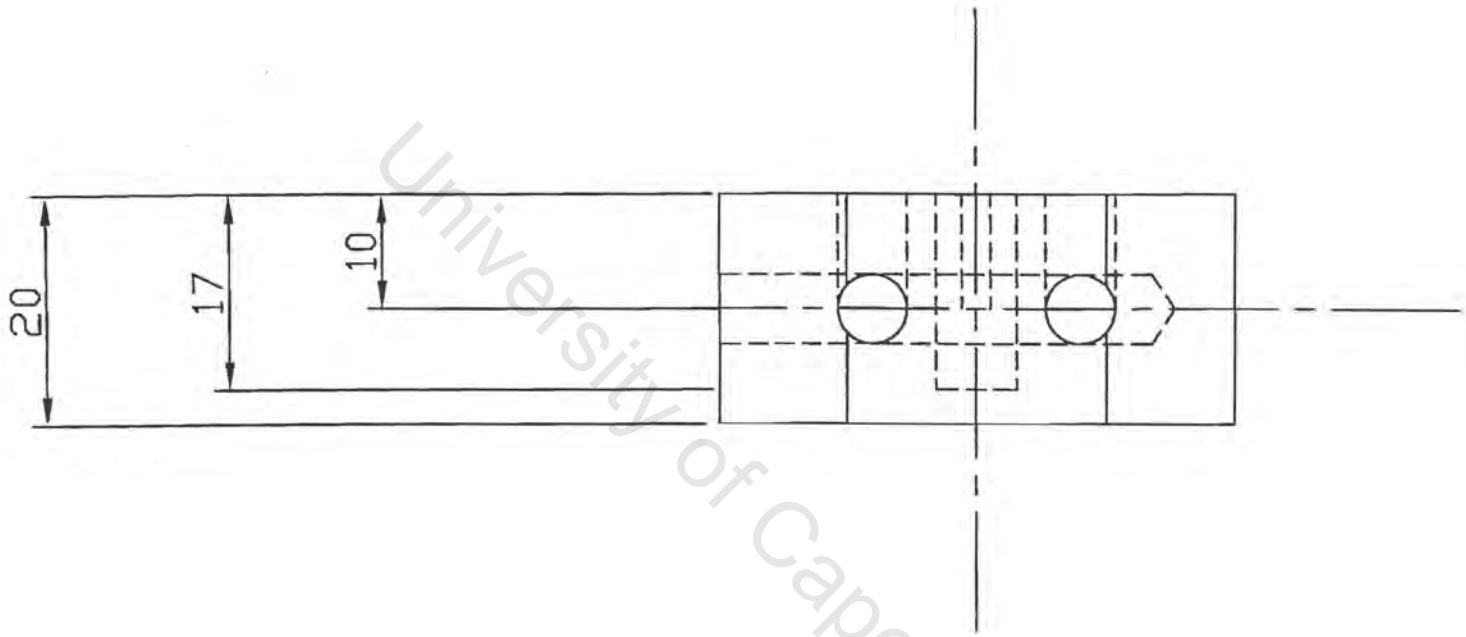

Figure 3.10: *A side view of the copper disk with the respective manufacturing dimensions*

3.7 OPERATIONAL PROCEDURE OF THE COOLING APPARATUS

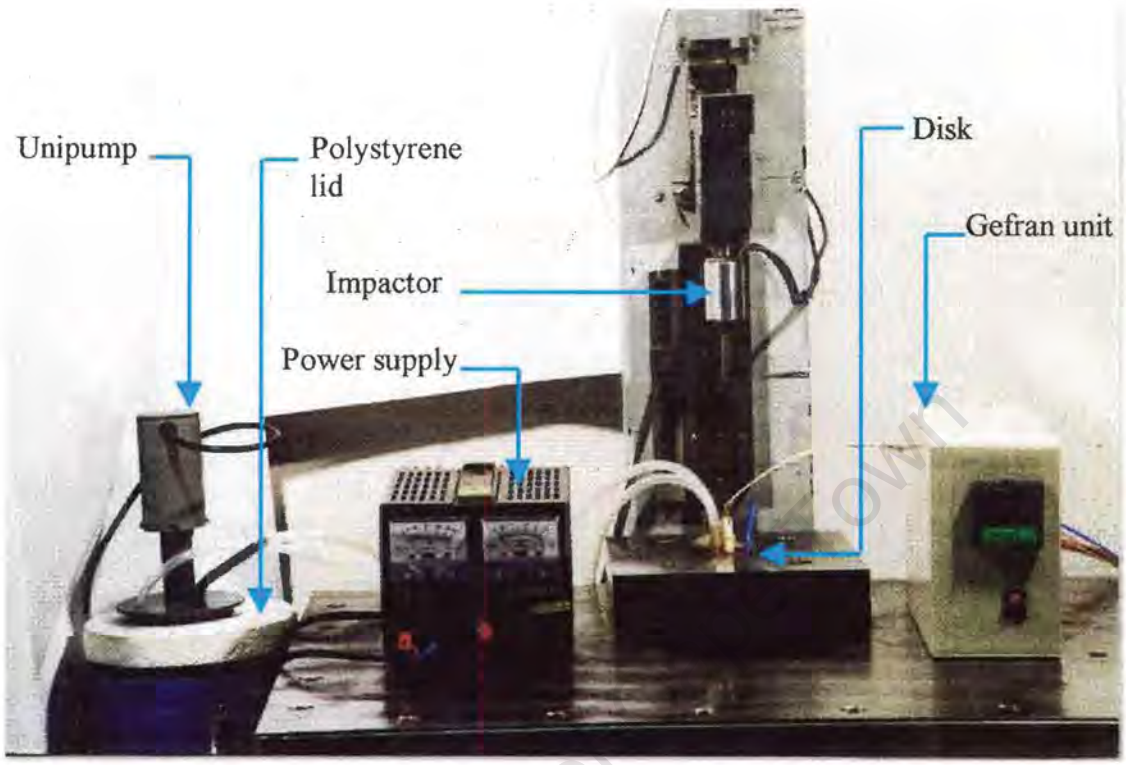

Figure 3.12: *Photograph of the cooling apparatus-set-up used at the base of the impact tester*

A photograph of the final set-up used during the impact testing procedure is shown in figure 3.12. The operation of the cooling apparatus is specific to the cooling rate of the type of material being cooled and the environment in which the apparatus is used. The copolymers were cooled for 15 minutes at a temperature which was -5°C lower than the desired temperature to accommodate for specimen heating upon removal of the disk from the specimen surface. The operational procedure for the use of the cooling disk system facility is as follows:

The Unipump should be thoroughly dried before use as any liquid residue will freeze in the pump shaft and prevent the rotary motion of the impeller and thus inhibit the circulation of the coolant. The Unipump is to be located in a upright position in the dewar using the polystyrene lid designed for this purpose. To prevent accidents due to the splashing of the coolant, the

Unipump should be gently lowered into the storage vessel or dewar containing the coolant. Power should be supplied to the pump only when immersed into the coolant.

The thermocouple and the heating element should be properly located in their respective holes in the copper disk. Moisture in the thermocouple locating hole should be avoided to attain accurate temperature readings of the disk. Ensure that a ceramic hollow tube encapsulates the length of the heating element exposed to the atmosphere for safety reasons as well as to allow for better heat dissipation.

Once power is supplied to the pump and the impeller begins to rotate, the coolant is circulating in the disk. The speed at which the impeller rotates can be controlled by adjusting the voltage supplied to the pump which further allows for ease of temperature regulation. The Gefran unit provides a digital display of the disk temperature and the desired temperature which should be set manually before the operation of the cooling disk system facility.

Care should be exercised during testing to avoid grotesque distortion of the silicone tubing as it would fail in a brittle manner due to the temperature of the coolant being lower than the glass transition temperature of the silicone tubing. The dewar may need to be refilled with the coolant at certain intervals depending on the coolant flow rate and the required specimen test temperature. Upon completion of the use of the cooling apparatus, the Unipump should be removed from the dewar only after the silicone tubing has attained its natural flexibility and should be dried thoroughly. The disk must also be thoroughly dried.

CHAPTER 4

EXPERIMENTAL TECHNIQUES

4.1 TEST MATERIALS

The copolymer under investigation in this research study is poly (propylene-ethylene) copolymer, which consists of polypropylene as the matrix polymer and the ethylene propylene rubber as the dispersed modifier particles.

4.2 TEST SPECIMENS

The polymer specimens are supplied by Sasol Polymers and are made by injection moulding as per the standards dictated in the ASTM D4101 and ISO 1873-2 procedures. The injection moulding process consists of molten polymer being injected into a cold mould cavity with the geometry of the desired shape. The cycle time period is around 60 seconds of which the cooling in the mould lasts approximately 25 seconds. All the specimens were tested in such a manner that the impactor (tup) penetrated the specimens at a direction perpendicular to that of the polymer molecules injected into the mould cavity. All the specimens were un-notched prior to the impact tests.

4.2.1 Test Specimen Dimensions

The initial circular test specimens of a 2 mm thickness were tested at room temperature using the drop weight impact tester. The tests yielded erroneous results due to excessive specimen vibration during the impact event. The vibration was detected by means of a plot of voltage as a function of time. This plot showed a deviation from the expected normal behaviour, which can be attributed to the specimen being improperly clamped. The specimen vibration was a result of two factors. Firstly, the specimen thickness was

insufficient and thereby allowing for lateral movement of the specimen during impact. Secondly, the specimen diameter of 60 mm did not provide enough material being clamped in the holder. The advent of excessive vibration was corrected by using square specimens of dimensions:

Length = 100 mm

Breadth = 100 mm

Thickness = 3 mm

4.2.2 Test Specimens Ethylene Content

To examine the effect of the ethylene content present in the copolymer, copolymers where the ethylene content varied between 0 and 13% was supplied by Sasol Polymers. The polymer with the 0% ethylene is the polypropylene homopolymer. The matrix grid shown below indicates the different grades of copolymer tested to investigate the influence of ethylene on the mechanical properties.

Specimen type	*Batch number*	*Ethylene content (wt %)*	*Nucleating agent*	*Melt flow index*
PP 1147 HQ7	Bx 5808X	0	Present	1.93
PP 2340 PC	Bx 5890Y	6.9	Present	16.8
PP 2540 H	Bx 6422Y	11.4	Present	1.77
PP 2648 M	Bx 6343Y	13.4	Present	9.0
PP 2648 RC	Bx 6321Y	12.0	Present	24.3

Table 4.1: *Tabulation of the specimen production parameters*

The PP 1147 HQ7 and PP 2540 H grades had a melt temperature of 230°C during moulding to assist the complete filling of the mould as they are high molecular weight grades.

The codes used in the specimen types can be deciphered using the format shown below.

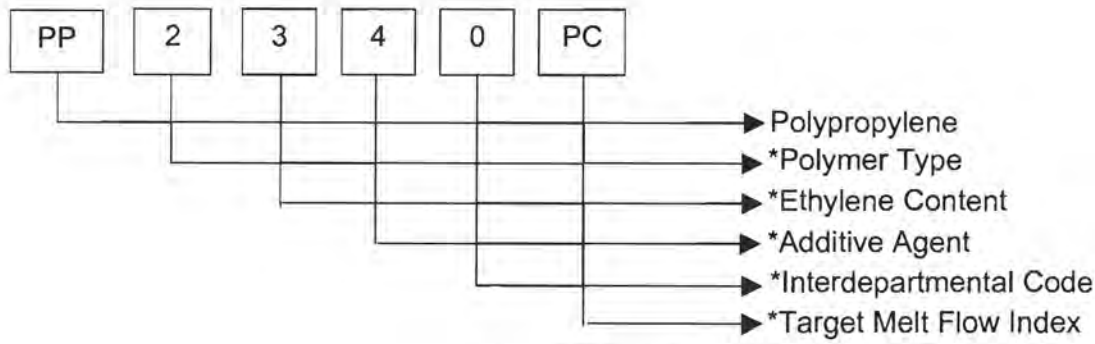

where the * sign means "An indication of"

Polymer Type	1	Homopolymer
	2	Block copolymer
	3	Random copolymer
Additive Agent	0	General additive package
	4	Nucleating additive package
Target Melt Flow Index	H	2.0 g/10min
	K	3.5 g/10min
	L	5.5 g/10min
	M	8.5 g/10min
	N	12 g/10min
	P	16 g/10min
	R	21 g/10min
	T	45 g/10min
Last Letter (in some cases)	C	Controlled rheology grade

Table 4.2: *Deciphering of the codes used in the polymer designation terminology*

4.2.3 Test Specimens Melt Temperature Variation

Sasol Polymers supplied two series of injection moulded specimens. These are referred to as the "A" and "B" series. The "A" series copolymers are injection moulded at a melt temperature of 200°C using a mould temperature

of 30°C. The "B" series samples were produced by increasing the melt temperature to 230°C, whilst keeping the mould temperature at 30°C.

Specimen type	Series	Ethylene content (wt %)	Melt flow index	Material supplier
PP 2348 M	"A" and "B"	6.4	7	TARGOR
PP 2648 RC	"A" and "B"	7.6	22	TPC
PP 2648 RC	"A" and "B"	10.4	22	DOW
PP 2648 RC	"A" and "B"	10.6	24	DOW

Table 4.3: *Tabulation of the manufacturing parameters used to produce the "A" and "B" series*

4.2.4 The Influence of Copolymer Types

Copolymers from various suppliers was used to manufacture the "A" series copolymers at varying levels of ethylene to examine the effect of varying the type of ethylene introduced into the polypropylene copolymers. The complete range of the "A' series is shown in table 4.4 below.

Specimen type	Series	Ethylene content (wt %)	Melt flow index (g/10m)	Material supplier
PP 2340 P	"A"	5.6	16	TPC
PP 2340 P	"A"	5.5	18	TPC
PP 2348 M	"A"	6.4	7	TARGOR
PP 2348 M	"A"	6.3	7	TARGOR
PP 2448 TC	"A"	6.7	42	DOW
PP 2448 TC	"A"	6.5	54	TPC
PP 2600 PC	"A"	10.2	17	TARGOR
PP 2648 RC	"A"	10.4	22	DOW
PP 2648 RC	"A"	10.6	24	DOW
PP 2648 RC	"A"	7.6	22	TPC

Table 4.4: *Tabulation of the various parameters used in the production of the "A" series*

4.3 TESTING APPARATUS: INSTRUMENTED DROP WEIGHT IMPACT TESTER

The impact tests were performed on an in-house built drop weight impact tester that was modified to include cryogenic temperature impact testing. The impact tester is instrumented to allow the impact data obtained during the impact event to be recorded onto a computer. For each impact event, three traces are recorded. Manipulating the acceleration history equations of the impactor acquired from the tup force measurements derives the three traces mentioned. The force imposed onto the specimen vs. the impact time, and the total deflection experienced by the specimen during the impact event can be obtained. The integral of the area under the force-deflection curve provides information of the impact energy absorbed by the specimen as a function of specimen deflection.

4.3.1 Impact Test Procedure

A photograph of the test apparatus shown in the figure 4.1 indicates the different components of the instrumented drop weight impact tester used in this investigation. The drop weight impact tester is calibrated according to the procedure described in the Results Section to obtain meaningful results. Prior to commencing of the impact test, a square test specimen is securely clamped into place by the use of bolts located on the top clamp plate. The tup and the cross-head beam should be hoisted to the required height by means of an electronic pulley attached to the cross-head beam. The copper disk is then placed onto the exposed section of the specimen surface and the coolant is permitted to flow from the storage dewar through the disk and pumped back into the dewar. The disk is placed onto the specimen ensuring direct physical contact for a period of 15 minutes.

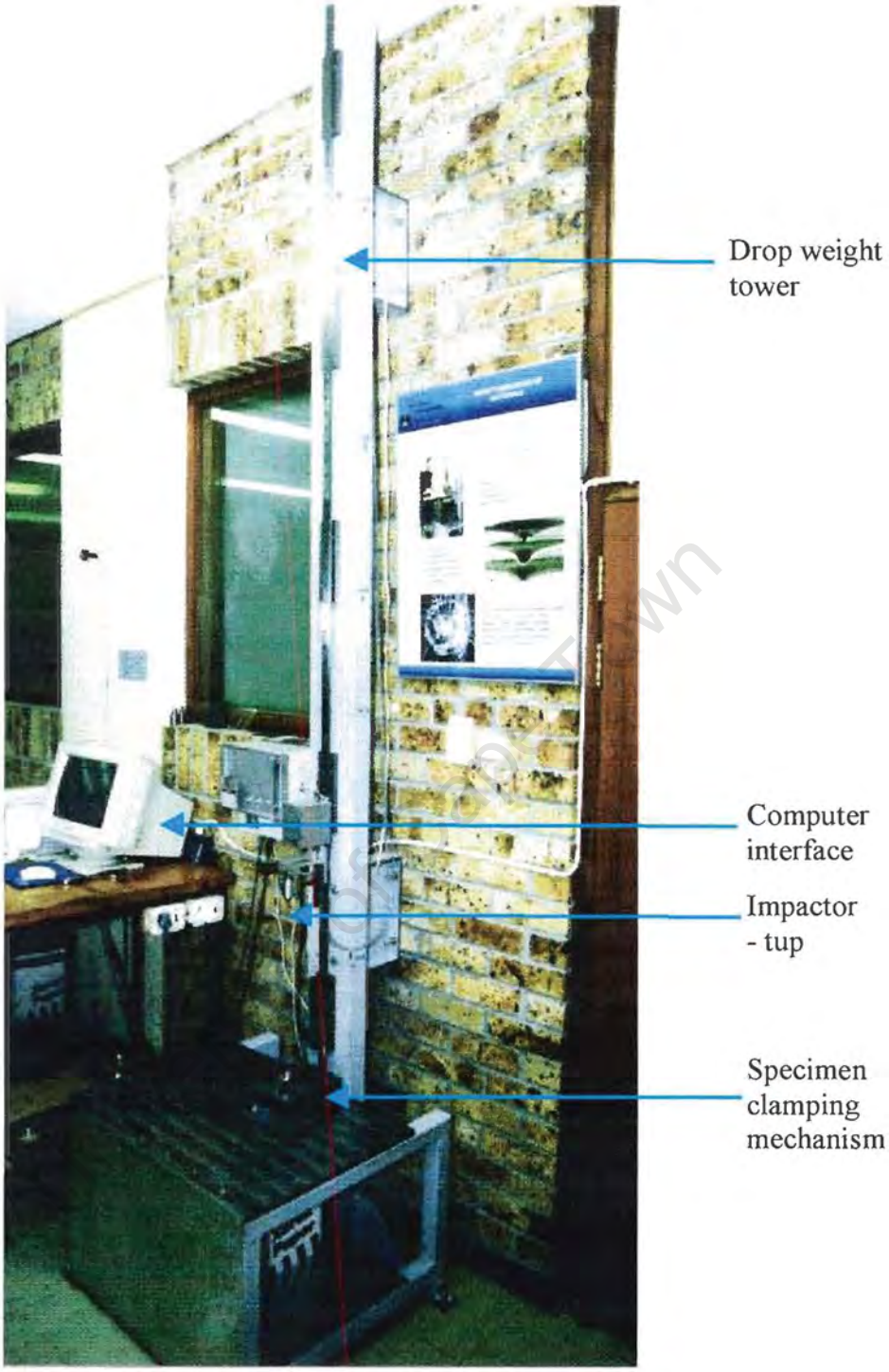

Figure 4.1: *Photograph of the in-house built instrumented drop weight impact tester*

The specimen temperature is monitored using the infra-red thermal device whereas the temperature of the cooling disk is controlled by a thermocouple. Parameters such as the load cell calibration coefficient, existing weight of the cross-head beam and the offset voltage are entered into the data acquisition computer program. When the appropriate temperature conditions required for

the impact test are met, the cooling disk is removed and the tup is released from the designated height and allowed to fall under the force of gravity until it makes contact with the specimen surface. This point marks the beginning of the impact event and the computer interface starts to record the necessary impact event details. The impact event ends when the tup velocity reaches zero. Provided specimen contact is made and the tup has fully penetrated the specimen thickness, the impact test is commissioned as being a successful one. The impact velocity of the tup at the onset of the impact event is noted. The impact data is copied into the Windows Notebook format, converted into the Microsoft Windows Excel format and analysed. The last step involves removal of the specimen from the clamping plates and appropriately labelled for future references.

4.3.2 The Tup Specifications

The hemispherical nosed tup or impactor having a shaft diameter and length of 8 and 50 mm, respectively was selected and used throughout the impact tests. A photograph of the tup and the cross-head system is shown in figure 4.2. The weight of the cross-head beam along with the tup and other components is 1.155 kg. The instrumented impact tests are carried out in the total penetration mode. In this mode, the tup must fully penetrate the specimen thickness i.e. the impact test is carried out to a point of complete failure in the specimen. Penetration is defined as the entrance of the impactor into the specimen followed by a complete passage or complete piercing of the specimen by the impactor. The release height of the tup is therefore varied to ensure that the potential energy accumulated in the cross-head beam is sufficient enough to just cause failure in the various specimens.

The tup impact velocity is the velocity of the tup at the instant in which the tup's hemispherical nose makes physical contact with the top surface of specimen. It is measured by means of optical limit switches located at the base of the tower railing through which the velocity flag on the cross-head beam passes and is recorded onto the computer. Due to the conversion of

potential energy into kinetic energy that occurs as a consequence of the motion of the tup under gravity, the impact velocity is dependent on the height at which the tup is allowed to fall from.

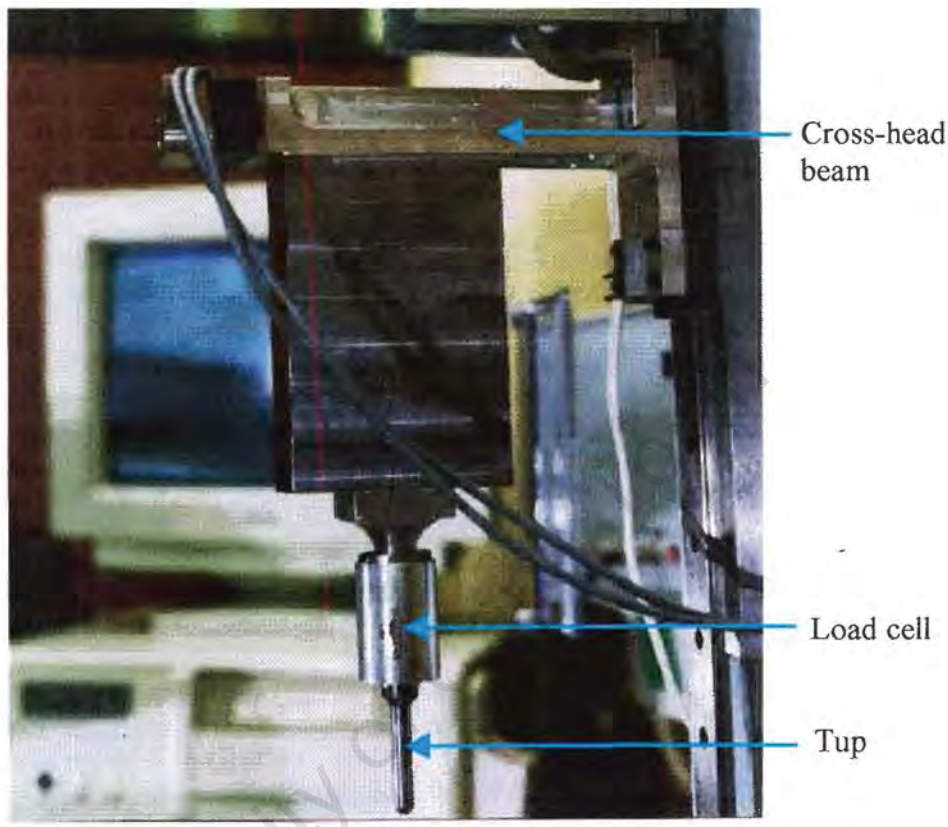

Figure 4.2: *Photograph of the different components that constitute the impactor*

4.3.3 Ambient Impact Testing Temperature

With the aid of the cryogenic temperature facility, the impact testing temperature is lowered from room temperature, 23°C, to -50°C at successive 10°C intervals. Thereafter, the impact test temperature intervals for each specimen grade is narrowed around their brittle-to-ductile transition to get a more accurate estimate of the brittle-to-ductile transition temperature. In addition some of the specimens were tested to obtain their impact response at temperatures ranging from 23°C to 40°C.

4.4 SCANNING ELECTRON MICROSCOPY

The scanning electron microscopy specimens are acquired from the same batch of specimens supplied for drop weight impact testing. This allows one to correlate the structural features with the mechanical property results obtained from the experiments conducted. The specimens are prepared by cutting them in strips of 15 mm X 100 mm. A notch is introduced into the surface of the specimen at approximately 20 mm along the strip of the copolymer. This is then inserted into a bath of liquid nitrogen for a period of 15 minutes. The strip is fractured and the fracture surface is etched by immersing the specimen into a heptane solution heated at 70°C for approximately 1/2 hour. The specimens are then placed into a solution of methanol for a period of 5 minutes in the ultrasonic bath for cleaning purposes.

Aluminium stubs are used to mount the specimens with the aid of some carbon dag. A SEM Coating Unit E5100 was used to sputter-coat the polymer specimens with a gold-palladium mixture. This is done to render them electrically conductive and to prevent charging of the specimens during microscopy. The sputter coating procedure is carried out using voltage of 2 kV and a current of 16-17 mA for 10 minutes. A silver conductive paint is then applied to the contact area between the specimen and the aluminium stub to minimise the effect of charging. A Cambridge S200 Stereo scanning electron microscope (SEM) is used for the detailed examination of the copolymer specimen's surface. To minimise radiation damage to the polymer, an accelerating voltage of 10 – 15 kV is used. The Joyce Loebl Image Analysis Software package in the Electro-Microscopy Unit (EM unit) is used to determine the average size of the etched rubber particles.

CHAPTER 5

RESULTS

5.1 RELIABILITY OF THE LOW TEMPERATURE IMPACT FACILITY

5.1.1 Load Cell Calibration

The cross-head beam, which consists of the tup, the load cell and the sensory equipment, is used to indent the specimens. The load cell makes use of a voltage signal corresponding to the applied load to obtain data for the plots of the force vs. time, force vs. deflection, energy vs. deflection and voltage vs. time. Thus, the load cell should firstly be calibrated to obtain accurate results. The calibration procedure involved removing the load cell and the tup from the in-house built drop weight impact tester and positioning it upside down in a compression cage on the Zwick Universal tensile testing machine. The load cell was then subjected to a series of successive compressive forces ranging from 0 kN to 20 kN.

At each successively applied load, the corresponding output voltage registered by the data acquisition computer system is recorded. The data acquisition system is electronically linked to the load cell by means of a signal processing unit. The two variables are then plotted against each other. Figure 5.1 shows a plot of the applied compressive load as a function of the output voltage. The slope of the best-fit line in the plot is used to determine a load cell calibration coefficient and a value of -6514 $N.V^{-1}$ was obtained from the graph. The x-intercept value of 0.0717 is the offset voltage measured on the load cell when no load is applied.

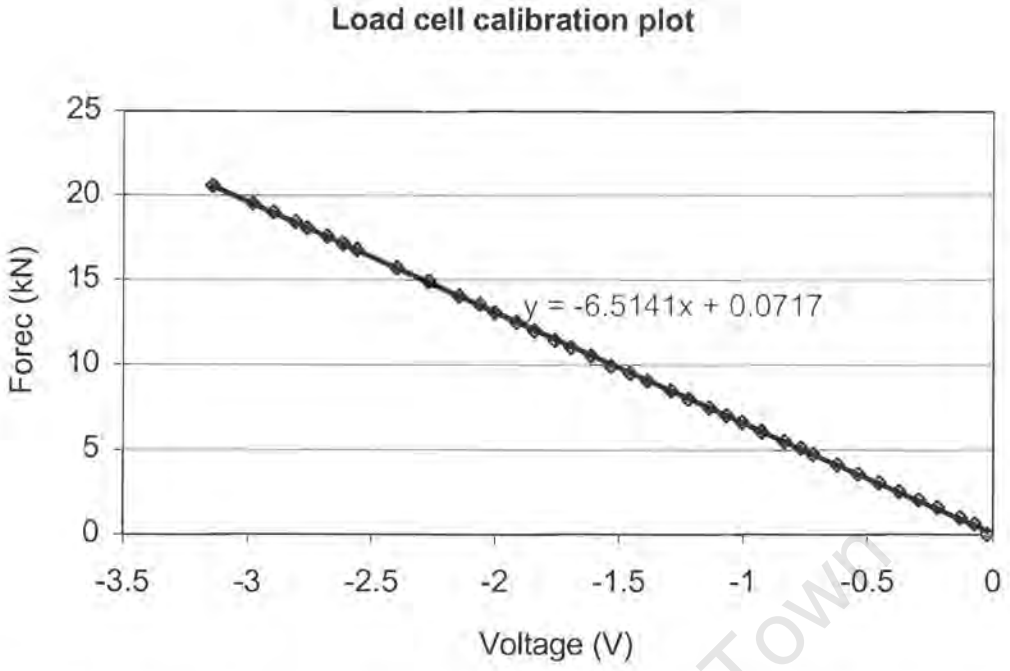

Figure 5.1: *Graph showing the load cell calibration coefficient from the data acquired*

5.1.2 The Effect of Specimen Thickness

The drop weight tests showed two distinct types of responses in terms of the voltage vs. time graphs when considering two different specimen thicknesses. Figure 5.2 is a plot for a circular copolymer specimen having a diameter of 60 mm and a thickness of 2 mm. When compared to figure 5.3, several features can be seen. The graph shown in figure 5.3 is that recorded for a 3 mm thick square specimen of length 100 mm. The extent of oscillations present in the voltage readings is dramatically reduced in figure 5.3 when the specimen dimensions are increased. The occurrence of specimen vibration during the impact event is confirmed by the excessive oscillations found in figure 5.2. The specimen vibration is a direct result of inadequate specimen clamping which is a synergistic effect of two factors, insufficient specimen thickness and diameter. A specimen thickness of only 2 mm causes vibration of the specimen in the vertical direction. Coupled to that, the specimen's diameter of 60 mm is unable to provide an acceptable level of specimen clamping which further contributes to the vibration.

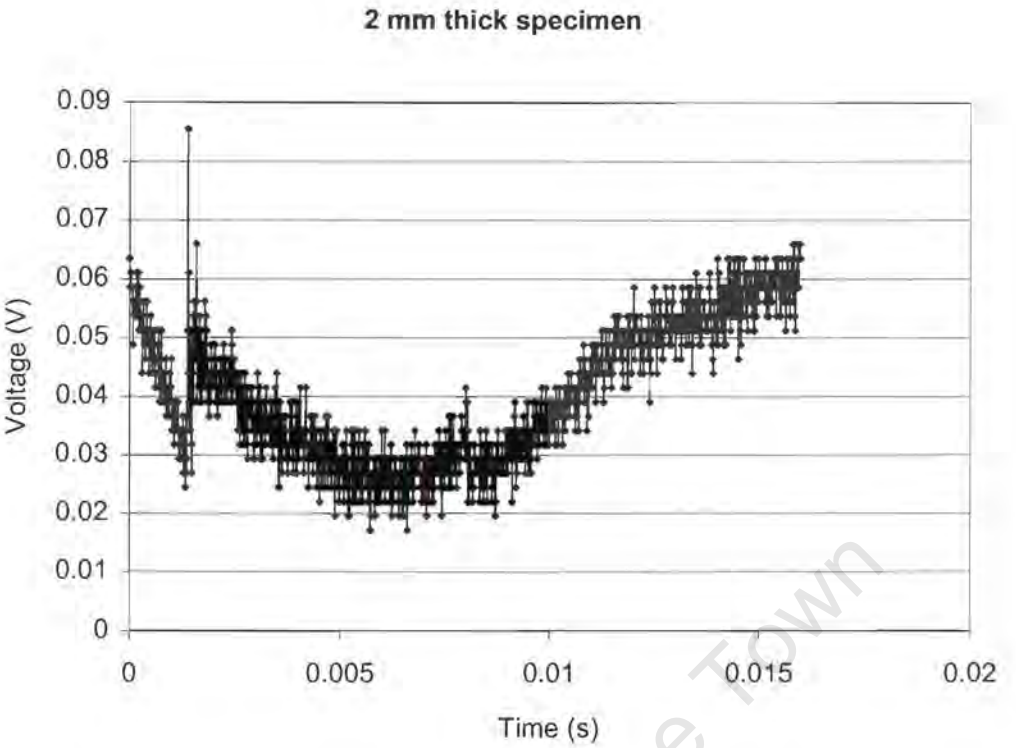

Figure 5.2: *Graph indicating the output voltages as a function of the impact duration for a circular 2 mm thick specimen*

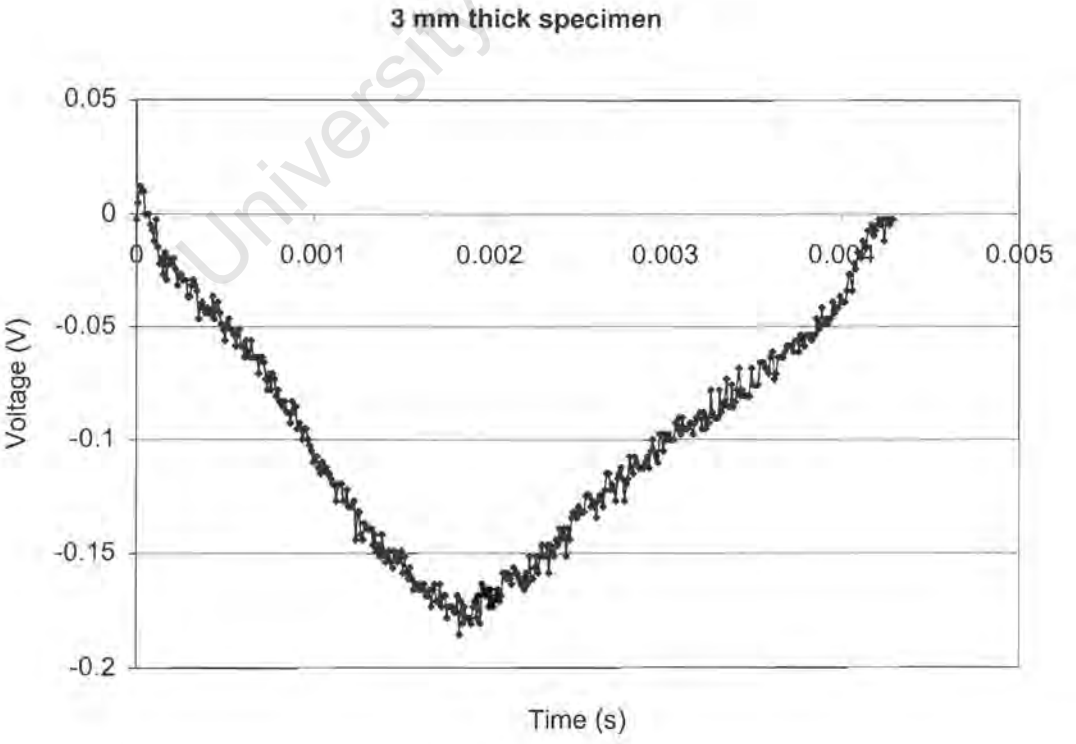

Figure 5.3: *Graph indicating the output voltages as a function of the impact duration for a square 3 mm thick specimen*

Increasing the specimen thickness to 3 mm and using a 100 mm square specimen significantly hinders the vibration of the specimen. The respective voltage data captured during impact event in figure 5.2 have positive values which is contradictory to the findings in the load cell calibration graph in figure 5.1. This is because a force exerted by the specimen onto the tup should exhibit a negative voltage as observed in figure 5.3. Adequate clamping and a specimen thickness of at least 3 mm lead to a more refined trendline of the voltage curve as in figure 5.3.

5.1.3 Infrared Emissivity Calibration

The Testo 826–T4 temperature measuring device required to be calibrated in order to accurately determine the specimen temperature during testing. The calibration is done by altering the emissivity factor of the thermal instrument until the direct contact and infrared temperature readings match within an acceptable margin of error. In this work, an acceptable margin of error is defined as the two readings being within 5% of each other. Table 5.1 shows the room temperature measurements of the various polypropylene grades using the two different measurement techniques. All of these readings are within the acceptable limit indicating that the infrared emissivity temperature measurement technique is reliable for testing the temperature of the polymer specimens.

Specimen type	*Direct contact measurement (°C)*	*Infrared measurement (°C)*	*Percentage error (%)*
PP 1147 HQ7	22.3	21.5	3.6
PP 2340 PC	22.5	22.0	2.2
PP 2540 H	21.8	21.0	3.7
PP 2648 M	22.1	21.5	2.7
PP 2648 RC	22.2	22.0	0.9

Table 5.1: *Tabulation of the results obtained using two different temperature measuring techniques*

5.1.4 Correlation of the Copper Disk Temperatures with the Polymer Specimen Temperatures

To validate the impact temperatures during the actual testing, temperature measurements of the copper disk and the polymer specimens are taken just prior to an impact test. The reliability of the test temperature readings is critical in terms of the accuracy of the impact test results where temperature is a variable parameter. To include representative polypropylene specimen grades in this study, the polypropylene homopolymer as well as low and high ethylene content polypropylene copolymers are examined. The temperature settings and the readings obtained are shown in table 5.2.

The temperature controller unit is set to a temperature of 5°C below the desired impact test temperature to compensate for specimen heating when the copper disk is removed. The specimen heating occurs during the time interval in which the copper disk is removed from the polymer specimen surface and the start of the impact event. This time interval was found to be between 13 and 15 seconds, during which time the specimen was measured to heat up by approximately 5°C.

The copper disk temperature is measured using a thermocouple. The polymer specimen temperature is measured by inserting the probe of the temperature measuring device into a hole drilled into the specimen. The equilibrium copper disk temperatures in table 5.2 are reached after allowing liquid nitrogen to circulate through the copper disk for a period of 15 minutes. The PP 2648 M specimen does not have a specimen temperature reading at a desired testing temperature of –50°C due to the temperature measurement capability limitations on the infrared measuring device. The results from table 5.2 show that the cryogenic temperature facility is capable of successfully lowering the polypropylene copolymer specimen temperatures down to –50°C. During the time that the copper disk is removed, the polymer specimen will heat up to a temperature within 2°C of the desired temperature.

Specimen type	Desired impact temperature (°C)	Temperature controller setting (°C)	Equilibrium copper disk temperature (°C)	Polymer specimen temperature (°C)
PP 1147 HQ7	23	N/A	N/A	22.0
	0	-5	-7	-5
	-10	-15	-15	-15.8
	-20	-25	-25	-25.3
	-30	-35	-34	-35.4
PP 2340 PC	23	N/A	N/A	22.0
	0	-5	-6	-5
	-10	-15	-15	-15
	-20	-25	-27	26.3
	-30	-35	-34	-35.6
PP 2648 M	23	N/A	N/A	22.1
	0	-5	-4	-3.8
	-10	-15	-12	-13.3
	-20	-25	-23	-25.8
	-30	-35	-36	-36
	-40	-45	-47	-47.3
	-50	-55	-58	- - -

Table 5.2: *Cryogenic temperature measurements of the copper disk and the various grades of polypropylene specimens*

Specimen type	Desired impact temperature (°C)	Temperature controller setting (°C)	Equilibrium copper disk temperature (°C)	Polymer specimen temperature (°C)
PP 1147 HQ7	30	31	30	31
	35	36	36	36.5
	40	41	41	42

Table 5.3: *Tabular representation of the high temperature settings for the polypropylene homopolymer*

Table 5.3 shows the temperature results obtained by heating the polypropylene homopolymer to 40°C. This was also done for the PP 2340 PC copolymer as both these polymers showed a brittle-to-ductile transition above room temperature. During the heating mode of operation, the temperature controller need only to be set at 1°C above the required impact test temperature as the cooling rate of the polymer specimen upon removal of the copper disk is sufficient to allow for a tolerance range of 2°C during the impact tests.

5.1.5 Reproducibility of the Impact Rig

The reproducibility of the impact results obtained using the instrumented drop weight impact tester is a function of two aspects. One is the material homogeneity and the other is dependent on the accuracy of testing rig. Assuming a consistent or negligible variation of material properties, the reproducibility of the impact results can therefore be said to be solely dependent on the reproducibility of the impact rig. To analyse the reproducibility of the rig, a methodology of worst case scenario is followed. Five impact tests (X_i) are done at a specific temperature, where $\overline{X}$ represents the mean impact energy for the 5 "identical" specimens tested. The standard deviation (σ_x) for the 5 impact energy values is also calculated. The test temperature is varied to incorporate the different cryogenic temperatures into the statistical analysis. The test temperature with the largest error band in impact energy is used in the analysis to determine the confidence level %.

Figure 5.4 is an impact energy curve obtained during the drop weight impact tests as a function of the test temperature using the PP 2648 M polypropylene copolymer. The curve is divided into three sections to analyse the data in the ductile, brittle-to-ductile transition and brittle regions of the curve. Table 5.4 is a summary of the individual impact energy results obtained at the three sections of the graph, the mean and standard deviation thereof. To determine the acceptability of the measured impact energy values, the mean energy value is used as a measure of the expected impact energy ($X_{expected}$).

Specimen type	Impact test number	Test temperature (°C)		
		-20	-40	-50
PP 2648 M	X_1	22.7	8.9	1.5
	X_2	22.4	11.3	2.3
	X_3	21.9	15.9	1.6
	X_4	22.7	9.5	1.8
	X_5	22.6	11.7	1.2
	$\overline{X}$	22.5	11.5	1.7
	σ_x	0.3	2.4	0.4

Table 5.4: *Summary of the impact energy data (J) obtained at the different temperatures of the graph in figure 5.4*

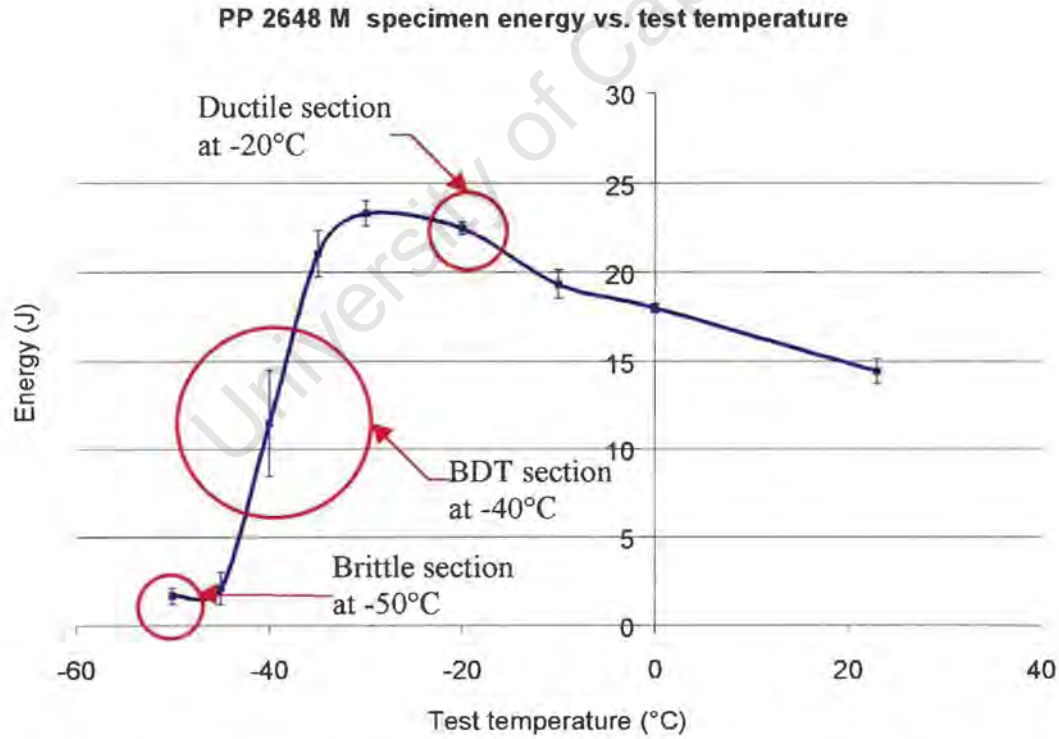

Figure 5.4: *Graph of the impact energy of the PP 2648 M specimen as a function of test temperature showing the three sections used for statistical analysis. The error bars indicate the minimum and maximum energy values obtained.*

The discrepancy between the expected value and the worst energy value (X_{worst}) recorded, i.e. furthest from the mean, is calculated by the equation 5.1 shown below:

$$\text{Discrepancy} = \left| X_{worst} - X_{expected} \right| \qquad \text{(Eq. 5.1)}$$

Since the confidence level of the impact test is determined by the largest error band in the impact tests, the –40°C impact tests are analysed as these show the largest standard deviation. Therefore, the discrepancy value would be 4.4 J. This is incorporated into equation 5.2 to obtain the number of standard deviations (t) by which X_{worst} differs from $X_{expected}$. In the –40°C case, a value of 1.8 is calculated.

$$t = \left\{ \frac{\left| X_{worst} - X_{expected} \right|}{\sigma_x} \right\} \qquad \text{(Eq. 5.2)}$$

$$\text{Probability (outside } t\sigma_x) = 1 - \text{Probability (within } t\sigma_x) \qquad \text{(Eq. 5.3)}$$

$$7.19\% = 100 - 92.81\%$$

Using the table of the normal error integral, the probability of obtaining an impact energy value that differs from $X_{expected}$ by t or more standard deviations can be found. This probability is given by equation 5.3. Therefore, it can be stated that under the assumptions of complete homogeneity in the impact specimens and the Gaussian distribution of the data that there exists only a 7.19% probability that the next impact energy value obtained would lie outside the distribution of the mean. Considering that this is the worst case scenario, the impact data at the other temperatures would therefore show an even lower probability of falling outside their minimum and maximum ranges. Thus, the impact rig and the incorporated cryogenic facility can confidently be used for purposes of determining the brittle-to-ductile transition in different grades of polypropylene copolymers.

5.2 EFFECT OF MATERIAL PARAMETERS ON IMPACT BEHAVIOUR

5.2.1 Melt Flow Index (MFI) Influence on Impact Energy Absorption

To study the effect of the melt flow index on the impact energy, it was necessary to minimise other factors that might contribute to energy absorption and thus provide misleading results. It was therefore decided to examine the effect of MFI in the copolymers and exclude the homopolymer from this analysis. All the copolymers were produced using a nucleating additive agent and thus did not affect this aspect of the investigation.

The ethylene content present in the copolymer is an important factor which also affects the drop weight impact energy of the copolymer. In order to minimise the influence of the ethylene content, it was decided to consider only the copolymers containing the higher percentage ethylene viz. the PP 2540 H, PP 2648 M and the PP 2648 RC specimens. In addition to the ethylene content factor, the brittle-to-ductile transition is yet another factor which should also be eliminated and thus the influence of MFI was studied at 23°C given that none of the three copolymers undergo any form of transition at this temperature.

Figure 5.6 displays an average of the energy results obtained from five drop weight impact tests as a function of the melt flow index of the specimens. The associated error bars are defined by the minimum and maximum values obtained during testing. Clearly, the melt flow index of a copolymer has an effect on its impact resistance as shown in the figure. From the limited data presented in the graph, it appears that there exists an exponential decrease in the absorbed impact energy with increasing MFI. The graph shows a 23% drop in the energy absorption of the polypropylene copolymer as its melt flow index increases from 1.77 to 24.3 g/10min.

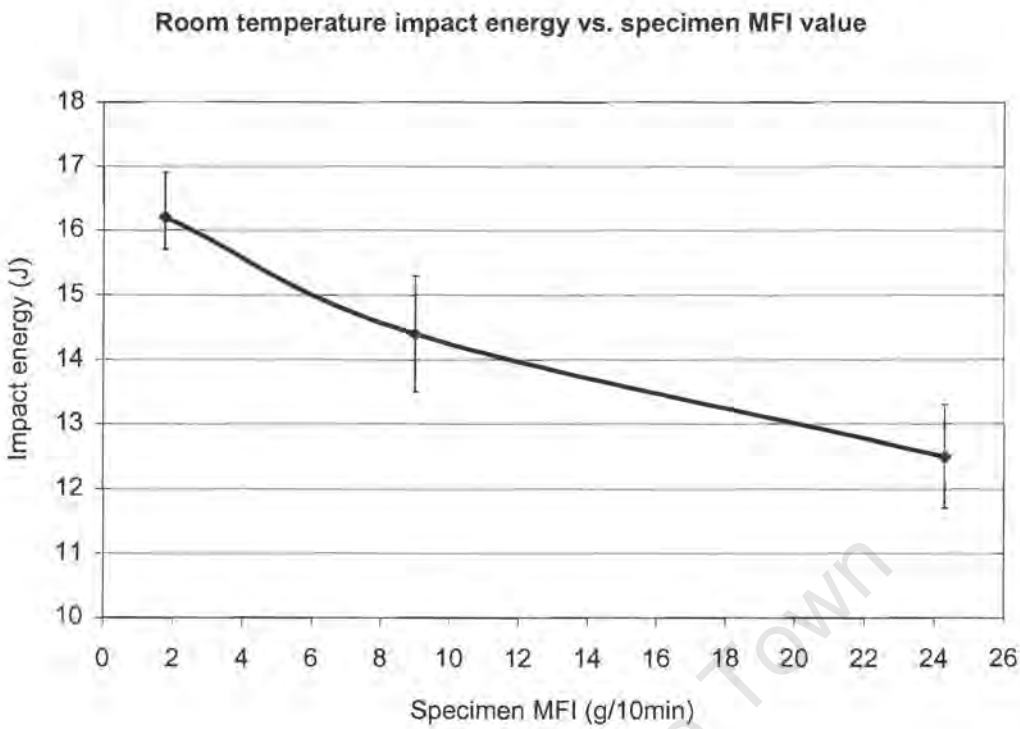

Figure 5.5: *Plot showing the decrease in impact energy observed as the specimen MFI values increase*

5.2.2 Ductility of the Polypropylene Polymers

The ductility ratio values in table 5.5 describe a measure of the ductility of the polymer specimens. These values can only be used to rank the materials in terms of their ductility and do not represent a material property of the polypropylene specimens. The tabulated data show that the effect of introducing low levels of the elastomer is not significant in terms of increasing their ductility. However, additions of the ethylene propylene rubber above 11% have definite implications on the specimen's ability to flow plastically.

The ductility ratio table shows that there is a correlation between the higher ethylene percentages and the resultant increased ductility of the copolymer specimens. It would appear that relatively low ethylene contents do not markedly affect the ductility of the copolymers as seen from the PP 2340 PC specimen containing 6.9% ethylene. Figure 5.6 is a plot of the ductility ratio

as a function of the specimen ethylene content that emphasises the increase in the ductility observed at higher percentages of ethylene content. The dotted line in the graph represents the trendline of the curve. The trendline is used only to show the observed ductility increase.

Specimen type	Ethylene content (wt %)	Ductility ratio (No units)
PP 1147 HQ7	0	0.10
PP 2340 PC	6.9	0.06
PP 2540 H	11.4	0.58
PP 2648 RC	12	0.51
PP 2648 M	13.4	0.58

***Table 5.5**: Tabulation of the ductility ratios in an impact test conducted at 23°C*

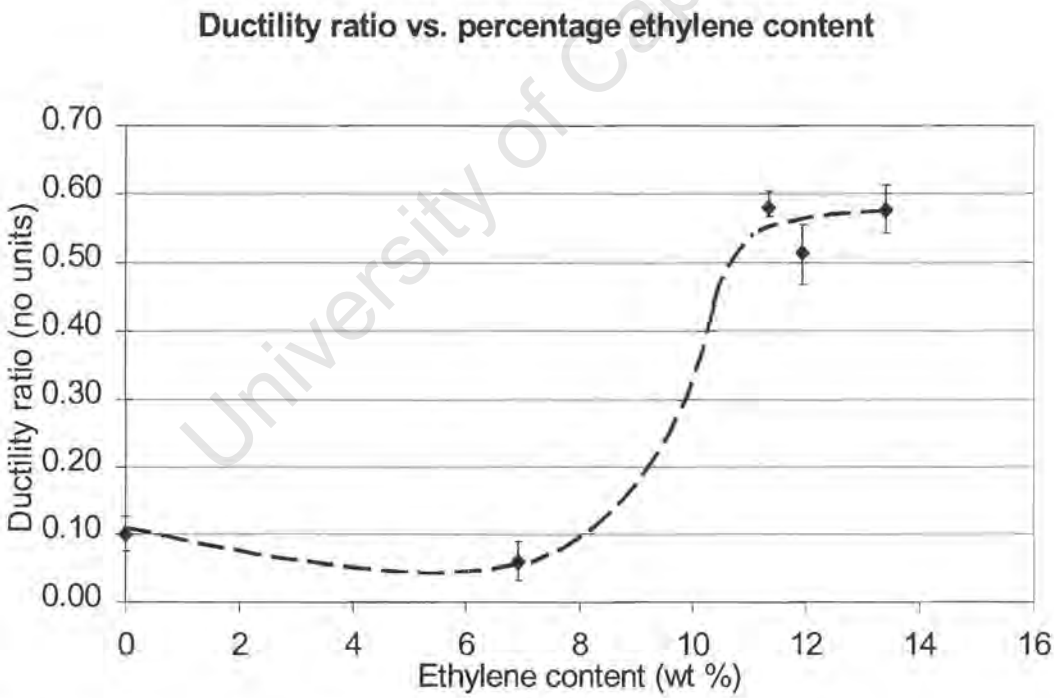

***Figure 5.6:** The plot shows the sharp increase in the specimen ductility at about 11% ethylene content*

5.2.3 Effect of Melt Temperature on Impact Behaviour

The "A" and "B" series copolymer specimens in table 4.3 were impact tested to determine the influence of increasing the melt temperature during the injection moulding stage on the energy absorption capability. The four different copolymers were both injection moulded at a melting temperature of 200°C ("A" series) and with a melt temperature of 230°C ("B" series). The graph in figure 5.7 shows an impact energy drop of between 1 to 8% as the melt temperature is increased to 30°C. The decrease in the impact energy is not very pronounced but appears to show mainly in the high percentages of ethylene content.

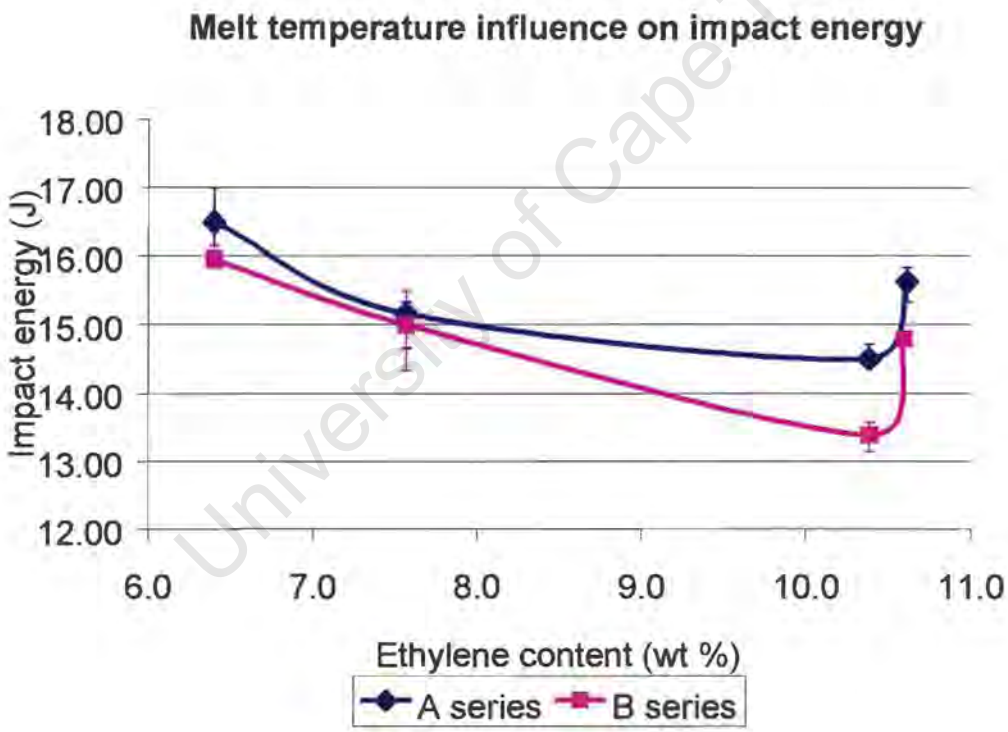

Figure 5.7: *Graph showing the change in impact energy with an increase in melt temperature*

5.2.4 Effect of Ethylene Content on the Impact Behaviour at 23°C

The copolymers listed in table 4.1 were used to examine the effect of ethylene content on the impact behaviour at 23°C. The polypropylene homopolymer was included as a reference material. All the drop weight impact tests were considered complete only when through penetration occurred. Increasing the impact energy and thus the force imposed onto the high % ethylene content specimens was done by raising the tup height to ensure through penetration.

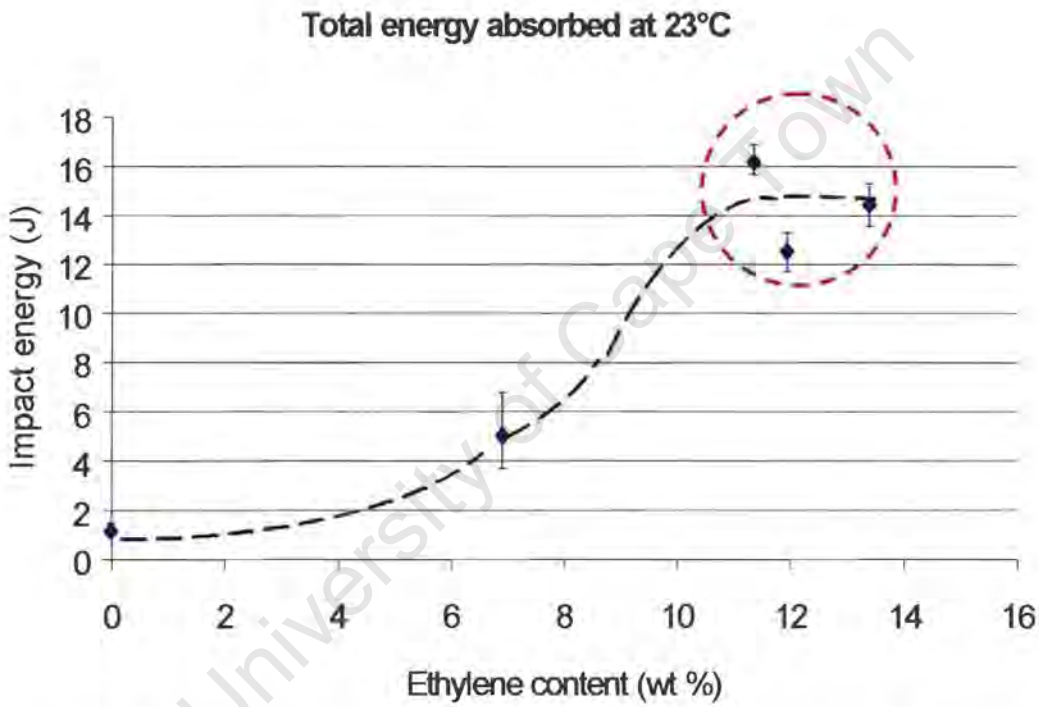

Figure 5.8: *Graph of the results obtained from the drop weight impact tests done 23°C*

All the data pertaining to the instrumented drop weight tests can be found in Appendix A at the end of the thesis. The specific percentages of ethylene content correlating to the various specimens can be found in section 4.2.2. Each data point on the graph in figure 5.8 is representative of an average of five impact tests. The error bars associated with the data points are calculated using the minimum and maximum energy values in the five impact tests. The homopolymer clearly shows the lowest energy absorbed during the impact test. The total energy absorbed increases with ethylene content until a

value of approximately 11% is reached following which some slight fluctuation is observed in the higher percentages of ethylene content.

The high ethylene content copolymers, encapsulated by the dotted circle in figure 5.8, show impact energies of nearly 14 times that of the homopolymer. The highest impact energy absorbed by the PP 2540 H copolymer can be attributed to it having the highest molecular weight (lowest MFI). Although this polypropylene grade had between 1 and 2% lower ethylene contents than the other two grades, the limited number of samples does not allow one to make conclusive judgements about the sensitivity of the molecular weight and ethylene content on impact strength.

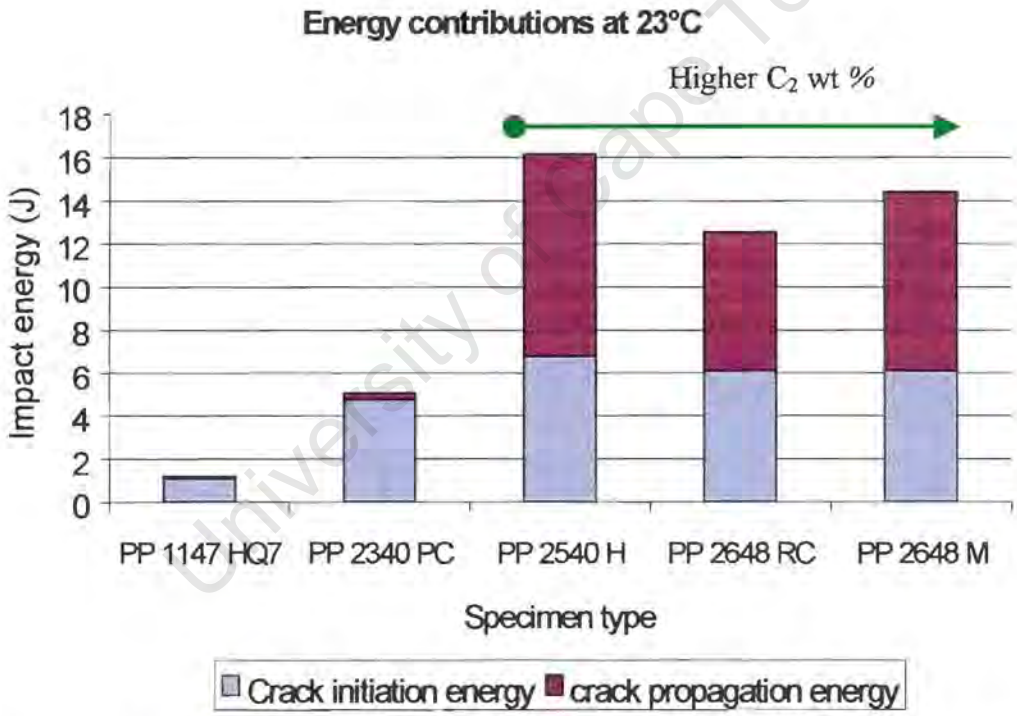

Figure 5.9: *Bar chart showing the increase in the crack propagation energy component of the total impact energy of the specimens*

An examination into the distribution behaviour of the specimens in figure 5.9 reveals that the total energy increases dramatically in the higher ethylene copolymers (refer to green line in figure 5.9) due to a contribution of more than 50% by the crack propagation energy to the total energy impact energy.

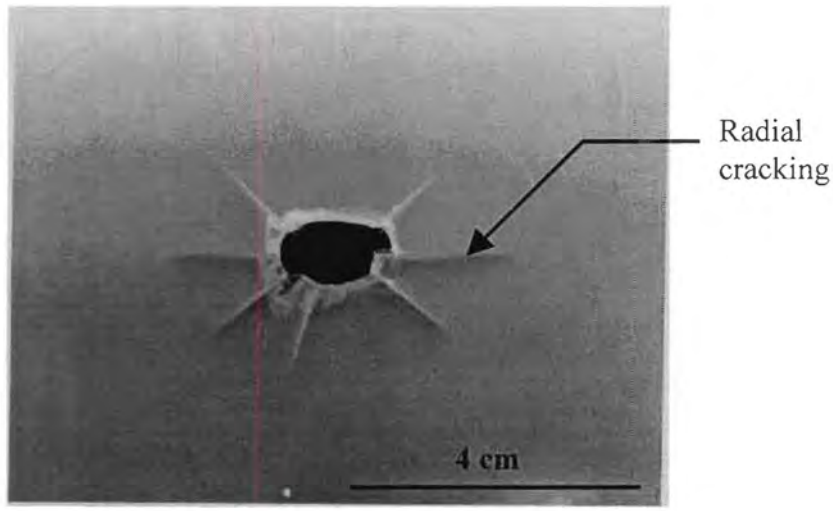

Figure 5.10: *Photograph of the impacted surface of a PP 1147 HQ7 homopolymer specimen*

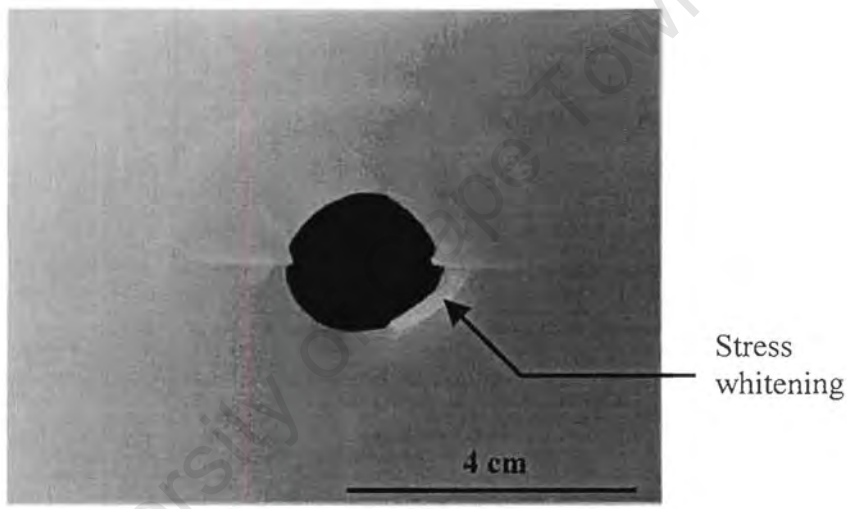

Figure 5.11: *Photograph of the impacted surface of a PP 2340 PC copolymer specimen*

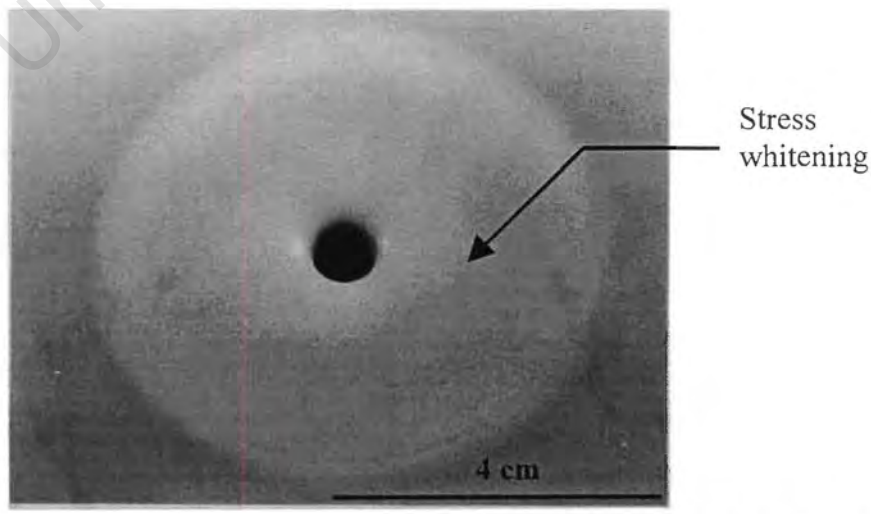

Figure 5.12: *Photograph of the impacted surface of a PP 2648 M copolymer specimen*

Comparatively, the low ethylene content specimen and the polypropylene homopolymer show a contribution of only 8% and 6%, respectively to crack propagation energy. The crack initiation energies of the different specimen grades show an increase with ethylene content before stabilising to about 40% of the total impact energy contribution. The homopolymer shows a brittle failure with radial cracking whilst a ductile type failure is observed in the high ethylene content specimen of PP 2648 M copolymer. This specimen also shows substantial stress whitening which was not observed in the homopolymer. The low ethylene content PP 2340 PC specimen shows some radial cracking with very little stress whitening.

5.2.5 Effect of Different Poly (Propylene – Ethylene) Copolymers on the Impact Energy

Poly (propylene – ethylene) copolymers manufactured by different companies viz., TPC, TARGOR and DOW were tested and compared with the grades produced by Sasol Polymers. A comprehensive list of these copolymers can be found in table 4.4. Figure 5.13 is a plot of the impact energies of the copolymers against their ethylene content. The impact tests were performed at room temperature. The limited copolymer specimens produced by each company and the type of analysis performed does, to an extent, limit the type of information obtained.

An increase in ethylene content and a decrease in melt flow index will tend to increase the impact strength of the copolymers. However, it is clear from table 4.4 and figure 5.13 that some grades have lower percentages of ethylene and relatively high melt flow indexes, yet their impact energies are about 3 times higher than the Sasol Polymers grade of PP 2340 PC. In fact, it would appear that these grades have impact energies in the range of 14 – 17 J, which is relatively insensitive to both, ethylene content and the melt flow index. These "anomalies" will be further analysed in terms of the microstructure of these grades in section 5.4. The higher ethylene content

Sasol Polymer grades have similar energy values as the other copolymer types although they contain a higher percentage of ethylene.

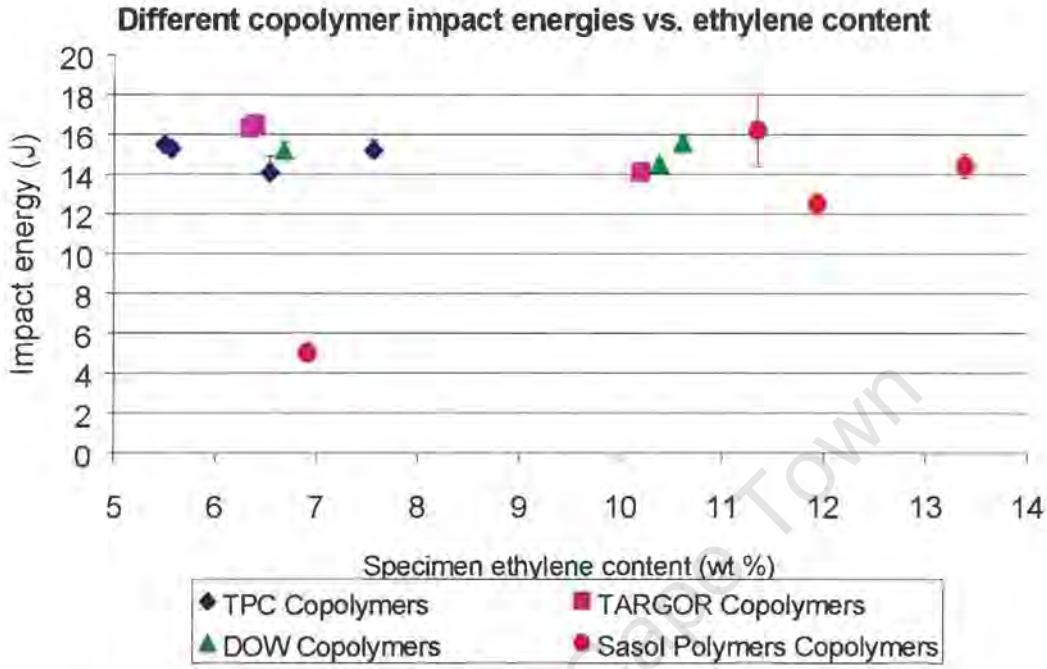

Figure 5.13: *Graph of the impact energies of the different copolymer types as a function of ethylene content*

5.2.6 Comparison of the Impact Ductility Ratio and Maximum Tensile Elongation %

The maximum elongation % data is obtained from tensile tests carried out on the copolymers at Sasol Polymers. This data can be found in Appendix B. The ductility ratio is obtained from the drop weight impact tests and is compared with the maximum tensile elongation % in figure 5.14. The error bars for the elongation data are not shown as only the average values were provided. Sasol Polymers did not test the homopolymer and thus only the copolymers are studied. The graph shows no particular correlation between the two properties. It is however noticed, that both PP 2648 RC and PP 2648 M specimens show a high ductility ratio and tensile elongation. The low tensile elongation % of the PP 2540 H (11.4% ethylene content) specimen can be attributed to its relatively high molecular weight (low melt flow index).

In section 5.2.2, a correlation was found between the ductility ratio and impact energy could be ascribed to the ductility ratios being obtained at high strain rates.

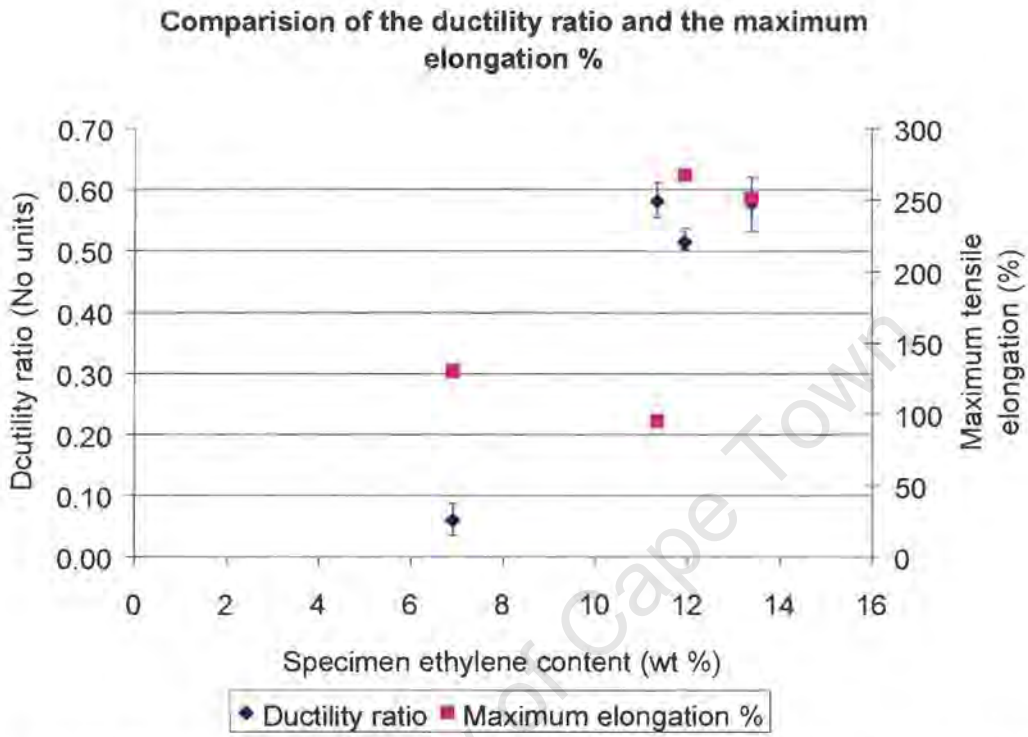

Figure 5.14: *Graph of the copolymer ductility ratio and maximum tensile elongation % as a function of the specimen ethylene content*

5.2.7 Comparison of the Drop Weight and Notched Izod Impact Results

Sasol Polymers performed the notched Izod impact tests and the results are analysed in order to compare them with the drop weight impact test results. The notched Izod impact data can be found in Appendix B. The test temperature and the specimen grades were varied to enable a more comprehensive comparison between the two testing techniques.

The results of the two impact test types are plotted in a graph shown in figure 5.15. The drop weight impact and notched impact test results are demarcated

by the diamond and square shaped data markers, respectively. The different ethylene contents of the specimens can be distinguished by the colour of the markers irrespective of the test type. Furthermore, a solid thin line is used to link the drop weight impact results for a particular specimen, whereas a dotted thick line is used for the notched Izod impact tests.

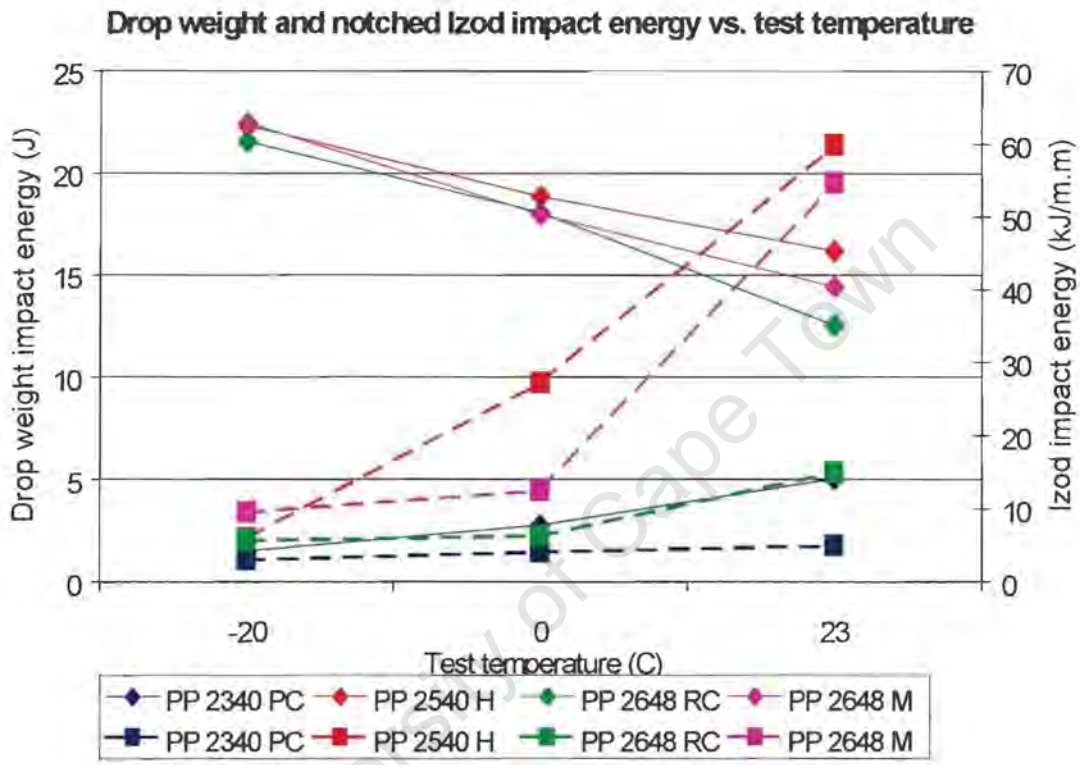

Figure 5.15: *Graph showing the difference in the notched impact and drop weight impact test results for various polypropylene specimens. The solid line denotes the drop weight impact test results and the dotted line denotes the notched Izod impact test results*

The polypropylene homopolymer was not tested by Sasol Polymers and was therefore also excluded from this study. The impact energies are plotted at test temperatures of 23°C and -20°C. The Izod impact test results show a drop in energy with decreasing test temperature for all the copolymers. The high ethylene containing copolymers show an increasing in drop weight impact energy with decreasing temperature. The low ethylene content PP 2340 PC specimen displays a decrease in drop weight impact energy as the test temperature is lowered.

5.3 EFFECT OF ETHYLENE CONTENT ON THE BDT TEMPERATURE

5.3.1 Determination of the BDT Temperature

The results of the drop weight impact tests carried out at various temperatures and for specimens of varying ethylene content are shown in table 5.6. These impact energy values are used to determine the brittle-to-ductile transition temperatures of the specimens. For each specimen type, five impact tests are conducted and the average impact energy together with their standard deviations is presented in the table. The individual impact curves can be found in Appendix C. Although a test temperature interval of 10°C was used to obtain the impact energy curves, further refinement of the temperature was required for some specimens to obtain a better indication of their brittle-to-ductile transition temperature. Hence a temperature interval of 5°C was used around the transition temperature of those specimens.

The maximum and minimum impact energies for all the tests fell within a confidence interval of more than 93% as was determined in section 5.1.5. The homopolymer and the low ethylene containing copolymer were tested at temperatures above room temperature as it was found that they displayed brittle behaviour even at room temperature. A graphical representation of the impact data is shown in figure 5.16 where the impact energy is plotted against test temperature for each polypropylene polymer type. The error bars indicate the minimum and maximum energy values obtained during impact testing.

The graphs in figure 5.16 clearly show that there exists a definite influence of test temperature on impact energy response of the different polypropylene grades. As the test temperature is lowered, a dramatic drop in impact energy occurs as the polymer behaviour changes from ductile to brittle over a narrow temperature band. This drop is associated with the brittle-to-ductile transition of the polymers and is significant in terms of the ability of energy absorption in the specimen.

Figure 5.16 also shows that the effect of adding increasing quantities of ethylene suppresses the onset of the brittle-to-ductile transition to lower temperatures. The brittle-to-ductile transition temperature is therefore also lowered. Narrowing the test temperature intervals to 5°C did produce a more accurate representation of the brittle-to-ductile transition in the polymer specimens. An examination of the higher ethylene content copolymer traces reveal that the impact energies increase with decreasing MFI down to the start of the brittle-to-ductile transition region for these copolymers. Moreover, as the test temperature is lowered to -50°C, it can be seen that there is no beneficial effect of copolymerizing polypropylene for impact energy enhancement at very low temperatures.

Test temp. (°C)	***Impact test specimen energies (J)***				
	PP1147 HQ7	***PP 2340 PC***	***PP 2540 H***	***PP 2648 RC***	***PP 2648 M***
40	14.9 (0.5)	- - -	- - -	- - -	- - -
35	14.9 (1.3)	12.4 (0.5)	- - -	- - -	- - -
30	1.9 (0.8)	12.1 (0.9)	- - -	- - -	- - -
23	1.2 (0.2)	5.0 (1.1)	16.2 (0.4)	12.5 (0.5)	14.4 (0.6)
0	1.7 (0.1)	2.8 (0.8)	18.9 (0.7)	18.1 (0.1)	18.0 (0.2)
-10	1.5 (0.3)	2.7 (0.4)	19.6 (0.1)	17.7 (0.5)	19.3 (0.7)
-20	1.3 (0.1)	1.5 (0.2)	22.3 (0.8)	21.6 (0.7)	22.5 (0.3)
-25	- - -	- - -	22.5 (0.3)	21.5 (0.5)	- - -
-30	1.1 (0.1)	0.8 (0.1)	9.7 (1.7)	12.7 (2.3)	23.3 (0.6)
-35	- - -	- - -	- - -	3.9 (1.8)	21.0 (1.0)
-40	- - -	- - -	9.3 (3.4)	2.5 (0.4)	11.5 (2.4)
-45	- - -	- - -	- - -	- - -	2.1 (0.7)
-50	- - -	- - -	- - -	1.6 (0.4)	1.7 (0.4)

Table 5.6: *Tabulation of the average impact energies and standard deviations of the specimens at various test temperatures*

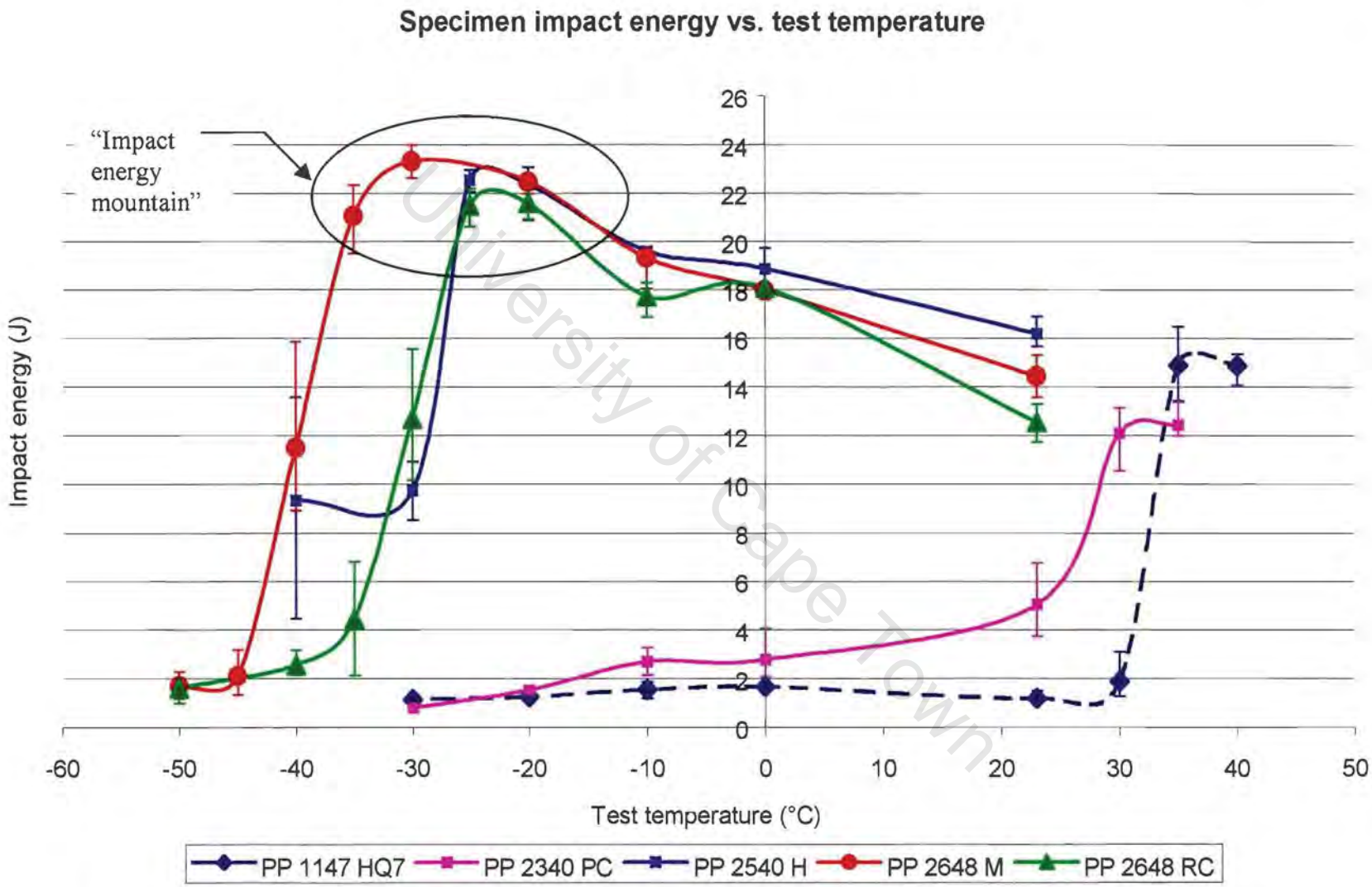

Figure 5.16: *Plot of the various polypropylene specimen drop weight impact energies as a function of their test temperature*

A significant consequence of decreasing the impact test temperature is the energy rise to a maximum value just before the occurrence of the brittle-to-ductile transition. This leads to a formation of an "impact energy mountain" in the impact vs. temperature curves. This behaviour is observed in the high ethylene content specimens and could also occur in the other two polymer specimens should their test temperature range be increased.

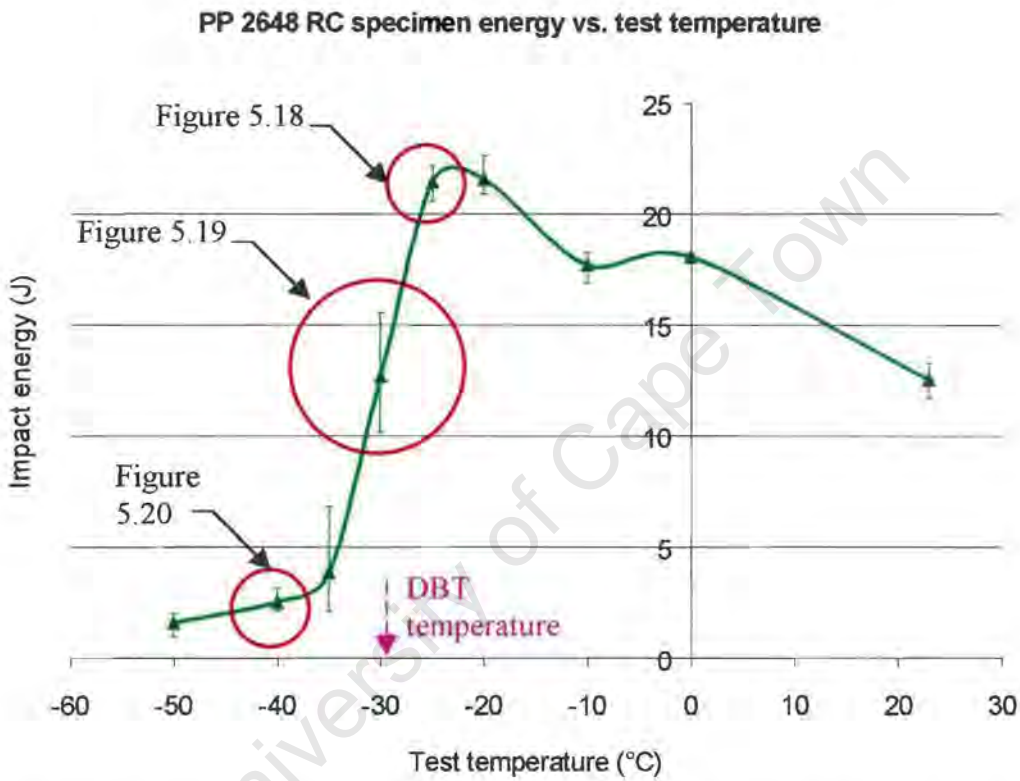

Figure 5.17: *Graph showing the three different regions of the PP 2648 RC trace from which the specimen photographs were obtained*

The PP 2648 RC specimens were chosen to examine the macroscopic effect of the brittle-to-ductile transition behaviour on the specimen's fracture behaviour. The fracture behaviour is examined by noting the characteristics and the pattern of deformation in the specimen at the three test temperatures viz., -25, -30 and -40°C as indicated by the circles in figure 5.17. Figure 5.17 is an impact energy trace of PP 2648 RC specimens. The three temperatures were chosen specifically to examine the specimen's fracture behaviour at a ductile, intermediate and a brittle stage.

Photographs of the impacted specimens at the various stages are shown in the figures as indicated in the graph. Figure 5.18 shows the underside of a specimen impacted in the ductile region. The protruding polymer lip is clear evidence of the gross deformation undergone by the specimen as a result of the impact event. The deformation behaviour seen is characteristic of a ductile mode of failure. The specimen appears to have drawn around the tup as it progressed or penetrated into the specimen thickness until a stage is reached that the polymer material in the shaft of the drawn cup thinned and suffered severe damage leading to the formation of a broken crown. Furthermore, two distinct circular regions of stress whitening are present. One of the stress whitening regions encompasses a circular area of 30 mm with the centre coinciding with the impact point of the tup. The second region of intense stress whitening can be seen in the form of a circumferential ring formed at the base clamping plate support diameter of 50 mm.

The underside of an impacted PP 2648 RC copolymer specimen impacted in the brittle-to-ductile region can be seen in figure 5.19. This photograph differs visibly from that in figure 5.18 with regard to specimen ductility and the absence of the drawn cup formation. Minimal stress whitening is noticed in the proximity of tup contact. The outer circular ring has a lower degree of stress whitening and the ring location is unchanged. However, minute radial cracks that appear to have been formed at the impact point can be seen to grow out towards the edge of the support ring in the clamping plate.

In addition to the formation of the radial cracks, the crack also propagates into the thickness of the specimen from the impact point as demarcated by the red arrow in figure 5.21. This behaviour is typical of the truncated cone type damage that occurs as a result of the Hertzian stresses induced in the polymer by the impact event. The photographic evidence of the specimen fracture surface suggests the occurrence of a brittle failure during impact.

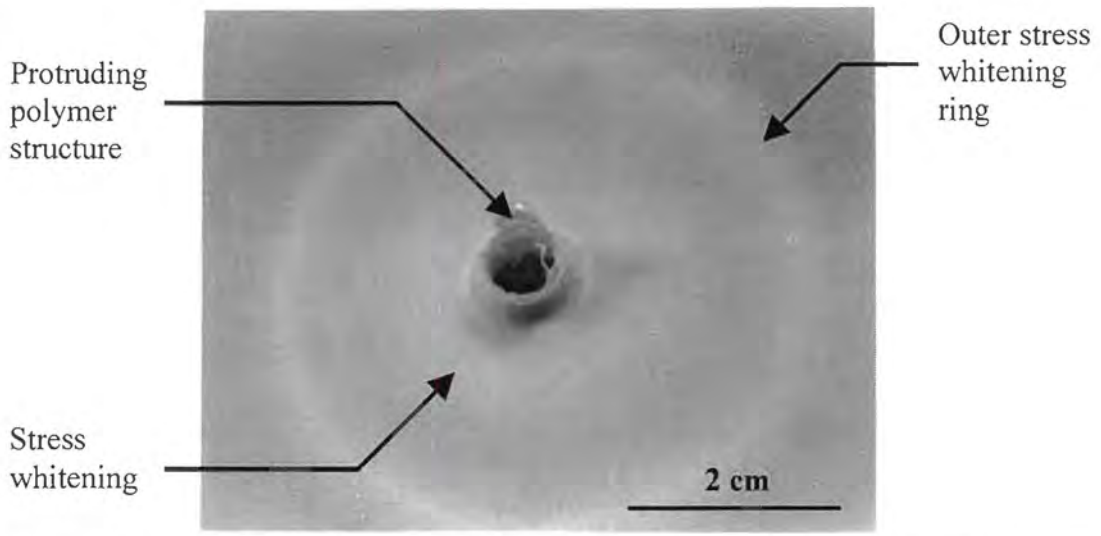

Figure 5.18: *Photograph of the underside of an impacted specimen in the ductile region*

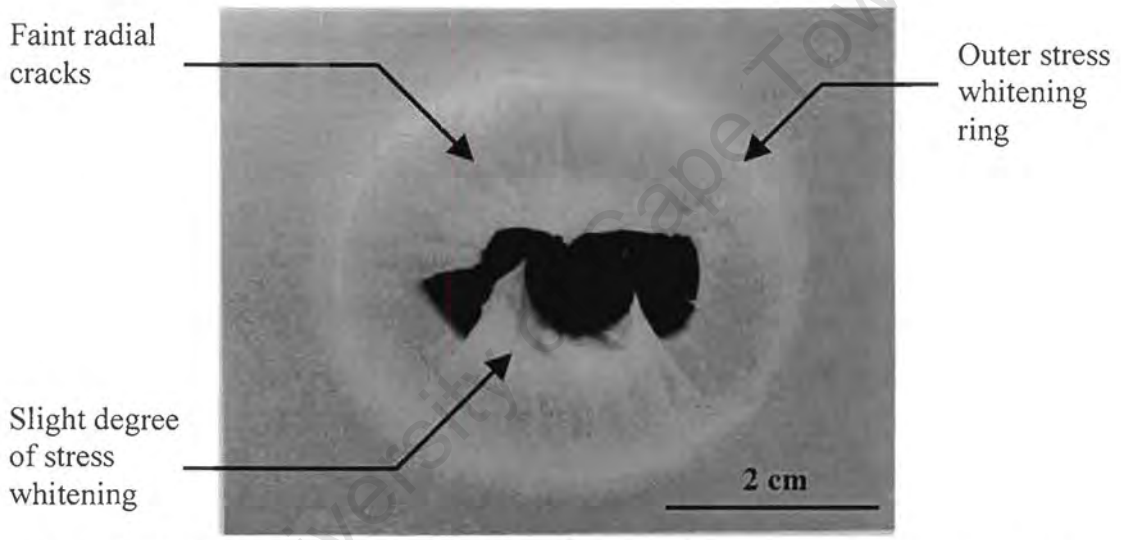

Figure 5.19: *Photograph of an impacted specimen in the brittle-to-ductile transition region*

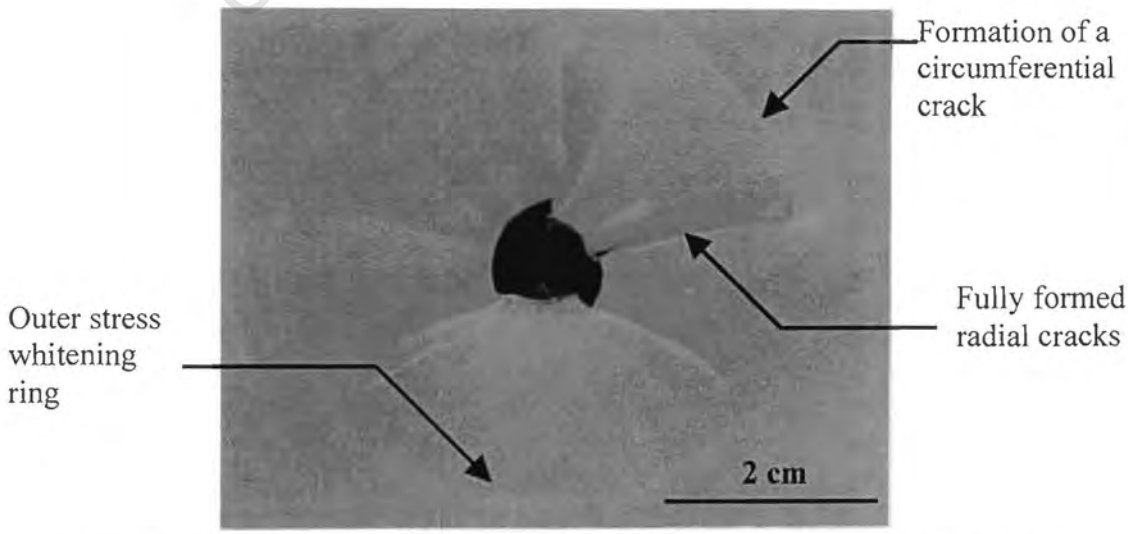

Figure 5.20: *Photograph of an impacted surface of the specimen in the brittle region*

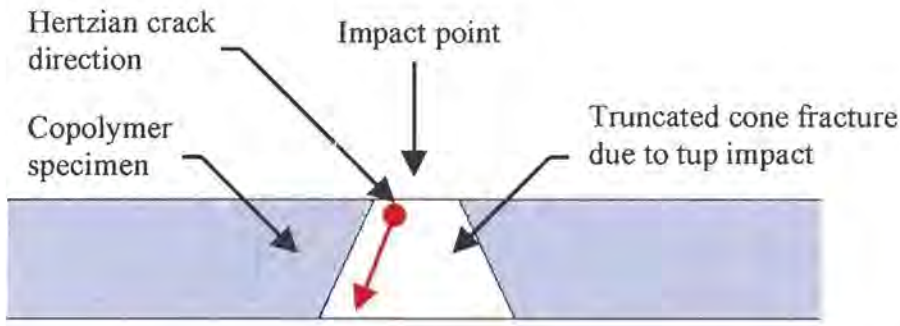

Figure 5.21: *Diagrammatic representation of a cross-section in the specimen showing the truncated cone fracture*

The photograph in figure 5.20 is representative of the impacted surface of a PP 2648 RC specimen at a test temperature of -40°C which is below the brittle-to-ductile transition. A truncated cone damage is also seen in this figure along with the absence of stress whitening. The radial cracks, though, are more visibly noticeable and manage to propagate to the edge of the support ring. Another crack pattern that differs from radial cracking is identified around the edges of the radial cracks. They are thus termed circumferential cracks. The advent of one such crack is shown in figure 5.20. It is important to note the formation of the faint outer stress whitening ring even at these low temperatures.

The specimen energy vs. test temperature graph shown in figure 5.16 is used to determine the brittle-to-ductile transition temperatures for the individual polymer specimens. The transition temperature is determined by following the methodology described in section 2.7, an example of which is shown in figure 5.17. The error associated with the transition temperature is obtained by plotting a trace of the maximum and minimum specimen energy value against test temperature and using them to determine the brittle-to-ductile transition temperatures. Table 5.7 shows the calculated brittle-to-ductile transition temperatures of the respective polymer specimens. The data in table 5.7 verifies that the brittle-to-ductile transition temperatures are suppressed to lower temperatures with increasing ethylene content.

Specimen type	Ethylene content (wt %)	Brittle-to-ductile transition temperature (°C)		
		Minimum	Average	Maximum
PP 1147 HQ 7	0	33	33	33
PP 2340 PC	6.9	27	27	28
PP 2540 H	11.4	-27	-27	-27
PP 2648 RC	12.0	-32	-30	-28
PP 2648 M	13.4	-42	-40	-38

Table 5.7: *Tabular representation of the brittle-to-ductile transition temperatures of the various specimen grades*

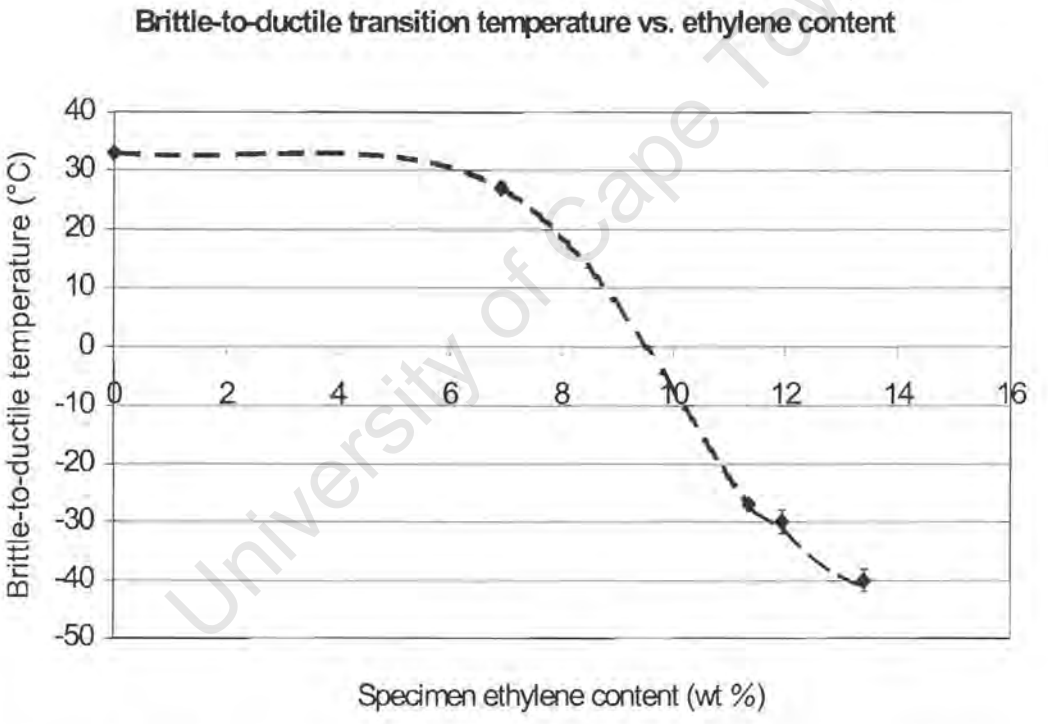

Figure 5.22: *Graph showing the dependence of the brittle-to-ductile transition temperature on the ethylene content*

Figure 5.22 is a plot of the brittle-to-ductile transition temperatures as a function of the ethylene content which illustrates the significance of adding the secondary EPR phase into the polypropylene matrix. The graph shows that the addition of small quantities of the secondary phase do not have a profound effect on decreasing the brittle-ductile transition temperatures as is

observed in additions of greater than 11%. A drastic drop of about 40°C is observed in the transition temperature between the PP 2340 PC and the PP 2540 H specimens.

5.3.2 Force Deflection Curves: Reproducibility of the Traces

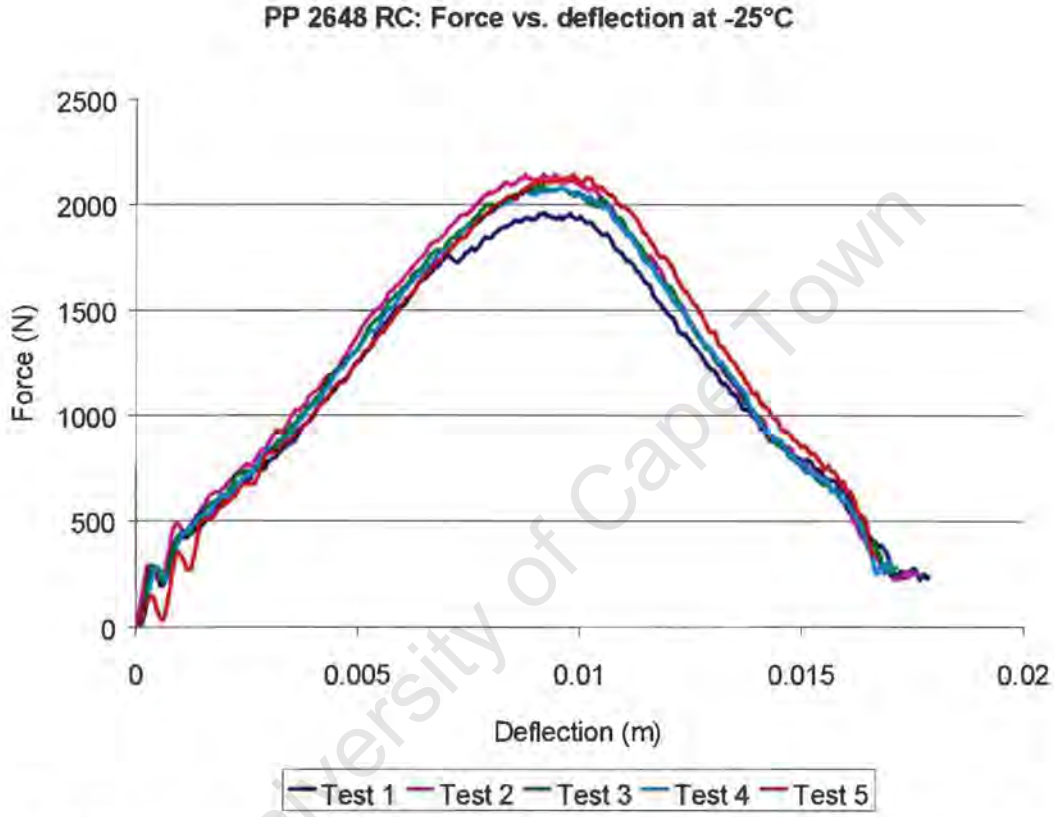

Figure 5.23: *Graph showing the reproducibility of five different force vs. deflection traces of the PP 2648 RC at a test temperature of -25°C*

The traces shown in figure 5.23 are for the PP 2648 RC specimens and are obtained by performing a series of 5 impact tests at a test temperature of -25°C. These traces are statistically analysed for their reproducibility thus giving an estimate of the reproducibility of the other force vs. deflection curves examined in this thesis. The mean impact force ($\overline{X}$) and the standard deviation (σ_x) are calculated from the individual force data (X_1 to X_5) obtained from the traces and are shown in table 5.8. The methodology of the worst case scenario explained in section 5.1.5 is used to determine the level of confidence.

Specimen type	Impact test number	Impact force measurement (N)	Δ between force and mean (N)
PP 2648 RC at -25°C	X_1	1958	116
	X_2	2141	67
	X_3	2085	11
	X_4	2065	9
	X_5	2121	47
	$\overline{X}$	2074	- - -
	σ_x	64	- - -

Table 5.8: *Summary of the impact force data obtained at a test temperature of -25°C*

The last column in table 5.8 shows the largest discrepancy is found in test number X_1. Thus this impact force measurement is used in equation 5.2 to calculate a value for t. The calculated value for t is 1.8. The table of the normal error integral and equation 5.3 indicate that the probability of the next impact force measurement lying outside the distribution of the mean force is 7.2%. The specimens are assumed to be homogeneous and to follow a Gaussian distribution.

5.3.3 Temperature Dependence of the Force Deflection Curves at Constant Ethylene Content

The statistical study for the force vs. deflection curves shows a 93% confidence interval, which is considered to be adequate and thus one force vs. deflection is selected from the impact tests at each test temperature. Figure 5.24 shows the force vs. deflection graphs of PP 2648 RC specimens showing the different traces obtained from test temperatures ranging from 23°C to -50°C. For this study, PP 2648 RC was chosen so that a correlation can be made with the photos in figures 5.18 – 20 and their representative traces. The traces in figure 5.24 can be used to analyse the effect of temperature on the specimen's response to an impact situation.

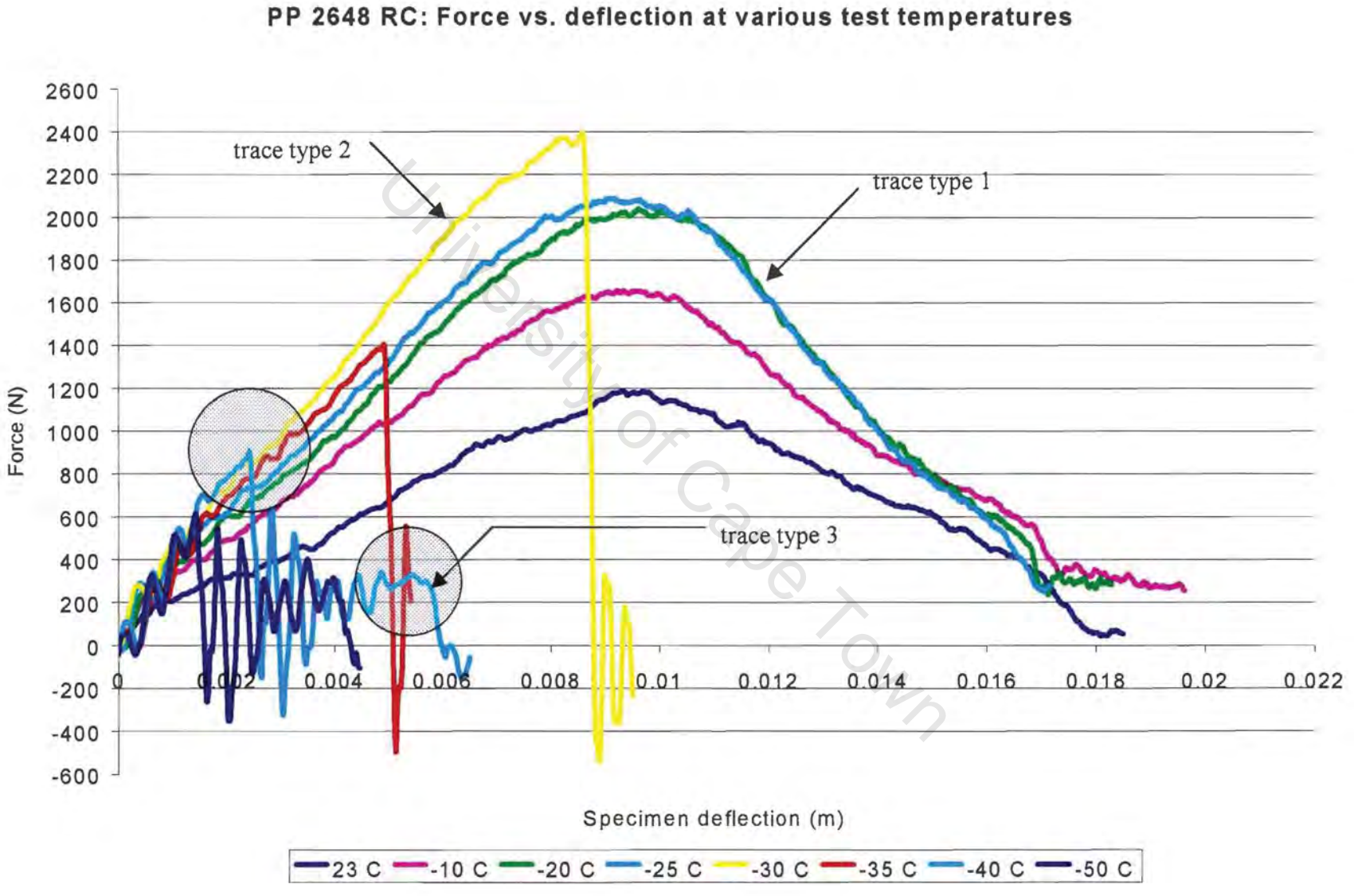

The traces show a gradual increase in the peak force sustained by the specimen as the test temperature is lowered to -30°C. As the test temperature lowered, specimen deflections do not change until a test temperature of -30°C is reached. At this point the specimen is in the brittle-to-ductile region and the deflection drops dramatically as seen in "trace type 2" in figure 5.24. Further lowering of test temperature decreases the peak force as well as the deflection of the specimen. As the test temperature is lowered to the brittle-to-ductile transition temperature of -30°C, an increase in the stiffness of the polymer specimen is observed by the increase in the slope of the elastic deformation region of the traces.

Three basic types of traces as indicated in figure 5.24 can be seen. The test temperatures that mark these traces are 23°C, -30°C and -40°C. Trace type 1 shows a gradual drop in the impact force as the impact test progresses past the peak force stage. The peak force in trace type 2, is followed by a sharp drop in impact force. Towards the end of the test, oscillations in the impact force that are associated with radial cracking are observed. Trace type 3 is different from the first two trace types in that it shows two different peak forces during the impact event. The first peak force is followed by comparatively large oscillations leading to a smaller secondary peak as indicated by the shaded area on trace type 3 in figure 5.24.

The contributions of the crack initiation and crack propagation energy to the total impact energy at the various test temperatures are shown in figure 5.25. An increase in the crack initiation and propagation energy is observed until a test temperature of -20°C is reached. According to the energy vs. temperature graph shown in figure 5.16, this temperature corresponds approximately to the "impact energy mountain". Until the transition is reached, the crack propagation energy constitutes more than 50% of the total energy. At the transition temperature, a dramatic drop in impact energy occurs. Below the brittle-to-ductile transition temperature, the crack propagation energy is less than 5% of the total impact energy.

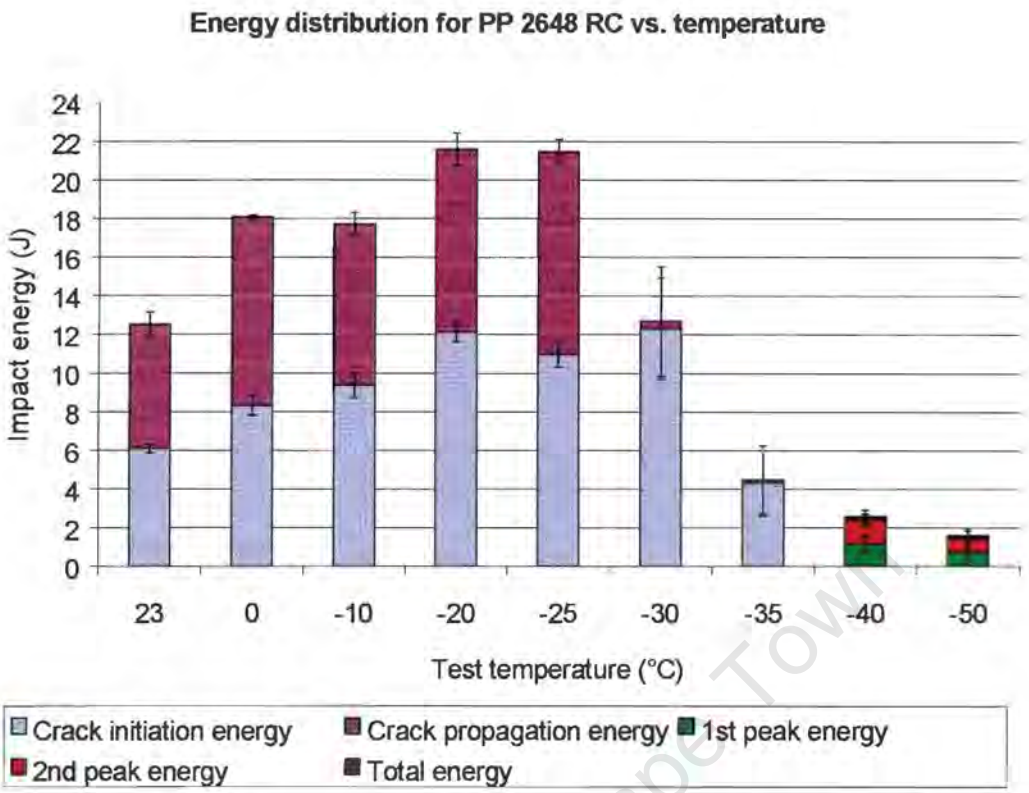

Figure 5.25: *Bar chart representing the different energy contributions of the total impact energy of the PP 2648 RC copolymer*

The brittle-to-ductile transition ends at -40°C introducing a different form of energy distribution to the impact energy. This produces a force vs. deflection trace of the type 3 in figure 5.24. Three different energy contributions are obtained viz., the energy at the first, the energy at the second peak and the final impact energy of the specimen. The first peak energy is associated with radial cracking whilst the secondary peak energy is associated with circumferential cracking.

5.3.4 Ethylene Content Dependence of the Force Deflection Curves at Constant Temperature

At a test temperature of -10°C, the high ethylene content specimen (PP 2540 H) showed ductile behaviour whereas the homopolymer displayed brittle behaviour and the low ethylene content specimen (PP 2340 PC) showed an

intermediate behaviour. Their respective force vs. deflection traces are plotted in figure 5.26.

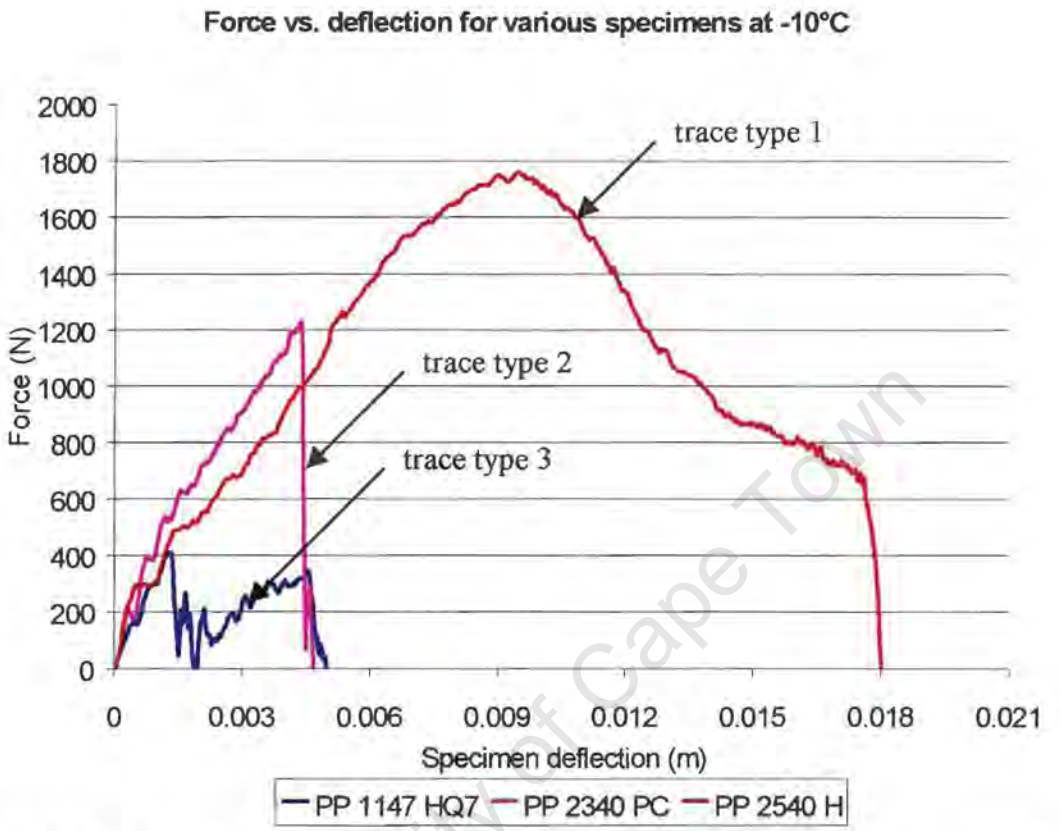

Figure 5.26: *Graphs of the different polypropylene specimen grades at a testing temperature of -10°C*

At this temperature, the peak force drops as the ethylene content increases. The impact response with decreasing ethylene content is similar to the effect of decreasing the test temperature at constant ethylene content. At this temperature, the homopolymer also shows two peaks associated with radial cracking and circumferential cracking as was observed for high ethylene content specimens at very low temperatures in section 5.3.3. The decrease in the ductility of the PP 2340 PC specimen is reflected in a specimen stiffness increase.

Figure 5.27 is a plot of the energy contributions of the respective polymer specimen traces shown in figure 5.26. The polypropylene homopolymer (0% ethylene) could not be analysed in terms of its crack initiation and propagation

energy primarily due to the two peak forces present in the force deflection trace. However, it is clear that ethylene additions of up to 6% have very little effect on impact energy. At low percent ethylene, the crack initiation energy contribution is high. The impact energy increases substantially in the high ethylene containing copolymers. These copolymers have similar contributions from both crack initiation and crack propagation energies.

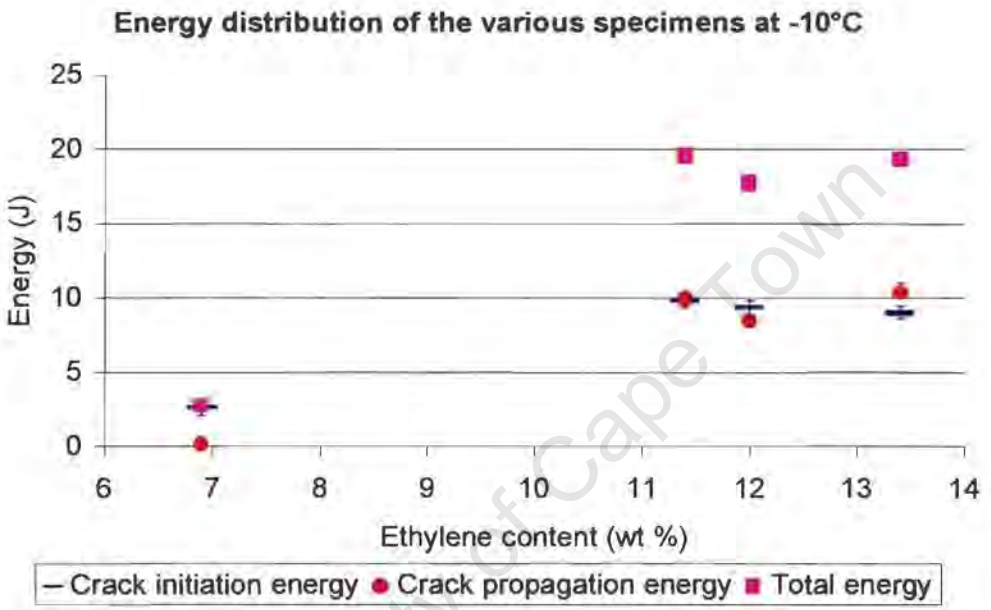

Figure 5.27: *Graph showing the influence of the various energy contributions on the total impact energy*

5.4 SCANNING ELECTRON MICROSCOPY

5.4.1 EPR Particle Analysis

The following SEM micrographs (figures 5.28 – 5.32) are taken of the etched specimens of poly (propylene-ethylene) copolymers in order of increasing ethylene content (see table 4.1). The etchant removes only the EPR particles. The polymer specimens can be identified by the figure captions. Figure 5.28 clearly shows the absence of the pores in the microstructure of the homopolymer polypropylene, whilst the copolymer specimens show a distribution of pores. There appears to be an increase in particle density with

increasing ethylene content. It would also appear that the high ethylene content copolymers have similar microstructure (figures 5.30, 5.31 and 5.32) as compared to the low ethylene containing copolymer of figure 5.29. The SEM pictures are followed by an analysis of the size of the EPR particles and the inter-particle spacing between them. This data is shown in table 5.9.

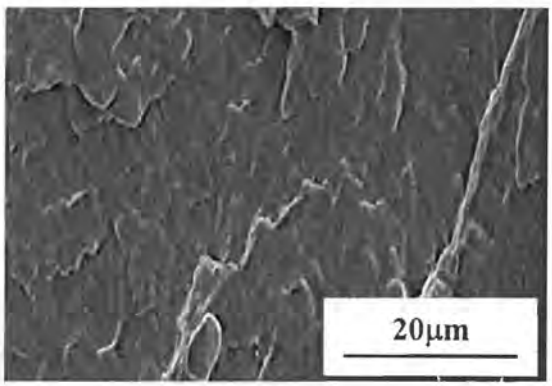

Figure 5.28: *Etched microstructure of PP 1147 HQ7 homopolymer*

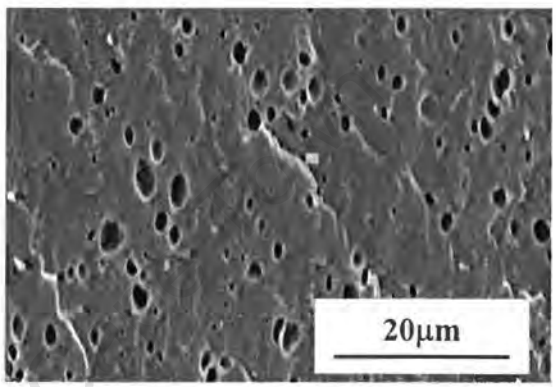

Figure 5.29: *Etched microstructure of PP 2340PC copolymer*

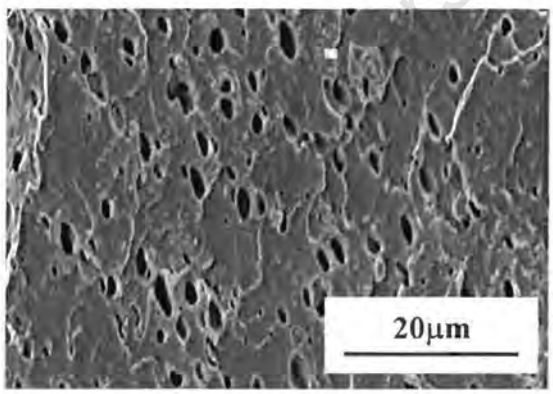

Figure 5.30: *Etched microstructure of PP 2540 H copolymer*

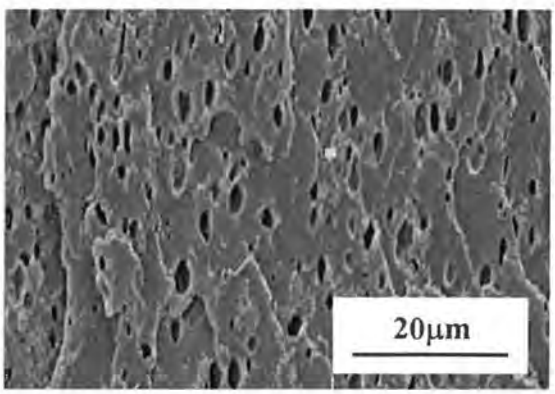

Figure 5.31: *Etched microstructure of PP 2648 M copolymer*

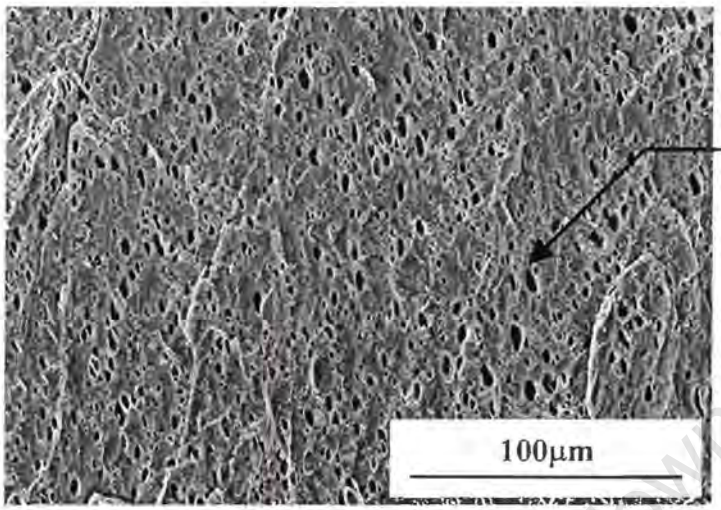

Figure 5.32: *Etched microstructure of PP 2648 RC copolymer*

Specimen type	*Ethylene content (wt %)*	*Average EPR particle size (μm)*	*Average EPR interparticle distance (μm)*
PP 1147 HQ7	0	0	0
PP 2340 PC	6.9	0.89	1.24
PP 2540 H	11.4	1.23	1.77
PP 2648 RC	12	1.23	1.32
PP 2648 M	13.4	1.18	1.26

Table 5.9: *Tabulation of the Sasol Polymer grades and their EPR particle characteristics*

Figures 5.33 to 5.42 are SEM micrographs of the microstructure of the polypropylene copolymers supplied by the various companies. To differentiate between the copolymer specimens, each micrograph is labelled with a figure caption stating the ethylene content of the copolymer and the company it was produced by (see also table 4.4). Table 5.10 shows the results obtained for the EPR particle analysis of these copolymers.

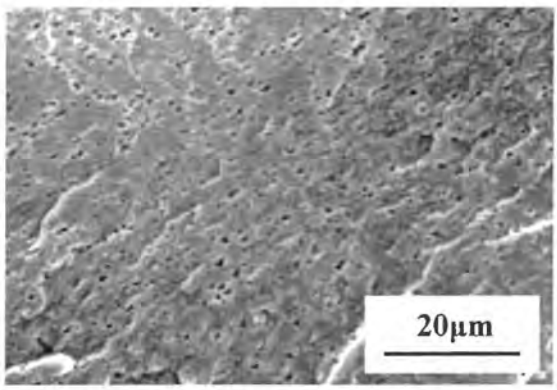

Figure 5.33: *5.5 ethylene % (TPC)*

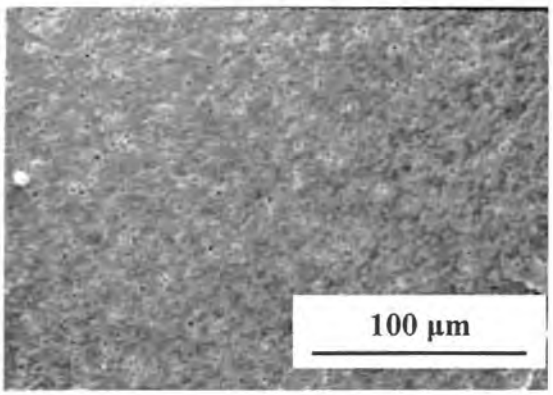

Figure 5.34: *5.6 ethylene % (TPC)*

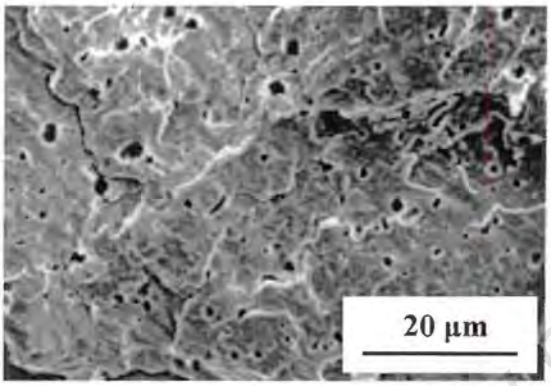

Figure 5.35: *6.5 ethylene % (TPC)*

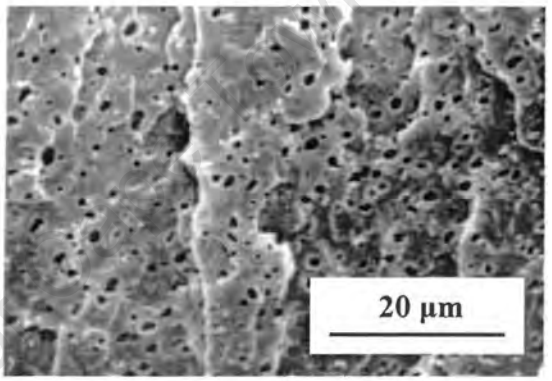

Figure 5.36: *7.6 ethylene % (TPC)*

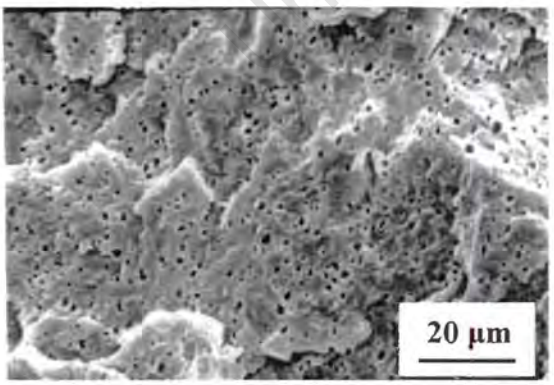

Figure 5.37: *6.3 ethylene % (TARGOR)*

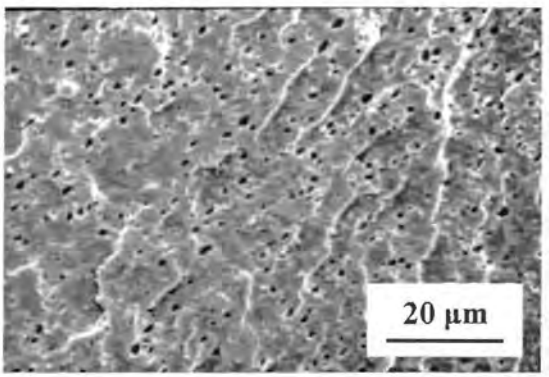

Figure 5.38: *6.4 ethylene % (TARGOR)*

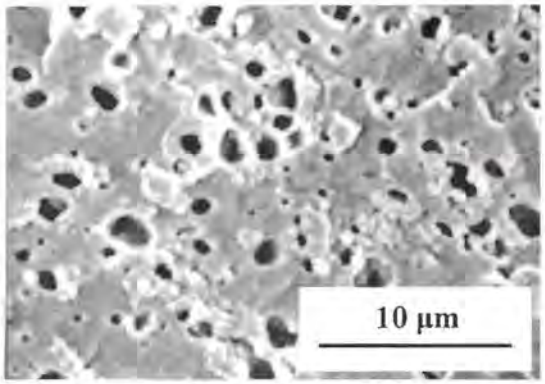

Figure 5.39: *10.2 ethylene % (TARGOR)*

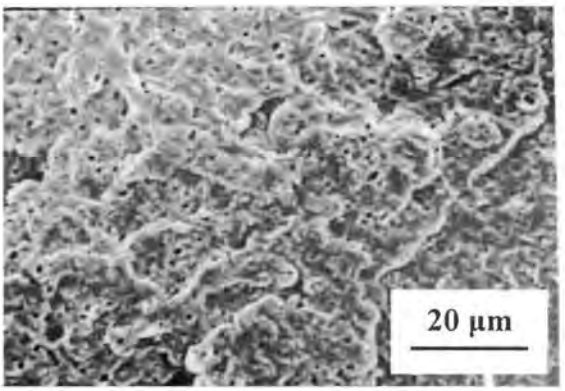

Figure 5.40: *6.7 ethylene % (DOW)*

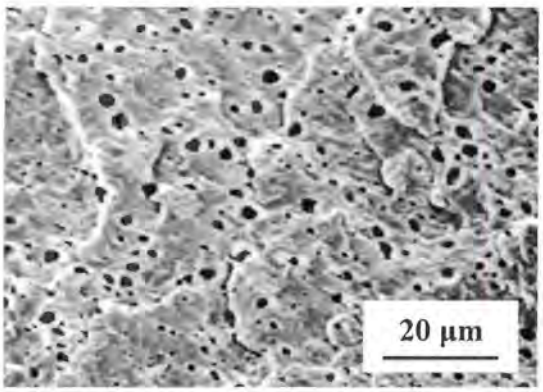

Figure 5.41: *10.4 ethylene % (DOW)*

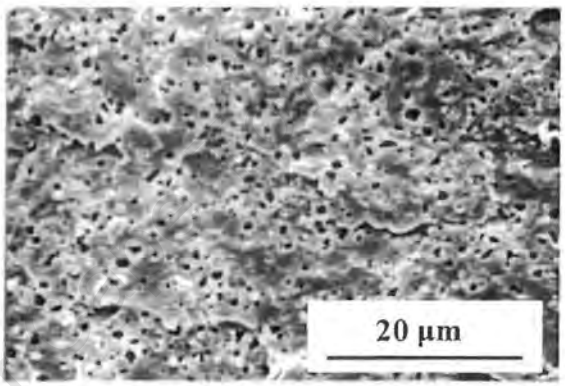

Figure 5.42: *10.6 ethylene % (DOW)*

Specimen type	*Ethylene content (wt %)*	*Average EPR particle size (µm)*	*Average EPR interparticle distance (µm)*
PP 2340 PC	5.5 (TPC)	0.59	1.35
PP 2340 PC	5.6 (TPC	1.19	3.29
PP 2448 TC	6.5 (TPC)	0.67	2.02
PP2648 RC	7.6 (TPC)	0.66	1.35
PP 2348 M	6.3 (TARGOR)	0.86	2.05
PP 2348 M	6.4 (TARGOR)	0.89	1.80
PP 2600 PC	10.21(TARGOR)	0.86	0.96
PP 2448 TC	6.7 (DOW)	0.80	1.83
PP2648 RC	10.39 (DOW)	1.31	2.17
PP2648 RC	10.62 (DOW)	0.62	1.75

Table 5.10: *Tabulation of the various copolymer types and their EPR particle characteristics*

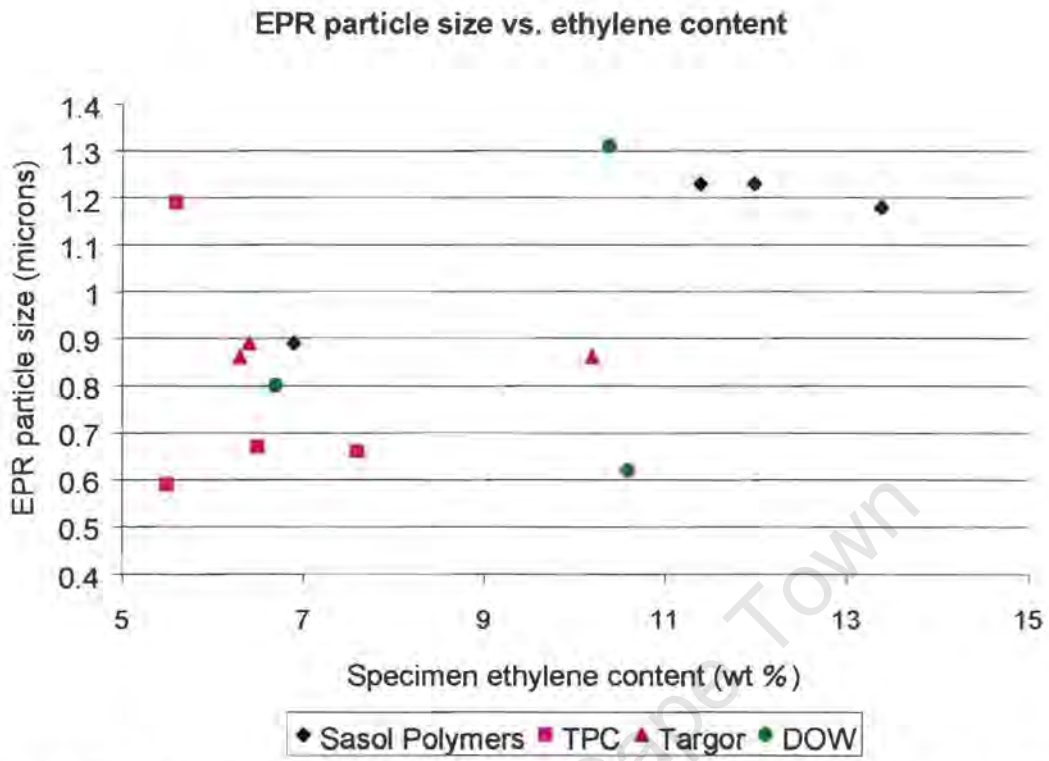

Figure 5.43: *Plot of the average EPR particle size of the copolymers as a function of their ethylene content*

Figure 5.43 shows the dependence of the average EPR particle sizes of the Sasol Polymer grades on the weight % of ethylene in the copolymer. The high ethylene containing grades show a larger EPR particle size compared to the low ethylene content PP 2340 PC grade. Literature suggests that polypropylene copolymer systems have an optimum particle size of approximately 0.4 μm. The SEM analysis results show that the EPR particle sizes range within a band of 0.6 μm to 1.3 μm.

Figure 5.44 is a graph of the EPR interparticle distance plotted against the specimen ethylene content. The interparticle distances are calculated by using the average EPR particle size and the area or volume fraction obtained from the analysis. It is expected that the interparticle distance between EPR particles should decrease with increasing ethylene content. However, the results in figure 5.44 do not follow this trend due to changes in the distribution of the EPR particle sizes within the specimen grades. The TARGOR

copolymers exhibit the expected decrease in the EPR interparticle distance with increasing ethylene content. It should be noted that the interparticle distances between the secondary EPR phase are concentrated within a band of 0.5 μm and 2.5 μm irrespective of the ethylene % as seen in figure 5.44.

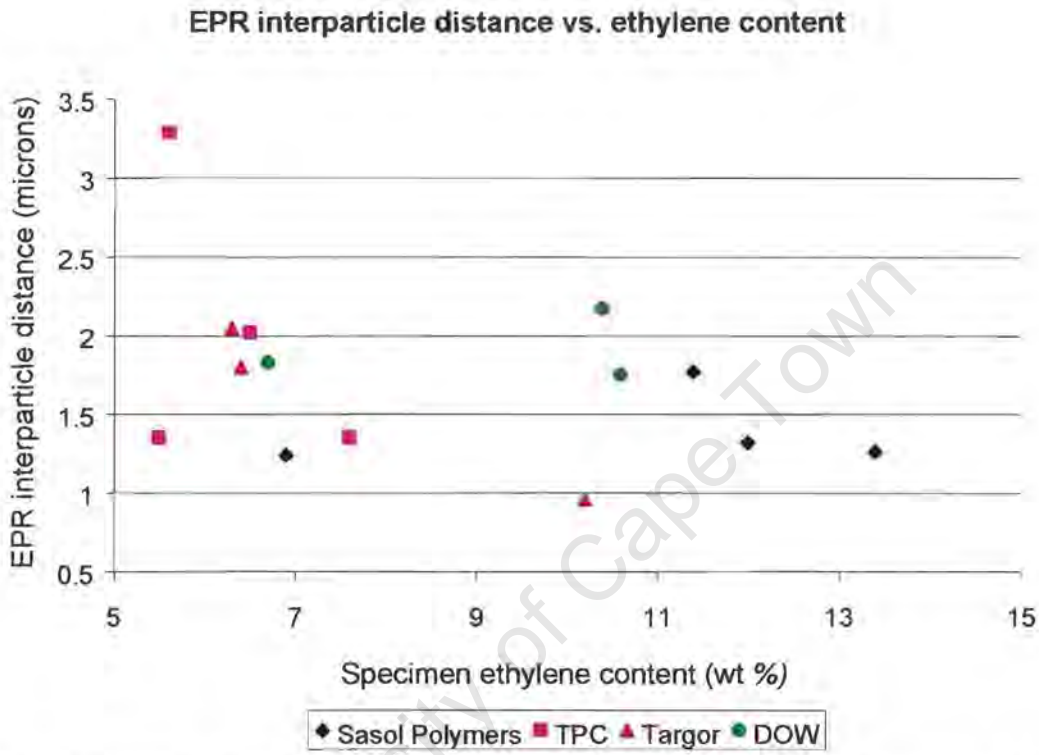

Figure 5.44: *Graph showing the average interparticle distance between the dispersed EPR particles in the different copolymer types*

The results shown in figure 5.43 and 5.44 can be explained by examining the particle size distribution graphs. Figure 5.45 shows the normalised EPR particle size distribution graphs for the Sasol Polymer grades. The number of EPR particles is normalised to allow for a valid comparison between different copolymers. All the Sasol Polymer grades as well as the TPC, DOW and TARGOR grades show the presence of a tail in the EPR particle size distribution plots. The length of the tail varies between the copolymers grades. In particular, the PP 2648 RC grade shows the longest tail amongst the Sasol Polymer grades.

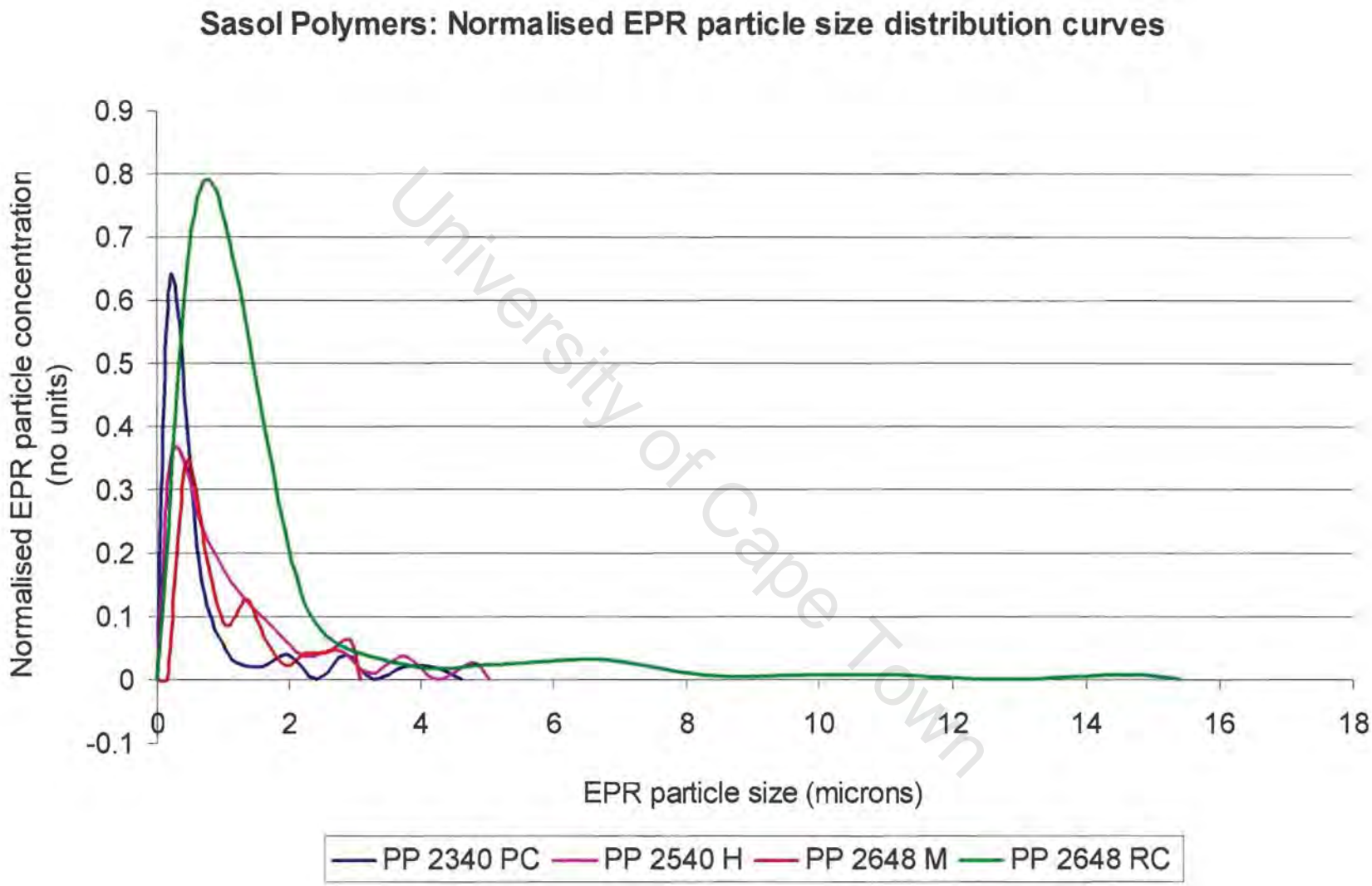

Figure 5.45: *Normalised EPR particle size distribution curves for the different Sasol Polymer grades*

The controlled rheology grades viz., PP 2340 PC and the PP 2648 RC show a symmetric particle size distribution about their peak values in the normalised distribution graphs. This is not the case with the other two polypropylene copolymer grades. The normalised particle size distribution graphs for the TPC, TARGOR and DOW copolymer types can be found in Appendix D. Table 5.11 shows the Karl Pearson coefficient of skewness of the normalised particle size distribution curves for the different copolymer grades.

Specimen type	***Supplier***	***Ethylene content (wt %)***	***Coefficient of skewness (no units)***
PP 2340 PC	Sasol Polymers	6.9	1.3
PP 2540 H	Sasol Polymers	11.4	1.1
PP 2648 RC	Sasol Polymers	12.0	1.1
PP 2648 M	Sasol Polymers	13.4	1.2
PP 2340 PC	TPC	5.5	0.7
PP 2340 PC	TPC	5.6	1.1
PP 2448 TC	TPC	6.5	1.1
PP 2648 RC	TPC	7.6	1.0
PP 2348 M	TARGOR	6.3	1.1
PP2348 M	TARGOR	6.4	0.9
PP 2600 PC	TARGOR	10.21	1.1
PP 2448 TC	DOW	6.7	1.1
PP 2648 RC	DOW	10.39	0.9
PP 2648 RC	DOW	10.62	0.8

Table 5.11: *Tabulation of the Karl Pearson coefficient of skewness*

The normalised particle size distribution curves for various copolymers with an ethylene range of between 5 to 7% are plotted in figure 5.46. Figure 5.47 shows the distribution curves for copolymers within an ethylene range of between 10 to 12%. The results of the analyses of these graphs are tabulated in table 5.11. There appears to be a correlation between the shape of the normalised distribution curves and the average interparticle distance between the EPR particles. A narrow distribution of particle sizes about the

peak particle size leads to a smaller interparticle distance as seen for the 5.5 ethylene % TPC grade in figure 5.46. The broader distribution curve of TPC containing 5.6% ethylene has a higher average interparticle distance. Similar trends can also be deduced from the higher ethylene containing copolymers in figure 5.47. The DOW grade with 10.39% ethylene has a higher interparticle distance compared to the DOW grade containing 10.62% ethylene due to a broader particle size distribution.

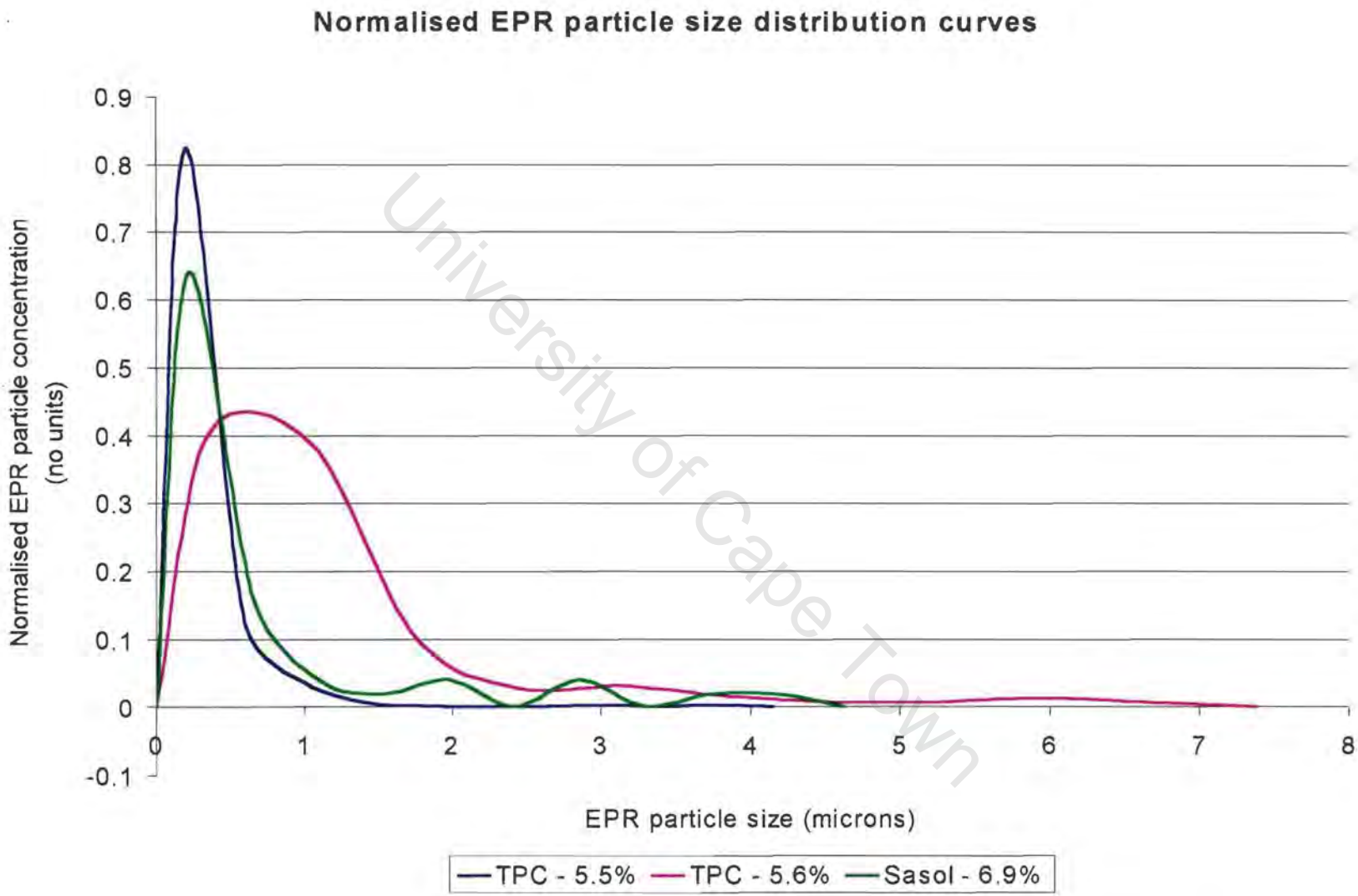

Figure 5.46: *Graphs of the normalised particle size distribution curves for an ethylene range of between 5 to 7%*

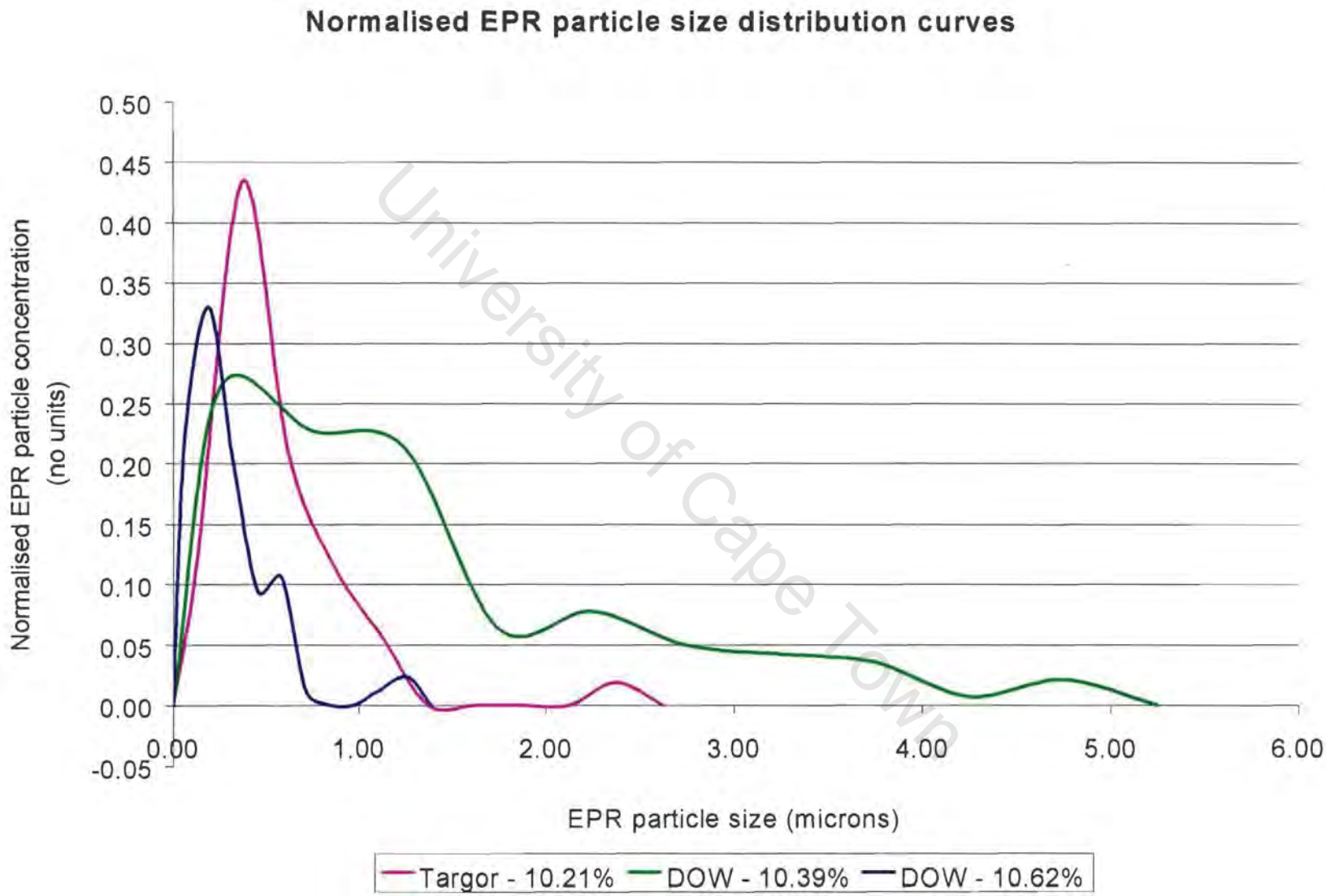

Figure 5.47: *Graphs of the normalised particle size distribution curves for an ethylene range of between 10 to 12%*

CHAPTER 6

DISCUSSION

The mechanical properties of copolymers are sensitive to their microstructure and to the type of loading imposed onto the copolymer. This investigation focuses on poly (propylene – ethylene) copolymers and their impact behaviour as their material parameters are varied. Of particular interest is the influence of temperature and ethylene content on the drop weight impact behaviour of the copolymers. An understanding of the influence of temperature and the material parameters contributes significantly to the efficient use of the poly (propylene-ethylene) copolymers in day to day applications.

6.1 THE REPRODUCIBILITY OF THE DROP WEIGHT IMPACT TEST RIG

The reproducibility of the impact test results obtained from the poly (propylene – ethylene) copolymers is dependent on the reproducibility of drop weight impact testing and on the homogeneity of the test specimens. To investigate the reproducibility of the drop weight impact tester, test parameters that could introduce variability were identified and investigated. These are the tup release height, load cell calibration coefficient and the incorporated cryogenic temperature facility. The tup release height was varied at constant copolymer type and test temperature. The load cell is responsible for determining the impact force during the test and was calibrated according to the methodology described in section 5.1.1 before the impact tests were performed. The statistical study of the force deflection curves (see section 5.3.2) showed a probability or confidence level of 93% which is also a measure of the accuracy of the load cell.

The function of the cryogenic temperature facility was to maintain a specified specimen impact test temperature. The test temperature was regulated by means of a temperature controller unit that has an accuracy of 0.5% full-scale ± 1°C. However, the operation of the cooling disk system requires that the copper disk be removed from the polymer specimen surface before the impact test is allowed to proceed. During the time period of the copper disk removal and tup contact with the polymer specimen, the specimen temperature rises by approximately 5°C. However, this time period is not constant and is a function of the operator's swiftness and the data acquisition software package since the release mechanism of the tup is triggered by a computer activated solenoid. This results in a 2°C operational accuracy of the low temperature facility.

The cooling disk system was used because it showed a number of advantages over the vapour cooling system and the coiled cooling system. The simplicity of the design and the physical contact between the copper disk and the polymer specimen were among the main advantages of the cooling disk system. It is possible to increase the accuracy of the test temperature by incorporating an environmental chamber around the specimen clamping mechanism. It was assumed that the Sasol Polymer test specimens had a homogenous microstructure in relation to the size, shape and spatial distribution of the EPR particles within each specimen grade. A constant test specimen thickness of 3 mm was used during impact testing as the 2 mm thick specimens yielded erroneous results due to excessive vibration. The specimen clamping mechanism was firmly secured before proceeding with the impact tests to minimise any possible vibration of the 3 mm thick test specimens.

6.2 INTERPRETATION OF THE IMPACT TEST RESULTS

The two most important plots obtained from an impact event are the impact force and the absorbed energy vs. specimen deflection. They provide vital information with respect to the specimen's response during an impact loading

event. Figure 6.1 illustrates the results obtained from the data acquisition software of the instrumented drop weight impact tester. The traces shown in figure 6.1 are overlays that demonstrate the reproducibility of the drop weight impact tester. A detailed description of the impact event is given in Appendix E. Information such as the total impact energy, crack initiation and propagation energies of the test specimens can be obtained by determining the respective areas under the force vs. deflection curve of those specimens.

This information can be used to calculate the ductility ratio and rank the specimens in terms of their ductility and ethylene content. These properties can be correlated with the obtained impact energies thereby allowing an understanding of the copolymer's response to an impact event. In addition to this, examining the slope of the trace between point A and B also provides a means to compare the modulus of the different copolymers.

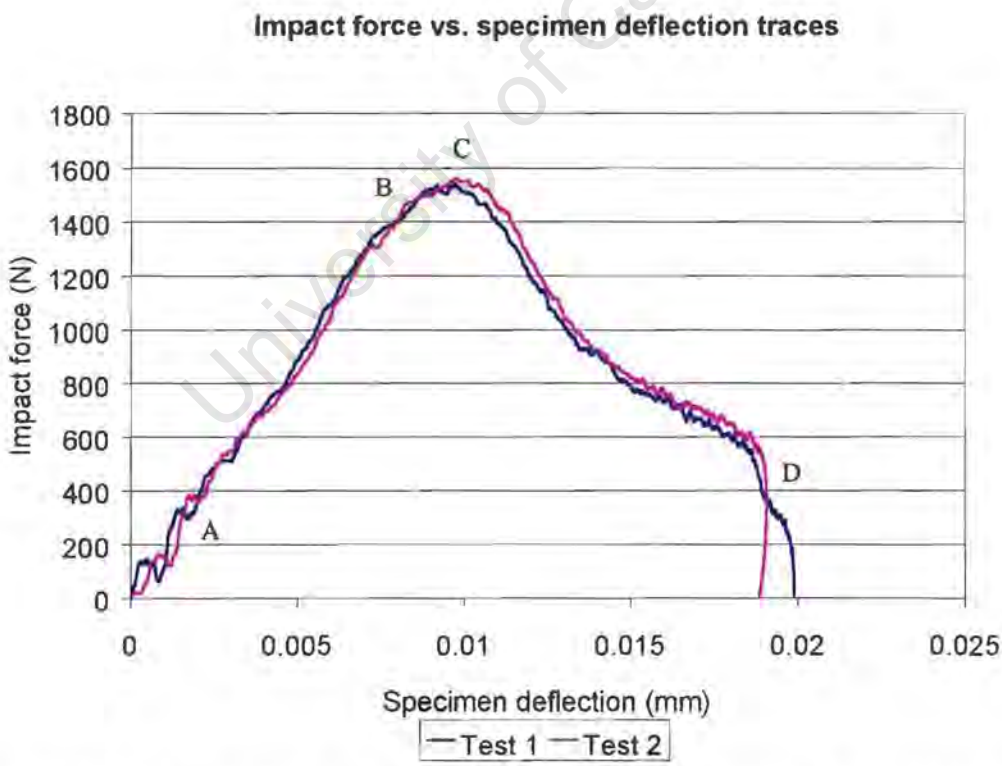

Figure 6.1: *Graph showing the plot of force as a function of deflection with the characteristic points in an impact event*

It was found that the modulus of the polypropylene copolymer increases with decreasing temperature until the test temperature reaches the brittle-to-ductile transition temperature of that particular copolymer. Further lowering of the test temperature, results in a dramatic drop in the copolymer's impact strength (refer to figure 5.24). It is postulated that at temperatures lower than the brittle-to-ductile transition temperature, crazes nucleate at a few sites only because it is more favourable for the nucleated crazes to propagate rather than for new craze sites to be nucleated.

Above the brittle-to-ductile transition temperature, both the crack initiation and crack propagation energy is high but as the test temperature is lowered below the brittle-to-ductile transition temperature, the crack propagation energy is very small as was shown in figure 5.25. At these temperatures the crazes still require a relatively high crack initiation energy but once the crazes are formed, they easily develop into a critical size leading to the formation of cracks. These cracks propagate either through chain scission or inter-spherulitically. At very low temperatures molecular relaxation does not offer a viable method for energy dissipation. Therefore shear yielding does not occur at these low temperatures and high strain rates. Van der Waal *et al* also did not find any evidence of crazing at very low temperatures[17].

At temperatures above the brittle-to-ductile transition temperature, it is easier to nucleate new crazes rather than to propagate the nucleated crazes because the crack propagation energy is higher than the crack initiation energy (refer to figure 5.25). Hence many crazes are formed which is manifested in the form of stress whitening as was shown in the example of figure 5.18.

As the ethylene content increases, the shape of the force vs. deflection traces change from a brittle to ductile type as seen in figure 5.26. The energy dissipated by the polymer increases with ethylene content due to an increase in the concentration of the EPR particles in the copolymer. Crazing occurs in all the polymers but the magnitude of crazing is reduced in the polypropylene homopolymer and the low ethylene content specimen as seen in figures 5.10,

and 5.11. Fewer crazes formed in the low ethylene containing copolymers since the concentration of EPR particles that can act as initiation sites for the crazes is low. The energy dissipated by the low ethylene content specimen as well as the homopolymer, in figure 5.26, is also reduced because the test temperature of -10°C is below their brittle-to-ductile transition temperature. It is important to note that the shape in the force vs. deflection trace with decreasing ethylene content at constant temperature is similar as that for decreasing test temperature with constant ethylene content.

6.3 THE BRITTLE-TO-DUCTILE TRANSITION

6.3.1 Effect of Ethylene Content

Figure 5.8 shows that the impact energy of the copolymers is higher than that of the polypropylene homopolymer. This is clearly a consequence of incorporating EPR into the polypropylene matrix. The rubber particles act as stress concentrators initiating a multitude of the deformation micro mechanisms such as multiple crazing, shear yielding and cavitation to enhance the toughness of the rubber modified polymers. These rubber particles are capable of limiting the growth of voids and crazes to a sub-critical size thus allowing the copolymers to absorb a greater amount of the impact energy before failure. Although the homopolymer is also able to nucleate crazes, the number and material volume over which the crazes nucleate is less than that of the copolymers.

The fundamental difference between the homopolymer and the copolymer is that the homopolymer is unable to limit the growth of these crazes due to the absence of the EPR particles. The crazes therefore develop into unstable cracks that propagate rapidly throughout the material leading to the low impact energy of the homopolymer. This can be deduced by the marked increase in the crack initiation energy of the copolymer specimens compared to that of the PP 1147 HQ7 homopolymer as was shown in figure 5.9. The

homopolymer exhibits a predominantly brittle failure mode at room temperature. In addition to this, the rubber particles also impart toughness to the poly (propylene – ethylene) copolymer through the contribution of the amorphous regions within the ethylene propylene rubber phase[2,8,13,27].

A closer examination of figure 5.8 shows that the impact energy of the high ethylene containing specimens viz., PP 2540 H, PP 2648 RC and PP 2648 M is substantially higher than the low ethylene content PP 2340 PC copolymer. The energy distribution graphs (refer to figure 5.9) show that the increased impact energy is due to a higher contribution of the crack propagation energy to the total impact energy.

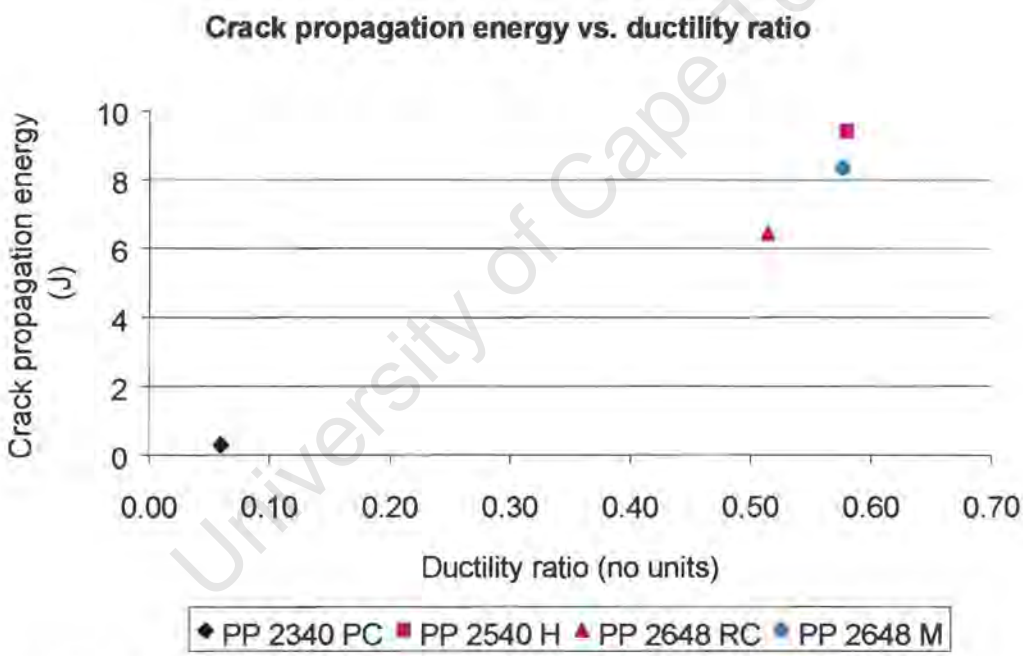

Figure 6.2: *Graph showing the relationship between the crack propagation energy and the ductility ratio*

The crack propagation energy is directly related to the ductility of the specimens as shown in figure 6.2. Figure 6.2 and the calculated ductility ratios in table 5.5 indicate that the PP 2340 PC copolymer tends to exhibit a minimal degree of plasticity. Thus comparatively, the PP 2340 PC is more brittle than the high ethylene content specimens as confirmed by the photograph shown in figure 5.11. This would indicate that the ability of the

material to flow and the extensive plastic drawing process during the impact event is also responsible for the observed higher impact energy of the higher ethylene content specimens. It should be borne in mind that the ductility ratios were obtained at high strain rates.

The brittle behaviour of the PP 2340 PC is most likely due to the combined effect of two factors viz., the EPR concentration and interparticle distance. The low concentration of EPR particles in a low ethylene content specimen reduces the number of nucleated crazes. These crazes reach a critical size due to the inefficiency of the craze termination process. Therefore unstable cracks are formed upon reaching the critical size and the copolymer fails in a brittle mode. A comparison of the stress whitening area, which is an indication of crazing, in figures 5.11 and 5.12 shows that the low ethylene copolymer does indeed craze but to a far lesser extent than the high ethylene copolymer.

The average EPR particle size of the PP 2340 PC specimens of 0.9 μm is smaller than that that of the higher ethylene containing Sasol copolymers of about 1.2 μm (refer to figure 5.43). Figure 5.45 shows that most of the EPR particles of the PP 2340 PC are closely distributed about the mean. In the event of the formation of a crack in the PP 2340 PC copolymer, the EPR particle is unable to arrest or influence the propagation of the crack due to its limited size in relation to the plastic zone of the crack. This further contributes to the brittle behaviour of the specimen and its reduced energy absorption capability[8].

The transformation from the brittle to ductile failure behaviour of the copolymers with increasing ethylene content is also attributed to the critical rubber content of the polypropylene system. The low rubber content copolymers, as in the PP 2340 PC copolymer, falls below the critical content required for ductile failure. The impact energy results in figure 5.8 show that the impact strength is increased dramatically above 11% ethylene content. At these ethylene concentrations, the impact strength can further be enhanced by using copolymers with a low melt flow index

6.3.2 The Brittle-to-DuctileTransition Temperature

It is evident from figure 5.16 that the impact test temperature has a profound influence on the observed impact behaviour of the poly (propylene – ethylene) copolymers and the polypropylene homopolymer. Each polymer shows a conspicuous reduction in their impact energy at a certain test temperature or more specifically their brittle-to-ductile transition temperature. The transition temperatures decrease with increasing ethylene content. The glass transition temperature of the EPR is approximately -50°C and an increase of the ethylene % in a copolymer decreases its brittle-to-ductile transition temperature.

At the same time, the EPR phase is amorphous and the overall crystallinity of the copolymer is reduced with increasing ethylene. Using differential scanning calorimetry (DSC), an inverse correlation between ethylene content and crystallinity was found by Mange[22]. The large difference in the brittle-to-ductile transition temperatures between the PP 2340 PC and PP 2540 H copolymers is related to the increase in rubber content of the PP 2540 H copolymer grade[8,13,18,34].

An increasing degree of crystallinity results in a yield strength that is higher than the ultimate strength of the polymer thus causing a brittle mode of failure in the specimens. This is observed in figure 5.26 where the PP 1147 HQ7 and the PP 2340 PC specimens show a sharp fall in their recorded impact force after reaching peak force. This is indicative of their low ductility compared to the damage tolerant high ethylene content PP 2540 H specimen which shows a gradual drop in impact force[34].

A comparison of figures 5.24 and 5.26 show that the effect of decreasing the impact test temperature is analogous to decreasing the ethylene content of the copolymers. Although only the PP 2648 RC force vs. deflection curves are analysed, the other copolymers show similar behaviour. The graphs in figure 5.24 show that the peak force of the PP 2648 RC specimen increases

until the test temperature is lowered to -30°C. The difficulty in molecular chain slippage and increase in activation energy with decreasing temperature increases this peak force. It is important to note that until a test temperature of -25°C is reached, the yield strength of the PP 2648 RC, although increasing, is still below its ultimate strength of the copolymer.

A comparison of the energy distribution bar chart in figure 5.25 shows that the crack initiation energy increases from a test temperature of 23°C to -20°C. It is therefore easier for crazes to nucleate at temperatures higher than -20°C. The high crack initiation energy at a test temperature -20°C would also imply that the energy dissipated per unit craze at this temperature is greater than at 23°C. Evidence of crazing is generally seen as stress whitening because this phenomenon is caused by the scattering of light due to the differences in the refractive index of the microfibrils and the unyielded polymer. No significant difference was noticed during visual comparison of the stress whitening regions of the impacted specimens at the two test temperatures indicating that the decrease in crazing at -20°C is not substantial as that below the brittle-to-ductile transition (see figure 5.20). Therefore the dissipated impact energy increases as the test temperature is lowered to -20°C. This increase is observed in the formation of the "impact energy mountain" in the energy vs. temperature curves shown in figure 5.16.

Further examination of figure 5.25 shows a distinct reduction in the crack propagation energy at a test temperature of -30°C which corresponds to the brittle-to-ductile transition temperature of the PP 2648 RC copolymer. At this temperature, the magnitude of stress whitening and therefore crazing is visibly reduced as was shown in figure 5.19. Since the crack initiation energy is still high, a fewer number of crazes are nucleated thus dissipating some of the impact energy. However, nucleated crazes continue to propagate and breakdown into cracks since very little additional energy (low crack propagation energy) is required to propagate an initiated craze at this temperature. Thus the copolymer's capability of dissipating the impact energy is severely retarded leading to a brittle failure mode. This leads to the drop in the energy on the left side of the "impact energy mountain". Thus the

occurrence of the "impact energy mountain" is a result of two opposing factors viz., the temperature induced brittleness of the copolymer and the multiple crazing toughening micro-mechanism. The process of chain scission and development of inter spherulitic cracks dominate at temperatures below the brittle-to-ductile transition whilst multiple crazing and shear yielding dominate the toughening mechanisms at temperatures above. Thus the nature of the brittle-to-ductile transition of rubber modified polypropylene is related to the deformation processes responsible for the dissipation of the impact energy.

Test temperatures of -40°C and –50°C show a multi-peaked phenomenon in the force vs. deflection that are related to the development and propagation of the radial and circumferential cracks. It also appears from figure 5.20 that the radial cracks occur first followed by the circumferential cracks. These energies could not be evaluated in terms of crack initiation and propagation energies due to the formation of the two peaks. Nonetheless, the total energy dissipated by the PP 2648 RC copolymer continues to decrease with decreasing temperature. It is noticed that the beneficial effect of incorporating the EPR phase into the polypropylene microstructure is lost at temperatures below the brittle-to-ductile transition temperature regardless of the ethylene content.

6.3.3 Influence of Stress State on Impact Energy

Although the physical data between the notched Izod and the drop weight impact tests cannot be compared, the impact behaviour of the copolymer specimens can be examined. Figure 5.15 shows that the impact response obtained from the two testing techniques differ in that the drop weight impact results of the high ethylene containing specimens show an increase in impact energy with decreasing temperature whereas the Izod test results show a decreasing energy trend. This difference can be related to the stress state imposed on the test specimens during testing.

In the case of the rubber modified polypropylene specimens, the decreasing Izod impact energy trend may be attributed to the higher "Izod brittle-to-ductile transition temperatures". The difference in the "Izod brittle-to ductile transition temperatures" and those obtained for the drop weight tests is a result of the severe triaxial stress state imposed onto the material in the vicinity of the notch tip during Izod impact testing. It would thus appear that the notched Izod tests were conducted below their "Izod brittle-to-ductile temperatures". In the drop weight impact test, the high ethylene containing specimens are yet to reach their brittle-to-ductile transition temperatures (-27 to -40°C) and are in the "impact energy mountain" stage of the energy vs. test temperature graph.

The low ethylene content copolymer has a brittle-to-ductile transition temperature of approximately 27°C and so any test below this temperature would result in brittle failure[27]. The effect of introducing a notch and the molecular orientation of the polymer relative to the impactor also would have an effect on the brittle-to-ductile transition relative to the test method employed.

6.3.4 Effect of Molecular Weight on Impact Strength

The reduction in the impact energy on copolymer specimens with similar ethylene content and increasing melt flow index was shown in figure 5.5. This trend was also found by Cieslinski *et al* on EPDM copolymers and by Marcus *et al* on polypropylene homopolymers[36,40]. To examine the effect of molecular weight, the impact tests were performed at room temperature. Stress whitening was observed in all three specimens indicating that the multiple crazing micro-mechanism was the dominant form of deformation during the impact event. It is known and has been shown that molecular weight is inversely related to the melt flow index in a log-linear fashion[40]. The toughening mechanism of multiple crazing is dependent on the degree of crystallinity of the copolymer since craze nucleation occurs within the amorphous content of the matrix polymer. Therefore, the portion of material available for the nucleation of crazes increases with decreasing melt flow

index. These crazes have tougher microfibrils as a result of the presence of chain entanglements. The intensity of the crazes is consequently increased with decreasing melt flow index leading to a greater extent of toughening and hence a larger impact energy. This explanation is supported by the observed increase in impact energy with decreasing melt flow index[8,41].

In this work, the molecular weight and ethylene content varied simultaneously and it is difficult to isolate the effect of molecular weight on impact strength alone. Previous studies on polypropylene homopolymers have shown that the Charpy and Izod impact strength decreases exponentially as the MFI is increased[40]. In figure 6.3 below, it can be seen that at low MFI's the impact strength is dramatically enhanced[43]. In the drop weight impact tests also, the 2540H grade had the highest impact strength primarily due to its relatively high molecular weight. In high molecular weight grades, the long chains are unable to crystallize to the same extent as with small chains. The molecular chains become increasingly entangled with increasing chain length and these chains can absorb more energy through chain conformation in an impact event i.e. making the polymer tougher. This would also explain the lower % tensile elongation in the very high molecular weight grades as the chain slippage becomes more difficult.

The low MFI grades are processed at higher melt temperatures which is deleterious for impact strength as high melt temperatures cause some EPR particles to coalesce and increase the average particle diameter and particle size distribution. A broad particle size distribution increases the average interparticle distance, which again is deleterious for impact strength. The Sasol grades tended to have long tails in their particle size distribution curves indicating a few particles that are disproportionately large. An analysis of the skewness factors in table 5.11 confirms this. The etching process does not distinguish between single and coalesced particle, and so this can only be deduced from previous work[2]. It is not clear to what extent the MFI in the copolymer grades affects the viscosity ratios as it is known that increasing the viscosity ratio results in a coarser particle size distribution.

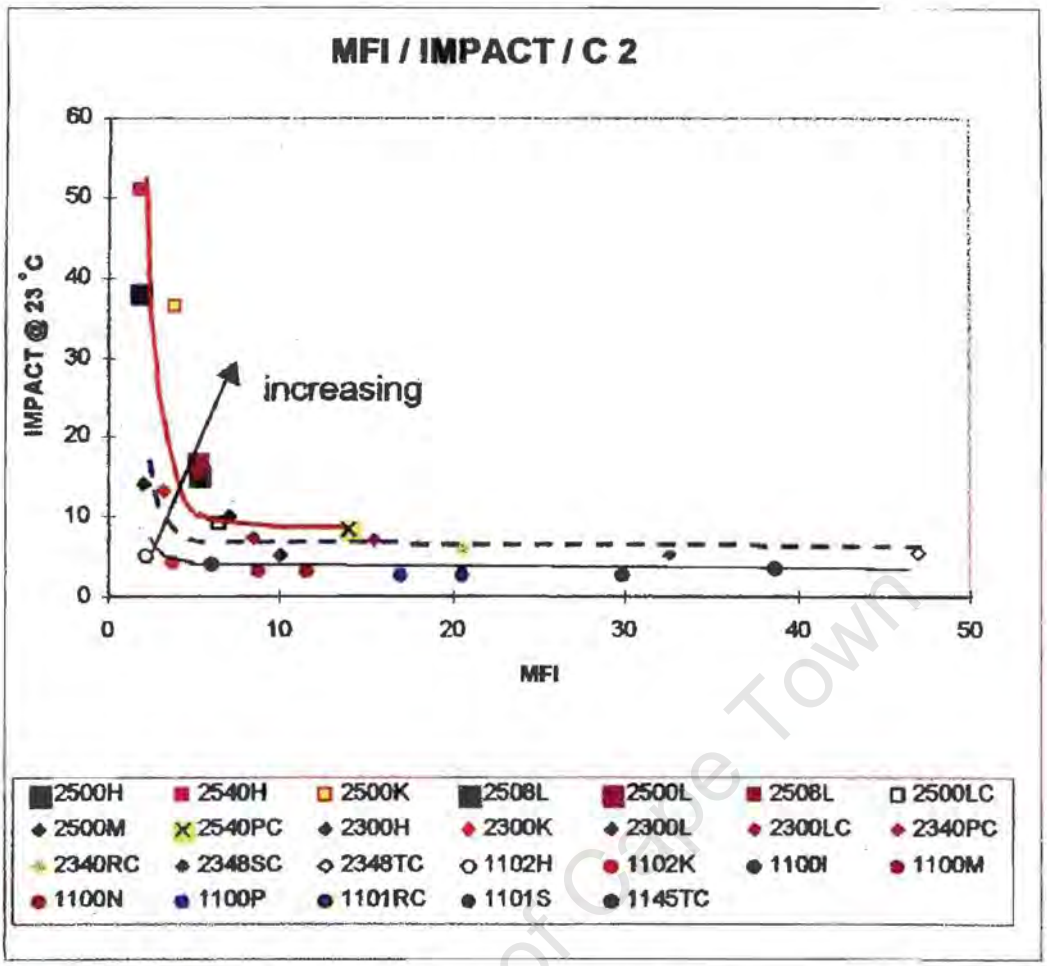

Figure 6.3: *Graph showing the inverse logarithmic relationship between the melt flow index and impact strength for various copolymer grades [after ref. 43].*

CHAPTER 7

CONCLUSIONS

- Instrumented drop weight impact testing is a useful tool to provide a means of characterizing and understanding the impact behaviour of poly (propylene – ethylene) copolymers. This form of impact testing is not limited to polymeric materials but can be used efficiently to examine other material types e.g., composites and metals. It is important to note that the results obtained from drop weight impact testing provide quantitative results which are to be used for comparing the impact properties of materials under specific test conditions. Important consideration should be given to the testing technique as the polymer may behave differently with different testing methods. The instrumented drop weight impact test provides a detailed account of the impact event. The rig was found to be reproducible to a confidence level of 93%.

- The cooling disk system was successfully incorporated into the in-house built instrumented drop weight impact tester and implemented to obtain impact energy results for the poly (propylene – ethylene) copolymers down to cryogenic temperatures of -50°C. This system was found to be advantageous over the vapour cooling system as well as the coiled cooling system. The cooling disk system showed an operational capability to within 2°C of the desired impact test temperature.

- Increasing additions of a low modulus elastomer such as ethylene propylene rubber (EPR) in polypropylene increases the low temperature impact toughness of the copolymer by suppressing its brittle-to-ductile transition temperatures. However, rubber modified polypropylene systems have a critical rubber content which should be

exceeded to optimize the impact strength of the copolymer. Other parameters such as the molecular weight of the polymers can also be increased to improve the impact resistance of the polypropylene specimens.

- The brittle-to-ductile transition plays an important role in the damage competition between the multiple crazing and shear yielding deformation micro-mechanisms. Prior to the occurrence of the brittle-to-ductile transition, multiple crazing and shear yielding are the predominant modes of deformation. After the transition, only a limited amount of the crazing micro-mechanism occurs due to the inability of molecular chain relaxation at these temperatures.

- Above the brittle-to-ductile transition temperature of a particular grade, stress whitening is observed in the polymer specimen after impact. At test temperatures much lower than the brittle-to-ductile transition temperature, radial and circumferential cracks are observed. It is noticed that a decrease in ethylene content of a copolymer is analogous to the lowering of the impact test temperature. Thus, the fracture behaviour of rubber modified polypropylene is dependent on both the test temperature and the ethylene content.

- Although a sensitivity analysis was not carried out on the melt flow index and the ethylene content, this investigation shows that a decrease in the melt flow index and an increase in the ethylene content favourably influences the impact strength of the polypropylene copolymers. The impact energies at below the brittle-to-ductile transition temperature are similar to that of the polypropylene homopolymer.

- No conclusive evidence could be found to substantiate the higher impact strength of the low ethylene content specimens of the DOW, TARGOR and TPC grades compared to that of the Sasol Polymer grades. This may be due to different production methods with concomitant changes in the microstructure of the ethylene propylene rubber phase. The viscosity ratio and the compatibility between the two phases may also be contributing factors to their higher impact energy. However, the high ethylene content Sasol Polymer grades showed similar energy absorption as the other grades.

CHAPTER 8

RECOMMENDATIONS FOR FUTURE WORK

- The addition of a high-speed video interface designed for viewing the specimen during the impact event can provide a useful means of correlating the impact data with actual visualization of fracture in the specimen. It would be particularly advantageous to have a timer in the video data so that the events of failure in the specimen can be related to the corresponding impact force, energy and specimen deflection.

- It would be important in terms of the accuracy in the impact results to eliminate the discrepancy associated with manual operation of the cooling disk system. This can be done by automating the process of removing the copper disk from the specimen surface.

- Investigate the impact properties of rigid particulate reinforced polypropylene systems and examine and compare the deformation mechanisms and impact behaviour with that of the rubber modified polypropylene systems.

REFERENCES

1 B. Sole, Sasol Polymers, Private Communication 1.

2 Moore E.P. Jr., ***"Polypropylene Handbook"***, Hanser/Gardner Publications, New York, 1996.

3 Callister W.D. Jr., ***"Materials Science and Engineering-An Introduction"***, 4th edition, John Wiley & Sons Inc., New York, 1996.

4 Fernando P.L. and Williams J.G., *"The Toughness of Copolymers of Polypropylene"*, **Polymer Engineering and Science**, 21, 1981, pp. 1003-1009.

5 Hongjun C., Xiaolie L., Xiangxu C., Dezhu M., Jianmin W. and Hongsheng T., *Structure and Properties of Impact Copolymer Propylene. II. Phase Structure and Crystalline Morphology"*, **Journal of Applied Polymer Science**, 71, 1999, pp. 103-113.

6 Kim G.M., Michler G.H., Gahleitner M. and Fiebig J., *"Relationship Between Morphology and Micromechanical Toughening Mechanisms in Modified Polypropylenes"*, **Journal of Applied Polymer Science**, 60, 1996, pp. 1391-1403.

7 Starke J.U., Michler G.H., Grellmann W., Seidler S., Gahleitner M., Fiebig J. and Nezbedova E., *"Fracture Toughness of Polypropylene Copolymers: Influence of Interparticle Distance and Temperature"*, **Polymer**, 39, 1998, pp. 75-82.

8 B. Sole, Sasol Polymers, Private Communication 2.

9 Marchal Y., Oldenhove B., Daoust D., Legras L. and Delannay F., *"Characterization of the Fracture Toughness of Rubber-Toughened Polypropylene Thin Plates"*, **Polymer Engineering and Science**, 38, 1998, pp. 2063-2071.

10 Ward I.M., ***"Mechanical Properties of Solid Polymers"***, John Wiley & Sons Ltd, New York, 1971.

11 Sugimoto M and Ishikawa M., *"Toughness of Polypropylene"*, **Polymer**, 36, 1995, pp. 3675-3682.

12 Flaris V. and Stachurski Z.H., *"The Mechanical Behaviour of Blends of Polyethylene, Polypropylene, and an Ethylene-Propylene Block Copolymer at -20°C"*, **Journal of Applied Polymer Science**, 45, 1992, pp. 1789-1798.

13 Liang J.Z. and Li R.K.Y., *"Rubber Toughening in Polypropylene: A Review"*, **Journal of Applied Polymer Science**, 77, 2000, pp. 409-417.

14 Van der Waal A., Verheul A.J.J. and Gaymans R.J., *"Polypropylene-Rubber Blends: 4. The Effect of the Rubber Particle Size on the Fracture Behaviour at Low and High Test Speed"*, **Polymer**, 40, 1999, pp. 6057-6065.

15 Montiel A.G., Keskkula H. and Paul D.R., *"Impact-Modified Nylon 6/Polypropylene Blends: 3. Deformation Mechanisms"*, **Polymer**, 36, 1995, pp. 4621-4637.

16 Birley, A.W., Haworth B. and Batchelor J., ***"Physics of Plastics: Processing, Properties and Materials Engineering"***, Carl Hanser Verlag, New York, 1992.

17 Van der Waal A. and Gaymans R.J., *"Polypropylene-Rubber Blends: 5. Deformation Mechanism During Fracture"*, **Polymer**, 40, 1999, pp. 6067-6075.

18 Van der Waal A., Nijhof R. and Gaymans R.J., *"Polypropylene-Rubber Blend: 2. The Effect of the Rubber Content on the Deformation and Impact Behaviour"*, **Polymer**, 40, 1999, pp. 6031-6044.

19 Tirosh J., Nachlis W. and Hunston D., *"Strength Behaviour of Toughened Polymers by Fibrous (or Particulate) Elastomer"*, **Mechanics of Materials**, 19, 1995, pp. 329-342.

20 Ficker H., Goeke G. and Walker D., *"Stress Whitening Resistant Polypropylene Impact Copolymers"*, **ANTEC**, 1988, pp. 741-744.

21 Klimek T.W., *"New Impact Copolymer Polypropylenes for FDA Applications"*, **SPO**, 1993, pp. 421-438.

22 Mange S., *"Structure-Property Relationships in Poly (Propylene-Ethylene) Copolymers"*, MSc Thesis, University of Cape Town, 1999.

23 Reed P.E., *" Falling Weight Impact Testing and Design"*, **Plastics, Rubber and Composites Processing and Applications**, 17, 1992, pp. 157-163.

24 Bucknall C.B., *"The Relevance of Impact Testing in the Materials Science of Polymers"*, **Plastics, Rubber and Composites Processing and Applications**, 17, 1992, pp. 141-144.

25 Schurmann B.L., Niebergall U., Severin N., Burger Ch., Stocker W. and Rabe J.P., *"Polyethylene (PEHD)/Polypropylene (iPP) Blends: Mechanical Properties, Structure and Morphology"*, **Polymer**, 39, 1998, pp. 5283-5291.

26 Ghaseminejhad M.N. and Parvizi-Majidi A., *"Impact Behaviour and Damage Tolerance of Woven Carbon Fibre-Reinforced Thermoplastic Composites"*, **Composites**, 21, 1990, pp. 155-168.

27 Perkins W.G., *"Polymer Toughness and Impact Resistance"*, **Polymer Engineering and Science**, 39, 1999, pp. 2445-2460.

28 Snoppy G., Reethamma J. and Varughese S.T.K.T., *"Blends of Isotactic Polypropylene and Nitrile Rubber: Morphology, Mechanical Properties and Comptibilization"*, **Polymer**, 36, 1995, pp. 4405-4416.

29 Liu T.M. and Baker W.E., *"Instrumented Dart Impact Evaluation of Linear Low Density Polyethylene at Controlled Impact Energy"*, **Polymer Engineering and Science**, 31, 1991, pp. 753-763.

30 Van der Waal A. and Gaymans R.J., *"Polypropylene-Rubber Blends: 3. The Effect of the Test Speed on the Fracture Behaviour"*, 40, 1999, pp. 6045-6055.

31 Mark J.E., Eisenberg A., Grasseley W. W., Mandelkern L., Samulski E.T., Koenig J.C. and Wignell G.D., ***"Physical Properties of Polymers"***, 2nd Edition, United Book Press, Baltimore, 1993.

32 "***Mechanical Behaviour of Materials: Proceedings of the International Conference on Mechanical Behaviour of Materials Vol III***", The Society of Materials Science, Japan, 1972.

33 Van der Waal A., Mulder J.J., Thijs H.A. and Gaymans R.J., *"Fracture of Polypropylene 1. The Effect of Molecular Weight and Temperature at Low and High Test Speed"*, **Polymer**, 39, 1998, pp. 5467-5475.

34 Van der Waal, A., Mulder J.J., Oderkerk J. and Gaymans R.J., *"Polypropylene-Rubber Blends: 1. The Effect of the Matrix Properties on the Impact Behaviour"*, **Polymer**, 39, 1998, pp. 6781-6787.

35 Jiang W., Tjong S.C. and Li R.K.Y., *"Brittle-Tough Transition in PP/EPDM Blends: Effects of Interparticle Distance and Tensile Deformation Speed"*, **Polymer**, 41, 2000, pp. 3479-3482.

36 Cieslinski R.C., Silvis H.C. and Murray D.J., *"Real-time Cryo-Deformation of Polypropylene and Impact-Modified Polypropylene in the Transmission Microscope"*, **Polymer**, 36, 1995, pp. 1827-1833.

37 Chou C.J., Vijayan K., Kirby D., Hiltner A. and Baer E., *"Ductile-to-Brittle Transition of Rubber Modified Polypropylene"*, **Journal of Materials Science**, 23, 1988, pp. 2521-2532.

38 Fernando P.L. and Williams J.G., *"Plane Stress and Plane Strain Fractures in Polypropylene"*, **Polymer Engineering and Science**, 20, 1980, pp. 215-220.

39 Liu Z.H., Zhang X.D., Zhu X.G., Qi Z.N. and Wang F.S., *"Effect of Morphology on the Brittle Ductile Transition of Polymer Blends: 1. A New Equation for Correlating Morphological Parameters"*, **Polymer**, 38, 1997, pp. 5267-5273.

40 Marcus K., Steinhobel C., Domingo M. and Marshall N, *"The Physical, Mechanical and Rheological Properties of Polypropylene: The Influence of Molecular Weight Averages and Molecular Weight Distribution"*, **International GPC Symposium '96**, 1996, pp. 3-33.

41 Lapique F., Meakin P., Feder J. and Jossang T., *"Relationships Between Microstructure, Fracture-Surface Morphology and Mechanical Properties in Ethylene and Propylene Polymers and Copolymers"*, **Journal of Applied Polymer Science**, 77, 2000, pp. 2370-2382.

42 D'Orazio L., Mancarella C., Martuscelli E., Cecchin G. and Corrieri R., *"Isotactic Polypropylene/Ethylene-co-Propylene Blends: Effects of the Copolymer Microstructure and Content on Rheology, Morphology and Properties of Injection Moulded Samples"*, **Polymer**, 40, 1999, pp. 2745-2757.

43 Marcus K., *"Copolymer Project Part 1: A Statistical Study on the Correlation Between Mechanical and Molecular Parameters: BNP Copolymers"*, **Polifin Internal Report**, 1997.

APPENDIX A

IMPACT DATA FOR SASOL POLYMER GRADES

Specimen type	*Ethylene content (wt %)*	*Impact velocity ($m.s^{-1}$)*	*Peak force (N)*	*Impact energy (J)*
PP 1147 HQ7	0	2.9	377	1.2
PP 2340 PC	6.9	4.0	1141	5.0
PP 2540 H	11.4	5.6	1310	16.2
PP 2648 RC	12.0	5.6	1174	12.5
PP 2648 M	13.4	5.6	1139	11.42

Table A-1: *Impact data for the Sasol Polymer grades tested at room temperature*

APPENDIX B

SASOL POLYMERS TEST DATA ON ALL COPOLYMER TYPES

Specimen types	Notched Izod impact test energy results (kJ/m^2)			Maximum elongation (%)
	23°C	0°C	-20°C	
PP 1147 HQ7	Specimen type not tested			
PP 2340 PC	5	4.1	3.1	130
PP 2540 H	60	27.3	6	95
PP 2648 RC	54	12.5	9.6	251
PP 2648 M	15	6.3	5.7	267

Table B-1: *Tabulated data of the Sasol Polymer grades*

Specimen types	Material supplier	Notched Izod impact test energy results (kJ/m^2)			Maximum elongation (%)
		23°C	0°C	-20°C	
PP 2340 P	TPC	5.8	3.6	3.3	37
PP 2340 P	TPC	6.1	3.7	3.3	58
PP 2348 M	TARGOR	8.8	4.7	3.6	95
PP 2348 M	TARGOR	5.5	3.7	3.3	56
PP 2448 TC	TPC	4.3	3.3	3.2	16
PP 2448 TC	DOW	4.9	3.5	3.2	34
PP 2600 PC	TARGOR	5.7	4.0	3.7	228
PP 2648 RC	DOW	5.0	3.4	3.4	82
PP 2648 RC	TPC	7.1	4.2	3.5	35
PP 2648 RC	DOW	9.1	4.9	4.1	67

Table B-2: *Tabulated data of the other copolymers grades*

APPENDIX C

IMPACT TRACES FOR THE SASOL GRADES AT DIFFERENT TEST TEMPERATURES

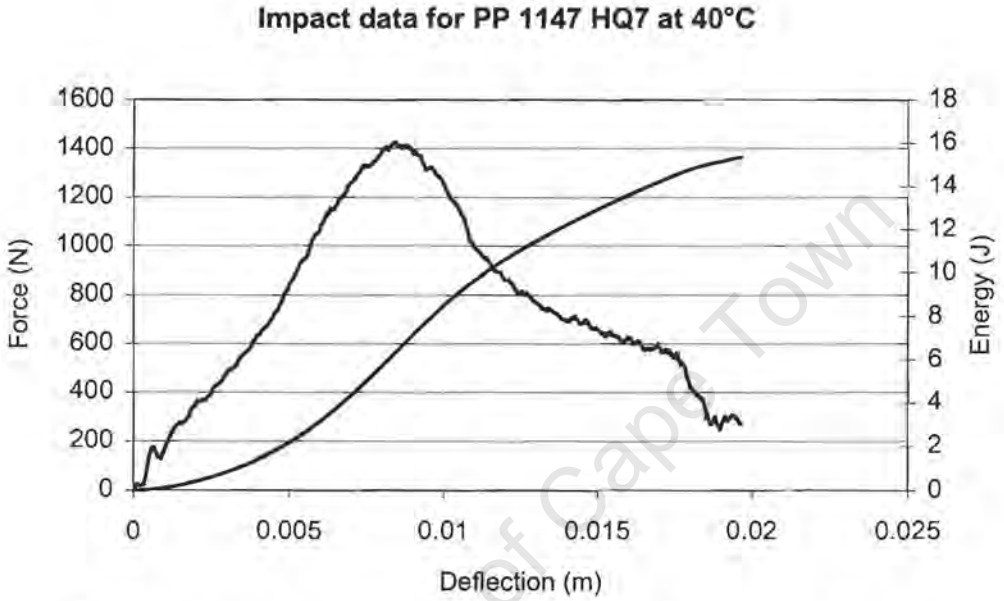

Figure C-1: *Impact traces for PP 1147 HQ7 at a test temperature of 40°C*

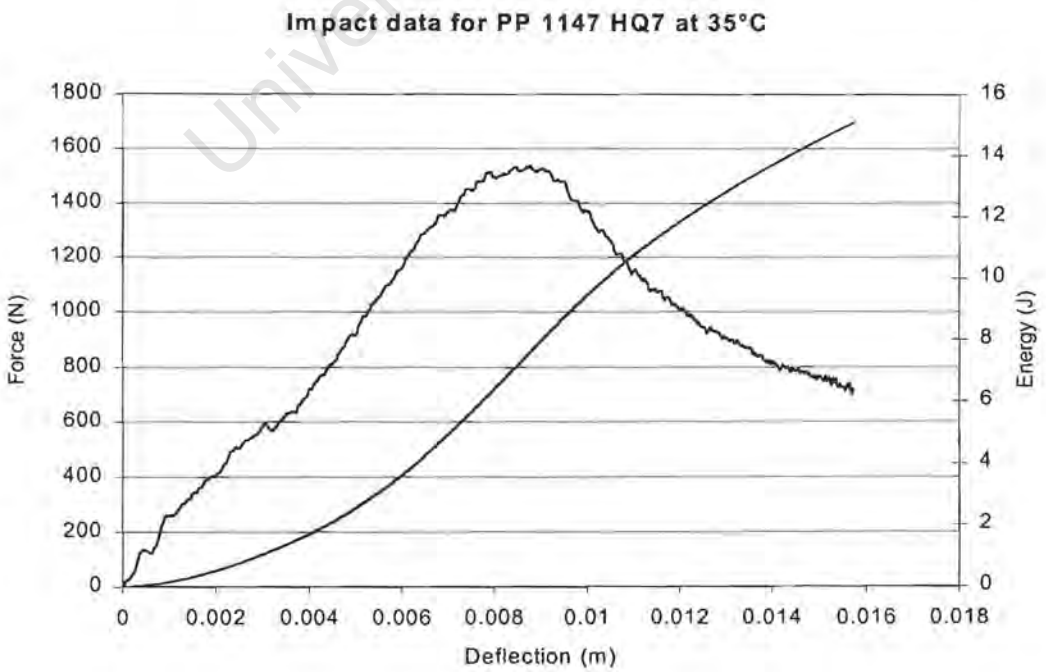

Figure C-2: *Impact traces for PP 1147 HQ7 at a test temperature of 35°C*

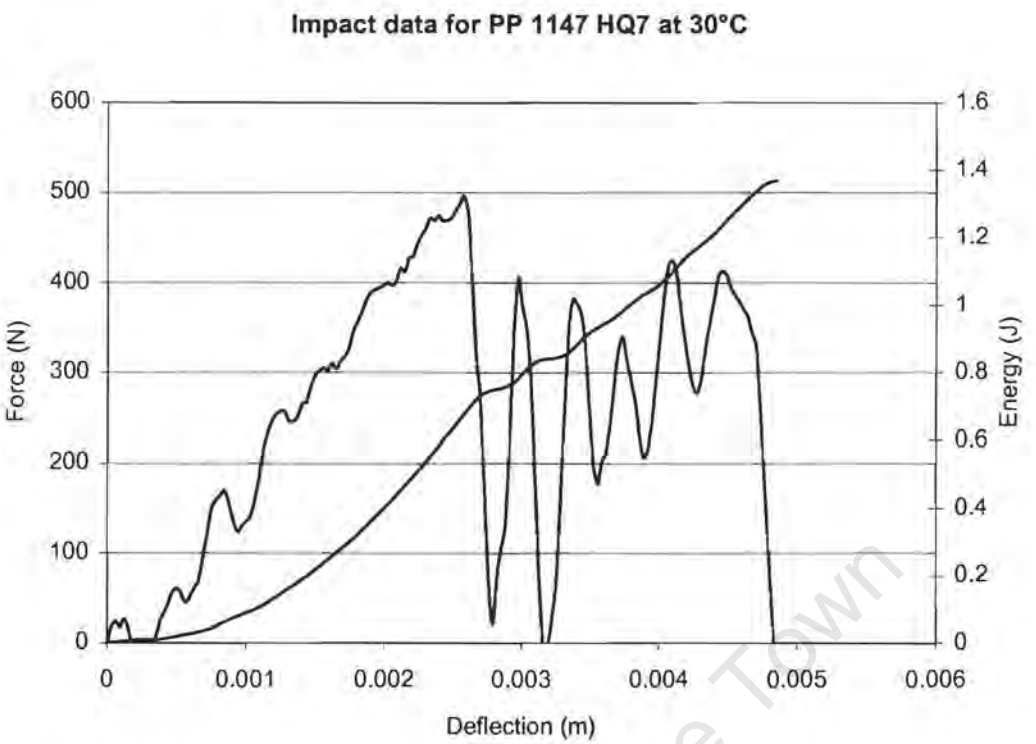

Figure C-3: *Impact traces for PP 1147 HQ7 at a test temperature of 30°C*

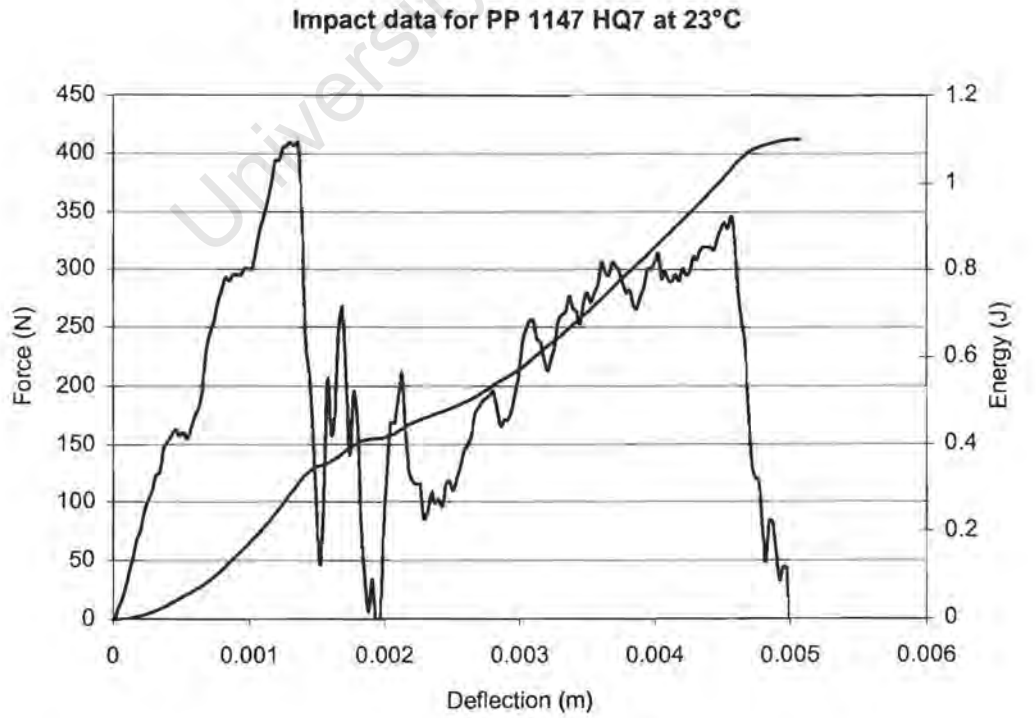

Figure C-4: *Impact traces for PP 1147 HQ7 at a test temperature of 23°C*

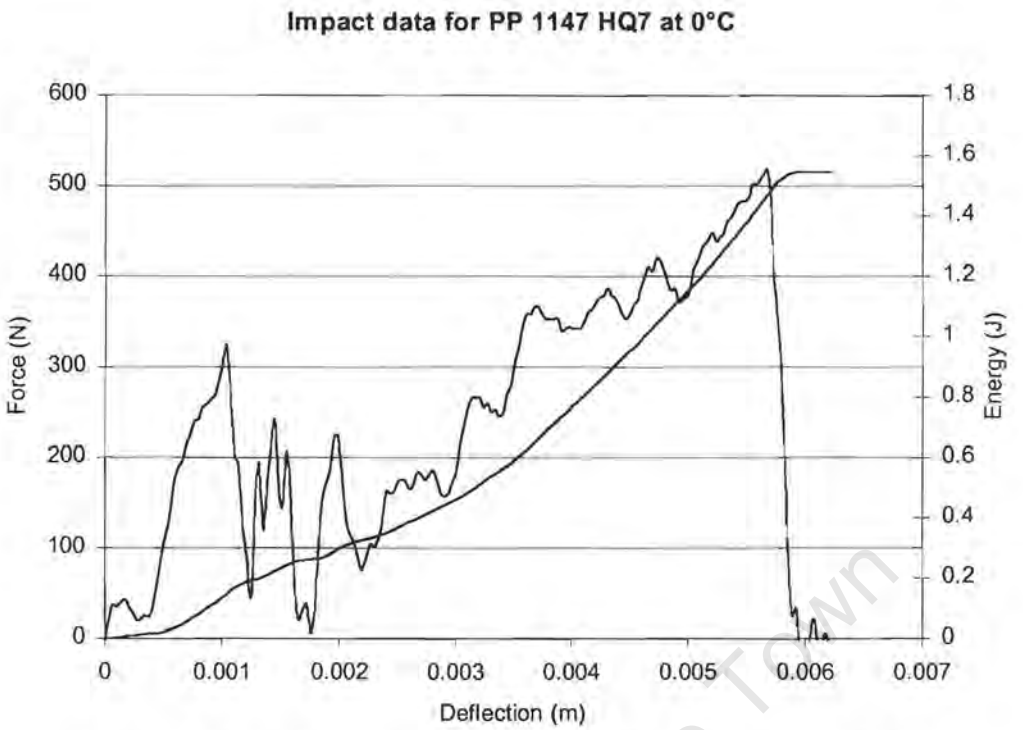

Figure C-5: *Impact traces for PP 1147 HQ7 at a test temperature of 0°C*

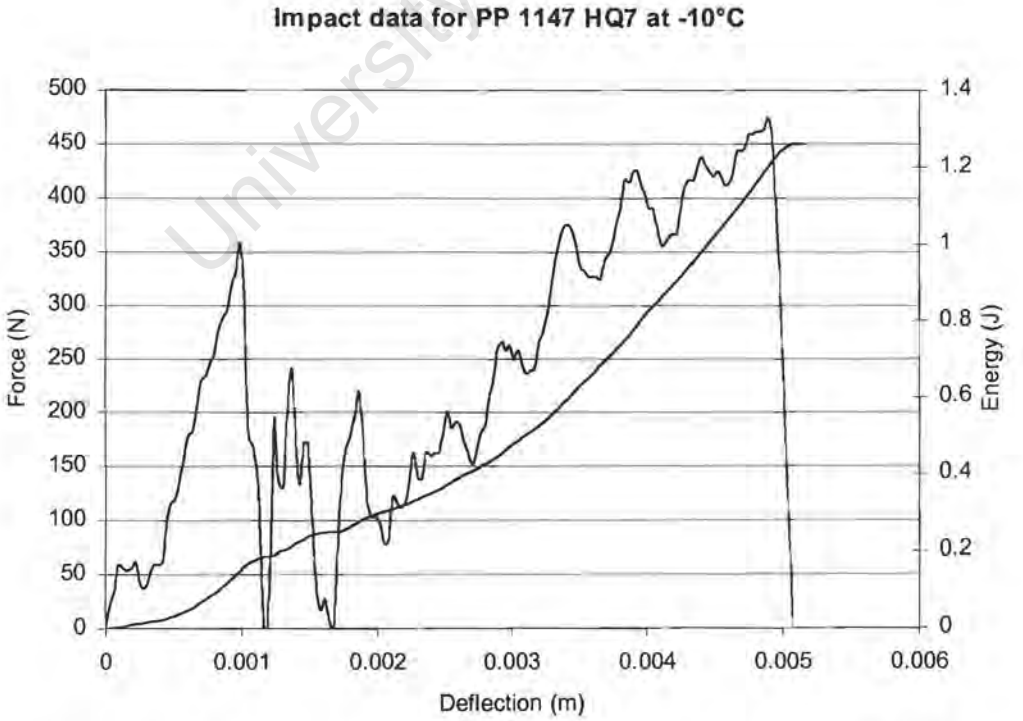

Figure C-6: *Impact traces for PP 1147 HQ7 at a test temperature of -10°C*

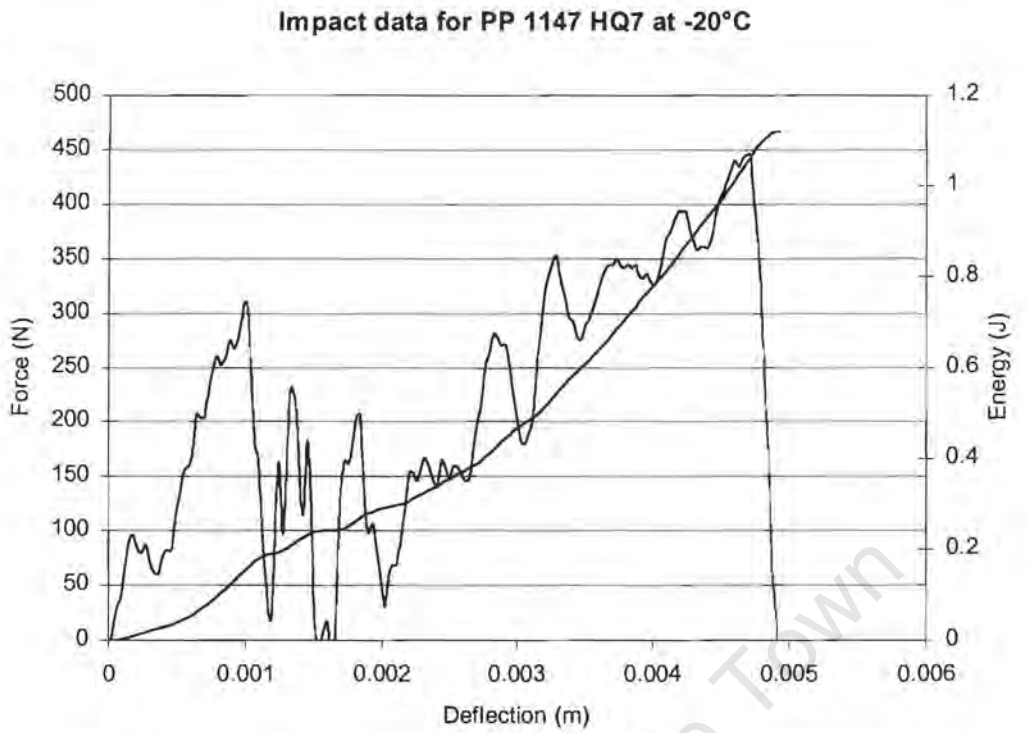

Figure C-7: *Impact traces for PP 1147 HQ7 at a test temperature of -20°C*

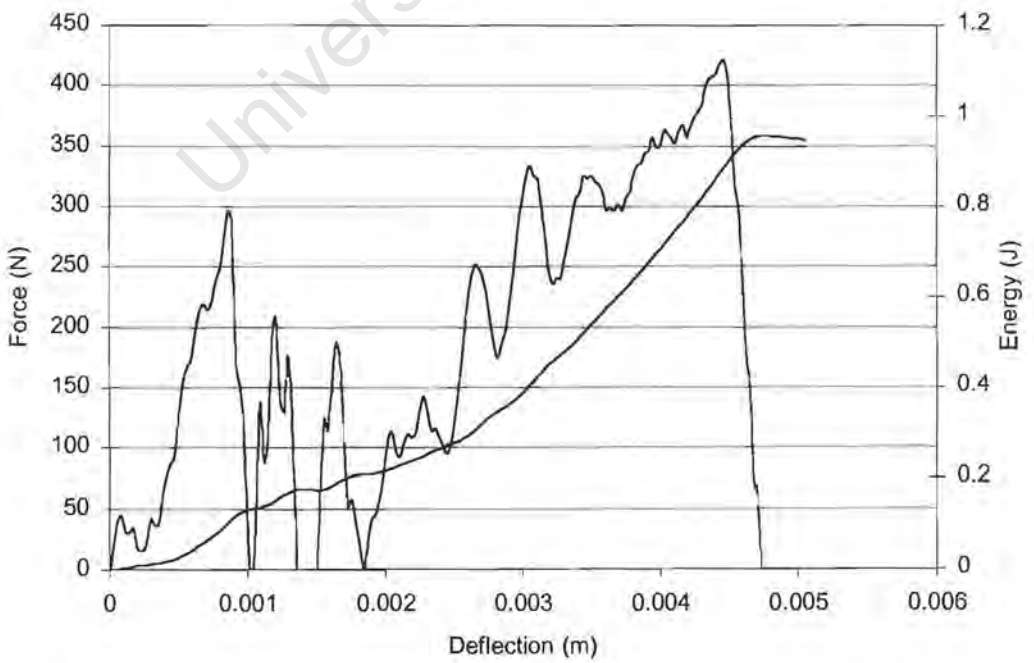

Figure C-8: *Impact traces for PP 1147 HQ7 at a test temperature of -30°C*

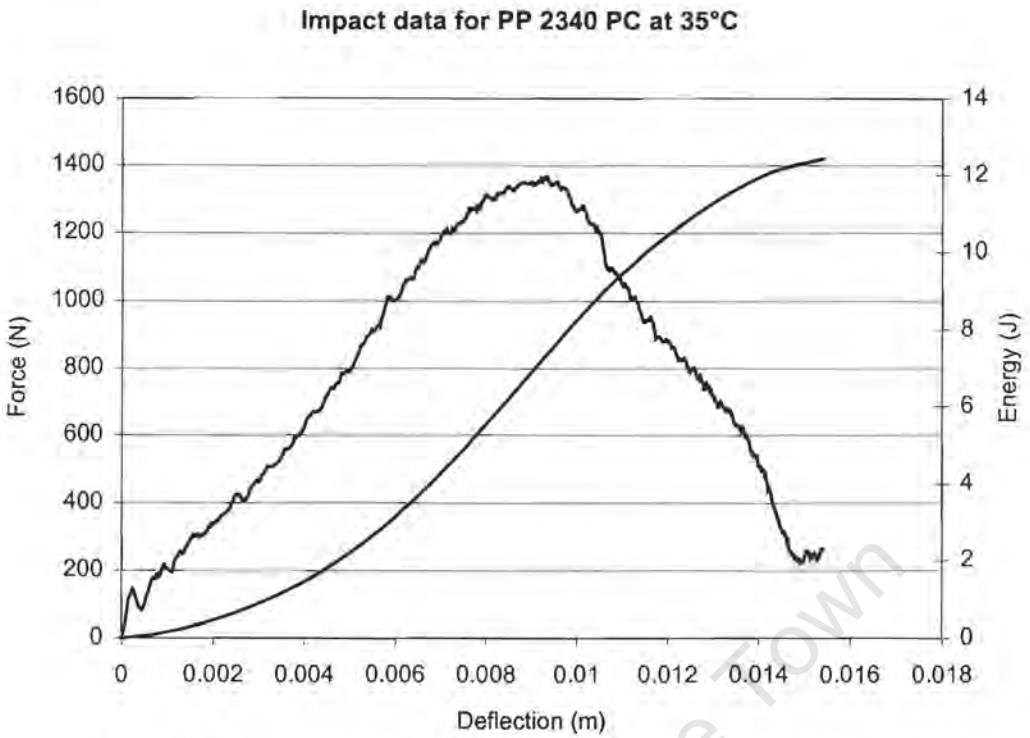

Figure C-9: *Impact traces for PP 2340 PC at a test temperature of 35°C*

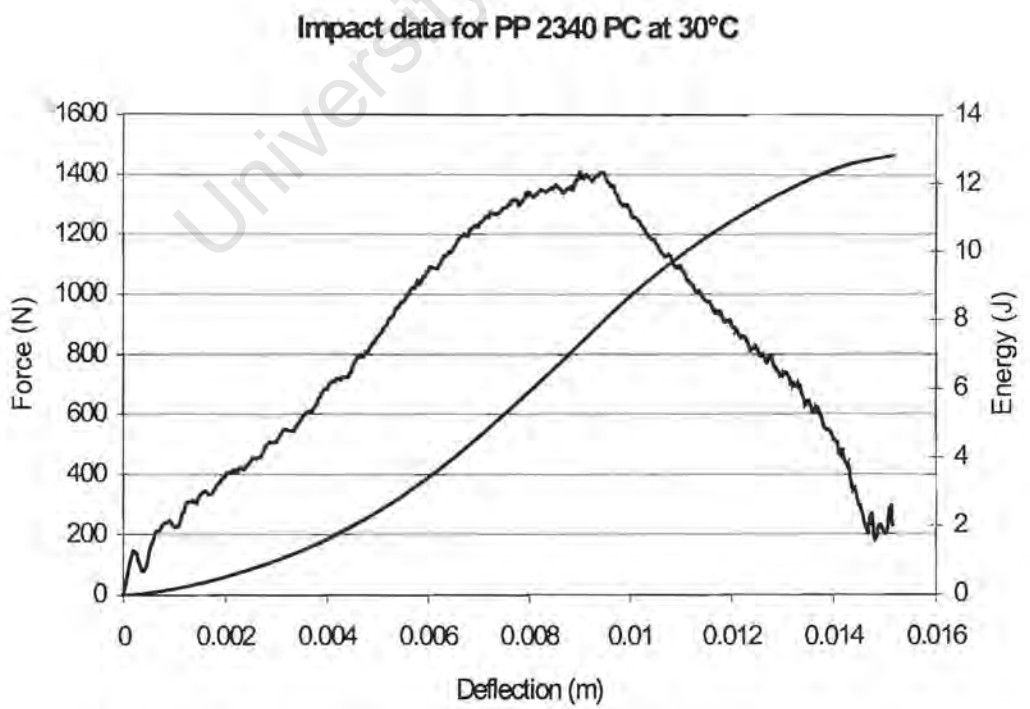

Figure C-10: *Impact traces for PP 2340 PC at a test temperature of 30°C*

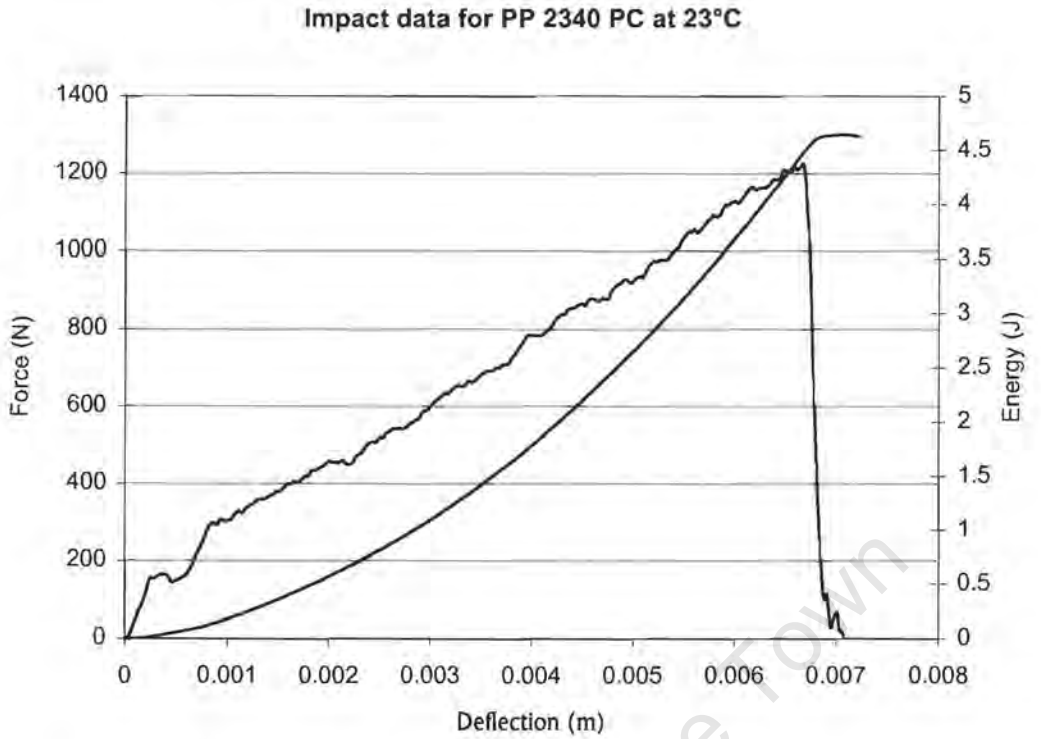

Figure C-11: *Impact traces for PP 2340 PC at a test temperature of 23°C*

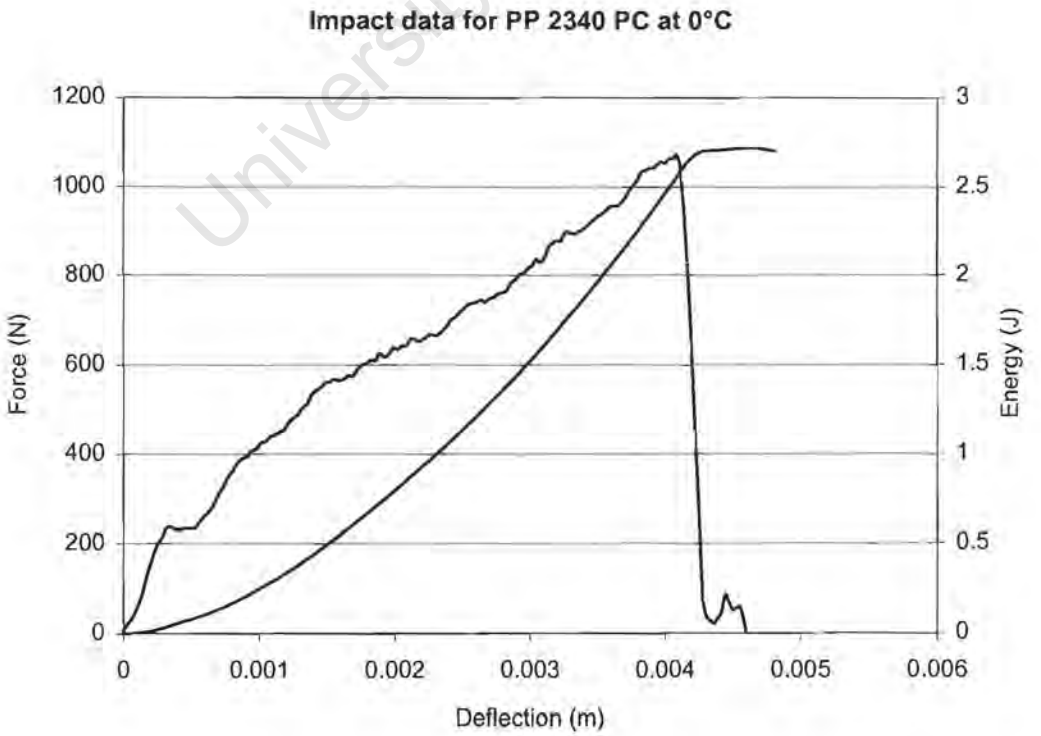

Figure C-12: *Impact traces for PP 2340 PC at a test temperature of 0°C*

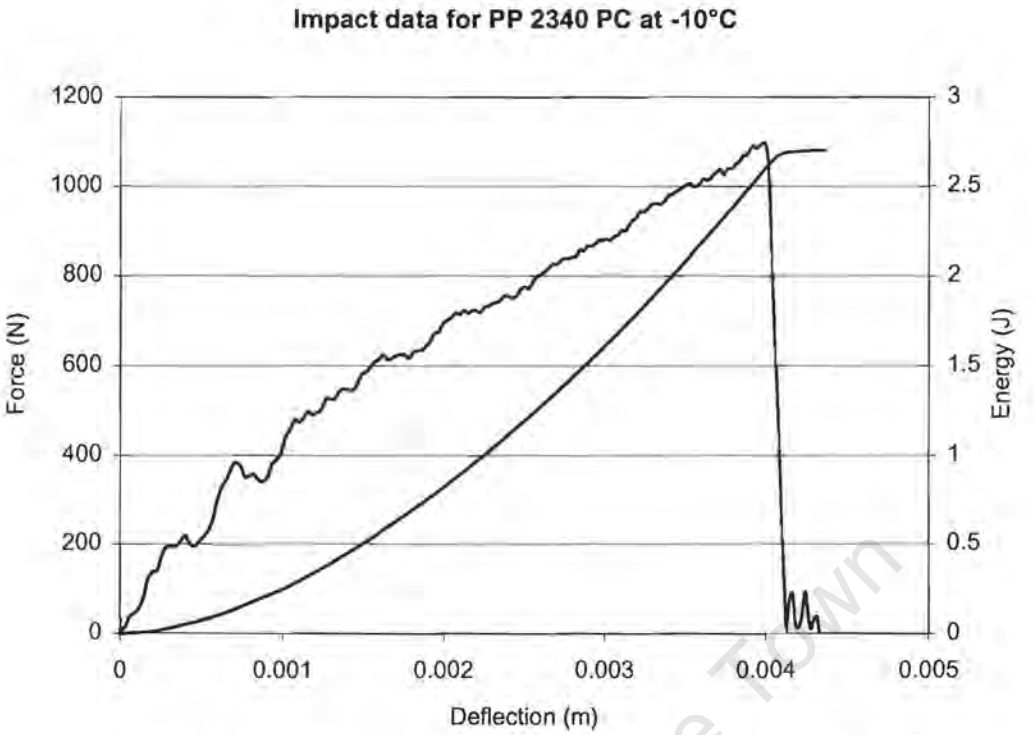

Figure C-13: *Impact traces for PP 2340 PC at a test temperature of -10°C*

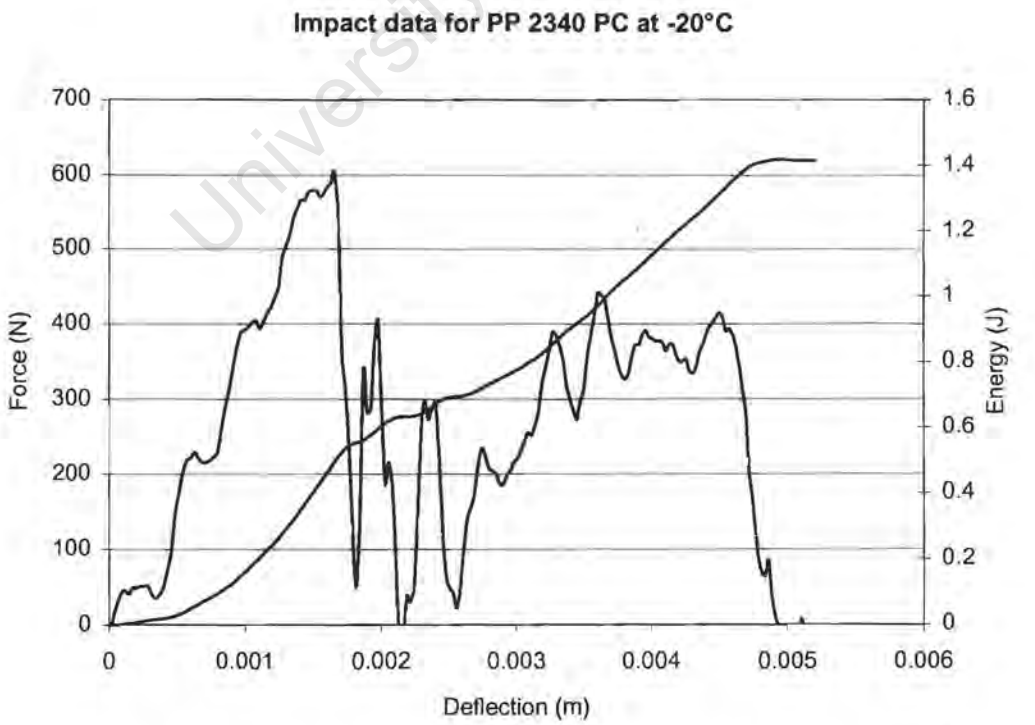

Figure C-14: *Impact traces for PP 2340 PC at a test temperature of -20°C*

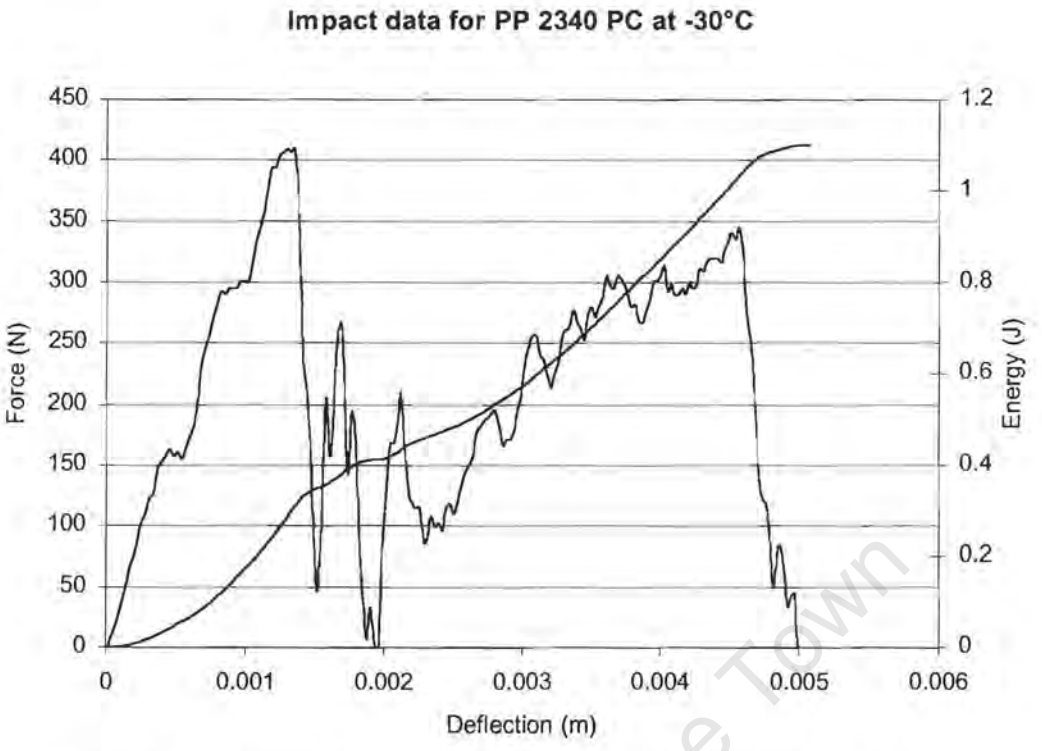

Figure C-15: *Impact traces for PP 2340 PC at a test temperature of -30°C*

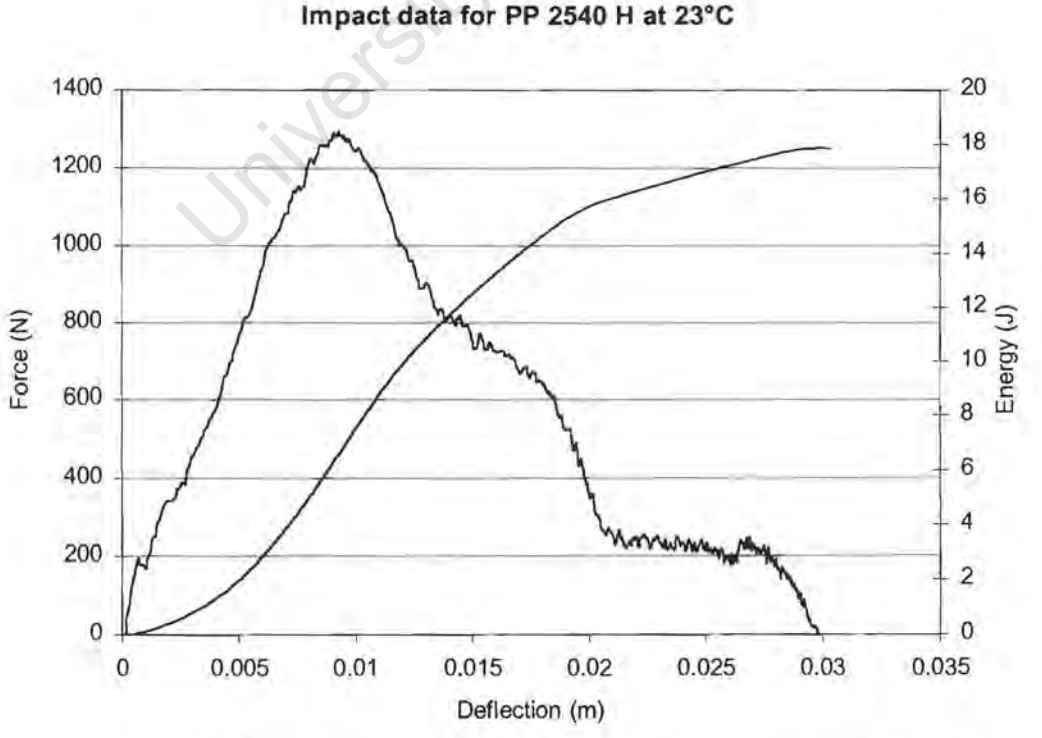

Figure C-16: *Impact traces for PP 2540 H at a test temperature of 23°C*

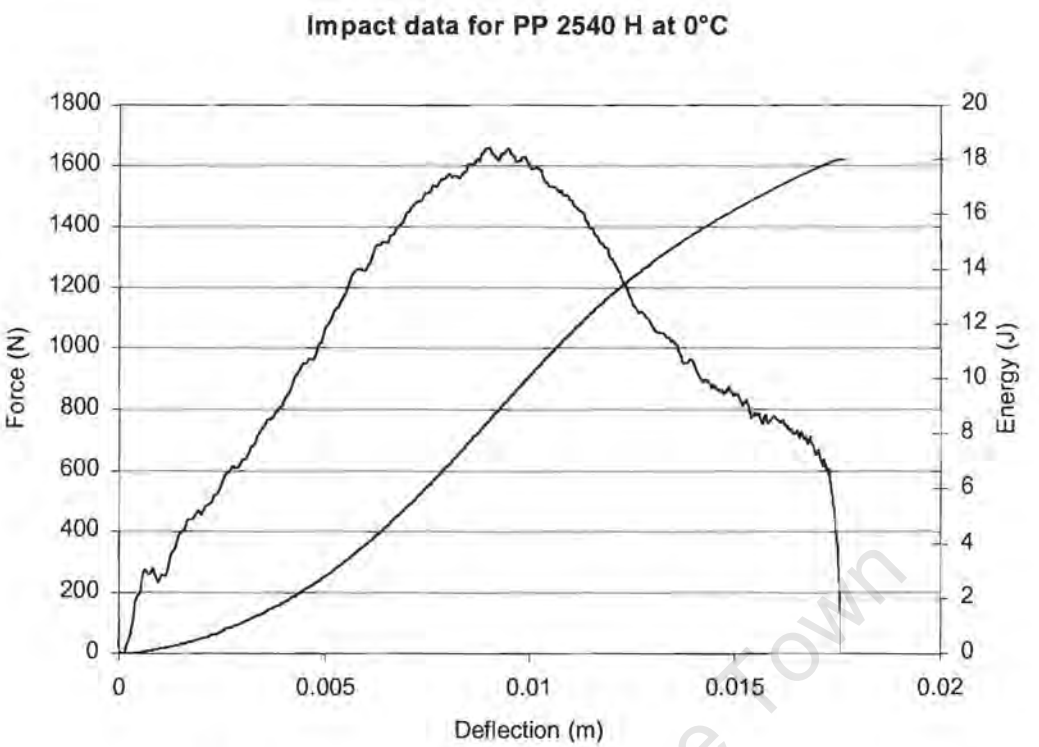

Figure C-17: *Impact traces for PP 2540 H at a test temperature of 0°C*

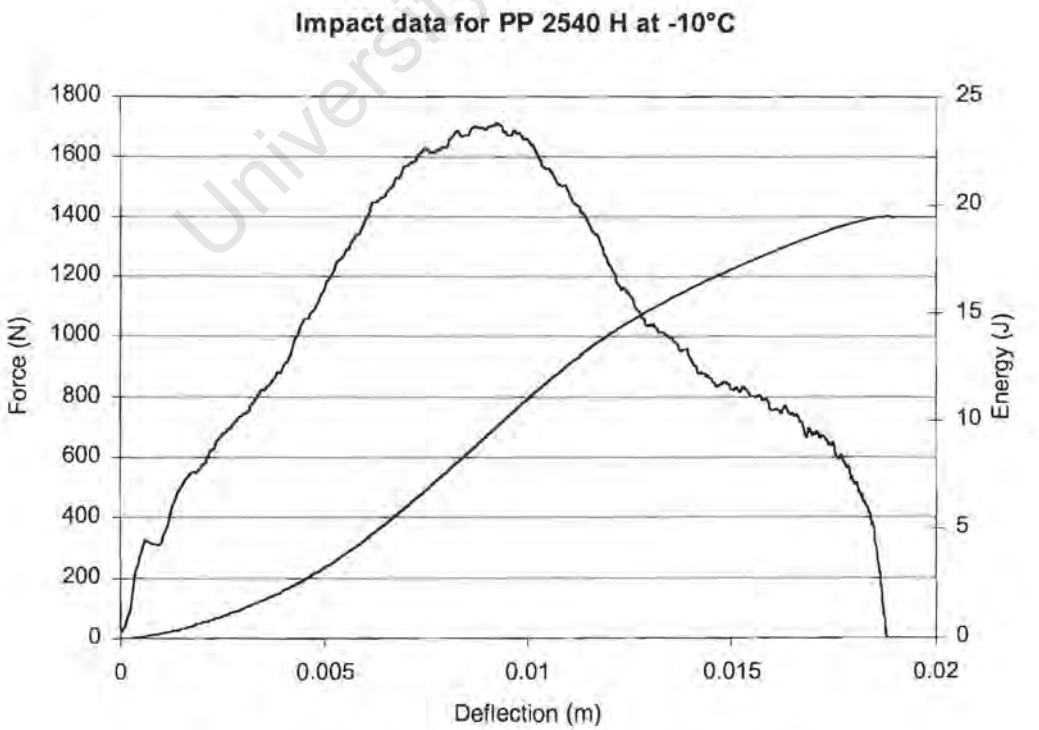

Figure C-18: *Impact traces for PP 2540 H at a test temperature of -10°C*

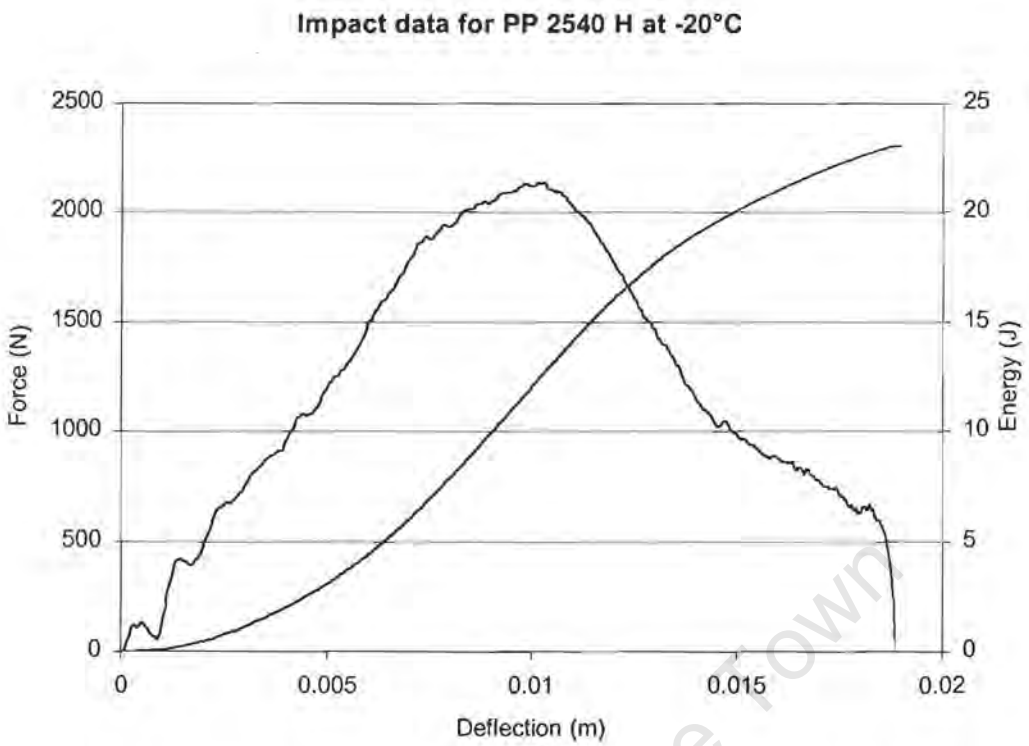

Figure C-19: *Impact traces for PP 2540 H at a test temperature of -20°C*

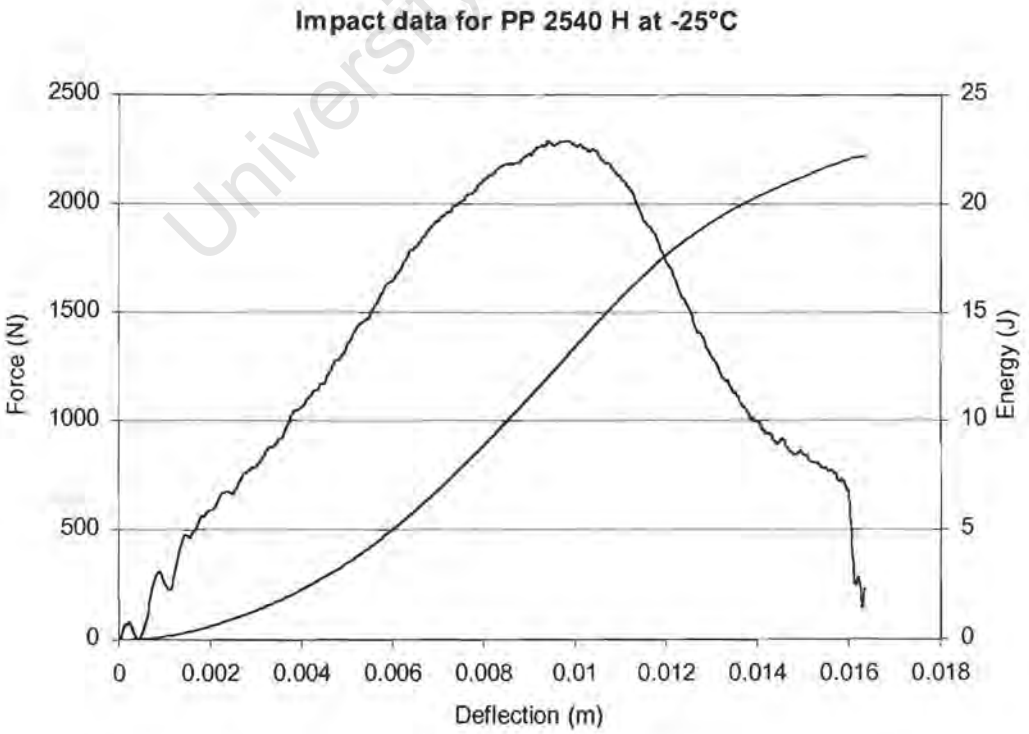

Figure C-20: *Impact traces for PP 2540 H at a test temperature of -25°C*

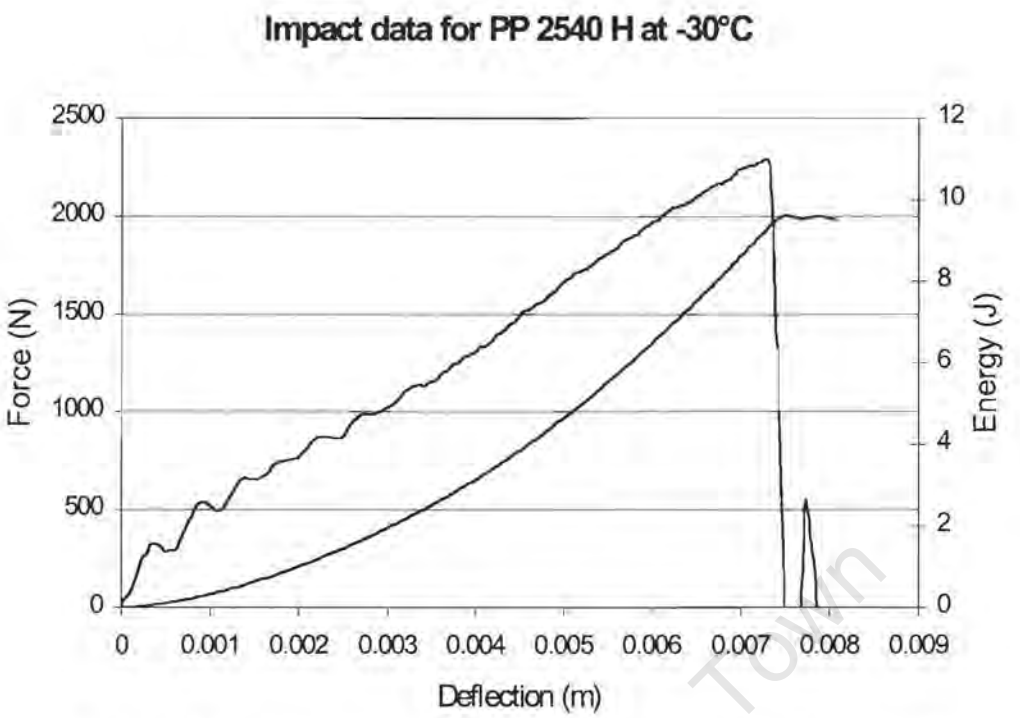

Figure C-21: *Impact traces for PP 2540 H at a test temperature of –30°C*

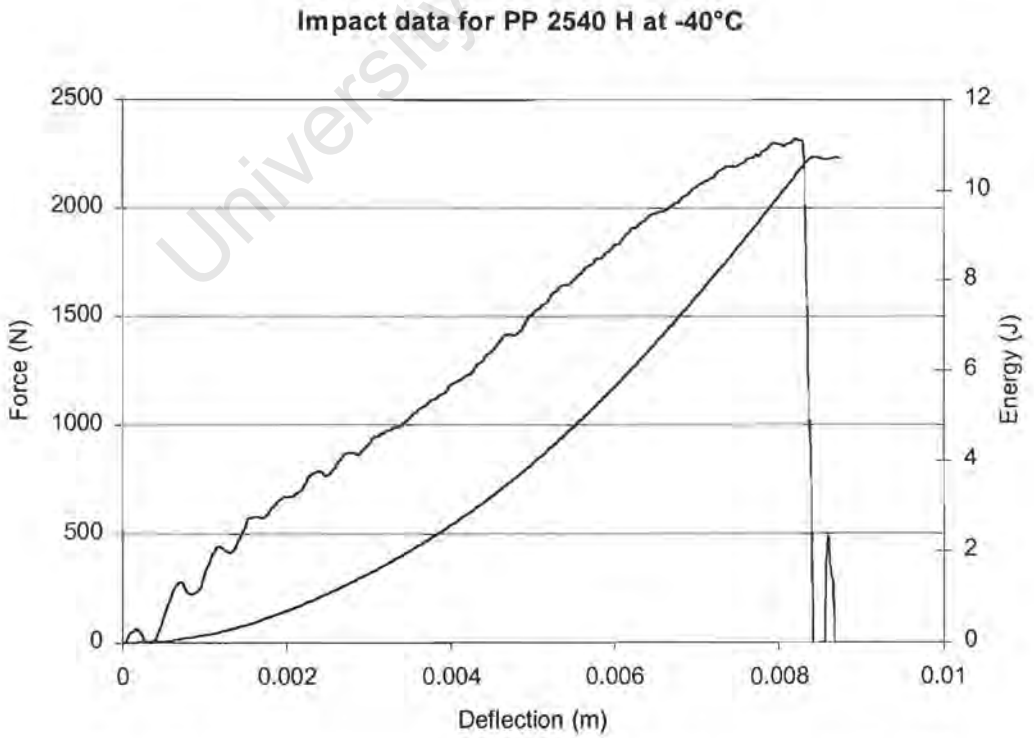

Figure C-22: *Impact traces for PP 2540 H at a test temperature of –40°C*

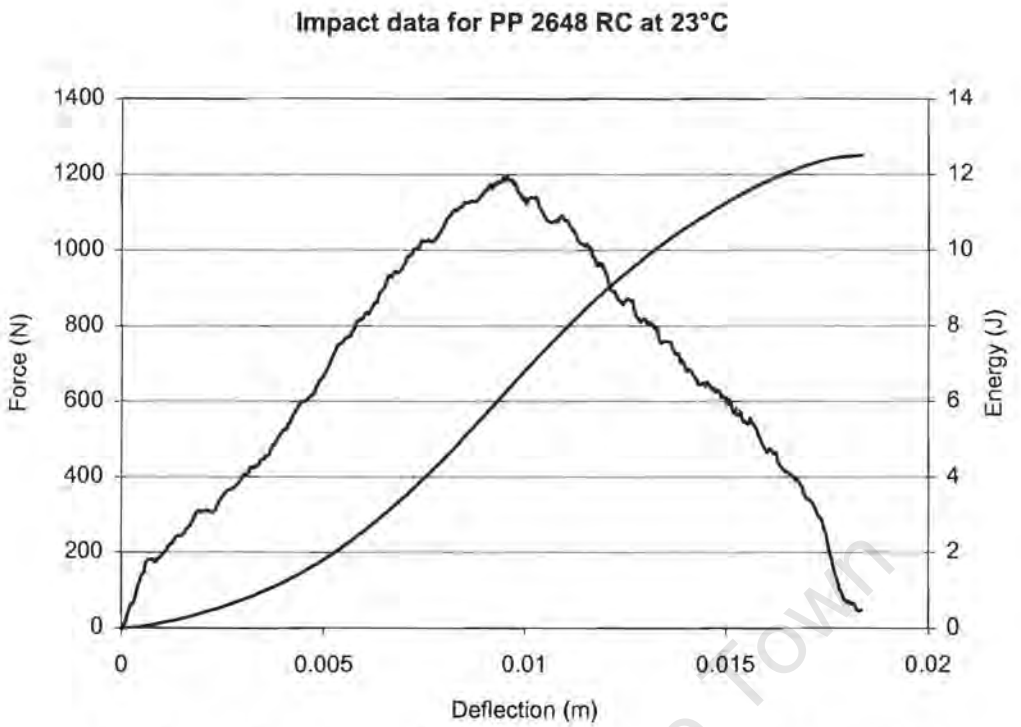

Figure C-23: *Impact traces for PP 2648 RC at a test temperature of 23°C*

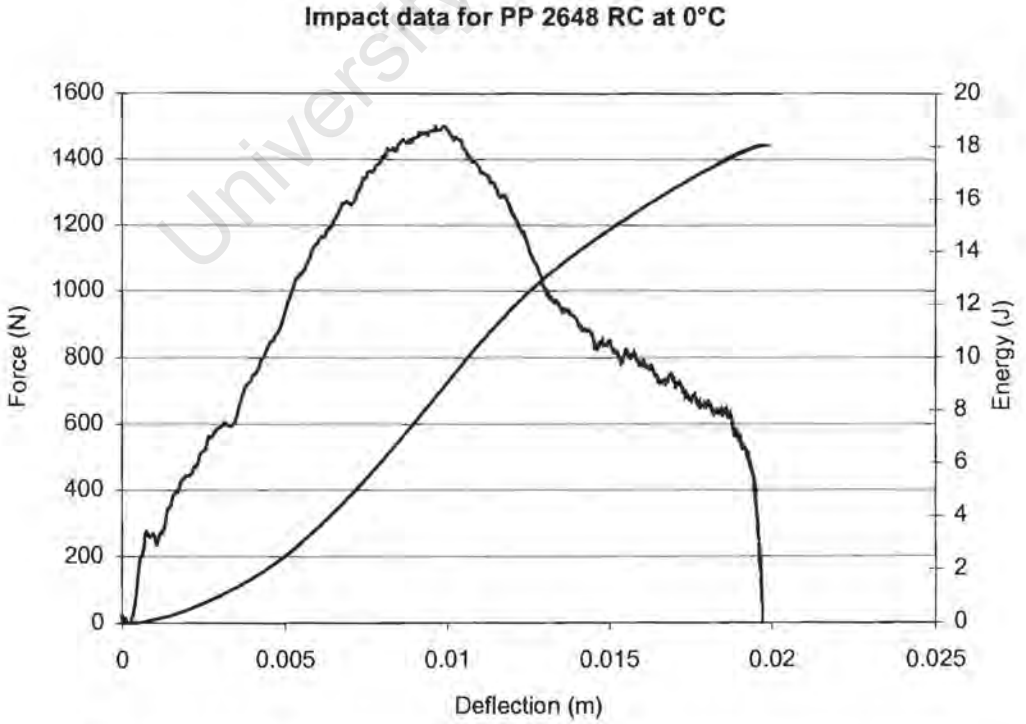

Figure C-24: *Impact traces for PP 2648 RC at a test temperature of 0°C*

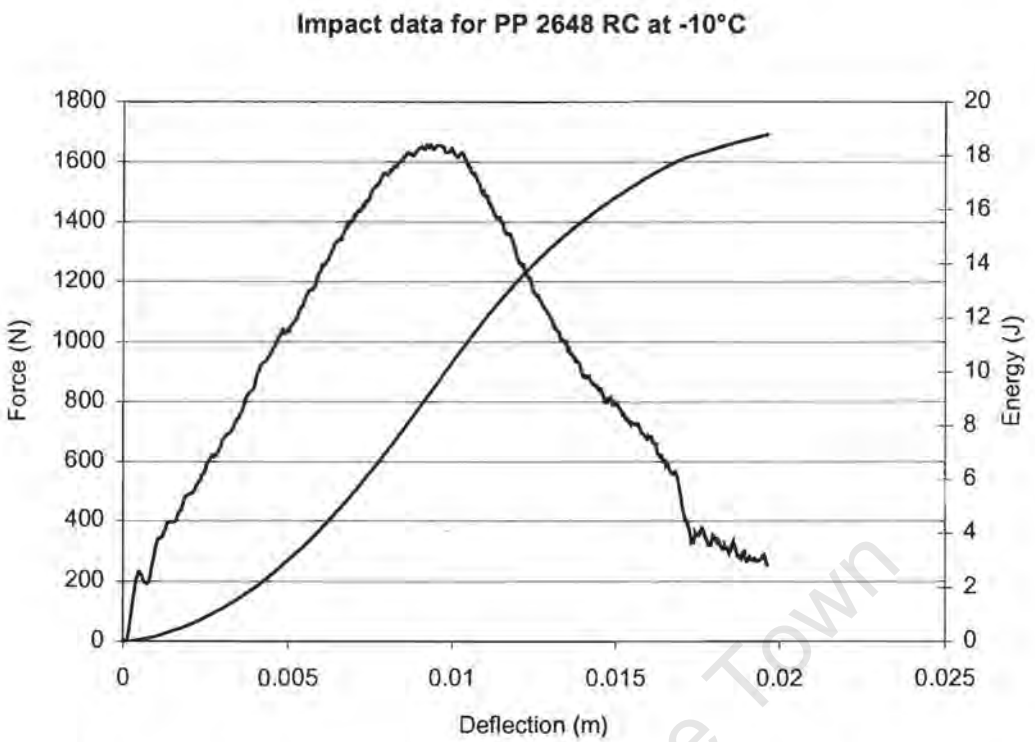

Figure C-25: *Impact traces for PP 2648 RC at a test temperature of -10°C*

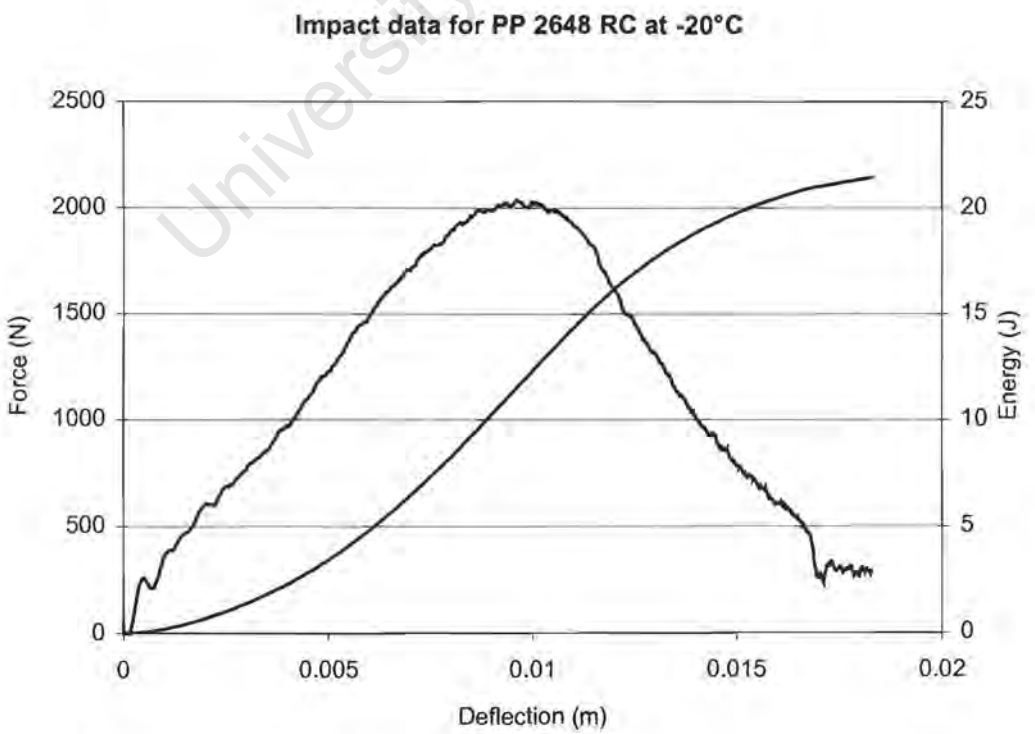

Figure C-26: *Impact traces for PP 2648 RC at a test temperature of -20°C*

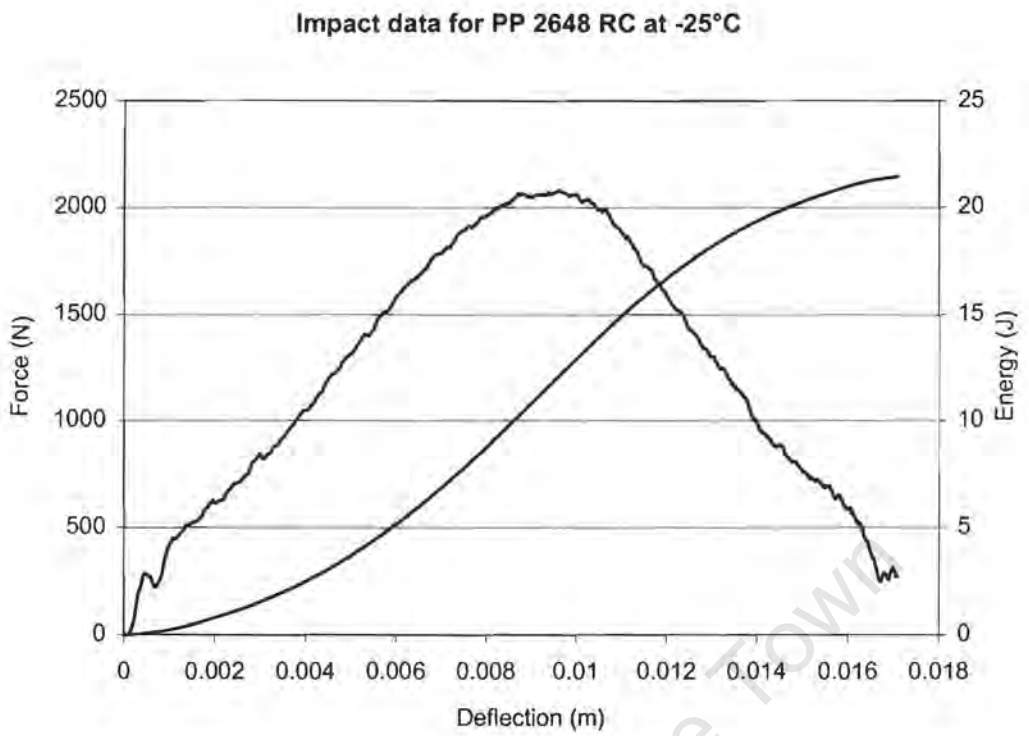

Figure C-27: *Impact traces for PP 2648 RC at a test temperature of -25°C*

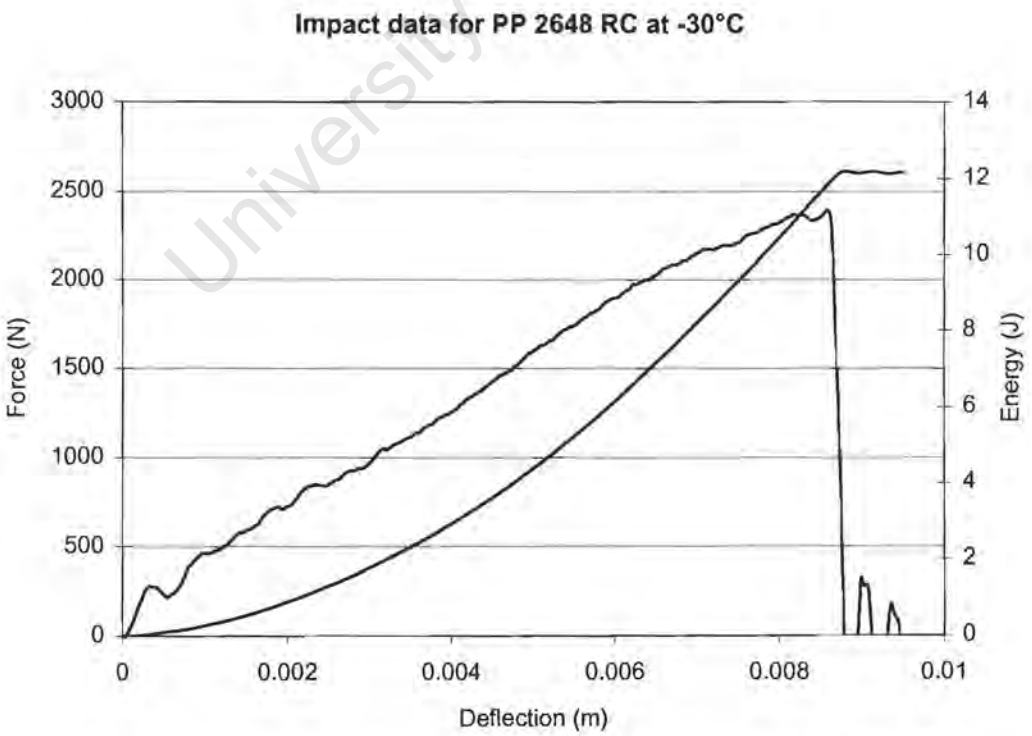

Figure C-28: *Impact traces for PP 2648 RC at a test temperature of -30°C*

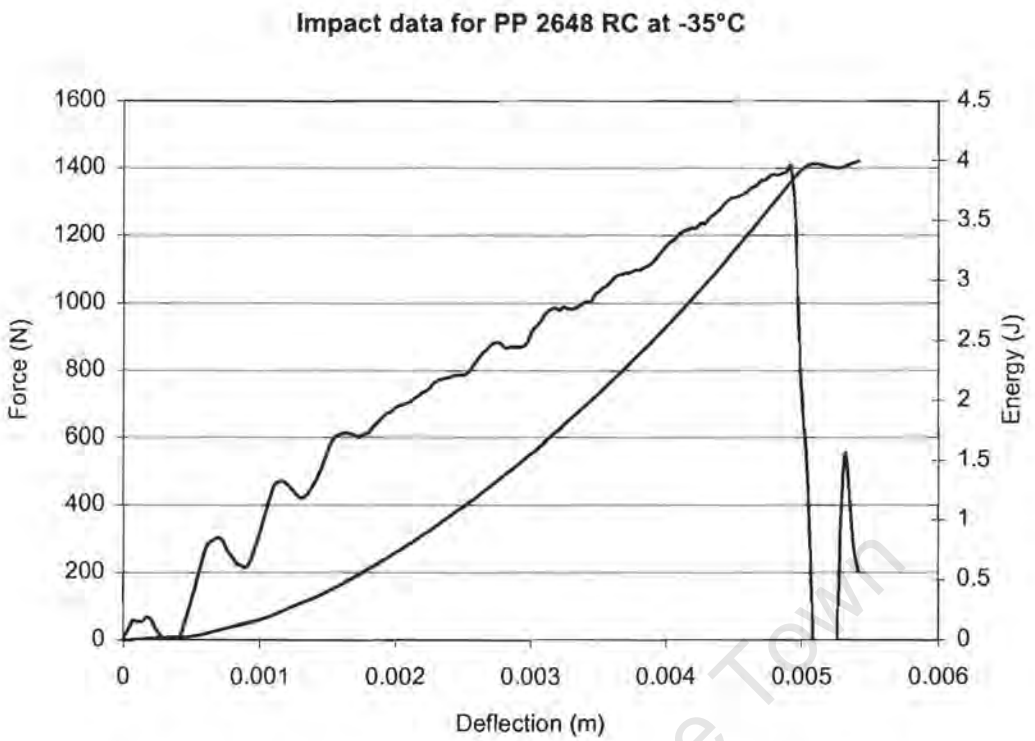

Figure C-29: *Impact traces for PP 2648 RC at a test temperature of -35°C*

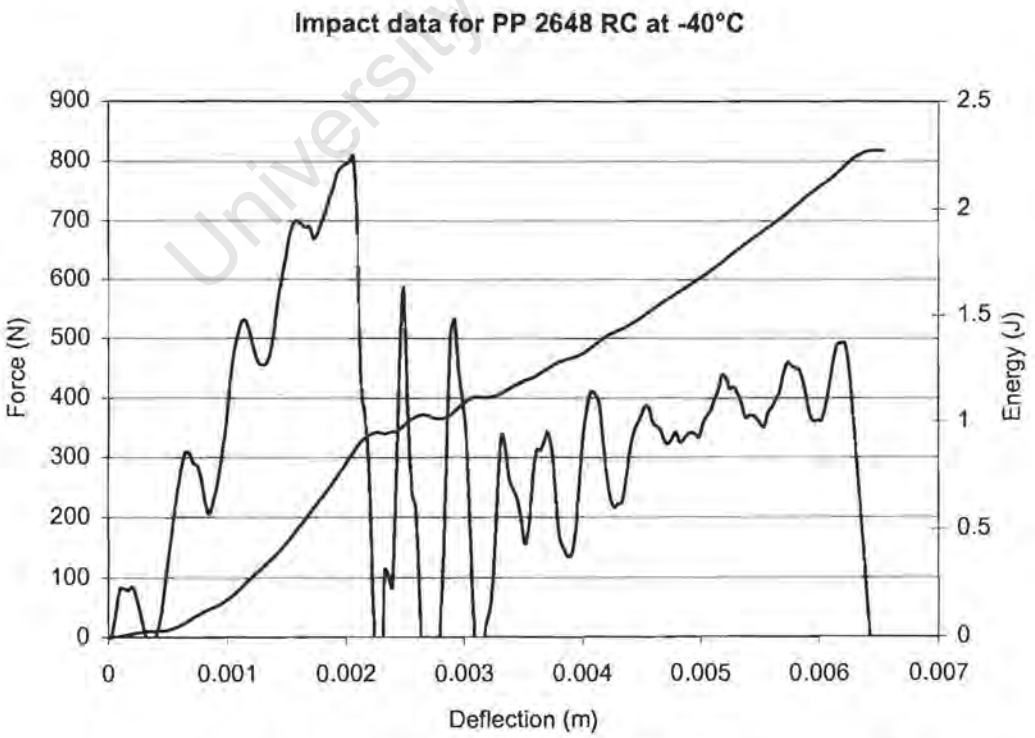

Figure C-30: *Impact traces for PP 2648 RC at a test temperature of -40°C*

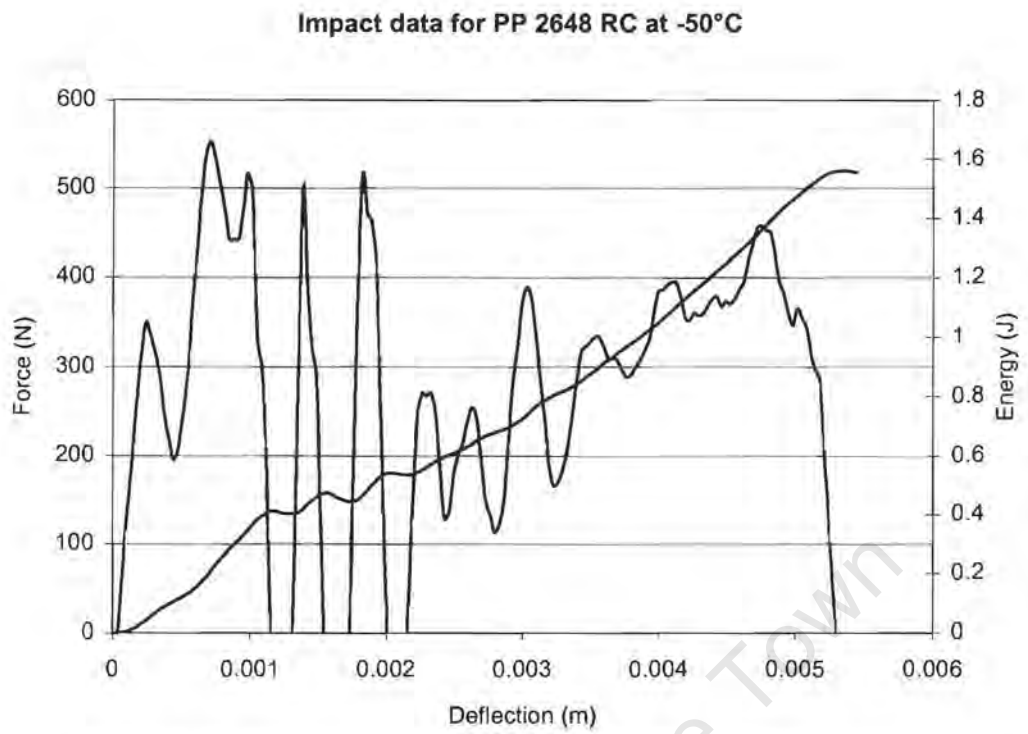

Figure C-31: *Impact traces for PP 2648 RC at a test temperature of -50°C*

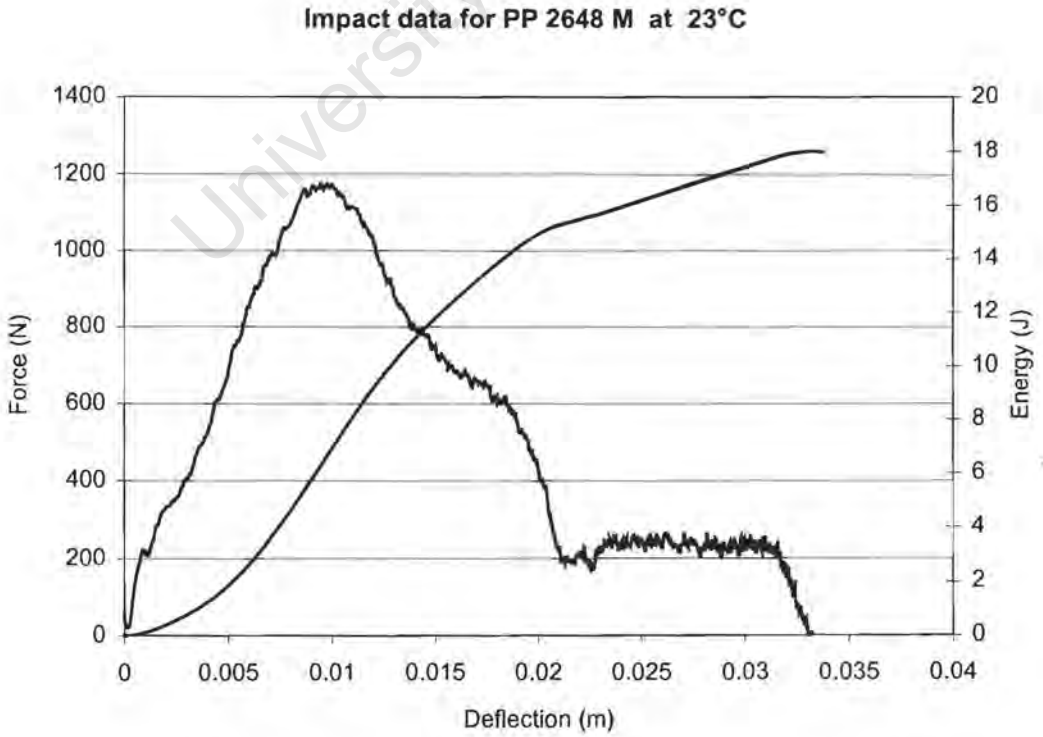

Figure C-32: *Impact traces for PP 2648 M at a test temperature of 23°C*

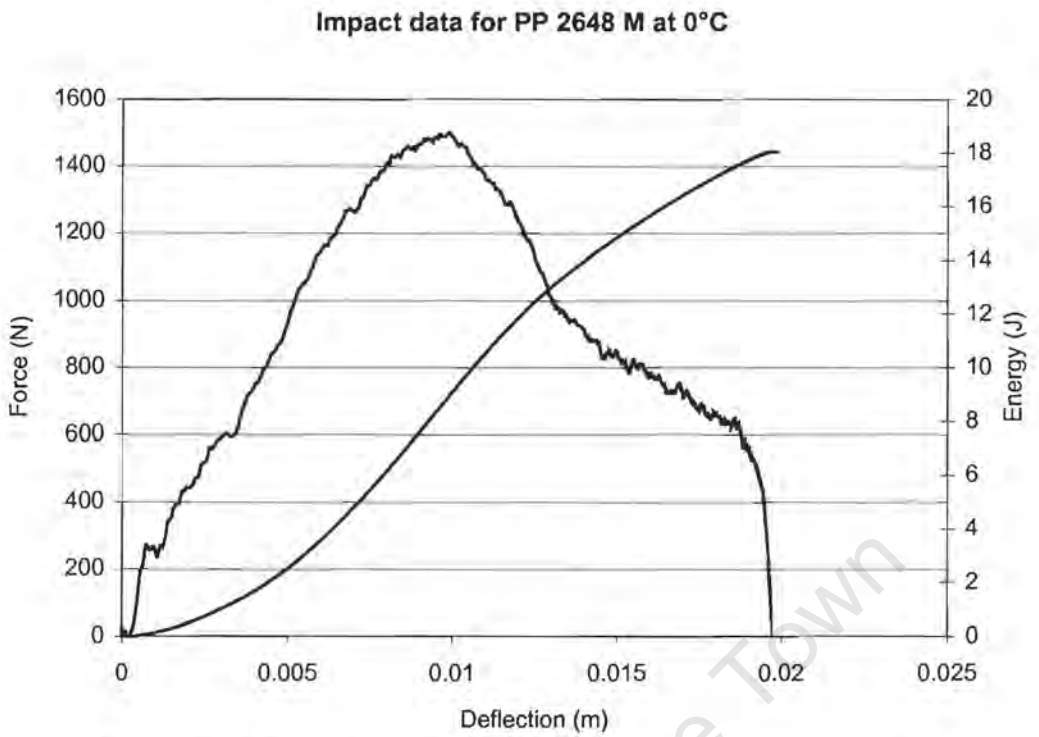

Figure C-33: *Impact traces for PP 2648 M at a test temperature of 0°C*

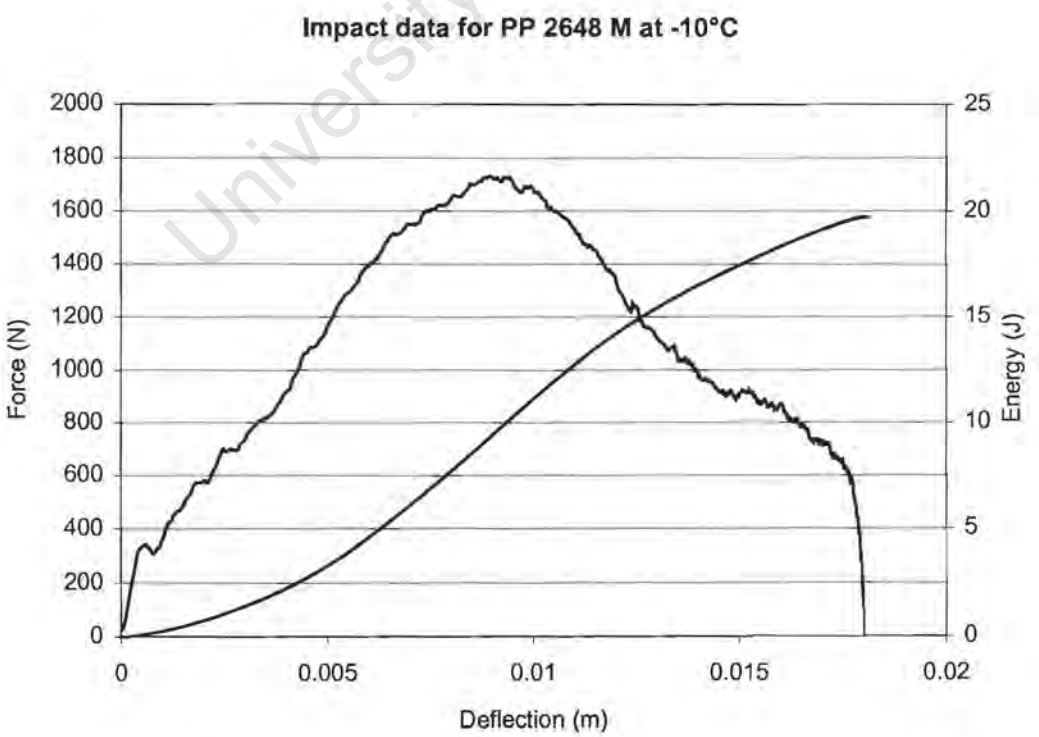

Figure C-34: *Impact traces for PP 2648 M at a test temperature of -10°C*

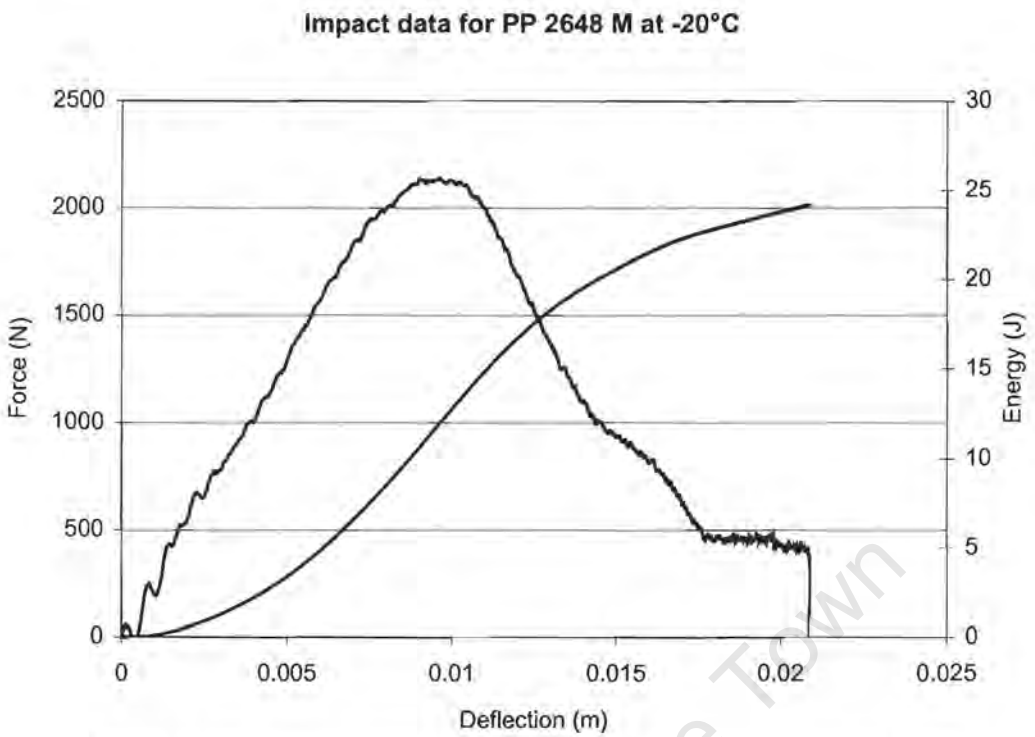

Figure C-35: *Impact traces for PP 2648 M at a test temperature of -20°C*

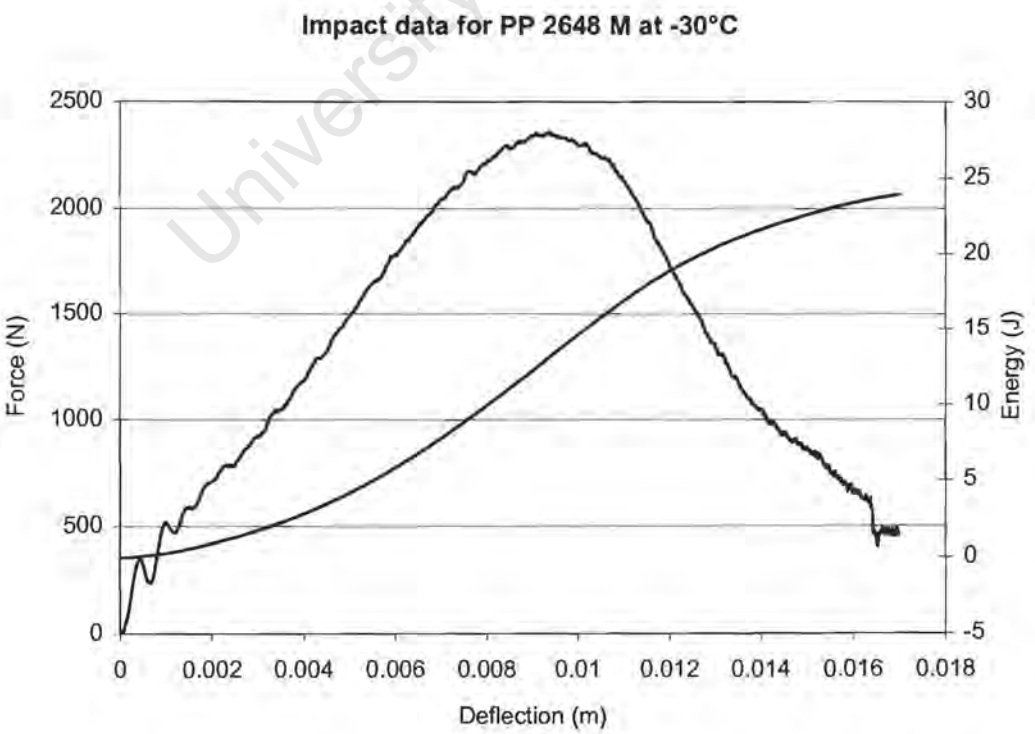

Figure C-36: *Impact traces for PP 2648 M at a test temperature of -30°C*

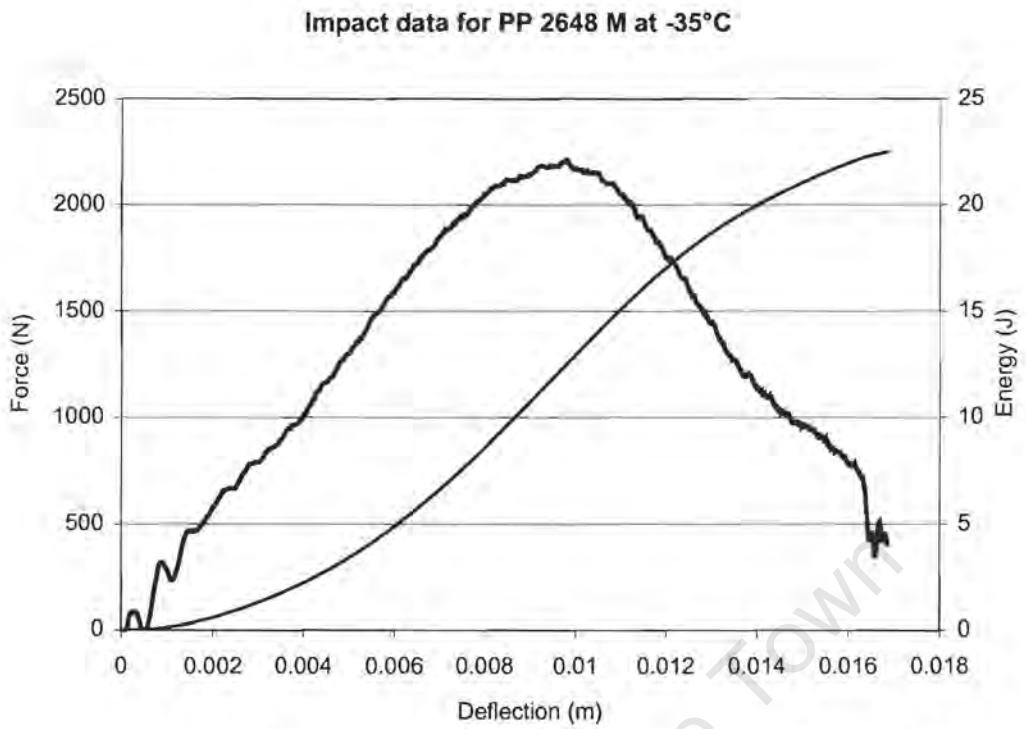

Figure C-37: *Impact traces for PP 2648 M at a test temperature of -35°C*

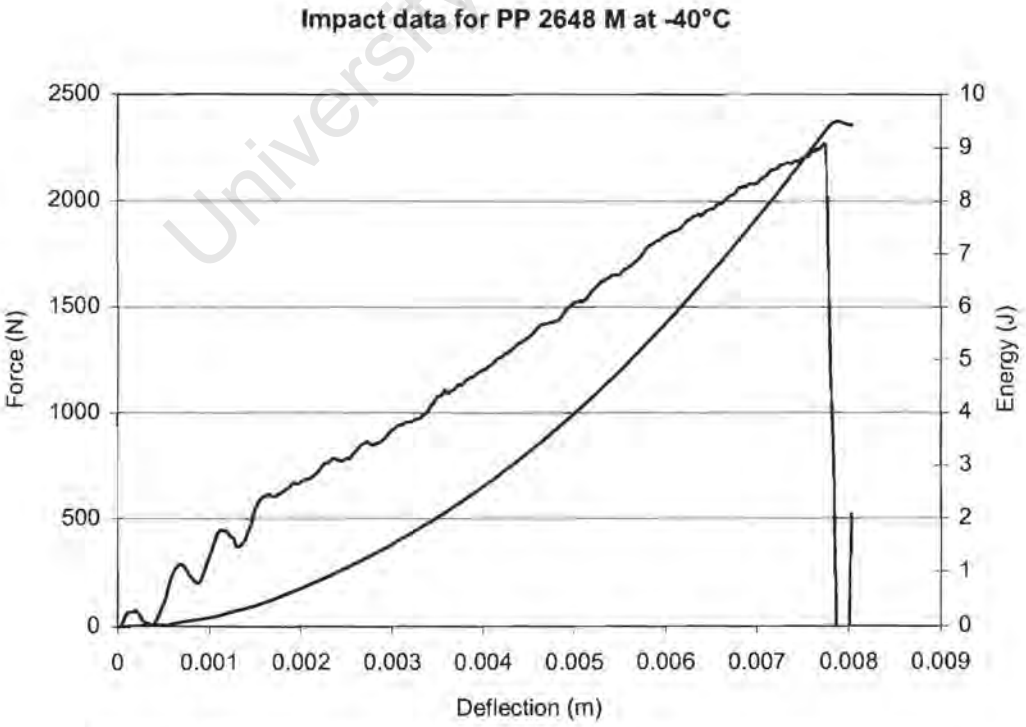

Figure C-38: *Impact traces for PP 2648 M at a test temperature of -40°C*

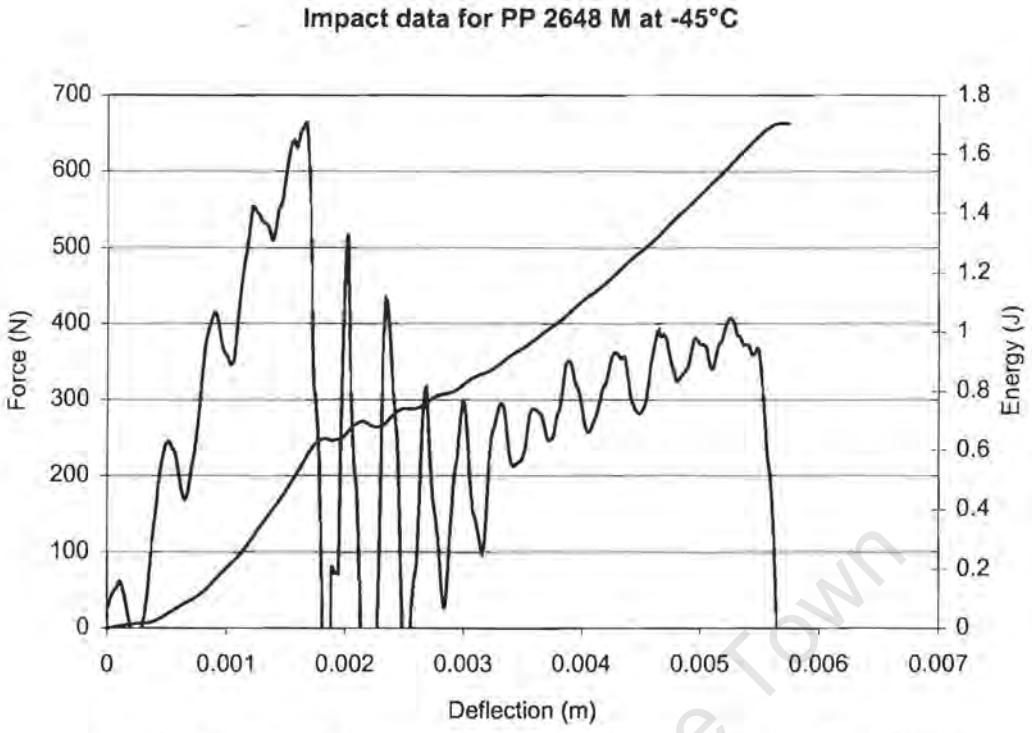

Figure C-39: *Impact traces for PP 2648 M at a test temperature of -45°C*

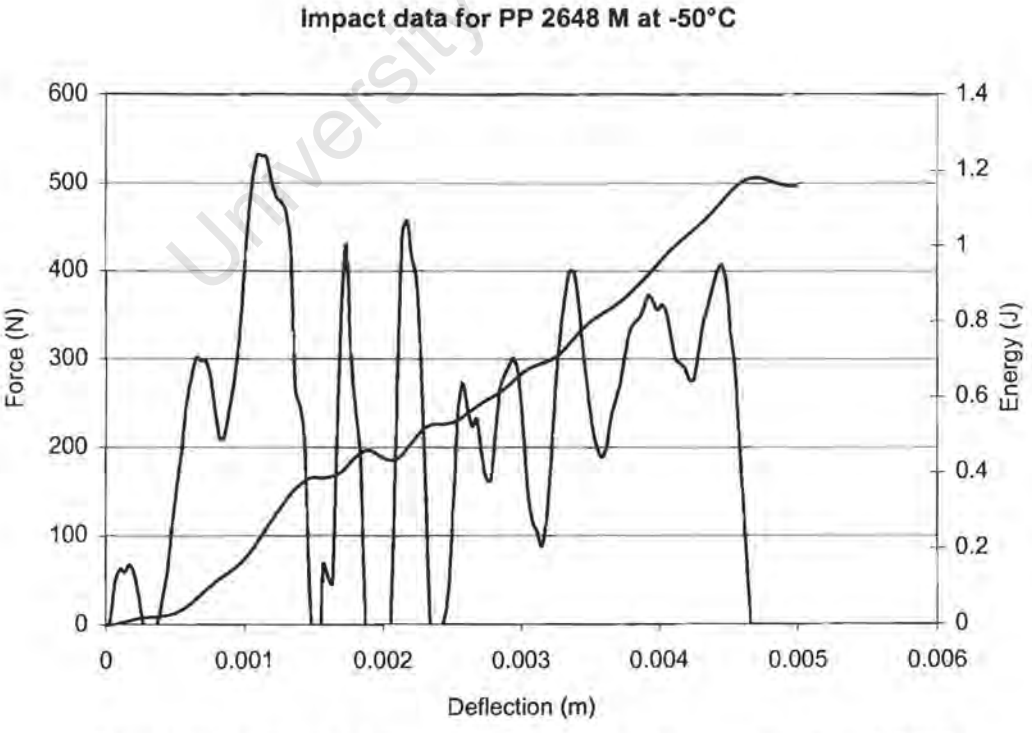

Figure C-40: *Impact traces for PP 2648 M at a test temperature of -50°C*

APPENDIX D

NORMALISED EPR PARTICLE SIZE DISTRIBUTION CURVES
FOR THE TPC, TARGOR AND DOW COPOLYMER TYPES

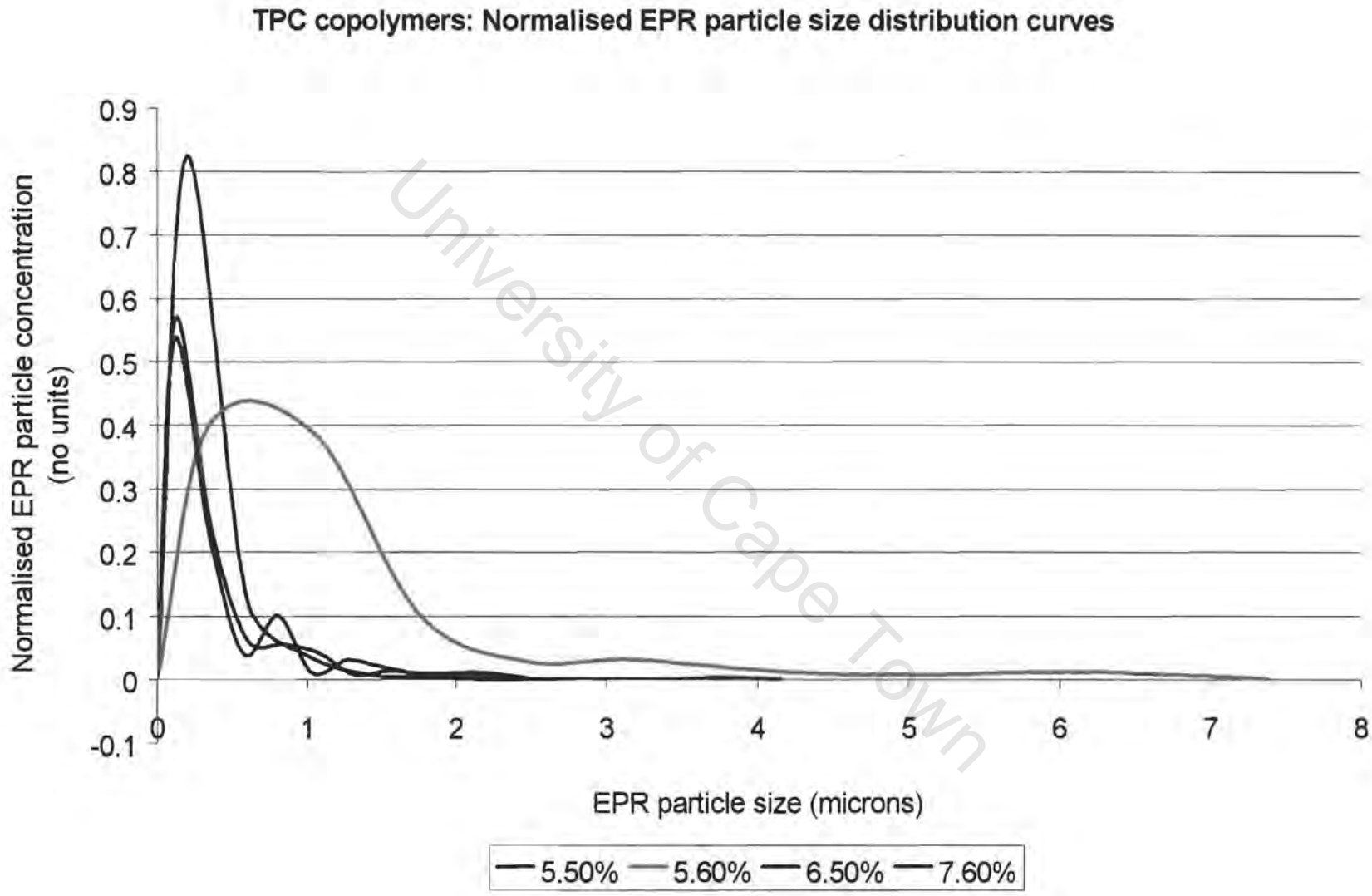

Table D-1: *Graphs of the normalised particle size distribution curves for the TPC copolymers*

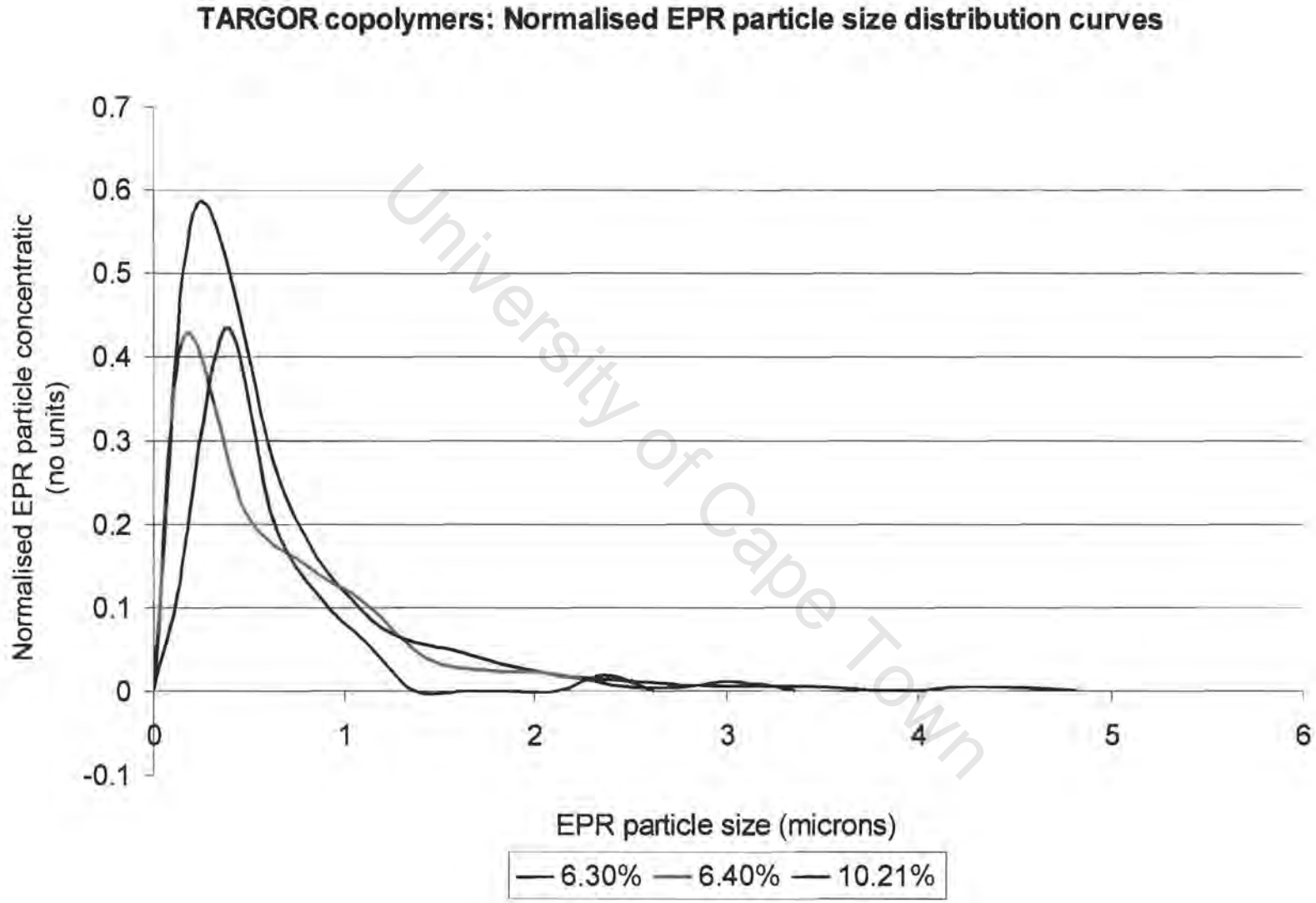

Table D-2: *Graphs of the normalised particle size distribution curves for the TARGOR copolymers*

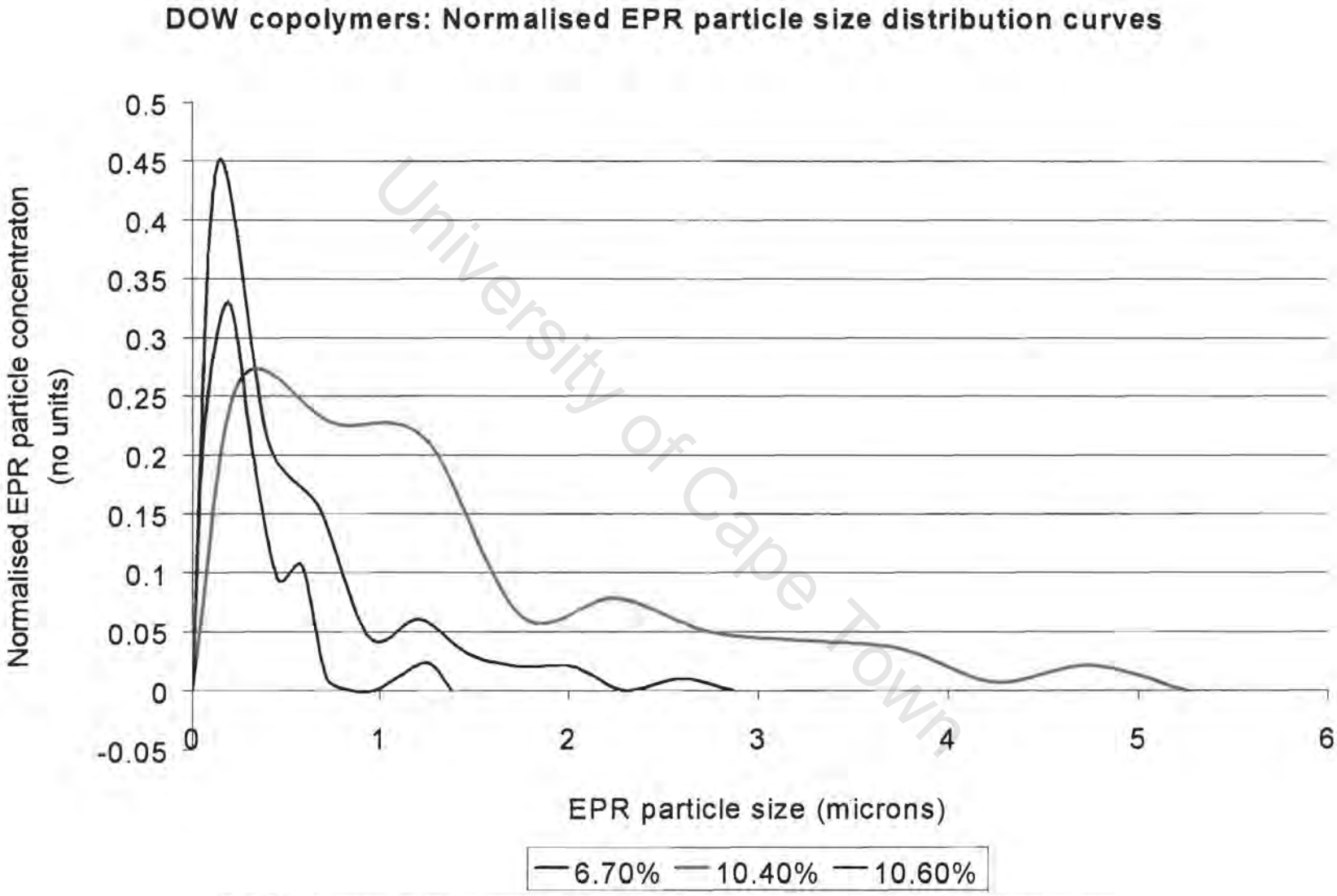

Table D-3: *Graphs of the normalised particle size distribution curves for the DOW copolymers*

APPENDIX E

A DETAILED DESCRIPTION OF THE IMPACT EVENT

Figure 6.1 shows that the curve generated during the impact event can be divided into four sections viz., A, B, C and D. Section A is known as the dynamic offset and does not describe any useful information. This section of the trace is representative of the disturbance of the loading response due to harmonic oscillations that are generated during the initial collision between the tup and the specimen surface. The end of section A in the trace indicates the start of the linear load deflection deformation behaviour of the polymer specimen. This behaviour is characterised by the specimen behaving as an elastically loaded structure. The onset of plastic or permanent mode of deformation starts at point B which is the yield point of the polymer specimen.

The first major deformation of the specimen occurs at point C. The corresponding impact force is the maximum load the specimen can withstand under an impact event before undergoing structural damage. This stage is associated with the appearance of macroscopic deformation characteristics in the specimen viz., cracks and tears. Stage C is followed by a conspicuous reduction in the rigidity of the specimen as indicated by the gradual drop in load after the completion of stage C. Point D is indicative of the end of the drop weight impact test. This is the failure point at which the specimen loses its structural integrity and therefore cannot sustain load any more. Some of the force vs. deflection traces show a constant impact force at this point which is a result of the frictional forces between the tup shaft and specimen.

The corresponding energy vs. specimen deflection graphs for the impact tests (see figure 6.1) are shown in figure E-1. The impact energy absorbed by the polymer increases continuously throughout the impact event. No reduction in the deflection of the specimen is noticed at the end of the test. This indicates

that the specimen did not posses any residual elastic energy at the termination of the impact event. More importantly, this is also an indication of the through penetration of the tup and a successful impact test. Should the specimen have any residual elastic energy, it is reflected by a decrease in the total specimen deflection at the end of the impact test. Thus the energy curves indicated by the graphs in figure E-1 is the total energy absorbed by the specimen during the impact event.

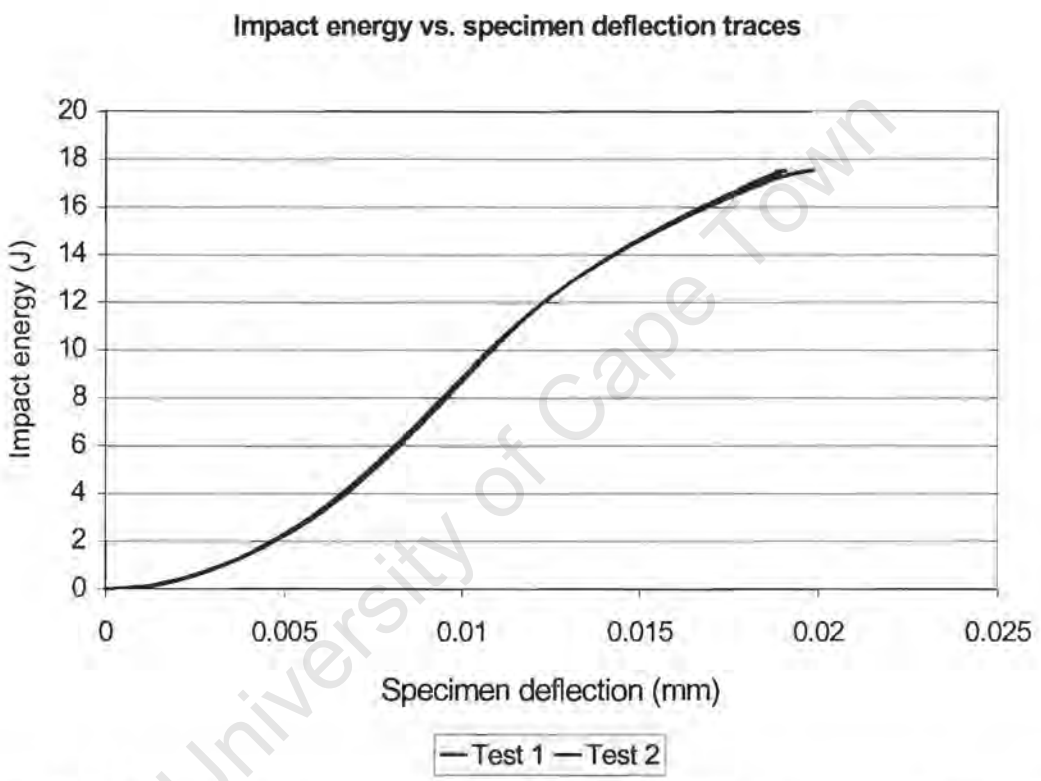

Figure E-1: *A plot of the traces showing the energy absorbed by the specimen as a function of specimen deflection*